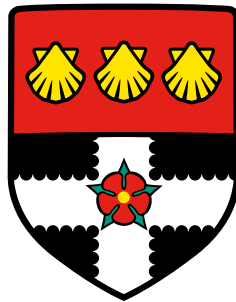


Supervisory Control Of Energy Storage In Rubber Tyred Gantry Cranes



Stefano Pietrosanti

School of Biological Sciences
University of Reading

This dissertation is submitted for the degree of
Doctor of Philosophy

December 2018

Declaration

I confirm that this is my own work and the use of all material from other sources has been properly and fully acknowledged.

All the material presented in this thesis, including material extracted from co-authored articles, is my own work unless explicitly stated.

Stefano Pietrosanti
December 2018

Acknowledgements

I would like to thank my supervisors, Prof William Holderbaum and Prof Victor Becerra, who helped and guided me from the start until the final stages of the research with their advice, constructive criticism and encouragement. This thesis would not have existed without the opportunity that they gave me, and I am grateful that they selected me to join this journey. Their support has been invaluable and allowed me to challenge myself in ways I would never have considered.

I would like to thank all the people involved in the Susports project, starting from Dr Rayner Mayer who initiated it from the noble objective of reducing greenhouse gases emissions. My sincere gratitude goes to Dr Ian Harrison who helped me throughout the journey and in particular to gather most of the data used in this work. Thanks to Dr Antonio Luque and Vicky Papaioannou for their collaboration and for sharing their research work with me. Thanks to all the other members of the Susports project who participated in this challenging program, and thanks especially to Climate KIC for funding this research. My gratitude extends to Wayne Travis and all those at the Port of Felixstowe who kindly donated their time to help metering data from cranes and explain day-to-day port operations.

The work undertaken by Dr Chris Knight for his MEng has laid the foundation for my research, therefore I want to express my gratitude to him for guiding me at the early stages of my PhD. Thanks to Maximilian Zangs for helping running the HTCondor cluster used for numerical calculations. I extend my gratitude also towards all the fellow doctoral students and researchers who provided their feedback and cooperation, among whom I would like to mention Feras Alasali, Timur Yunusov, Monica Armengol, Anthony Nnaji, Chris Shackleton and Charles Moorey.

My gratitude goes to the University academic and technical staff, especially to those at the former School of Systems Engineering. In particular I would like to thank Dr Ben Potter and Prof Paul Sharkey who provided invaluable advice, as well as Steve Gould, Nick Dove, Nick Gurr and Anthony Worrall who facilitated my work with their technical knowledge.

My thanks goes to my friends and to my sister who supported and comforted me during this long process. My most sincere thanks to my parents Luciano and Stefania for their inspiration and encouragement throughout my whole life. Without them I would not have been able to fulfil my desire of starting this PhD.

My final thoughts are reserved for Eva, whose unconditional support has made all this possible. She has always been to my side, providing encouragement during challenging times and cheering me up when pessimism was creeping in my mind. Her energy, patience and love brought out the best in me and gave me the strength to complete this journey to the end.

Abstract

Container terminals are crucial elements in the global trade of goods, however they are also responsible for massive greenhouse gases emissions. One of the key elements in a terminal is the Rubber Tyred Gantry (RTG) crane, which is used to stack containers in the yard. The energy efficiency of this machine can be greatly improved with the use of energy storage by taking advantage of the energy recovered when lowering a container. This thesis presents a study on supervisory control systems for energy storage, designed to determine the instantaneous power output that provides the best benefits with the limited resources provided by the energy storage device. Background research and data analysis provide indication on the energy flows in the system, leading to the development of an RTG crane model, which is validated using data measured on a real crane. The addition of the model of a flywheel energy storage system produces a hybrid RTG crane model, which is used to simulate three proposed supervisory control strategies developed specifically for this application. The characteristics of the supervisory control systems and results from the simulation are compared and analysed in detail in order to determine the quality of the control systems in a real application.

Table of contents

List of figures	xv
List of tables	xxi
Nomenclature	xxiii
1 Introduction	1
1.1 Motivation	2
1.2 Problem statement	4
1.3 Objectives of the research	5
1.4 Publications emerging from this work	5
1.5 Outline of the thesis	6
2 Literature review	9
2.1 Energy storage systems	9
2.1.1 Renewable energy production	10
2.1.2 Power networks	11
2.1.3 Hybrid electric vehicles	11
2.1.4 RTG cranes	12
2.2 Control of energy storage	13
2.2.1 Low-level control of energy storage	13

2.2.2	Supervisory control	14
2.3	Modelling	18
2.4	Summary	20
3	The Rubber Tyred Gantry cranes and opportunities for increasing energy efficiency	23
3.1	Description of the crane	24
3.2	Main electrical components	25
3.2.1	Power supply	25
3.2.2	Electric motors	26
3.2.3	Auxiliary systems	28
3.3	Typical lift cycle	29
3.3.1	Import and export	30
3.3.2	Housekeeping	31
3.3.3	Gantry movements	31
3.3.4	Idle time	32
3.4	Crane used at the Port of Felixstowe	33
3.5	Energy and power flows of RTG cranes	34
3.6	Statistical analysis of the typical activity in a container terminal	38
3.6.1	Container weight	38
3.6.2	Interval between lifts	38
3.6.3	Duration of container lift	39
3.6.4	Average power	41
3.6.5	Energy consumption	41
3.7	System topology	42
3.8	Potential opportunities for improving efficiency	45
3.8.1	Energy recovery	45

3.8.2	Reduction of peak power demand	47
3.9	Energy storage	49
3.9.1	Batteries	50
3.9.2	Super-capacitors	52
3.9.3	Flywheels	54
3.9.4	Comparison of energy storage systems	55
3.10	Active Front-End	56
3.11	Summary	58
4	Design and low-level control of flywheel energy storage systems	61
4.1	Mechanical flywheel	61
4.2	Sizing of storage	64
4.2.1	Characteristics of the storage	64
4.2.2	Example of a physical flywheel	65
4.3	Powering a flywheel	65
4.3.1	Induction motor	66
4.3.2	Permanent magnet motor	66
4.3.3	Homopolar induction motors	67
4.3.4	Switched reluctance motor	67
4.4	Control of a switched reluctance motor	68
4.5	Summary	72
5	Modelling	73
5.1	Model of an RTG crane	73
5.1.1	Hoist motor	74
5.1.2	Load applied to the hoist motor	75
5.1.3	Primary source	84
5.1.4	Additional secondary elements of the model	88

5.1.5	Validation of the RTG model	89
5.2	Model of energy storage	93
5.2.1	Generic energy storage model	93
5.2.2	Generic flywheel energy storage model	98
5.2.3	Specific flywheel energy storage model	100
5.2.4	Comparison of energy storage models	105
5.3	Hybrid RTG crane model	110
5.4	Summary	110
6	Supervisory control strategies	113
6.1	Proportional-integral supervisory control	114
6.1.1	DC bus voltage control	115
6.1.2	Power sharing control	117
6.1.3	Simulation and results	120
6.1.4	Analysis of the results	122
6.2	Optimal supervisory control based on stochastic modelling	126
6.2.1	Lift duration	127
6.2.2	Problem definition	127
6.2.3	Optimal power management strategy	129
6.2.4	Simulation and results	133
6.2.5	Analysis of the results	137
6.3	Fuzzy logic supervisory control	140
6.3.1	Membership functions	141
6.3.2	Rules	146
6.3.3	Defuzzification	150
6.3.4	The output	151
6.3.5	Simulation and results	153

6.3.6	Analysis of the results	156
6.4	Summary	157
7	Analysis and comparison of supervisory control strategies	159
7.1	Hybrid RTG simulation	159
7.1.1	Energy consumption	162
7.1.2	Peak power demand	163
7.1.3	Estimated fuel consumption	165
7.1.4	Impact on the ESS	165
7.2	Analysis of supervisory control strategies	169
7.2.1	PI control strategy	169
7.2.2	Optimal	170
7.2.3	Fuzzy Logic	171
7.3	Feasibility, tuning and implementation	173
7.3.1	Tuning difficulty of supervisory controllers	173
7.3.2	Portability and generalisation	174
7.3.3	Computational burden	175
7.4	Sensitivity analysis	175
7.4.1	Change in energy capacity	176
7.4.2	Change in maximum power output	180
7.5	Summary	185
8	Conclusions	187
8.1	Summary and conclusions	187
8.1.1	Summary of the thesis	187
8.1.2	Summary of the chapters	188
8.1.3	Assumptions	191
8.1.4	Overview of original contributions to knowledge	192

8.2	Future work	192
8.2.1	Models and simulations	192
8.2.2	Crane Activity	193
8.2.3	Supervisory control strategies	194
	References	197
	Appendix A Characteristics of the RTG crane used as a reference in this work	207
	Appendix B Moment of Inertia of a Cylinder	209
B.1	Hollow cylinder	209
	Appendix C Stability and error rejection of the DC voltage PI control	211
	Appendix D Proof to the CDF Theorem	215
	Appendix E Membership functions	217
E.1	Inputs	217
E.1.1	Input 1: flywheel speed (in RPM) <i>FESSspeed</i>	217
E.1.2	Input 2: hoist motor power (in W) <i>HoistPower</i>	218
E.1.3	Input 3: DC bus voltage (in V) <i>DCbusV</i>	219
E.2	Outputs	220
E.2.1	Output 1: FLC output	220
	Appendix F Run the Matlab scripts	223
F.1	Optimal control calculations	223
F.2	Hybrid RTG crane model	224

List of figures

1.1	RTG crane lifting a container at the MSC terminal in Valencia, Spain. . . .	2
3.1	RTG crane	25
3.2	Satellite view	26
3.3	Spreader	27
3.4	Crane schematic	28
3.5	Basic crane movements	29
3.6	Terminal tractor	30
3.7	Sequence of RTG movements	31
3.8	Crane in a port	32
3.9	Illustrative power flow during a lift	35
3.10	Energy consumed and regenerated in each phase	36
3.11	Illustrative lift: hoist and trolley speed	37
3.12	Illustrative lift: hoist position	37
3.13	Statistics on container weight	39
3.14	Statistics on intervals between lifts	40
3.15	Histogram of duration of lifts	41
3.16	Distribution of lift duration with various loads	42
3.17	Average power during lifts and lowerings	43
3.18	Energy flow during lifts and lowerings	43

3.19	Three-phase conductor bar that powers RTG cranes at the Port of Felixstowe.	44
3.20	Basic topology of the RTG crane	45
3.21	Consumed, potential and regenerated energy of standard lifts	47
3.22	Power demand as percentage of time	48
3.23	Example of powersharing: power	50
3.24	Example of powersharing: energy	51
3.25	Topology of crane equipped with energy storage	52
3.26	Rangone chart	53
3.27	Differences between a crane equipped with a diode rectifier and an AFE [1].	57
3.28	Topology of an RTG crane equipped with AFE	58
4.1	Power limits for a flywheel with torque constraints	63
4.2	Basic visualisation of a 6/4 switched reluctance motor.	67
4.3	Inductance and current of a single phase of an SR motor	69
4.4	Single phase of a SR motor converter	70
4.5	Diagram of the low-level controller for the SR motor.	71
5.1	Diagram of the connections for the model of the hoist motor	75
5.2	Measured power and speed of the hoist motor when lifting a 19 tonne container.	75
5.3	Mechanical system of the hoist motor with parallel ropes.	76
5.4	Hoist motor speed and power consumption when lifting a 25 t container . .	77
5.5	Ratio between vertical speed and rope speed in function of rope length. . .	79
5.6	simplified 1-rope geometry of an hoist mechanism	80
5.7	Forces imposed on container	81
5.8	Load torque of hoist motor from calculations	84
5.9	Fuel consumption of a Volvo Penta TAD1641GE diesel generator	85
5.10	VSC control system used in the AFE model	87
5.11	Simulink model of the brake resistor and resistor chopper.	88

5.12	Simulink model of the RTG crane	90
5.13	Comparison of measured and simulated data, series of lifts	91
5.14	Comparison of measured and simulated data, single lift	92
5.15	Comparison of measured and simulated data, 24 hours	92
5.16	Simulink model of the three-phase energy storage system	94
5.17	Simulation of a three-phase ESS supplying power during voltage sags	95
5.18	Generic DC energy storage system model implemented in Simulink	97
5.19	Switched reluctance motor model implemented in Simulink	99
5.20	Diagram of the components of the specific FESS model.	101
5.21	Measurements from a flywheel during a spin-down compared to the model	103
5.22	Mechanical power lost from friction at various rotational speeds.	104
5.23	Mechanical flywheel implemented in Simulink	105
5.24	Simulink blocks that read the instantaneous motor values from data	106
5.25	Simulink model of the specific energy storage system	107
5.26	Comparison of the three ESS models: power reference and storage outputs.	108
5.27	Comparison of the three ESS models: energy stored.	109
5.28	Comparison of the three ESS models: spin-down test.	109
5.29	Simplified diagram of the hybrid RTG crane model.	110
6.1	Supervisory control strategies presented in this chapter.	114
6.2	DC bus voltage fluctuations due to the activity of the hoist motor	115
6.3	Diagram of the RTG crane represented as basic electrical elements.	116
6.4	Output of the power sharing PI depending on load power P_L . P_M is the power threshold chosen below which the ESS does not intervene. P_S is the maximum power output of the ESS.	118
6.5	Power sharing and DC voltage control diagram	119

6.6	Hoist power against DC bus voltage; every dot represents a data point collected at 10 Hz. The power sharing and voltage PI working areas are highlighted, showing that no activity happens in the overlapping zone.	121
6.7	PI control strategy, full simulation	122
6.8	PI control strategy, lift cycle	123
6.9	Histogram of the lift durations	135
6.10	PCHIP interpolant of the CDF	136
6.11	Examples of control points calculated in the minimisation	137
6.12	Optimal control strategy, full simulation	138
6.13	Optimal control strategy, lift cycle	139
6.14	Structure of a fuzzy system.	140
6.15	Example of membership functions for a FLC.	142
6.16	Fuzzification process of the three inputs and their associated fuzzy sets. . .	145
6.17	Membership functions of the Fuzzy Logic Controller.	146
6.18	Examples of an FLC inference stage.	147
6.19	Example of the defuzzification process	151
6.20	Output of the Fuzzy Logic Controller, normal speed	152
6.21	Output of the Fuzzy Logic Controller, speed outside boundaries	153
6.22	Hoist power vs. DC bus voltage	154
6.23	Fuzzy logic control, full simulation	154
6.24	Fuzzy logic control, lift cycle	155
6.25	Example of the fuzzy logic process for 2 peculiar states.	157
7.1	Energy consumption of the hybrid RTG crane in the six days recorded. . . .	161
7.2	Energy consumption of the hybrid RTG crane in the six scenarios.	162
7.3	Percentage of time that the RTG crane load is above specified thresholds. .	164
7.4	Estimated fuel consumption in the six scenarios.	166

7.5	Average absolute power output of the storage device under the supervisory controllers.	167
7.6	Average energy stored in the ESS under the supervisory controllers.	168
7.7	Variation in energy capacity: consumed energy	177
7.8	Variation in energy capacity: peak power demand	178
7.9	Variation in power rating: energy demand	182
7.10	Variation in power rating: peak power demand	183
B.1	Hollow cylinder.	210
C.1	Control system topology for the PI supervisory control system.	213
F.1	QR code linking to the zip file containing the Matlab scripts.	224

List of tables

3.1	Energy flows during a lift cycle	36
3.2	Statistical information collected in 4 days	40
3.3	Energy consumed and regenerated during standard lifts	46
3.4	Comparison of energy storage technologies in use on RTG cranes.	56
4.1	Comparison of electric motor technologies	68
5.1	Measured ranges for geometrical parameters of the crane	79
5.2	Volvo Penta TAD1641GE diesel generator fuel consumption	85
5.3	Energy consumption of a single RTG crane for 24 hours	91
5.4	RTG model validation results for power	91
5.5	Parameters of the flywheel and best-fit values.	103
5.6	Comparison of energy storage models.	108
6.1	PI controllers parameters used in the simulation.	122
6.2	Parameters used for the calculation of the optimal control strategy	133
6.3	Parameters of the Gamma distribution which fits the lift duration data.	134
6.4	Parameters of the numerical minimisation.	136
6.5	Input and output signals of the FLC with their associated symbols.	145
6.6	Rules defined for the FLC.	150
7.1	List of RTG configurations simulated	160

7.2	Results of the simulation: energy consumption	163
7.3	Results of the simulation: peak power demand	164
7.4	Results of the simulation: fuel consumption	165
7.5	Changes in primary source energy consumption when varying the energy storage capacity	179
7.6	Changes in primary source peak power demand when varying the energy storage capacity	179
7.7	Changes in primary source energy consumption when varying ESS maximum power output	181
7.8	Changes in primary source peak power demand when varying ESS maximum power output	181
7.9	Main advantages and disadvantages of each control strategy	184
A.1	Characteristics of the RTG crane in use at the Port of Felixstowe	207

Nomenclature

Roman Symbols

$D(\cdot)$ cost function associated with energy production

D_{tot} total cost associated with energy production

E stored energy, [J]

E_{max} energy capacity of the storage, [J]

$F_L(t)$ Cumulative Distribution Function associated with the distribution L

$f_L(t)$ probability that an event occurs at time t when defined by a distribution L

I inertia, [$Kg \cdot m^2$]

m_c weight of a container, [kg]

m_s weight of the spreader, [kg]

$p_d(t)$ instantaneous power dissipated by the brake resistors, [W]

$p_f(t)$ instantaneous mechanical power of the flywheel, [W]

$p_g(t)$ instantaneous power of the primary source, [W]

P_L constant power demand of the load, [W]

$p_L(t)$ instantaneous power of the load, [W]

P_M primary power threshold of the power sharing PI, [W]

P_s maximum power output of the storage, [W]

$p_s(t)$ instantaneous power of the energy storage system, [W]

$P^*(k, L, E_0, P_s, \eta_1, \eta_2)$ Optimal power strategy for an energy storage system

$T(t)$ torque, [Nm]

$T_g(t)$ generating torque, [Nm]

$T_m(t)$ motoring torque, [Nm]

$U(t)$ potential energy, [J]

V_M DC bus voltage threshold of the voltage PI controller, [V]

Greek Symbols

α, β constant parameters that define a Gamma distribution

ω rotational speed, [rad/s]

ω_{max} maximum rotational speed of the flywheel, [rad/s]

ω_{min} minimum rotational speed of the flywheel, [rad/s]

Acronyms / Abbreviations

AFE Active Front-End

CO₂e Carbon Dioxide equivalent, a unit of global warming potential for greenhouse gases

CVT Continuously Variable Transmission

D-RTG Diesel Powered RTG cranes

E-RTG Electric Powered RTG cranes

ESS Energy Storage System

EV Electric Vehicle

FESS Flywheel Energy Storage System

FLC Fuzzy Logic Controller

HEV Hybrid Electric Vehicle

MOM Middle of Maximum, a defuzzification method

PCHIP Piecewise Cubic Hermite Interpolating Polynomial

PM Permanent Magnet motor

PoF Port of Felixstowe, the largest shipping port in the UK

RTG Rubber-Tyred Gantry crane

SC Super-capacitor, a high energy density capacitor

SoC State of Charge of a storage unit

SR Switched Reluctance motor

TEU Twenty-foot equivalent unit, a unit of cargo volume

ZPMC Shanghai Zhenhua Heavy Industries Company Limited, a crane manufacturer

Chapter 1

Introduction

Rubber Tyred Gantry (RTG) cranes are machines designed to stack containers in shipping terminals, including container ports. They are a key element of the logistics of a terminal yard, and are associated with a high energy consumption. They use large electric motors to raise containers weighing up to 40 tonnes for heights that can reach 20 metres, each crane consuming more than 800 kWh per day [2]. A crane lifting a container, like the one showed in Figure 1.1, can use over 2 kWh over the course of just 30 seconds. Part of this energy is stored as potential energy in the container; therefore, when a load is lowered, energy is recovered by the hoist motor and most of it is dissipated in brake resistors. This otherwise wasted energy could be recovered and re-used by installing energy storage systems. The effectiveness of the storage device can be enhanced by carefully adjusting its power output. In order to achieve this, it is possible to use supervisory control systems that select the best instantaneous power output depending on the conditions of the crane and its activity.

This thesis presents research in supervisory control strategies for energy storage that aims at reducing the RTG energy consumption and impact on the terminal power network. A supervisory control strategy requires a good understanding of the problem and a rigorous testing process to verify its effectiveness. The research that led to this thesis focused mainly on the development of supervisory control strategies, however it also sought to maintain a pragmatic approach and employ rigorous verification procedures.

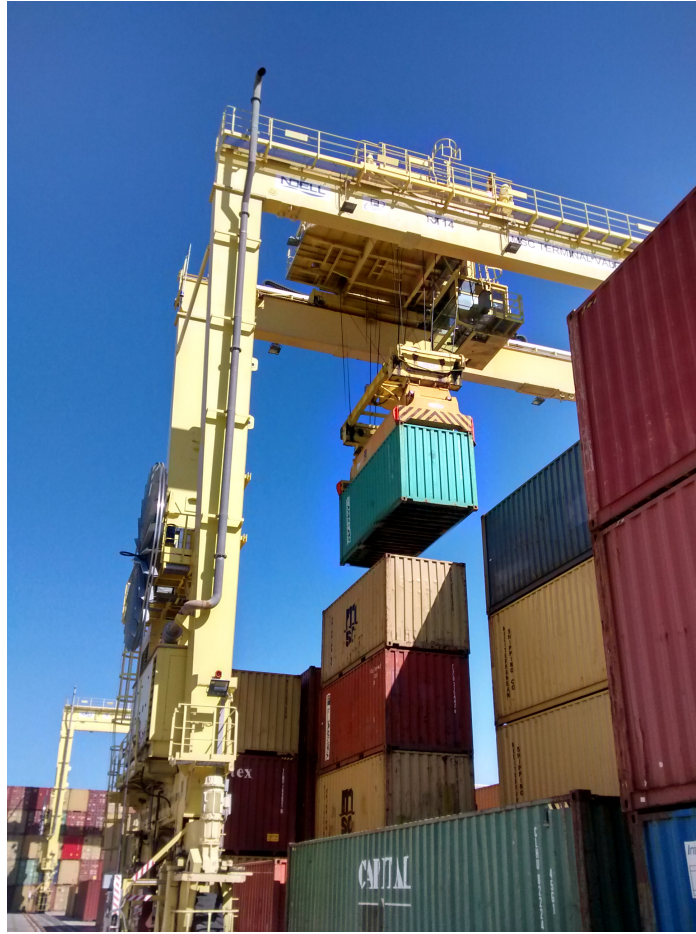


Fig. 1.1 RTG crane lifting a container at the MSC terminal in Valencia, Spain.

1.1 Motivation

Goods are being transported around the world at an unprecedented pace. The World Trade Organization reports that in the years 2010-2014 the volume of merchandise goods increased by an average of 3.5% yearly surpassing the value of 18 trillion US dollars [3]. Goods are transported by land and air but mostly by sea, with 90% of the total trade being seaborne [4]. Most of the imported goods that can be found on a supermarket shelf in the UK have been transported by sea in a standard intermodal container [5], with containerised trade reaching a global volume of 171 million TEU¹ in 2014 [6]. Container terminals handle the transshipping of cargo from one transport medium to the other, for example from sea to land, using purpose built cranes that consume large amounts of energy. Faced with the steady increase in global trade, port operators are actively pushing for higher efficiency

¹Twenty-foot Equivalent Unit

in the container handling process in order to increase revenue, reduce energy costs and greenhouse gases emissions [6]. The logistics and transportation sector is striving to find innovative solutions that increase efficiency. Technologies already exist that could allow tangible improvements to the energy efficiency, for example energy recovery and storage solutions. However it is first necessary to analyse the potential benefits and opportunities given by storage, as well as develop effective, feasible and economically valuable solutions for port operators. As Acciaro and Wilmsmeier say, “*Numerous technological solutions are available to reduce energy consumption. However, the uptake of these technologies is often hampered by economic, regulatory, managerial or technical barriers and, in general, by a lack of financial incentives or of knowledge.*” [7]

A great incentive for increasing efficiency is the potential reduction of greenhouse gas emissions from container cranes, which account for a large share of the land-side emissions in a container port. To give the reader an indication of the magnitude of the emissions, the Port of Felixstowe (the largest port in the UK) produces every year over 35,000 tonnes of CO₂e² exclusively from the activity of RTG cranes [8]. A small but meaningful increase in efficiency could have massive effects on the global energy consumption and CO₂ emissions from container ports such as Felixstowe.

The work that led to this thesis was focused on innovative solutions aimed at improving the efficiency of RTG cranes by using energy storage, in particular by developing effective control strategies that are able to exploit well the opportunities offered by energy storage. A reduction in their environmental impact could be achieved by implementing such control strategies as part of an energy storage system. The purpose of this thesis is then to demonstrate that energy storage in container cranes is a feasible solution, and that bespoke power management strategies can provide an effective and efficient benefit in terms of energy savings and reduction of the impact of cranes on the environment and container terminal operations.

As will be shown in the following chapter, the adoption of energy storage in container cranes is only at its early stages. There are areas not completely covered by current literature yet, for example there is a lack of a validated model of an RTG crane on which to test the benefits of storage. Power management strategies are still fairly basic and there is a wide array of techniques that need to be developed and tested for this particular application. This thesis has then the objective to develop and test control strategies for energy storage on a validated model based on actual measurements. An energy storage device will be devised for

²Carbon Dioxide equivalent

this particular application, showing the theoretical and practical feasibility of energy storage on RTG cranes.

1.2 Problem statement

Container terminals can reduce their energy consumption and greenhouse gases emissions by increasing the efficiency of RTG cranes. It would also be advantageous to reduce peak power demand from each RTG crane due to the ensuing benefits to the power infrastructure and generator sizing. Energy storage can be an effective tool to achieve these beneficial improvements when utilised properly.

The costs of implementing and maintaining energy storage units could disrupt adoption if proper care is not used in studying the application, sizing and, most importantly, the power management strategy. The following steps had to be followed during the research that led to this thesis:

- A study of the RTG crane as an electro-mechanical system composed of multiple elements working together to perform a task;
- A thorough analysis of the activity of the typical RTG crane, necessary for the quantification of power and energy flows that characterise the system;
- Modelling the RTG crane using powerful software that allows to test solutions to increase efficiency;
- An analysis and comparison of energy storage technologies in order to choose the one that best suits the requirements;
- Develop fast and reliable low-level control systems for the storage devices;
- Develop supervisory control strategies that can increase the efficiency of the crane, making the most of on the limited storage resources;
- An analysis and comparison of the supervisory control systems using, as a reference, real data and the RTG model.

1.3 Objectives of the research

The key features discussed in the motivation and the gaps in the literature identified in Chapter 2 lead to the following list of objectives:

1. Perform a study of the RTG crane and its activity in order to find opportunities for increasing its efficiency by introducing additional components, including energy storage;
2. Develop a validated and accurate model of an RTG crane;
3. Create a model of a storage system that is suitable for use in RTG cranes and that can be interfaced with the RTG model;
4. Develop a low-level control system for the storage device that is incorporated into the RTG crane model;
5. Propose improvements on existing supervisory control strategies;
6. Propose novel supervisory control strategies for energy storage in RTG cranes;
7. Perform a thorough analysis and comparison of the supervisory control strategies.

1.4 Publications emerging from this work

Part of the outcomes of the research presented in this thesis have been featured in the following publications:

Conference papers

- S. Pietrosanti, W. Holderbaum, and V. M. Becerra, “Modelling power flow in a hoist motor of a Rubber Tyred Gantry crane,” in *2015 IEEE Industry Applications Society Annual Meeting*, 2015.
- S. Pietrosanti, I. Harrison, A. Luque, W. Holderbaum, and V. M. Becerra, “Net energy savings in Rubber Tyred Gantry cranes equipped with an active front end,” in *2016 IEEE 16th International Conference on Environment and Electrical Engineering (EEEIC)*, 2016.

- A. Luque, I. Harrison, S. Pietrosanti, F. M. M. Alasali, W. Holderbaum, R. M. Mayer, and V. M. Becerra, “Energy reduction on eRTG,” in *2016 IEEE 16th International Conference on Environment and Electrical Engineering (EEEIC)*, 2016.

Journal papers

- S. Pietrosanti, W. Holderbaum, and V. Becerra, “Optimal Power Management Strategy for Energy Storage with Stochastic Loads,” *Energies*, vol. 9, no. 3, p. 175, Mar. 2016 (featured in the cover of the issue).
- S. Pietrosanti, W. Holderbaum, and V. M. Becerra, “Modeling Power Flow in a Hoist Motor of a Rubber-Tired Gantry Crane,” *IEEE Transactions on Industry Applications*, vol. 52, no. 3, pp. 2088–2094, May 2016.
- V. Papaioannou, S. Pietrosanti, W. Holderbaum, V. M. Becerra and R. Mayer, “Analysis of energy usage for RTG cranes,” *Energy*, vol. 125, pp. 337-344, 2017.
- I. Harrison, S. Pietrosanti, A. Luque, R. Mayer and W. Holderbaum, “Recording and Analysing Measurements from an RTG Crane,” *Measurement*, vol. 125, p 284-293, Sep. 2018.

1.5 Outline of the thesis

This chapter presented the background to the research and introduced the motivations behind this work. The rest of the thesis is structured in chapters as follows: Chapter 2 presents in detail the issues that this research aims to tackle, including a thorough description of the RTG crane and its typical activity in a container terminal. The power and energy flows during a typical lift are explained in detail, providing a clear prospect of the electrical components and flows involved. A statistical analysis is also included in order to provide the foundation on which to build the RTG model and the supervisory control strategies. Chapter 3 introduces the low-level control system developed for a flywheel energy storage system, which will then be included in the storage models described in Chapter 4. As well as the flywheel storage models, Chapter 4 presents the RTG crane model which will be used to develop, test and assess the quality of the supervisory control strategies. Chapter 5 is exclusively focused on supervisory control strategies produced in this research, explaining in detail the development processes and the motivations behind each. The supervisory control strategies

are then assessed and compared in Chapter 6, discussing their benefits and shortcomings. Finally, Chapter 7 contains the concluding remarks and highlights the importance of this research, with recommendations for future work.

Chapter 2

Literature review

This chapter aims to provide a critical review of the key works reported in the literature that are relevant to the research topics examined in this thesis. The literature review is divided into three main areas:

- Energy storage systems, discussing the technology and applications;
- Control of energy storage, including low-level and supervisory control systems;
- Modelling, in particular regarding simulating the power flows of RTG cranes.

2.1 Energy storage systems

The issue of desynchronising the production and consumption of energy has been historically tackled using a wide range of technologies: accumulating burning wood during the summer allows for heat production in the colder months of the year; mechanical clocks are powered by a spring that only needs to be reloaded periodically; flywheels in internal combustion engines reduce speed fluctuations. Vast amounts of energy are saved daily by hydroelectric dams built to provide easily accessible energy: water can be released when power is in high demand. Pumped hydro storage has been used since the start of the 20th century for providing peak power demand [9, 10] and in 2012 it accounted for 99% of the storage capacity in the world [11]. The geographical restrictions make it unsuitable for small scale storage in power systems, whereas other technologies developed in the second half of the century are more suited to this. These include batteries [12, 13], flywheels [14, 15] and

super-capacitors [16, 17]. These three technologies are the most commonly used in power systems where electrical energy needs to be stored locally for a period of time which can range from milliseconds to months or even years [10, 18].

Large scale storage, as in the case of the aforementioned pumped hydro, is used to compensate for seasonal or daily fluctuations in power production and demand. The capacitor that smooths voltage fluctuations in a full-bridge rectifier is an example of very fast storage, being charged and discharged tens of times per second. The operation of cranes in container terminals is, however, characterised by dynamics that have a time horizon of seconds and minutes, because they are synchronised with container lifts. This research is focused on systems that are composed of a primary energy source (e.g. a diesel generator or the electrical grid) and a dynamic load that is characterised by considerable variability.

In container terminals, energy storage can be used in conjunction with RTG cranes in order to reduce energy consumption by recovering potential energy when lowering containers [19–22]. Most RTG cranes dissipate this energy into heat using dump resistors, whilst storage could absorb recovered energy that would be reused in a subsequent lift.

2.1.1 Renewable energy production

The power output of renewable energy sources can be highly variable and it may be necessary to use energy storage to help achieve the grid code requirements [18]. Some forms of renewable energy production, like the aforementioned hydroelectric plants, possess inherent storage capabilities [10]. On the other hand, wind turbines and solar plants are affected by external factors that cause very high variability in the power output. Energy storage solutions for these applications focus on mitigating the unpredictable power fluctuations [18]. Supervisory control systems for renewable energy production focus on maintaining a constant power output either by compensating sudden changes in output [23] or longer (~ 1 hour) power fluctuations [24]. The application of storage in renewable generation, nonetheless, differs from the use on RTG cranes due to the dissimilar objective and power flows: an RTG crane is characterised by intermittent high power demand that burden a primary source, whilst renewable generation is continuous but afflicted by high variation. Storage on an RTG crane operates only when a crane is lifting or lowering a container, whilst storage in a wind farm is continuously compensating the power output. However, the techniques used in renewable energy production can be adapted to supervisory control in cranes. Fuzzy logic

control in [23] and optimal control in [25] have been used with flywheel storage, showing the potential of these technologies when associated with advanced supervisory control systems.

2.1.2 Power networks

As discussed above, energy storage is beneficial in reducing the variability in the supply side, but another use of storage is to tackle variability in the demand side. For instance, power networks in residential areas can be reinforced by using storage, reducing the need of increasing the capacity of the network when demand reaches a peak. Seasonal and daily peaks can be dealt with by using energy stored during low-demand periods [26, 27]. Power demand from multiple buildings is aggregated and this tends to eliminate fluctuations seen in a single household, then a supervisory control can be designed to predict deviation from the baseline and act accordingly [28]. Research on energy storage in power networks may not be immediately applied to an RTG crane, but it offers an insight of the technologies and strategies that can be applied when multiple RTGs are connected to a single grid.

2.1.3 Hybrid electric vehicles

Batteries, flywheels and Super-Capacitors (SC) have reached a maturity that allows them to be used locally in a vehicle or a mobile gantry crane. A well-known example is the use with Hybrid Electric Vehicles (HEV) which are usually equipped with batteries and/or other form of storage [29]. Hybrid vehicles are powered by a fossil-fuel primary power source and a storage system that can provide peak power and recover energy using regenerative braking. Energy storage is clearly a key element of HEVs, as the vehicle has to store efficiently the recovered energy, minimising the use of the primary source [30]. HEVs have similar dynamics to the RTG crane, as the demand has high variability and energy can be recovered and reused. The size and weight constraints for the storage are more stringent in HEV with respect to larger and heavier RTG cranes, therefore the actual storage devices will differ [10]. Nonetheless, the control strategies have common objectives and similar challenges; it is not surprising, then, that the research relative to control of energy storage in HEVs can be used as an inspiration for RTGs, as will be shown in the following sections.

2.1.4 RTG cranes

An early study on energy storage in cranes was presented by Liang and Virvalo in 2001, storing energy in an hydraulic system [31]. In this work, the authors proposed an hydraulic energy storage system for hydraulic cranes: accumulators store potential energy recovered from lowering loads. This mechanical device is completely passive, and it is not possible to control the energy delivered by the stores. For a system to be versatile for any magnitude of loads and operation, it requires controlling of the power being delivered by the storage. This can be easily achieved with cranes powered by electric motors using electric energy storage systems.

The technology behind flywheel electric energy storage allowed for its use in RTG cranes. Toliyat *et al.* firstly introduced them in [32], where it is demonstrated how it is possible to store the energy and control the power using back-to-back converters and a permanent magnet synchronous machine. An application for this technology has been found by Flynn *et al.* in [19], where an RTG equipped with flywheel storage is described. In this paper the authors produce experimental results of flywheel storage being charged by a crane lowering a load, and then using the stored energy for subsequent lifts. The technology used has been commercialised by Vycon specifically for use in RTG cranes [33]. The control system used is discussed in more detail in Section 2.2.

Supercapacitors, and later batteries, have been extensively used in RTG cranes. The first paper on supercapacitors in RTG cranes was presented by Kim *et al.* in 2006 [34], whilst batteries were first used by Baalbergen *et al.* only in 2009 as the energy densities and lifetime of Li-ion batteries had sufficiently improved by then [20]. At the time of writing, the most complete work on energy storage in cranes have been produced by Hellendoorn, Mulder *et al.* in [22] and [35], followed by Antonelli *et al.* [36]. The achievements presented in these papers will be discussed in more detail in the next section.

Storage in RTG cranes is now a reality, driven by environmental and economic interests. Crane manufacturers are thus offering hybrid solutions for those customers who want to reduce energy consumption and greenhouse gases emission, increasing efficiency [37]. Positive preliminary results and industrial involvement caused an increase in interest of the academic environment towards storage in cranes. Next section will present the key articles about energy storage in RTG cranes, focusing on their contribution on low-level control and supervisory control.

2.2 Control of energy storage

The research presented in this thesis focuses on the control of energy storage, in particular controlling the power flowing to and from it in order to maximise the multiple benefits that can be potentially obtained. This is achieved in two steps: controlling the storage system at a low-level ensuring that a reference power output is followed, and then developing a supervisory control system that sets the reference power output to a level that is deemed beneficial for the whole system.

2.2.1 Low-level control of energy storage

This research is based on the assumption that an energy storage device needs to deliver a precise electric power output (or input) following an external reference signal. In order to do so, a low-level controller needs to handle the dynamics of the storage, whichever is the method of storing energy. Batteries and SCs are charged and discharged by varying the voltage and current applied to them, usually using DC/DC converters [10, 38–40]. Controlling the power flow is then achieved by acting on the converter according to the desired power output and the state of the DC link.

Flywheels are controlled by acting on the motor that powers them. By changing the rotational speed it is possible to generate a power flow in the electrical machine. A storage control system can implement one of the state-of-the-art controllers used in conjunction with electrical machines, achieving high efficiency [14, 41–43].

A low-level controller also needs to maintain the storage in its operating limits, including minimum and maximum charge level. This is particularly important for batteries, as deep discharges and high temperatures can degrade them, therefore they often require an advanced battery management system [10]. Super-capacitors are also susceptible to damage but to a lower degree than batteries. Flywheel storage requires a monitoring system as well, but they are even easier to manage as they are more robust and have less energy and power constraints. In general, low-level controllers implement some sort of monitoring that can limit the power output regardless of the reference input, safeguarding the condition of the storage [18].

2.2.2 Supervisory control

Choosing the right reference value for the energy storage power output is not a trivial problem, as it highly depends on the status of the system. Some authors preferred limiting the complexity of the control system by passively supplying stored energy when requested by the load and focus on the sizing of the storage and the primary generator [36]. However, an advanced supervisor may provide greater flexibility and ensure a better utilisation of the energy and power resources. It achieves that by monitoring the parameters of the system and the storage itself, assessing the situation and adjusting the instantaneous reference power output in order to reach a global objective, for example increase the efficiency of the crane over a longer period of time than a single lift cycle. In fact, the reference value supplied by the supervisor may not maximise instantaneous energy savings, and instead preserve stored energy for when it may be indispensable, resulting in substantial increases in efficiency.

There is a wide variety of techniques that can be used for a supervisory control system, and this section analyses those present in the literature that have produced promising results.

Rule-based and PI controllers

The simplest solution is to determine a constant reference depending on the operating mode of the system: a rule-based controller. This type of controller outputs a reference value by processing the input with logic expressions; they are based on intuition and human expertise without the need of a priori knowledge of the operating cycle [30]. Ignoring, for the moment, the technical differences between the operation of a hybrid RTG crane and an HEV, it is possible to look at the research related to supervisory controllers in hybrid electric vehicles for inspiration. A type of rule-based control is introduced by Phillips *et al.* in [44] where a finite-state machine reads the status of an HEV (generating, regenerating, clutch engaged, etc.) to determine the demand to each subsystem (including the battery storage). Other examples of finite-state machines are presented by Salmasi *et al.* in [30].

Rule-based controllers have also been implemented in hybrid RTG cranes. Baalbergen *et al.* in [20] compares various supervisory strategies aimed at reducing the lifetime costs of equipment and fuel in hybrid RTG cranes. The most promising strategy emerging from the article consists in switching on the generator for a limited period of time for charging an SC bank, which in turns powers the crane for the rest of the time. The crane then fluctuates between two states: one where the storage passively powers the whole crane, and another where the generator produces constant power (at the maximum rated level). This simple

but effective control strategy has also been applied by Iannuzzi *et al.* [45], and also by Niu *et al.* in [46] where a large battery powers the crane and it is recharged by the generator when reaching a low state of charge. Note that the strategies proposed in [20, 45, 46] do not consider managing the power output of the storage, which exclusively depends on the intensity of the load. It would be highly beneficial to dissociate the output of the storage from the intensity of the load, and instead focus on global objectives. Focusing on the instantaneous load may reduce the overall efficiency of the system, because the remaining stored energy may be better used in the future. These papers focus solely on the instantaneous benefits given by the storage, disregarding favourable opportunities offered by supervisory control.

Rule-based control systems, as those described above, possess inherent key limitations. The choice of the discrete states and the associated control outputs determine the quality of the controller: it needs to be finely tuned for the single application. This is expressed in more detail by Pisu *et al.* in [47] where a finite-state machine control for HEV is analysed; the conclusion is that this type of controller can only provide satisfying results after extensive calibration, greatly reducing portability and versatility. As will be shown in Chapter 3, RTG cranes are subjected to a wide range of power and energy demands, therefore the rule-based control systems are often associated with PI controllers that allow for variability in the state of the system, especially the load.

Voltage control in a hybrid crane is the method chosen by Kim *et al.* [34] and Li *et al.* [48], where PI controllers track a voltage error and produce a reference output that is fed into the storage, absorbing energy when the voltage raises in the regeneration phase and feeding energy back to the system when voltage is low. Zhao *et al.* [49] introduce a double PI loop to control the power flowing through two storage devices: a SC bank (fast inner loop) and a battery (slow outer loop); the system controls the voltage in the DC link of a crane limiting voltage fluctuations during all the phases; the battery is used as the primary energy source. Flynn *et al.* [19] also introduce a storage system that compensates for voltage hikes in the regeneration phase of a hybrid crane, although the control is left to the proprietary storage device. In the aforementioned paper, however, a net separation is introduced between the control systems responsible for the charge and discharge of the storage: it is charged using voltage control and discharged by outputting a power which is proportional to the load power. Xu *et al.* [50] also differentiate the two phases using different control strategies, however the voltage control is used in the discharging phase; it is not clear though how the charging phase is managed, as the paper limits its scope to the technical implementation of flywheel storage

in a crane. Ndokaj *et al.* [40] follow a similar approach to [19] when discharging: the storage provides a current which is proportional to the load current of a hybrid crane. Voltage control for charging the storage in a hybrid crane then appears to be a relatively simple but effective solution when the storage is uniquely charged using regenerated energy [19, 34]. However, the discharge phase requires more attention: power delivered by the storage can be controlled in order to achieve global objectives and increase overall efficiency. At the time of writing there is no example of hybrid cranes charged using voltage control that also implement a more sophisticated and effective power sharing control when discharging. An investigation by Antonelli *et al.* in [36] shows that a power-sharing technique can reduce massively the energy consumption when it is associated with a reduction in the diesel generator size. As shown in [20], a constant power output of the primary source would be preferable to a value proportional to the load (as is currently done in [19, 40, 45, 46]).

Fuzzy logic control

A deterministic rule-based supervisory control is bound to output a constant reference associated to discrete states of the system. It can be possible to increase the robustness and adaptivity of a rule-based control system by introducing fuzzy logic [30]. Fuzzy Logic Controllers (FLCs) are based on fuzzy input sets and linguistic rules, selecting an output that does not need to be limited to a small number of discrete values [51, 52]. Although the use of FLCs is widespread in power systems [53, 30], there is currently very little research related to fuzzy logic controllers in hybrid RTG cranes, even though Xu in [50] recommends fuzzy control for extending his work. Fuzzy logic controllers in HEVs have been the subject of extensive research, and many articles can be found presenting advanced techniques. For example, Schouten *et al.* [54] show the use of a hybrid vehicle with batteries where the FLC receives as input the state of charge of the storage and the motor speed. Ferreira *et al.* in [55] add fuel cells and SCs as well, increasing the complexity; the FLC is relatively simple, though, showing a quality of fuzzy logic: high effectiveness with low complexity. Salmasi in [30] presents other examples of noteworthy uses of FLCs in HEVs, and compares them to other existing control systems.

As already mentioned, there appears to be a lack of rigorous and extensive research related to the application of FLCs to RTG cranes, compared to what is available for HEVs. The only published paper with this topic is [56], where the possibility of using an FLC is hinted but no controller is presented. However, the EnD thesis written by Knight [57] presents in detail an FLC for flywheel storage. The control strategy is focused on reacting

to changes in the voltage, with high symmetry between the consumption and regeneration phases; the behaviour of the controller is then similar to a voltage controller, with added tweaks that modify the output depending on the load and the state of charge of the storage. Whilst its performance is not at the same level of other control system in the literature, it is a good starting point for the development of an advanced FLC for hybrid RTGs. Contrary to what is available for HEVs, there is no advanced FLC developed for hybrid RTGs that exploits as much as possible the ability of fuzzy logic to handle complex systems, for example separating the generating and demand phases of the RTG.

Optimal control

A supervisory control system can add flexibility to a hybrid system, enabling the introduction of a Power Management Strategy (PMS). A PMS focuses on obtaining benefits that have a larger horizon than the single instant on which most of the control strategies discussed previously are based. For example, a PMS may decide to keep energy stored even if the crane is demanding power, if needed in the future. It is possible to find a PMS that maximises the benefits over a certain time interval by using optimal control [58]. In [30] and [47] this type of control is assessed for its qualities in HEVs, with many examples presented. In HEVs, like in RTGs, the objective is often to reduce energy consumption, therefore optimal control strategies have been developed that minimise a cost function which includes energy costs. The ideal horizon spans the entire lifetime of the storage, but predicting the future demand is often very challenging: it would be necessary to know the future movements, the weights involved and also the power flows associated with them. For these reasons, a global solution is difficult to obtain [30], therefore the horizon is either restricted to a single known cycle (as in the case of standard vehicle driving cycles [59]) or other techniques are used, including equivalent fuel consumption [60] or stochastic approaches [61]. Rowe *et al.* in [26, 27] present an optimisation algorithm for storage in power networks, where the demand is characterised by seasonal or daily variation around a baseline. This type of variability is different from the one observed in cranes, where the load is characterised by short high-power pulses corresponding to a lifting event. However, inspiration for optimal control strategies for RTG cranes can come from a related field: hybrid micro-grids. They can be characterised by sudden high-power demand on the storage (typically due to variability in the primary power supply). Optimal control of storage in micro grids has been tackled in [62–65], but the work done by Levron and Shmilovitz in [66] is particularly interesting, where the optimal control problem includes the limited energy capacity of the storage, which

is a very important issue in the RTG application as the high power demand and the limited available space reduce the maximum energy capacity. The authors aim to reduce primary energy consumption with the assumption of perfect knowledge of the power demand over time; as will be explained in the following chapter, this is unfortunately not possible with RTGs because power demand cannot be easily predicted. In a later paper by the same authors, the focus moves to peak shaving, but the assumption of complete knowledge of the load still stands [67]. These articles are two good examples of a potential optimal control strategy for RTG cranes, and the issue with the knowledge of the load could be tackled by exploiting stochastic properties of the RTG crane activity. Such properties could become evident after an analysis of the activity of RTG cranes.

A paper by Hellendoorn *et al.* [22], along with the linked thesis by Mulder [35], presents the only published application of optimal control for hybrid RTG cranes. Their work is based on the minimisation of fuel consumption of a hybrid RTG crane equipped with supercapacitors. The specific consumption of the diesel generator powering the crane is measured in order to find the optimal working conditions of the generator. The SC storage is modelled as well and a minimisation strategy that aims to find the SC output power that minimises fuel consumption in a lift cycle is developed. The load power is estimated using a prediction algorithm, and the eventual future fuel cost is included in the cost function, reducing the issue caused by not having perfect knowledge of future power consumption. The strategy applied by the authors is called “equivalent consumption minimisation strategy” and it is widely used with HEVs [30, 47]; a requirement of this strategy is the knowledge of the instantaneous fuel consumption of the diesel generator. If this information is not available or if a crane is electric powered, this strategy cannot be applied. The authors chose to minimise fuel consumption exclusively, whilst it could be beneficial to also reduce peak power consumption, as will be shown later in this thesis.

2.3 Modelling of RTG cranes and flywheel storage systems

The study of supervisory control systems is often associated with an analysis of their benefits, either experimentally or by using computer models. The implementation of storage in RTG cranes has been studied experimentally in [20] with a small-scale laboratory test, whilst it has been tested in [19, 22, 46, 34] with a full-size crane. Nonetheless, other authors developed computer models of a crane in order to test the hybrid systems. Toliyat *et al.* [32] and Xu *et al.* [50] used the *Powersim* simulation software *PSIM* to model the power electronics

components that interface an RTG crane with a permanent magnet motor powering a flywheel. In these two papers, the crane itself is not modelled, as they focus on the storage system implementation. Antonelli *et al.* in [36] use the non-proprietary modelling tool *Modelica* to model an RTG crane equipped with a generic storage device and a power-sharing control system.

Modelling a flywheel energy storage system consists in modelling the electric motor powering a rotational mass. The non-trivial part, then, consists in reproducing the dynamics of the electric machine chosen. For reasons that will be explained in Chapter 4, it was decided to use a switched reluctance machine. Le-Huy and Brunelle [68, 69] developed an accurate model of a switched reluctance motor using *MATLAB/Simulink*, and this model is a solid foundation for a flywheel energy storage model presented later in this thesis.

The use of *MATLAB* and *Simulink* for modelling power systems is widespread, often using the *Simscape Power Systems* toolbox [70], formerly called “*SimPowerSystems*”, which enables the simulation of the complex dynamics characterising large electrical systems [71]. In the specific topic of hybrid RTG cranes, *MATLAB/Simulink* has been used in the literature to simulate the effect of adding storage to a crane. Iannuzzi *et al.* [45] developed a *SimPowerSystems* model to test the addition of a super-capacitor bank to a crane, analysing the energy savings opportunities. The crane itself is represented by a three-phase induction motor which is the main hoist motor of the crane. Similar topologies are studied by Di Napoli *et al.* [72] and Ndokaj *et al.* [40], again using the *SimPowerSystems* toolbox. The energy and power flows in a hybrid crane formed by multiple motors and super capacitor storage are studied by Li *et al.* in [48], again using *MATLAB/Simulink* software. Zhao *et al.* in [49] presents a more detailed simulation of battery and super capacitor storage in hybrid RTG cranes. In this paper, the crane is modelled in *SimPowerSystems* as a single motor that represents the total power load of the crane, and the authors show the benefits of adding both batteries and super capacitors by simulating a typical lift cycle. All the models presented above are lacking a validation process, for example comparing data produced by simulations with data measured on an actual crane.

The only author presenting a model of an hybrid RTG with flywheel energy storage is Knight in [56, 57, 73]. The model is developed in *SimPowerSystems* and it reproduces the power and energy flows of the hoist motor in an RTG crane, as well as the dynamics of a flywheel energy storage. This is the only known RTG model that has been subjected to a validation process, but it still shows limited accuracy. This model has been the inspiration for the model presented in this thesis, but it needed a complete redevelopment as high quality

data collected in 2016 allowed for a higher accuracy and better reproduction of the electrical signals. One of the objectives of the research presented in this thesis is to produce a high quality validated model of the crane that matches measured data.

2.4 Summary

This chapter provided an analysis of the literature published on the topics of energy storage systems, RTG cranes, control of energy storage and control strategies for energy storage in RTG cranes. The literature shows a robust presence of papers regarding energy storage in power applications, like for example the use in electric vehicles. However, there is still only a limited number of papers focused on RTG cranes, and only few of them discuss control strategies for energy storage. In particular, this literature research revealed the following gaps in the currently published research:

- Only limited data has been published on the power and energy consumption of an RTG crane during normal operation. Crane manufacturer and terminal operators provided aggregated information available on the overall energy and power consumption. Some data points can be extracted from previous works, however most authors concentrated on single lift cycles that last less than two minutes. A more thorough data collection and analysis must be performed in order to identify and quantify the energy and power flows in a crane over a longer period of time and under different conditions. This gap in the literature is linked to the first objective of the research listed in Section 1.3.
- RTG crane models have been used in some of the works, however none of the articles available in the literature performed simulations on validated models of RTG cranes, excluding the model presented in [56] which shows insufficient modelling accuracy. This gap is linked to research objective number 2.
- In the area of supervisory control systems for RTG cranes, all articles focus uniquely on energy savings or reduction of peak power demand. It will be shown in this thesis how both objectives should and can be tackled at the same time within the same control strategies. This gap is linked to research objective number 5.
- Very little variety of supervisory control strategy techniques for RTGs is present in the literature. This is mostly due to the early stages of this research, and there is the need of introducing other well-known techniques to this particular application. For example,

there is very limited research on optimal supervisory control in RTG cranes, as well as fuzzy logic control. This gap is linked to research objective number 6.

- No supervisory control comparison for RTG cranes has been published yet (excluding comparisons with systems *without* supervisory control). Therefore, there is a clear necessity for a comparative analysis of supervisory control strategies. This gap is linked to research objective number 7.

Chapter 3

The Rubber Tyred Gantry cranes and opportunities for increasing energy efficiency

Global trade is facilitated by the presence of a standard transport medium: an aluminium box called intermodal container. First used in 1956 and standardised in the 1960s, containers have now become a key element in the movement of goods. They facilitate the transport of any class of item by standardising the dimensions and weight of shipping items [5]. Container terminals have been built around the standard container, transshipping them between different transport vehicles using machines that have been designed exclusively to move containers. One of these machines is the Rubber Tyred Gantry (RTG) crane, which is used to stack and unstack containers while waiting to be moved to and from cargo ships, trains and trucks. The RTG crane, shown in Figure 3.1, can stack up to 6 containers on top of each other, straddling rows of 8 containers or more, with stacks that can reach lengths of hundreds of meters. Container terminals make extensive use of RTG cranes as they allow for high container density, faster operations, higher throughput and reduced land requirements.

This chapter defines the RTG crane under analysis and its operations in order to identify potential strategies for increasing the efficiency of RTG cranes. In order to do so, a series of objectives have been delineated in order to clearly define the background and the final goal of this research.

The first objective is to analyse the main electrical components that generate the main power and energy flows in the RTG crane during normal operation. There are very specific

power flows in the crane that have a central role in potential efficiency improvements. This chapter will analyse the electrical topology and will describe the function of the main electrical components during a generic lift cycle.

A second set of objectives for this chapter is related to the daily activity of the crane in a container terminal. The knowledge of the energy consumption of a crane during a single lift cycle is not useful on its own. To get a better understanding of the potential benefits of energy storage, it is necessary to analyse the statistical information of lift cycles. Are they all characterised by the same energy consumption? Do they all have the same duration? Are they very frequent or are there long periods of idle time? All these questions need to be answered if we want to choose an appropriate method for increasing the efficiency of the crane over a period longer than a single lift cycle.

The third objective of this chapter is to define the potential opportunities given by energy storage in order to then define the objectives that an RTG crane should achieve when equipped with energy storage. They must come from practical necessities and will be justified by the analysis of the crane topology and operations. Assumptions defined earlier will also be clarified and put into context, explaining their impact.

The fourth and final objective for this chapter is to use the information gathered previously and study storage devices in order to identify the one most suited for the objectives. The choice will depend not only on the energy and power flows of the crane, but also on its daily activity (e.g. frequency and duration of lifts) and on the measurable objectives defined earlier. The two chosen objectives will be described and justified in detail.

3.1 Description of the crane

RTGs are relatively large cranes used for container handling in container yards, can reach 25 m of height and can lift standard intermodal containers weighting up to 40 t. They are designed to straddle lanes of containers in order to create compact stacks by minimising the area needed for manoeuvre and steering. Figure 3.2 shows a satellite image of 5 RTG cranes in use at the Port of Felixstowe and it is possible to see how they straddle lanes of containers. The peculiar structure of this type of crane allows it to raise and lower containers vertically and move them horizontally without any need for a counterbalance.

In order to safely lock to a container, RTG cranes use a “spreader” (Figure 3.3), so called as it can change its length in order to accommodate container of different sizes. The spreader

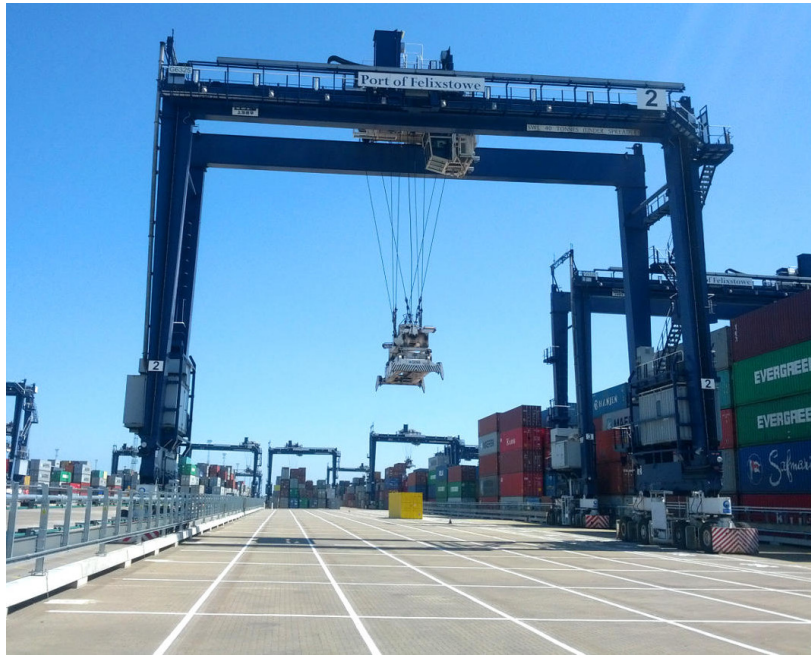


Fig. 3.1 RTG crane in use at the Port of Felixstowe [74].

attaches to a container using twist locks and it hangs from the “headblock” of the crane using 4 to 12 ropes that are used for both lifting and stabilisation. The spreader itself can weigh up to 13 tonnes, meaning that an unloaded crane consumes a large quantity of energy just by hoisting it. A container can weigh up to 40 tonnes, and usually the maximum load of an RTG crane is around 52 tonnes. In Sections 3.3 to 3.5 is explained in more detail how the typical lift cycle is performed and what is the power and energy consumed by the crane.

3.2 Main electrical components

An RTG crane is a complex system of interconnected mechanical and electrical components, although normal operation involves mainly: power supply, electric motors and auxiliary systems. Figure 3.4 shows a simple schematic of the main components of a crane, which are discussed in detail below.

3.2.1 Power supply

The main power source of an RTG crane can be either a diesel generator in diesel-powered RTGs (D-RTG) or the electrical power network of the terminal (E-RTG). The first case is



Fig. 3.2 Satellite view of container stacks and RTG cranes at the Port of Felixstowe. Imagery ©2016 Google, Map data ©2016 Google.

more common in older and smaller terminals due to the legacy equipment and the flexibility of local generation. In larger and busier terminals it is now very common to find cranes powered by the local network, as the energy and maintenance costs are lower but the infrastructure costs are higher and are often only justified for large installations. In general, E-RTG are now being favoured as they are associated with an overall reduction in costs and a dramatic decrease in CO₂ emissions [75–77] and many ports are now converting old D-RTGs into electric motivated by cost reduction and environmental regulations [78].

In both cases, the source is assumed to be a generic, single and infinite three-phase source which powers the motors as well as the auxiliary systems (which include lighting and air conditioning).

3.2.2 Electric motors

Most of the energy consumed by a crane is used to lift loads vertically; this action is performed by one or more hoist motors, mainly squirrel-cage induction machines, rated from 125 kW up to 400 kW [19, 34, 2]. A second group of large electric motors perform lateral movements of the “trolley”, which comprises of the control cabin and the headblock. The

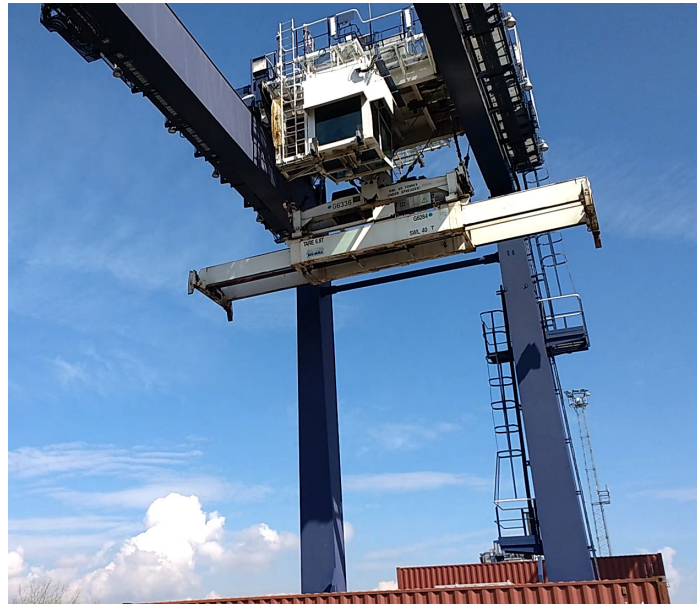


Fig. 3.3 Photo of an RTG crane with a spreader (in white) set for loading 40' containers.

trolley moves laterally along rails and it is moved by a set of induction motors rated from 20 to 40 kW. The third group of large motors is in charge of moving the crane itself in the terminal yard and are called gantry motors. They are rated for approximately 45 kW each and are usually characterised by lower energy consumption compared to the other groups as gantry movements are less frequent and short. Modern cranes are equipped with additional motors that perform anti-skew action but they are at least an order of magnitude less powerful than the hoist motors.

The electric motors in older RTG cranes are connected directly to the AC feed through variable frequency and variable voltage AC/AC power converters, and resistor banks are connected to the DC stage of each converter. A more modern design, shared by most manufacturers, includes a common DC bus to feed all the motors, where a diode rectifier converts AC power from the primary power source to DC which is then converted back to AC by the drives. The regenerated energy is fed into the DC bus, allowing other motors to use part of the recovered energy, while all the surplus energy is then dumped into shared brake resistors. The brake resistors are used to dissipate the regenerated energy when braking (e.g. when lowering a container) and are automatically activated by an increase in bus voltage. The design that includes a DC bus reduces the costs of the electrical components and it is also modular and more versatile as it allows the installation of additional devices, including energy storage systems which can charge and discharge power from and to any motor connected to the DC bus.

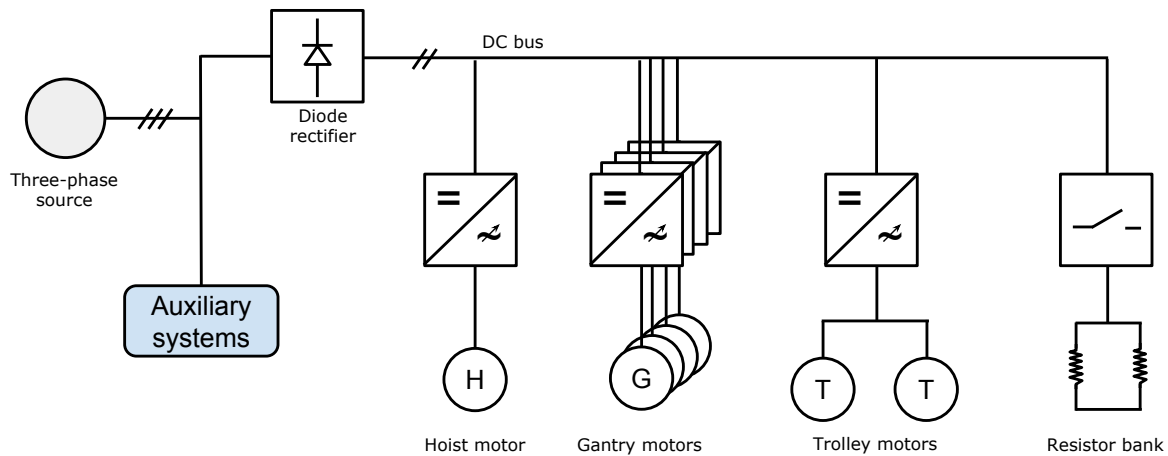


Fig. 3.4 Schematic of the main electrical components of the RTG crane used as a reference for this work.

The proliferation of electric powered RTGs can cause issues with power quality in the terminal power network since this is not usually designed to handle the unexpected additional load. The need for better power quality has led to the introduction of E-RTG cranes equipped with an Active Front-End (AFE), replacing the diode rectifier. An AFE adds two main benefits: an increased power quality and regenerative capabilities. Those benefits are discussed in more detail in Section 3.10.

3.2.3 Auxiliary systems

The crane continuously require energy for auxiliary systems even when idling. Control systems, lighting (especially at night), and air conditioning are examples of auxiliary systems and are characterised by a constant but relatively small power consumption. An energy storage system could help power those systems but the characteristics of the application (around 20 kW of constant power consumption) are not well suited with the energy storage device used when the crane is operating. This is because the typical lift consumes high power for short periods of time (tens of seconds) while auxiliaries demand relatively high energy spread over a long period of time (hours). The different demand dynamics of auxiliary systems are not handled by the same storage device managing pulsed power demand, therefore auxiliaries are not included in this research.

3.3 Typical lift cycle

An RTG crane can perform three basic movements [2], shown in Figure 3.5:

- “Hoist movement”, where the spreader (and a container, when present) is moved vertically along the z axis;
- “Trolley movement”, in which the headblock moves horizontally along the y axis (with the crane standing still);
- “Gantry movement”, where the crane moves along the container stack, usually along the x axis, although it can move horizontally in any direction when not straddling a stack.

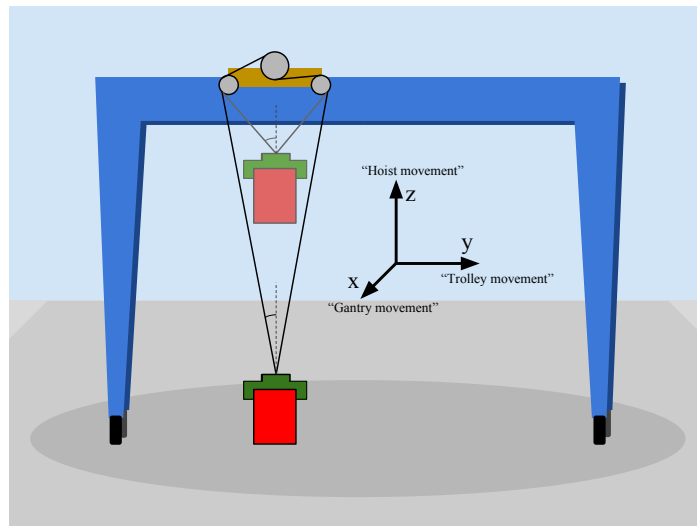


Fig. 3.5 Basic movements in the X-Y-Z space that the crane can perform [2].

The trolley and hoist movements can be performed simultaneously, whilst the gantry movement cannot be performed with an hoist movement for safety reasons. As will be shown in Section 3.5, the hoist movement is the most power and energy intensive, and also it is the only major source of regenerated energy; for these reasons the hoist motor is the main subject of this study, as it creates opportunities for a significant increase in the energy efficiency of an RTG crane.

The typical activity of the crane can be divided into four categories:

1. “Import” and “export”, when a container is transferred from a ship or land transport to a stack and vice versa;



Fig. 3.6 Terminal tractor used to move containers around container terminals.

2. “Housekeeping”, when containers are rearranged in the stack (e.g. when the container needed is hidden below a different container);
3. “Gantry movements”, when the crane itself moves along the stack or around the terminal;
4. “Idle time”, when the crane is powered on but not performing any action.

3.3.1 Import and export

In the first two cases, the container starts or ends on a terminal tractor (Figure 3.6) that carries the container to or from a different area of the terminal. As shown in Figure 3.7a, when a container is loaded onto a stack the whole movement is composed by three phases: from point 1 to point 2 with a vertical movement from the Terminal Tractor (TT) to a safe height, a horizontal movement to point 3 above the destination row, and subsequently a downward vertical movement to the final position (point 4) of the container. The height reached by the container depends on various factors including the presence of other containers in the stack, as it is not necessary to reach the top of the crane for each lift. The driver will usually perform a movement similar to the one shown in Figure 3.7b where the hoist and trolley movements are combined when lifting and lowering. The same sequence, in reverse motion, is performed when a container is unloaded from the stack and placed on the terminal tractor. Figure 3.8 shows an RTG crane moving a container from a stack to a terminal tractor: notice how the container is not at full height.

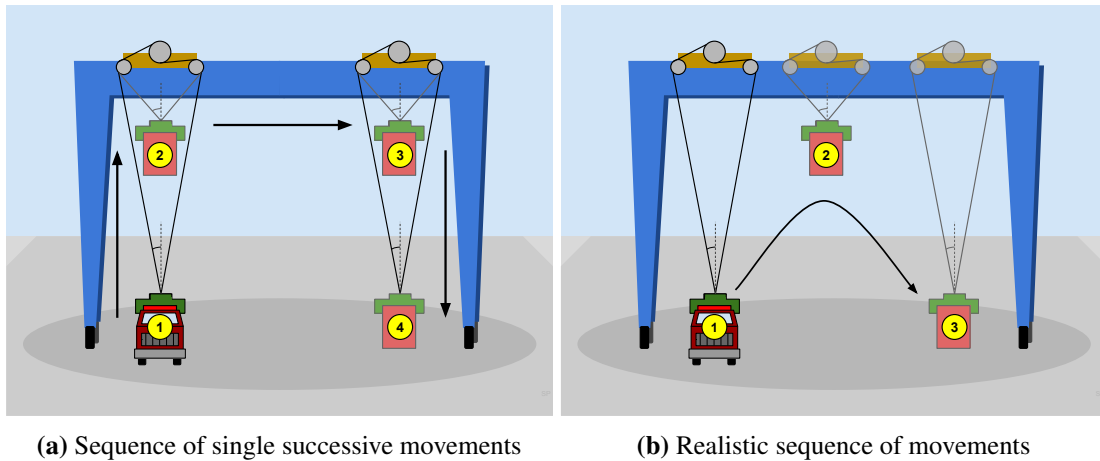


Fig. 3.7 RTG moving a container from a terminal tractor to the stack

3.3.2 Housekeeping

It can occur that the container which needs to be picked by the crane is inaccessible because it is under one or more containers. In that case it is necessary to reposition the stack in order to access that particular container; this is done by lifting and moving containers for short distances, executing a sequence of lifts, lowers and lateral movements. It is possible but unlikely that a gantry movement is performed by the crane for housekeeping purposes, as in general gantry movements are not performed with a container as it is not time-efficient to move containers to a different row. Housekeeping movements can also be performed when requested by the terminal operator for safety reasons: in case of high winds a tall stack is at risk of collapsing. Levelling the stacks by the reducing the height of the tallest stack can help increasing the stability, thus idling cranes may be asked to reposition containers by the logistics centre in the terminal. The lift sequence of a crane performing housekeeping is similar to the one associated with import and export, with the only difference being the energy consumed; this is because the container does not need to be moved by a large distance. In this research, housekeeping movements are treated as standard movements as they are characterised by similar power profiles.

3.3.3 Gantry movements

RTG cranes have wheels that allow them to move horizontally along a stack and also, when required, the wheels are rotated and the crane can travel around the yard. Gantry movements are relatively rare when compared to hoist movements and they are also less energy intensive.



Fig. 3.8 RTG crane moving a container (in red) to a terminal truck (bottom right).

They are relatively short, as well, as the majority of the movements involve moving along the container stacks to a different row. A very small percentage of the movements involve moving the crane to a different stack or to move towards a maintenance yard and they can last for tens of minutes. Gantry movements are analysed in this work in order to show their energy and power impact on the crane; nonetheless, they are infrequent and also they do not offer regenerative opportunities (see Section 3.5). Therefore, they have been ignored during the development of the crane model and the control strategies.

3.3.4 Idle time

An RTG crane can spend a large portion of time waiting for movement orders or terminal tractors to arrive. This proportion of time depends on the level of activity of the terminal, but it usually is in the range of 20% to 60% [2]. The energy consumption of a crane depends on this value as a higher activity is reflected into a higher energy consumption. From an energy storage point of view, an idling crane does not offer any opportunity for improving the efficiency of the crane apart from supplying the idle energy demand. In E-RTGs, an idling crane has little impact on the power network and storage solutions would not be useful. Diesel powered RTG cranes, on the other hand, consume a non negligible quantity of fuel when idle, as the diesel generator is kept active during the idling period. A single energy storage solution may help mitigating this problem by powering auxiliary systems, however

this work cannot be used for this application as the characteristics of the storage are not suitable for both a high power demand and high energy capacity [10, 79]. A reduction in idle fuel consumption is usually achieved by modifying diesel generators to work in dual or multi-speed mode, thus reducing speed and fuel consumption when a crane is idle.

3.4 Crane used at the Port of Felixstowe

The Port of Felixstowe (PoF) is the largest container port in the UK with an annual handling volume of over 4 million Twenty-foot Equivalent Unit (TEU), equivalent to 40% of the UK container volume [8], and the port is inevitably associated with a high energy consumption. One of the major contributors in the energy consumption is the fleet of around 60 RTG cranes that handle containers in the terminal yards. An objective of the research presented in this thesis is to reduce the energy consumption of RTG cranes, potentially leading to major energy savings and reductions in greenhouse gases emissions in PoF and any container terminal that employs RTG cranes.

The work presented in this thesis is mostly based on the operation of a generic RTG, although a specific model of crane is used as a reference for simulations and analysis of the control strategies. The most prevalent model of RTG crane at PoF is a diesel-powered 16 wheels crane rated for a maximum container weight of 40 tonnes, manufactured by Shanghai Zhenhua Heavy Industries Company Limited (ZPMC). A picture of the crane can be seen in Figure 3.1 and the full list of characteristics is presented in Table A.1, in Appendix A, at page 207. This particular model of RTG crane has been chosen since it possesses a very common electrical configuration that is shared with most of the modern RTG cranes. In particular, it is equipped with induction motors connected to a common DC bus which is powered by a three-phase source.

The main electrical components of this model of RTG crane were modelled in MATLAB/Simulink using the Simscape Power Systems toolbox and the model was validated using data recorded by the University of Reading using bespoke metering equipment [80]. The following Sections will explain in more detail the typical lift cycle of a crane and its associated power and energy consumption.

3.5 Energy and power flows of RTG cranes

An RTG crane in use at the Port of Felixstowe was instrumented with logging equipment that is able to record the activity and power flows during normal operation. The objective of the data collection is to study the operation of a crane for characterising the energy dynamics, in order to develop an accurate model. This section presents a summary of the results obtained from analysing the data, focusing on the energy and power dynamics of the crane.

Whilst some of the energy is consumed by auxiliary systems (lighting, air-conditioning, etc.), most of it is used by electric motors, whose consumption varies depending on the activity. Figure 3.9 shows the crane power flow during an illustrative lift cycle. The data was generated during a controlled test where a container weighing 19 tonnes was lifted and lowered back into the initial position. An additional gantry movement is added at the end with the objective of visualising the power flows during that particular phase; therefore, the time axis does not represent the actual time elapsed between the last two phases. The complete lift cycles is composed of the following 7 phases:

- A: The spreader starts from a resting position at the top of the RTG crane and it is lowered over a container which is resting on top of a terminal tractor. During this phase the hoist motor regenerates an average of 75 kW, with the exception of a sag caused by the sudden deceleration of the load. Duration: 29.4 seconds.
- B: The hoist motor lifts a 19 tonne container for the full height of the crane, creating a significant power demand. An initial peak is caused by the power required to accelerate the load up to steady state speed. The power consumption appears to increase over time, however this is due to the peculiar geometry of the crane (see Section 5.1.2). Duration: 35.4 seconds.
- C: The container is moved horizontally by the trolley motors towards the horizontal final position. The power consumption is lower than in the previous phase, highlighting the difference in power demand between hoist and trolley motors. A trolley movement regenerates negligible energy. Duration: 33.5 seconds.
- D: When above the final position, the container is lowered in place and the hoist motor regenerates into the DC bus. Note that the power magnitude, although high, is lower than in phase B due to the presence of power losses in both the mechanical parts (gears, sheaves) and electrical components (motor, converter). Duration: 27.8 seconds.

- E: The spreader is lifted back up to its resting vertical position and power flows into the hoist motor. The initial acceleration peak is accentuated by the lower steady state power consumption. Duration: 37.2 seconds.
- F: The trolley moves back into the original position. The power consumption appears lower than phase C, however the differences are minimal compared to phases B, D and E. Duration: 37.3 seconds.
- G: In this phase the crane itself moves along the stack, performing a gantry movement. The power flow shown in phase G in Figure 3.9 is caused uniquely by the gantry motors, and very little energy is regenerated during braking. Duration: 81 seconds.

Figures 3.11 and 3.12 show, respectively, the speed of hoist and trolley motor, and the vertical position of the spreader during the illustrative lift.

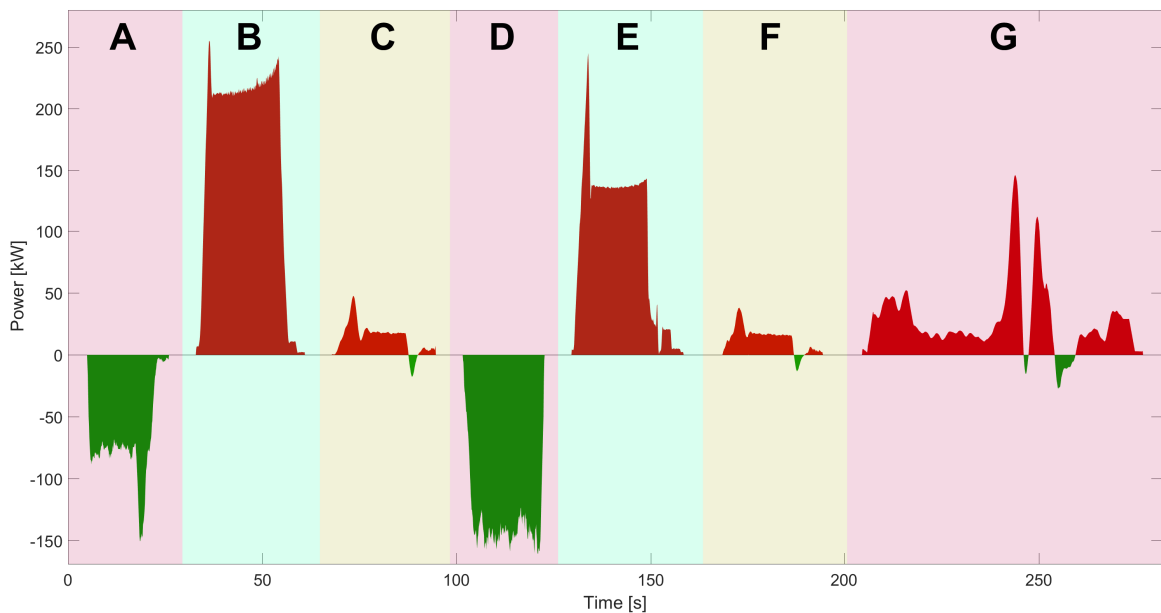


Fig. 3.9 Power flow of an RTG crane performing an illustrative lift cycle of a 19 tonne container from a terminal truck to the yard, followed by a gantry movement.

Table 3.1 presents information on the energy flow in each phase, divided into consumed (from the three phase supply to the motor), regenerated (from the motor to the brake resistors) and net consumption (consumed minus regenerated); the consumed and regenerated energy is also shown in Figure 3.10. It is clear from the table and figures that most of the energy is consumed by the hoist motor when performing an hoist movement, either with just the spreader or with a container attached. Trolley and gantry movements generally do not

regenerate significant amounts of energy [2], therefore in this work it is assumed that only phases characterised by hoist movements will generate meaningful amounts of energy.

Crane drivers usually perform multiple movements at once, overlapping the phases. Hoist and trolley motors may draw power at the same time causing an increase in demand on the primary source during a hoist phase. Nonetheless, Table 3.1 and Figure 3.10 show that the trolley energy consumption is a fraction of the hoist, and for simplicity it is convenient to consider the individual power demand of the hoist motor as the typical demand of an RTG crane when lifting a container.

Table 3.1 Energy consumption and regeneration for the various phases of the illustrative lift cycle

Phase	Motors	Energy consumed	Energy regenerated	Net energy consumed
A	Hoist	0.00 Wh	397.12 Wh	-397.12 Wh
B	Hoist	1257.95 Wh	0.00 Wh	1257.95 Wh
C	Trolley	106.67 Wh	6.55 Wh	100.12 Wh
D	Hoist	0.00 Wh	765.35 Wh	-765.35 Wh
E	Hoist	765.13 Wh	0.00 Wh	765.13 Wh
F	Trolley	94.90 Wh	4.84 Wh	90.06 Wh
G	Gantry	569.75 Wh	22.64 Wh	547.11 Wh

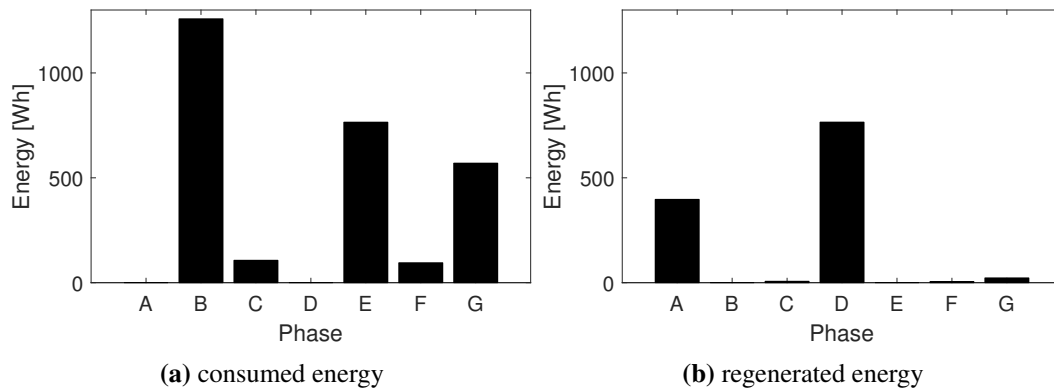


Fig. 3.10 Energy consumed and regenerated in each phase of the illustrative lift.

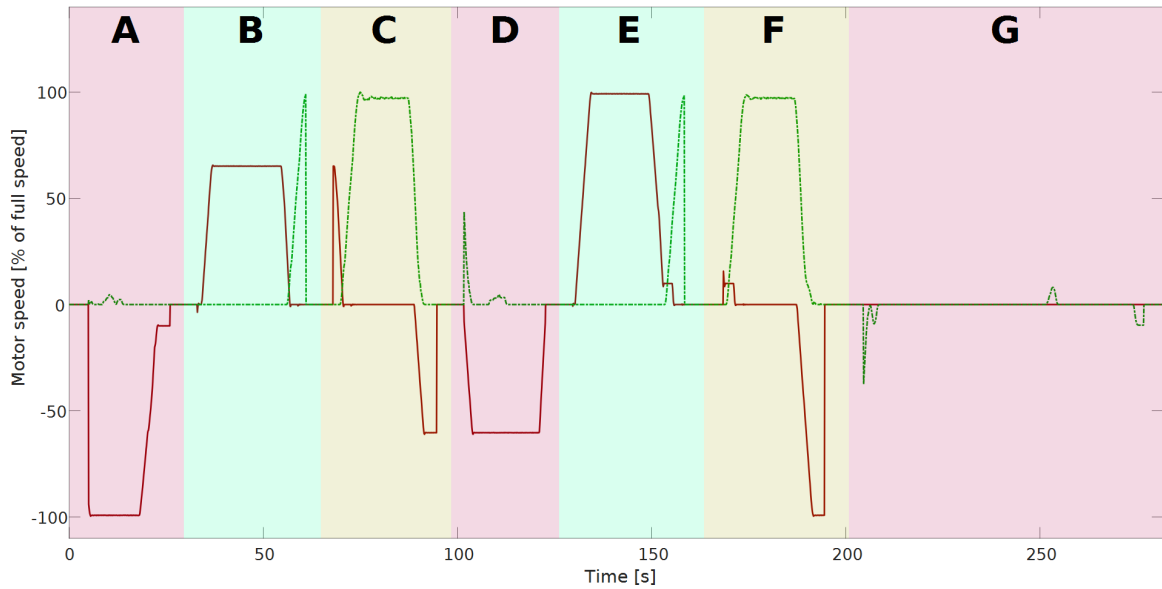


Fig. 3.11 Hoist motor (red solid line) and trolley motor speed during the illustrative lift.

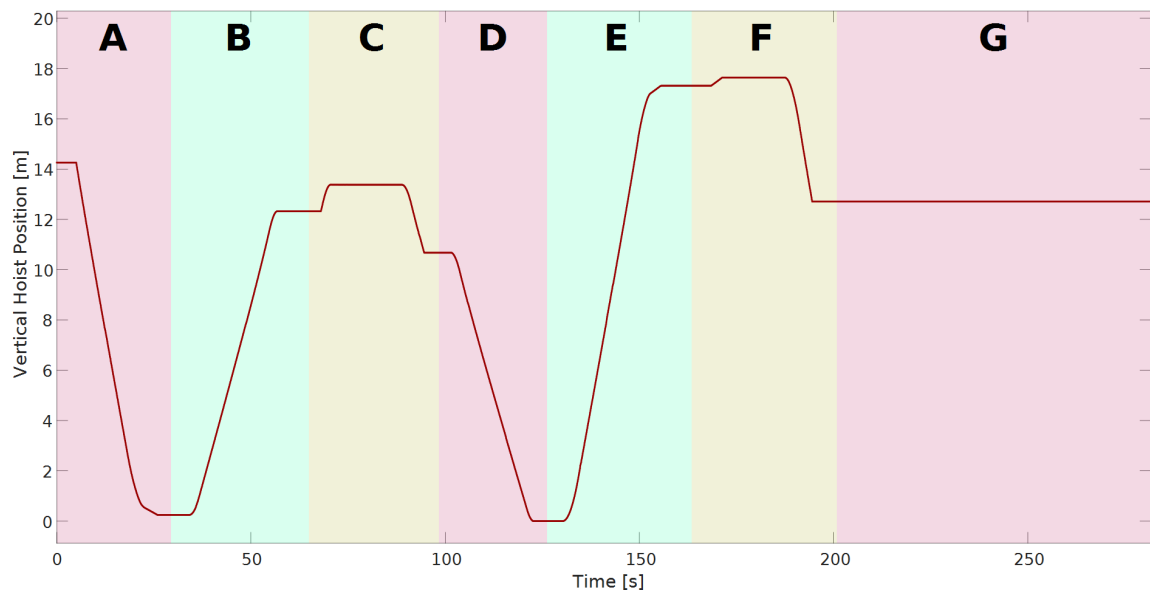


Fig. 3.12 Vertical position of the spreader during the illustrative lift.

3.6 Statistical analysis of the typical activity in a container terminal

The data collection on the RTG crane in use at the Port of Felixstowe includes monitoring the activity of a crane in terms of frequency of lift cycles, weight of the containers, duration of container lifts and statistics on power and energy consumptions. The information presented in this section, extracted from data collected for a duration of 4 days, has offered insight on the activity of an RTG crane in terms of the frequency and intensity of movements performed by the crane. Beside providing information necessary to the implementation of energy storage, this information also quantifies the work performed by an RTG crane in a container yard; part of the analysis and results shown in this section have been published as a journal paper in *Measurements* [2].

3.6.1 Container weight

Container weight is already measured by the crane since it is a safety requirement (to avoid exceeding maximum load). Furthermore, this information needs to be gathered as mandated by the International Maritime Organization [81]. The mechanical energy U required to lift a container is proportional to its weight m :

$$U = mg\Delta h \quad (3.1)$$

where g is the acceleration of gravity and Δh is the change of height. A terminal characterised by a larger fraction of heavy containers will result in a higher energy consumption. Container weights were measured and their distribution over 4 days is shown in Figure 3.13. Weight distribution is concentrated around two peaks, respectively at 10 and 27 tons. Table 3.2 shows the statistical values extracted from the measured weights.

3.6.2 Interval between lifts

The rating of the crane power system is highly dependent on the amount of time that passes between phases of high power demand, as it is dependent on the average power demand. Together with the measurement of the loads and the duration of lifts, this information can

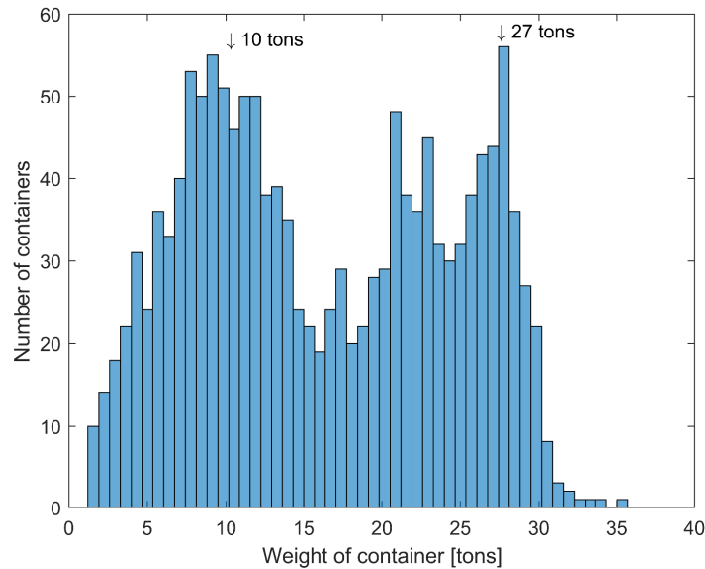


Fig. 3.13 Histogram of the number of containers with the measured weight, data collected over a period of 4 days (1934 lifts) [2].

help assess the characteristics of power demand. At comparable energy levels, short and frequent high power loads can be harder to manage compared to continuous low power loads.

The intervals between a spreader lock and the subsequent relock (indications that a container has been moved) were measured over a period of 4 days. The results are presented in Figure 3.14 and Table 3.2. Intervals above 5 minutes were discarded as they indicate that the crane has been idle and also they are few in number compared with the number of lift moves.

3.6.3 Duration of container lift

The primary energy source of the crane must provide high power during the duration of the container lift, since the hoist motor is the highest rated electrical machine in the crane. Masses of up to 52 tons (container plus spreader) are lifted for a duration of up to 65 seconds, with a peak power that can reach 400 kW. It then becomes very important to estimate the duration of the typical lifts, which depends on the height that the container needs to reach and the mass of the load.

The average lift duration also changes depending on the characteristics of the container terminal. Small and busy terminals will have containers densely placed in high stacks, while

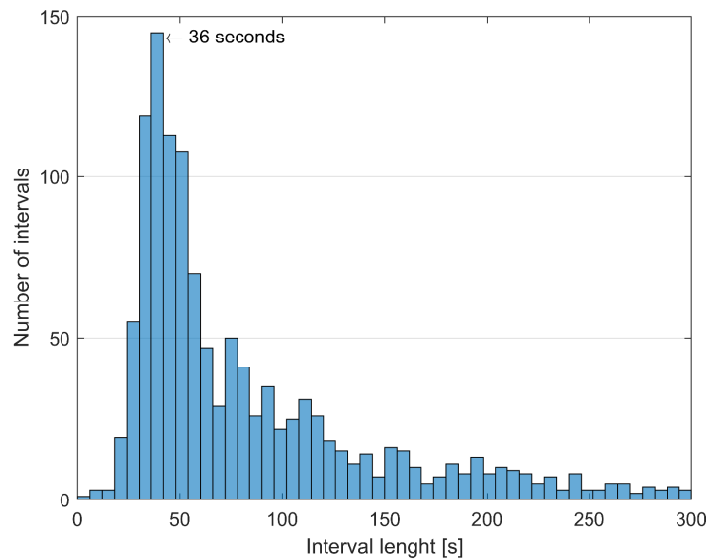


Fig. 3.14 Histogram of the duration of the intervals between lifts, data collected over a period of 4 days (1934 lifts) [2].

larger ports with low activity will prefer lower stacks. The height of the stacks will then influence the lift duration. The distribution of lift durations measured at the Port of Felixstowe is presented in Figure 3.15.

The maximum speed at which the container is lifted depends on the weight of the containers, with lighter containers lifted at a vertical speed of 52 metres per minute, while at full load (40 tons) the speed is limited to 26 metres per minute; this results in a slight increase of the duration of the lift when lifting containers of higher mass, as shown in Figure 3.16.

Table 3.2 Statistical information on container weight, duration of intervals between lifts and duration of lifts. Data collected over a period of 4 days.

	Container weight	Interval between lifts	Lift duration
Maximum value	32.3 tons	298.5 s	65.6 s
Minimum value	1.2 tons	4.5 s	1.0 s
Mean value	16.3 tons	83.0 s	22.1 s
Median value	15.3 tons	58.0 s	21.0 s

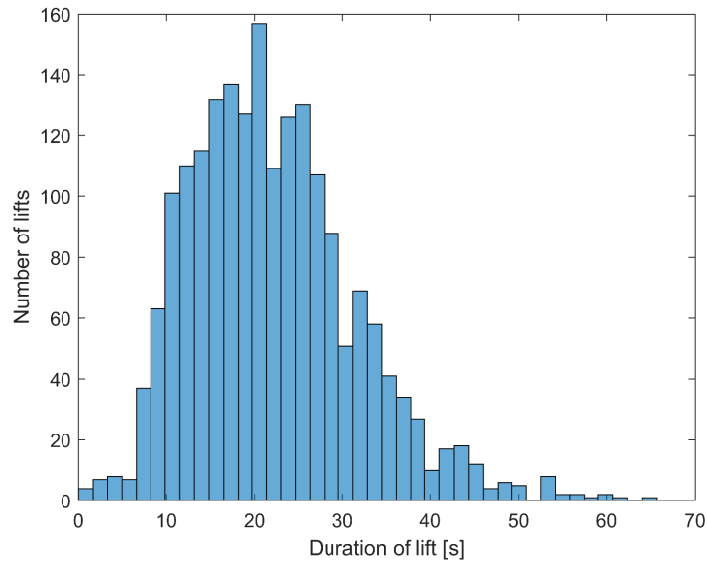


Fig. 3.15 Histogram of the number of lifts with the measured duration, data collected over a period of 4 days (1934 lifts) [2].

3.6.4 Average power

The data collected over four days were analysed in order to quantify the average power during hoist movements, divided into lifts and lowerings. The average power is calculated as the mean power in the interval of time when the hoist motor is moving in a single direction (upwards or downwards). In the 4 days, 1528 lifts and 1507 lowerings were identified from complete lift cycles (lasting at least 3 seconds). Figure 3.17 shows the histogram extracted from the analysis. Most of the lifts (Figure 3.17a) are concentrated between 50 and 200 kW, with a median of 97 kW. An 80th percentile of 146 kW indicates that 80% of the lifts are below that value. Lowerings (Figure 3.17b) are concentrated around the median value of -42 kW, with the 80th percentile at -73.5 kW. This information will be useful when a choice needs to be made regarding the power rating of an energy storage system: the ESS will need to be able to produce a power output comparable to those values.

3.6.5 Energy consumption

The data above was further analysed to calculate the energy consumed or regenerated during a lift or a lowering, respectively. Figure 3.18 shows the data, indicating that most of the lifts consume (and regenerate) relatively low energy. The median value for the consumed energy

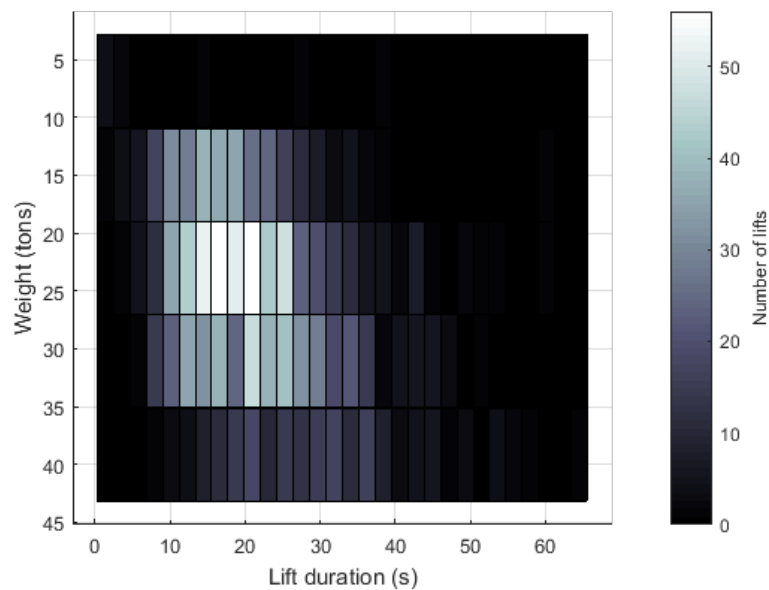


Fig. 3.16 Distribution of lift durations. The brightness increases with the number of lifts associated to a particular mass/duration combination [2].

is 0.463 kWh while the 80th percentile is 0.880 kWh. Lowerings have a median value of -0.287 kWh and the 80th percentile is at -0.601 kWh. This analysis will help choosing the energy capacity of the energy storage, i.e. the maximum amount of energy that the ESS can store and deliver.

3.7 System topology

The data collected and analysed will become useful for the development of effective control strategies only when studied alongside the topology of the electrical systems in the crane. The data needs to be put into context with the pathways followed by the energy during the crane's daily activity.

The RTG crane under analysis, described in Section 3.4, was originally powered exclusively by a diesel generator. Recently, it has been fitted with a connection to the terminal power network through a conductor bar running along the stack (Figure 3.19), allowing it to be powered by the three-phase grid instead of using the diesel generator. In this work the source was modelled as an infinite capacity three-phase source, capable of delivering any instantaneous power $p_g(t) \geq 0 \forall t > 0$ to the DC bus through a (single-quadrant) diode rectifier. The assumptions on the primary source are justified by the fact that the power

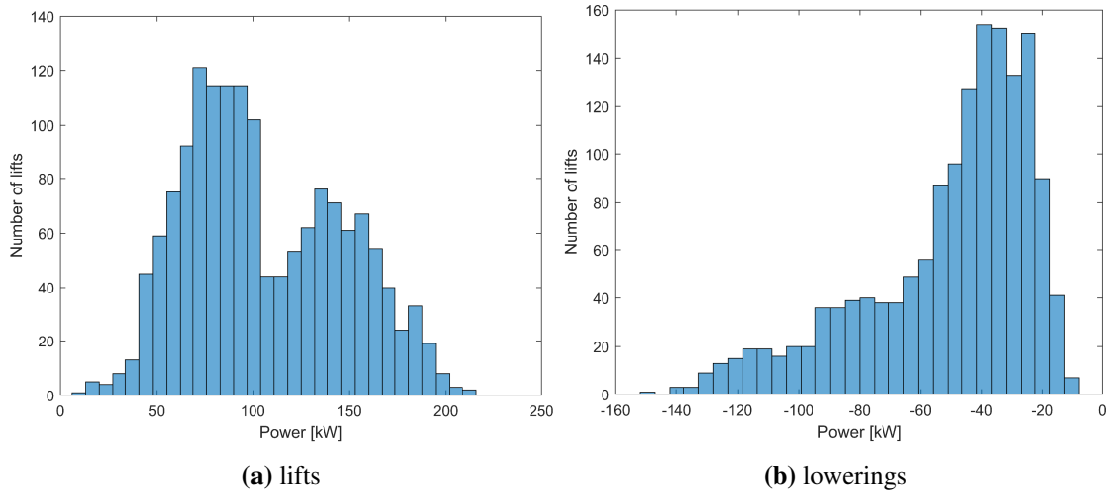


Fig. 3.17 Histograms of the average power consumption during a lift or lowering.

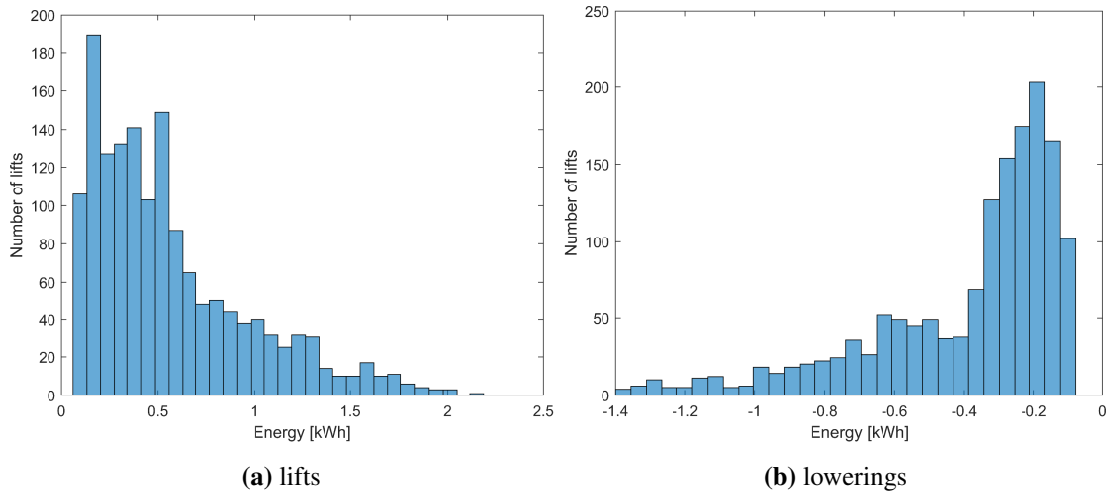


Fig. 3.18 Histograms of the energy consumption or regeneration in a lift or lowering.

rating of the primary source will be higher than the maximum power demand of the crane. The primary source has no energy limitation as it is supposed to be either the electrical grid or a diesel generator, both capable of supplying the energy required during a lift cycle. Furthermore, the time dynamics of the electrical components of the crane are assumed to be slower than the main power source in order to guarantee the correct operation of the crane. These assumptions are justified by the consideration that RTG cranes currently operating in container terminals perform normally with their own primary supply and without any additional power source.

The main motors (hoist, gantry, trolley, etc.) are all connected to the shared DC bus and are modelled as a single load which demands power $p_L(t)$ which changes with the

activity; the motors regenerate power during braking so the instantaneous value of $p_L(t)$ can be negative. Most of the energy consumption and almost all the energy recovery is due to the hoist motor, thus the load will be approximated as the power flow of the hoist motor (see Section 3.5). Brake resistors engage automatically when the DC bus voltage raises above 750 V, absorbing all the regenerated energy; the power dissipated into the brake resistor $p_d(t)$ is assumed unbounded and can only flow in a single direction: $p_d(t) \geq 0 \forall t > 0$. Hence, the power flow can be described by the following equation:

$$p_g(t) = p_L(t) + p_d(t) \quad (3.2)$$

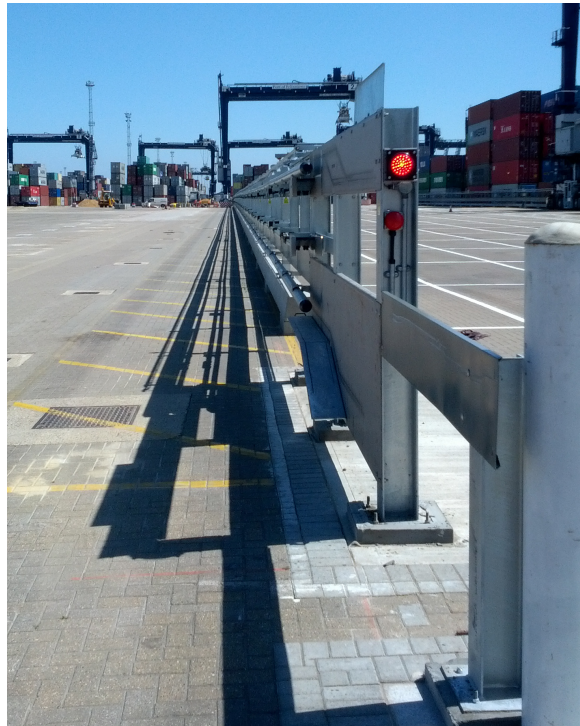


Fig. 3.19 Three-phase conductor bar that powers RTG cranes at the Port of Felixstowe.

The power flows are also visualised in Figure 3.20. The regenerated energy is dissipated into the brake resistors, wasting significant amounts of energy and increasing the greenhouse gases emission from RTG cranes, especially diesel powered ones.

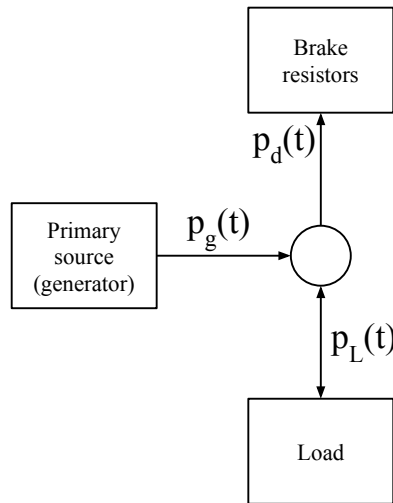


Fig. 3.20 Diagram showing the basic topology of an RTG crane.

3.8 Potential opportunities for improving efficiency

3.8.1 Energy recovery

Energy dissipated into the brake resistor is permanently lost as heat and the efficiency of the crane would increase if there was the possibility of recovering the energy. The data studied in Section 3.6.5 shows that, in four days, the hoist motor consumes 1306 kWh. The amount of wasted energy is non-negligible: in the same period, the hoist motor regenerates 737 kWh, more than 56% of the consumed energy. Recovering this wasted energy would save a container terminal approximately 67.25 MWh per RTG crane per year; in a diesel powered crane this equals to the consumption of 16.48 tonnes of diesel fuel [82], using a very conservative estimate and assuming that the motor is never idling. This amount of diesel fuel is associated with an emission of 52.14 tonnes of CO₂ [83]. There are environmental benefits in recovering this energy in terminals, especially those characterised by tens of cranes working simultaneously. The savings are less significant in electric powered cranes since the cost and pollution associated with electrical energy production is lower. In the UK, these electric energy savings are equivalent to a reduction of 48.42 tonnes of CO₂ emissions [84]. If the share of renewable energy production increases, the CO₂ emissions will decrease, strengthening the cause for E-RTGs as environmentally friendlier cranes.

It has been shown that a crane regenerates large amounts of energy during the daily activity, but how much does it regenerate in one single lift cycle? This information is crucial,

as it relates to the time that passes between consuming and reusing the energy: if energy consumption and recovery in a single lift cycle are comparable, the energy can be reused quickly without having to store it for relatively long periods. Controlled tests were performed at the Port of Felixstowe with a crane executing standard lifts of known container weights in order to measure accurately the power flows. Voltage and current consumption of the hoist motor were recorded as well as the vertical position of the spreader; this information was then used to calculate the consumed and regenerated energy which were compared with the potential energy $\Delta U(t)$ gained by the spreader:

$$\Delta U(t) = (m_c + m_s)g\Delta h(t) \quad (3.3)$$

where m_c is the container weight, m_s is the spreader weight (measured at 12.5 tonnes) and $h(t)$ is the vertical position of the spreader. The empty spreader and an empty container were lifted and then lowered, with the final height equal to the initial one, therefore the potential energy gained during the lift is equal to the one lost in the lowering. The voltage and current of the hoist motor were recorded with a sampling time of 0.1 seconds and the energies were calculated with a trapezoidal integration as follows:

$$E = \frac{T_s}{2} \sum_{k=1}^N (i(k+1)v(k+1) - i(k)v(k)) \quad (3.4)$$

where E is the total energy calculated, T_s is the sampling time, N is the number of samples collected, and $i(k)$, $v(k)$ are the DC current and voltage at the sample time $k \in \mathbb{N}$, respectively. Table 3.3 and Figure 3.21 show the values extracted from the analysis. Table 3.3 also shows the ratios between consumed, potential and regenerated energy, indicating that the mechanical and electrical losses are relatively small. Note that, for this particular analysis, the regenerated energy was inverted in sign in order to facilitate the comparison.

Table 3.3 Comparison of electrical energy consumed, mechanical potential energy and electrical energy regenerated when performing standard lifts with various container weights.

Container mass	Consumed energy	Potential energy	Regenerated energy	Potential/ consumed	Regenerated/ consumed	Regenerated/ potential
0 t	746.58 Wh	575.93 Wh	395.21 Wh	77.1%	52.9%	68.6%
5.5 t	760.56 Wh	607.34 Wh	524.28 Wh	79.9%	68.9%	86.3%
19 t	1302.2 Wh	1072.5 Wh	900.31 Wh	82.4%	69.1%	83.9%

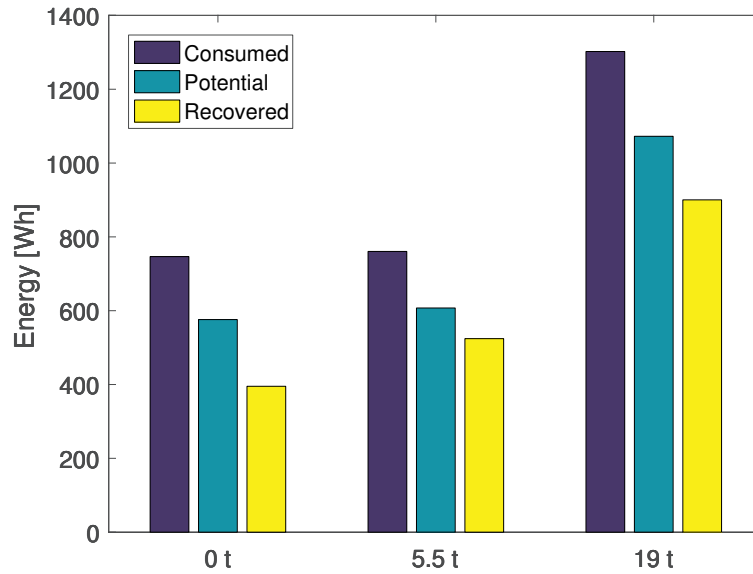


Fig. 3.21 Chart showing electrical energy consumed, mechanical potential energy and electrical energy regenerated when performing standard lifts with various container weights.

Storage capacity and power rating are limited, it is then necessary to decide on when and how to use the stored energy. Furthermore, in this particular application the demand and regeneration are not easily predictable and non-negligible losses are present. These factors will make it non trivial to develop an effective control strategy, as it is not beneficial to manage power flows passively. The next section will explain why it may be preferable to actively manage power and energy in order to achieve a second very important objective: peak power demand reduction.

3.8.2 Reduction of peak power demand

One of the potential opportunities of reusing stored energy is to minimise peak power demand, by effectively lowering the maximum value of the power demand over time. Data collected for 4 days on an RTG was analysed to calculate the percentage of time that the primary source outputs certain values of power. As shown in Figure 3.22, 76% of the time the crane is demanding less than 16 kW, but the primary power source needs to be rated for the highest possible power demand. The data shows that the maximum power demand during the 4 days is 350 kW, and this is the least power that needs to be available to the crane in normal conditions.

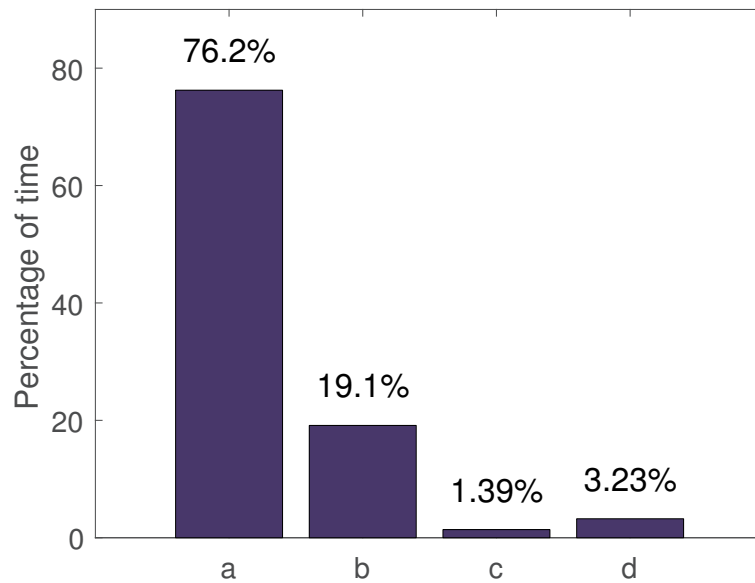


Fig. 3.22 Chart showing the percentage of time that the crane demand a certain amount of power to the primary source. a) $p_g < 16kW$, b) $16kW \leq p_g < 150kW$, c) $150kW \leq p_g < 200kW$, d) $200kW \leq p_g$.

The benefits of reducing the peak demand for diesel powered RTGs come from a reduction in the size of the generator: lower peak power demand allows for diesel generators with lower power rating that usually consume less fuel when idling. Idle fuel consumption is effectively wasted energy as the crane does not perform any activity apart from keeping the generator spinning and powering the auxiliaries.

Energy storage can perform a so-called peak shaving operation where it provides power to the system in order to limit the maximum power demanded to the generator. This operation requires the storage system to supply all the excess power. RTG cranes, like most industrial equipment, can self-limit their maximum power consumption, but this is associated in increased lift cycle times because of reduced movements speeds. This undesirable effect can then be mitigated by implementing a peak-shaving solution in the energy storage device, significantly reducing the fraction of time when the RTG crane needs to operate in reduced power mode. This solution allows port operators to decrease the maximum power rating of the primary source of the crane by swapping a large generator for a smaller one. This operation, so called “genset retrofit”, is a viable solution for reducing fuel consumption in container terminals [36, 75, 78] and has been performed in many terminals, but it needs to be associated with changes in either the operation of the crane or, preferably, by adding energy storage equipment that can provide the peak power.

A second issue related to generators comes from fast transients in power demand that are associated with high fuel consumption and excessive greenhouse gases emission, therefore a fast peak shaving device that smooths power transients will effectively reduce the environmental impact of an RTG crane.

Electric powered RTGs are less affected by high power demand as the electrical grid can normally provide the power levels needed without any major impact on efficiency. On the other hand, the electrical infrastructure of a container terminal needs to be designed around the worst case scenario: cranes lifting at full load. This may result in avoidable high capital investments.

Terminal operators may be hesitant in converting D-RTGs into more environmentally friendly E-RTG cranes since the costs and efforts associated with upgrading the local power network can be immense. It would be beneficial to reduce the maximum power draw of an RTG crane by supplying power from an energy storage device during peak demand. This operation, called peak shaving, is performed by supplying enough power from the ESS to maintain the load visible to the primary source below a predetermined threshold, lower than the crane's highest possible power demand [67, 85]. Adding a peak shaving device to either the crane or the local network could reduce dramatically the infrastructure costs, allowing terminals to reduce the dependence on fossil fuels by converting more cranes to electric.

Figure 3.23 shows an example of a peak shaving device limiting the maximum amount of power demanded to the primary source. In normal conditions, the maximum load is over 150 kW while the device, in the example, is limiting it to approximately 75 kW. The storage device starts the test with 3.34 MJ of stored energy and ends it with 2.54 after 18 seconds. Figure 3.24 shows the profile of the energy stored in the peak shaving ESS.

This thesis will show how recovering energy and reducing peak power demand could be achieved, either individually or in combination, by using energy storage associated with carefully planned control strategies.

3.9 Energy storage

The opportunities discussed in Section 3.8 may be implemented by using a device that is able to store energy for later use. The diagram in Figure 3.25 shows how an energy storage unit can add a new pathway for the regenerated energy that does not necessarily mean dissipating it as heat in the brake resistors:

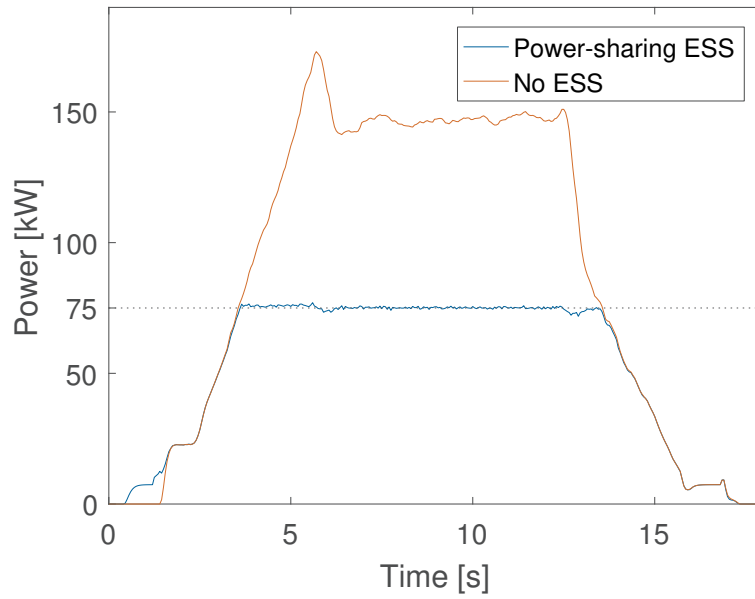


Fig. 3.23 Power demand on the primary supply of an RTG crane with and without a peak shaving device.

$$p_g(t) = p_L(t) + p_d(t) + p_s(t) \quad (3.5)$$

where $p_s(t)$ is the power flow of the energy storage system.

An effective energy storage system will act on the instantaneous value of $p_s(t)$, managing the stored energy $E(t)$:

$$E(t) = \int p_s(t) dt. \quad (3.6)$$

Energy storage can come in multiple forms, for example chemical, electrochemical and mechanical. For the particular application on an RTG crane there are few technologies that, at the moment, have the right characteristics: batteries, supercapacitors and flywheels.

3.9.1 Batteries

Electrical energy is converted into chemical energy by supplying a current to an anode and a cathode immersed in an electrolyte. The most common battery in the market is the lead-acid battery invented by Plante in 1859 which consists of alternated pairs of lead and lead dioxide plates immersed in a solution of sulphuric acid [86]. The short life-cycle and the low energy

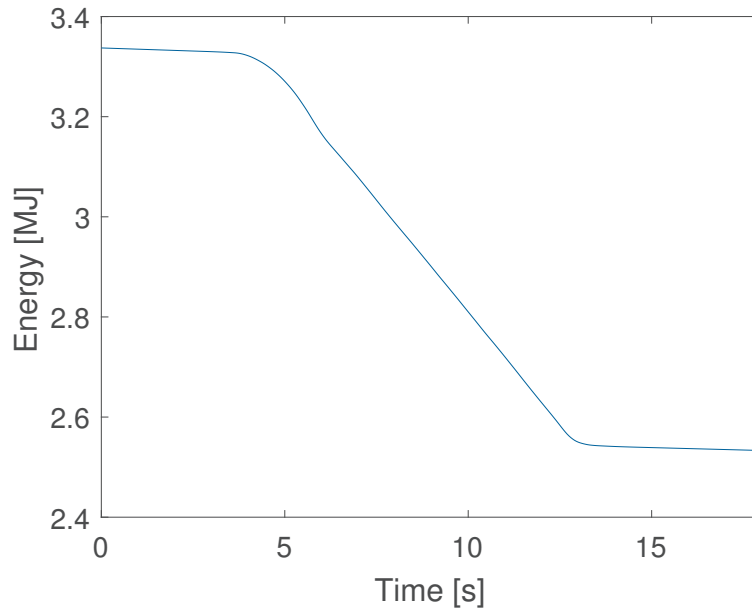


Fig. 3.24 Energy stored in the peak shaving ESS.

density (the amount of energy that can be stored in a unit of volume) make them unsuitable for storing large quantities of energy. Advancements in technology led to the development of Lithium-ion batteries, which feature higher energy densities, typically 200 to 400 Wh/l, and specific energy of 75 to 200 Wh/kg [87, 88]. The power density and the specific power are, respectively, 1.5 – 10 kW/l and typically 0.15 – 0.5 kW/kg.

The diffusion of electric and hybrid vehicles and the widespread adoption of lithium-ion batteries led to the decrease of costs, making them suitable for use in a RTG crane. The weakness of chemical energy storage is due to the relatively low power density: the amount of instantaneous power that can be transferred by the battery is low in relation to their size [79] (see Figure 3.26). This can be a limiting factor for recovering the energy from lowering a container because the power flow from the hoist motors reach peak values in the order of hundreds of kW (see Section 3.5). Nonetheless, the high energy density allow for a large amount of stored energy. Another drawback of using batteries is the limited life-cycle due to degradation. The number of charge-discharge cycles is limited to the tens of thousands in the best scenario, and high temperatures and deep discharges (typical in a crane) lower this number. This shortcoming also forces to install charge control circuits that add complexity and cost, as well as increasing the environmental impact due to the disposed batteries [10].

Commercial RTG cranes equipped with batteries are already present on the market. MJ EcoPower developed a hybrid RTG crane equipped with a 400 Ah lithium-ion battery

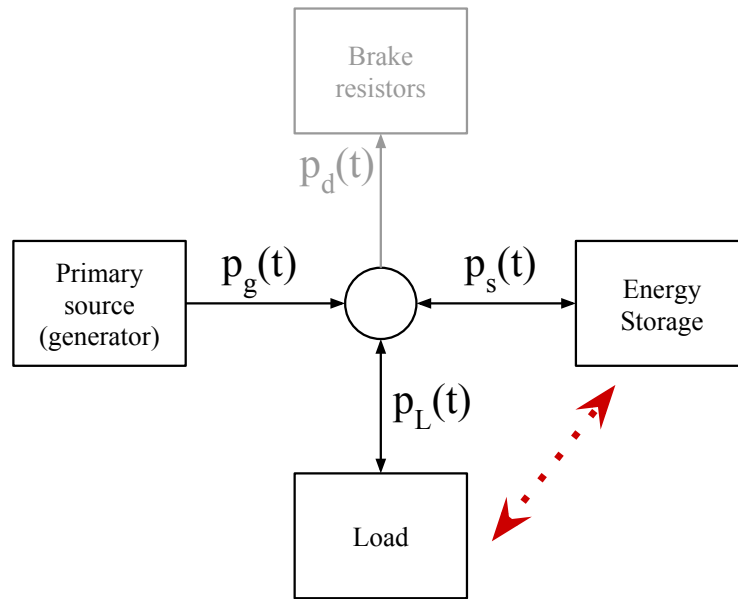


Fig. 3.25 Topology of an RTG crane equipped with energy storage with in red the new pathway for energy.

[89] which showed a 72% and 35% fuel consumption reduction when idle and under load, respectively.

3.9.2 Super-capacitors

Super-Capacitors (SC), also called ultracapacitors, are high-capacity electrochemical elements that store energy in the form of an electrostatic field. The power density of SCs is very high and can be considered infinite as the limiting factor is often the power rating of the associated converter. On the other hand, the specific energy is orders of magnitude lower than the batteries: 0.1 – 5 Wh/kg [88], 0.05 – 5 Wh/kg [87], while the energy density does not go above 10 Wh/l [87].

SCs are suitable for short high-power bursts and for this reason they are used for absorbing and supplying peak power. As discussed in Section 3.5, RTG cranes do have in fact power profiles that are often composed of power peaks, for example when accelerating a container from the ground to the maximum vertical speed. For this reason, SCs are used in hybrid RTGs for peak shaving and power sharing [34, 90–92].

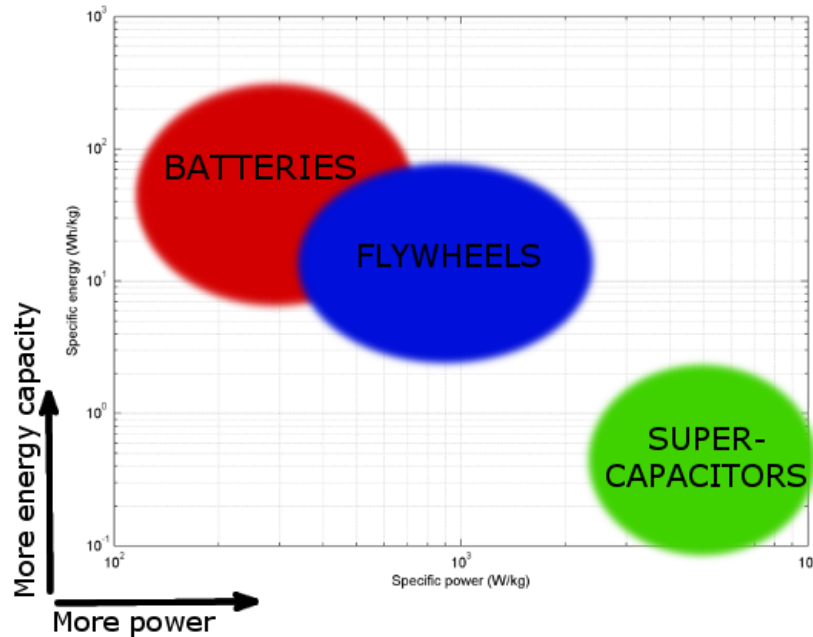


Fig. 3.26 Comparison of the power and energy densities of common energy storage technologies (Ragone chart).

In [90] a Finite-State Machine (FSM) is used to determine the status of the crane (raising a container, lowering a container, idling) and to act accordingly. The SC provides voltage control when the container is accelerated upwards while the generator spins up, then the SC works in power control to share the lifting effort with the generator; when the crane lowers a container the DC bus voltage increases and the SC is set to regulate the voltage anomaly, absorbing power. Results show a reduction of around 30% in fuel consumption.

In [34] the SC intervenes when the load weight exceeds a predetermined value, helping the generator by controlling the frequency (the generator frequency decreases as it struggles to generate more power) supplying power. In case of smaller loads and when the SC voltage exceeds a threshold, the SC controls the DC bus voltage absorbing energy or maintaining the voltage above the activation level of the rectifier diodes. When the SC voltage is low and load weight is low the super-capacitor is charged from the generator, while it is charged by recovered energy only when SC voltage is high. Results show around 30% fuel consumption reduction.

3.9.3 Flywheels

A rotating mass can be used for accumulating electrical energy when connected to electrical motors. A rotating mass stores an amount of energy $E(t)$ [93]:

$$E(t) = \frac{1}{2}I\omega(t)^2 \quad (3.7)$$

where $I [Kg \cdot m^2]$ is the inertia of the flywheel (along the rotational axis) and $\omega(t) [rad/s]$ is the rotational speed. It can be seen that increasing the inertia will increase the amount of energy that can be stored, but it is also evident that the speed has a quadratic effect on the energy, resulting in an increased focus on achieving high rotational speed to obtain high energy capacity. Energy is transferred to the flywheel when the flywheel is accelerated, whilst when the flywheel is decelerated the stored energy decreases.

Modern Flywheel Energy Storage Systems (FESS) are composed by a rotating element made by metal (steel, titanium alloy) or other materials (glass fibre, carbon fibre, Kevlar) suited to withstand the tensile stress caused by centrifugal forces. The moving element is an electric motor (or a continuously variable transmission in the case of a connection to a mechanical system) usually in the form of an induction motor, a permanent magnets synchronous motor or a Switched Reluctance (SR) motor.

High standing losses make flywheels inadequate for long-term storage, for this reason they are only used for storing energy for short periods of time (like those required by RTG cranes between lowering and lifting) but they do not limit the number and frequency of charge-discharge cycles [10].

The ample choice in geometries and materials of the rotating element helps to achieve different objectives. Heavier, slower and cheaper steel-based flywheels offer lower losses and high energy density, while lighter and faster composite flywheels offer higher specific energy in environments where adding weight should be avoided. The range of operational speed of a FESS is kept above a certain threshold to avoid applying high tangential forces to the rotating mass at high power (and torque) levels, nonetheless power density and specific power depend mostly on the electrical machine used to power the system. This is because the electrical machine needs to be able to supply high power and high torque in a wide range of speeds, with a high average power; this requires a careful study on operating temperatures, cooling and deformations to avoid reducing the lifetime of the machine.

If higher energy density and efficiency are required, flywheels can be designed to rotate in vacuum and with magnetic bearings [94, 95], thus reducing winding and friction losses but increasing costs and complexity.

Studies show that FESSs have the following properties: energy density is 20 – 80 Wh/l, power density 1000 – 5000 W/l, specific energy 5 – 100 Wh/kg and specific power 0.4 – 1.5 kW/kg [87, 88, 96]. This places the FESS between batteries and SCs in terms of specific energy and power. For the particular application with wind turbines, the FESS has been found the most economical energy storage method for holding energy for less than 10 minutes [24]. There is no similar comparison for the use of different storages in RTG cranes at the date of publication.

A FESS has been tested on a RTG crane by Flynn et al. in [19]; the storage system comprises of two flywheels, each powered by a 150 kW permanent magnet synchronous motor and with a maximum energy capacity of 4.57 MJ (1.27 kWh). The total usable energy capacity is 2.12 MJ (0.59 kWh) due to speed limitations. The author claims that the use of high-speed flywheels can offer higher efficiency, longer life-cycle, reduced temperature concerns and increased reliability with respect to other solutions based on supercapacitors. The control algorithm speeds up the flywheels up to the minimum speed of 10,000 RPM, then redirects recovered energy from a lowering event to the storage increasing the flywheel speeds up to a maximum of 20,000 RPM. At the start of a lift, the flywheels provide most of the required power by limiting the engine power to 50 kW; after the power peak (due to the initial acceleration) the flywheel power is reduced to 120 kW while the generator ramps up gradually providing the rest of the power. The FESS tested on a crane reduced the fuel consumption of 20.9% with a significant reduction in particulate emission (66.7%).

3.9.4 Comparison of energy storage systems

The analysis presented in Section 3.5 showed that the ESS used in a typical crane should be able to store around 1 - 2 kWh of energy. It also needs to be able to deliver 100 - 200 kW and maintain it for a period of time of around 30 seconds. The chart shown in Figure 3.26 shows what the three technologies can offer in terms of energy and power, with the batteries allowing for larger energy capacity but reduced power outputs, and supercapacitors allowing for virtually unlimited power draws but very little energy density. In Table 3.4 it is presented a summary of the technologies and their qualities related to a possible implementation on a container crane.

Table 3.4 Comparison of energy storage technologies in use on RTG cranes.

	Advantages	Disadvantages
Batteries	<ul style="list-style-type: none"> • High energy density • Can store energy for longer periods of time 	<ul style="list-style-type: none"> • Low power density • Short life-cycle • High environmental impact
Supercap.	<ul style="list-style-type: none"> • High power density • Low complexity • Long life-cycle 	<ul style="list-style-type: none"> • Low energy density • Medium-high standing losses
Flywheels	<ul style="list-style-type: none"> • Mid-range energy and power density • Wide temperature range • Long life-cycle 	<ul style="list-style-type: none"> • High standing losses

While batteries and supercapacitors energy storage systems are the most common choices for storing recovered kinetic energy, a technology that shows good potential is flywheels [18]. The added complexity due to the presence of the motor (and associated control logic) is compensated by the increased durability and less stringent limitation in temperature and vibration [87, 88]. The only limitation that cannot be overcome is the short period of time that the energy can be kept stored, but this limitation is partially shared with supercapacitors as they tend to have relatively high self-discharge rates [87].

Flywheel energy storage has been chosen in this thesis because its characteristics match the requirements highlighted in Section 3.6 in terms of power and energy density, with the duration of lift cycles being below the threshold where flywheels were found to be more economical [24]. Flywheel storage is also preferable because of its expected lifetime: the motor and flywheel assembly match the life expectancy of the crane's mechanical and electrical components and require similar maintenance, without losing any significant energy capacity over time.

3.10 Active Front-End

To recover energy from a crane it is not necessary to use energy storage, and one alternative is to use Active Front-End rectifiers. The main use for AFEs in the generic application is to improve power quality, both reducing harmonics and stabilising the power factor to the desired value. Their use is widespread and well documented in the literature [97–101].

Consequently, crane manufacturers are equipping new models of E-RTGs with AFEs in order to obtain high power quality, reducing the total harmonic distortion below 3%, an order of magnitude less than what achieved with passive filters [102, 103]. An important benefit of AFEs is the regenerative capacity of the crane: energy regenerated when lowering containers is not dissipated into heat but can be regenerated into the supply network, as is shown in Figure 3.27. This property, which comes from the regenerative capabilities of an AFE, could potentially reduce the energy consumption of a container terminal if the energy recovered from one crane is simultaneously used by different cranes. The basic diagram in Figure 3.28 shows how the energy can be fed back into the primary source instead of having to be necessarily redirected to the brake resistors.

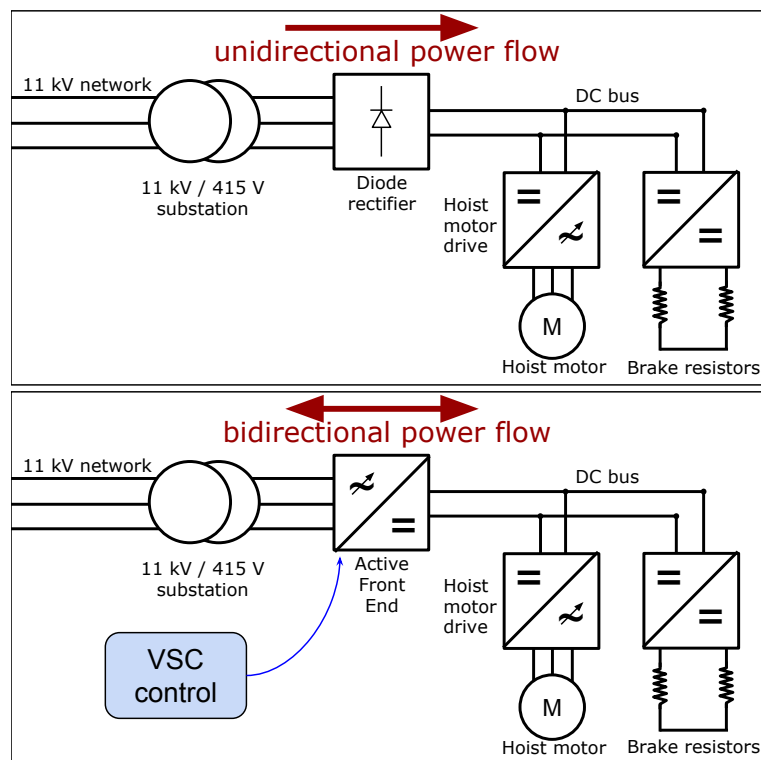


Fig. 3.27 Differences between a crane equipped with a diode rectifier and an AFE [1].

Active Front-Ends are an alternative solution to energy storage for reducing energy consumption in ports, however it is not possible to control the time when the energy is regenerated, thus it is necessary to ensure that there is an instantaneous power demand, in the rest of the local network, that matches the power regenerated. Furthermore, this restriction does not allow the application of peak shaving techniques without a careful coordination of multiple cranes. Additionally, the potential issues related to excessive regeneration need

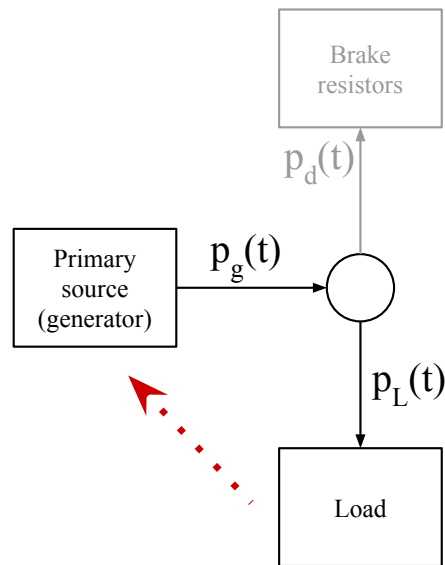


Fig. 3.28 Topology of an RTG crane equipped with AFE with in red the alternative pathway for energy.

to be taken into account: the container terminal could create complications in the regional power network if certain conditions occur. If excessive energy is produced, it is necessarily dumped into the regional power network. Depending on the local regulations, distributors could fine the terminal operators if this occurs.

In summary, energy storage offers higher flexibility and could be used to achieve a combination of energy savings and peak power demand reduction, whilst AFEs could only achieve energy savings when in particular conditions [1]. In Section 5.1.3 the effect of adding an AFE to a crane will be shown in more detail, including what energy savings could potentially be obtained and under which assumptions.

3.11 Summary

This chapter described the RTG crane as a key element in a container terminal and also as a system composed of multiple electrical elements which perform distinct tasks. When the crane is operating, the individual elements and tasks are intertwined in order to produce movements that for a typical lift cycle, described in detail in this chapter. The actual crane used as a reference for this work is also introduced, as well as the port in which it is operating. The energy and power flows of the crane are presented and described in an illustrative lift

cycle and also from measurements taken directly from a real crane. This analysis allowed the identification of the key electrical elements and the associated power flows during a generic lift cycle. The energy exchange has been quantified, providing a necessary foundation that is the base of this research. To the date of writing, this is the only publicly accessible comprehensive research on the energy flow in an RTG crane that present a high sampling rate (up to 100 Hz) and long-term data acquisition, with all the main electrical components metered and analysed. The measurement system used to gather high resolution data from the crane, and its associated data analysis tool, has been the base of a journal paper published in *Measurement (Elsevier)* [80].

Statistical information on daily activity has been provided in this chapter. This information provides an insight on the normal activity of the crane throughout multiple days and not only limited to a single lift cycle. This information not only helped define the characteristics of the energy flows, it also will be used to define the desired characteristics of a most suited storage device (see Chapter 6). The statistical analysis of the typical activity of an RTG crane in a container crane, presented in this chapter, was not present in the literature and it has been incorporated in a journal paper published in *Energy (Elsevier)* [2].

This chapter also presented a clear definition of the potential objectives that an RTG crane can achieve when equipped with energy storage. Those objectives have been motivated by practical necessities as well as the analysis of power and energy flows presented earlier. The first objective is to reduce energy consumption, which can lead to energy costs savings and a reduction in greenhouse gases emissions. The second objective is peak power reduction, which can reduce the impact of container lifts on RTGs, mitigating high power demands that are relatively infrequent. These objectives will be referenced to throughout this thesis, including during the choice of energy storage technology or when designing the supervisory control strategies.

Finally, this chapter presented an analysis on the most common energy storage technologies and their use. From all the information provided in this chapter it was possible to compare each technology and identify the one most suited for achieving the objectives of energy saving and reduction in peak power demand. Flywheel technology has been chosen for its ability to provide high power outputs with lower cost and size, and because its disadvantages are not an issue in the context of RTG crane operations. Active front-ends, a common alternative to energy storage in RTG cranes, was also analysed. The study showed limited flexibility and the impossibility to achieve both objectives stated earlier. A confer-

ence paper on this study has been presented at the *16th IEEE International Conference on Environment and Electrical Engineering* [1].

The objective of this thesis is to produce supervisory control systems for energy storage in RTG cranes, and this chapter provides the infrastructure on which this research is based. The problem has been defined by quantifying its electrical and statistical features. The objectives have also been defined by analysing the operation of the crane and practical necessities. The tool through which it is possible to achieve the objectives is the energy storage device, whose necessary characteristics have been set and will be the base of the next chapter, where it will be discussed whether it is possible to produce a storage device with those desired features.

Chapter 4

Design and low-level control of flywheel energy storage systems

The objective of this chapter is to present a flywheel energy storage device that is in line with the characteristics required by the application (defined in Chapter 3). Firstly the requirements will be determined, taking into account the analysis performed in previous chapters that indicated the energy and power flows in an RTG crane. Then the requirements are analysed in order to characterise a mechanical flywheel that is suitable for the task and that could be plausibly built in reality with existing technologies. Electric motor technologies will also be presented that are suitable for the use with flywheels and their qualities will be compared as well as the limitations. Finally, a low-level control of an electrical motor will be presented which will enable the control of the power flow to a flywheel.

4.1 Mechanical flywheel

As described in Section 3.9.3, a rotating mass possesses kinetic energy that is proportional to the inertia of the rotating mass along the rotational axis and also proportional to the square of the rotational speed, as specified in (3.7). A flywheel tends to maintain its rotational speed due to inertia, and any change in speed is the effect of a force (in this case, torque) applied externally. The mechanical power $p_f(t)$ transmitted to the flywheel is the derivative of the energy:

$$p_f(t) = \frac{dE(t)}{dt} = I\omega(t)\frac{d\omega(t)}{dt} = \tau(t)\omega(t) \quad (4.1)$$

where

$$\tau(t) = I \frac{d\omega(t)}{dt}, \quad (4.2)$$

hence the torque that is necessary to impose when a certain power is desired is the following:

$$\tau(t) = \frac{p_f(t)}{\omega(t)}. \quad (4.3)$$

It is possible to control the mechanical power flow of a flywheel storage by controlling the torque using an electric motor or, alternatively, with a mechanical transmission like a Continuously Variable Transmission (CVT)[104]. In a real system, the presence of mechanical friction and air causes the flywheel to slow down over time; to take into account losses $\tau_l(t)$ and including a controlled external torque $\tau_c(t)$, (4.1) becomes:

$$p_f(t) = (\tau_c(t) - \tau_l(t)) \omega(t) \quad (4.4)$$

with $\tau_l(t)$ being usually dependent on the rotational speed due to windage and friction losses in the bearings. Running the flywheel in vacuum and using low-friction or magnetic bearings can reduce the magnitude of $\tau_l(t)$ but in general this is a non-negligible value and it leads to high standing losses [10].

The rotational speed achievable by an actual flywheel is limited by the physical properties of the material it is composed of, the bearings, the mechanical connection to the external mover as well as the external mover itself. When rotating, the material situated at the maximum distance from the rotational axis will experience a radial force proportional to the square of the rotational speed $\omega(t)$, therefore it is not surprising that this will be the limiting factor when determining the maximum allowed speed. The maximum ideal energy capacity of a flywheel is then limited and equivalent to the kinetic energy associated with the maximum speed. A real system will also have limitations in the torque that can be handled by either the external mover (motor, CVT) or the flywheel itself, resulting in very limited power in the low speed range. An example is shown in Figure 4.1 where it is indicated the maximum power that can be delivered to a flywheel with various torque limits (from Eq. (4.1)). At low speeds the maximum allowed power is very low, and if we set an arbitrary threshold at 150 kW (dashed horizontal line) the flywheel can only operate above 750, 375 and 250 rad/s for torque limits of, respectively, 200, 400 and 600 Nm. Therefore, a real flywheel will need to operate in speed ranges that present a positive minimum speed; this

results in a lower actual energy capacity E_{max} which is expressed by the following equation:

$$E_{max} = \frac{1}{2}I(\omega_{max}^2 - \omega_{min}^2) \leq \frac{1}{2}I\omega_{max}^2 \quad (4.5)$$

with ω_{max} and $\omega_{min} > 0$ being the maximum and minimum speed, respectively. The instantaneous energy stored in a flywheel with bounded speed is the following:

$$E(t) = \frac{1}{2}I(\omega(t)^2 - \omega_{min}^2). \quad (4.6)$$

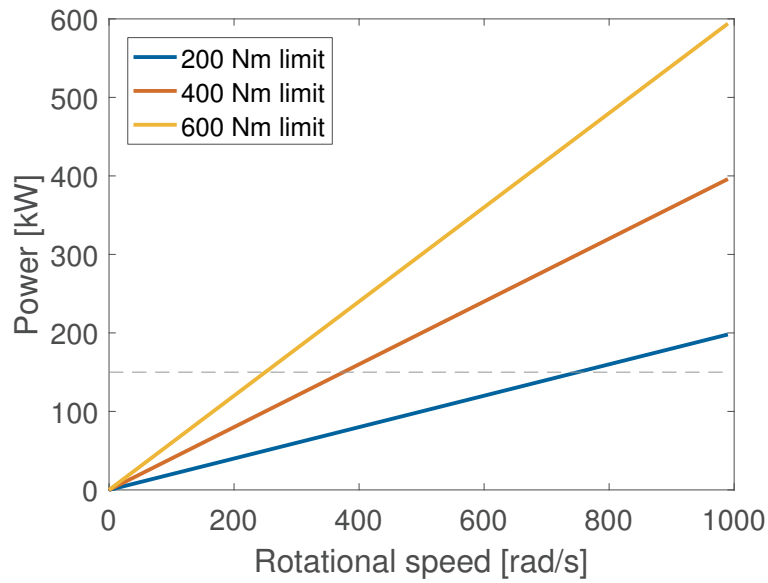


Fig. 4.1 Upper power limit that can be transferred to and from a flywheel in the presence of various torque limitations with respect to the rotational speed.

It is often useful to use the State of Charge (SoC) of an energy storage, defined as the stored energy normalised with respect to the capacity:

$$SoC(t) = \frac{E(t)}{E_{max}} \quad (4.7)$$

which, following (4.6), can be expressed as following:

$$SoC(t) = \frac{\omega(t)^2 - \omega_{min}^2}{\omega_{max}^2 - \omega_{min}^2} \quad (4.8)$$

and it is bounded between 0 and 1 during normal operation.

4.2 Sizing of storage

From the analysis performed in Section 3.6.5 and from the considerations in Section 3.9.4 it is possible to determine the possible size of the storage in order to define a set of characteristics that will be used for the rest of the research. As will be shown later, the control of energy storage is not completely dependent on the characteristics of the storage device but it is necessary to tune the parameters of the control in order to suit it for the particular system and application. In this section it will be also discussed whether it is effectively possible to build a storage of certain characteristics with current technology.

The aim of this section is to show how, in theory, a flywheel storage of the proposed characteristics is feasible and, most importantly, what are the limitations that will need to be taken into consideration when developing a control strategy.

4.2.1 Characteristics of the storage

The distribution of energy consumed by each lift occurred in 4 days of normal activity is shown in Section 3.6.5. The vast majority of lifts consume relatively little energy, with 80 % of them consuming less than 0.88 kWh. It is necessary to demonstrate that a flywheel energy storage device can be constructed with enough energy capacity to hold substantial amounts of energy and, at the same time, adhere to unavoidable constraints of size and mass. The value chosen for this demonstration is 1 kWh, which is a representative upper bound for a device that needs to store enough energy to provide meaningful performance but still not too much to eliminate the scarcity that is driving this research. As Figure 3.18a shows, 1 kWh provides enough energy to power most lifts, but some will necessary require the use of primary power, providing a realistic challenge that is the motivation for advanced supervisory control systems. For the same reason as above, the power requirement is set to 150 kW given that 80% of the lifts demand an average power of 146 kW. The range of speeds is calculated given the properties of the material that compose the flywheel as well as the maximum allowed torque (see Section 4.1).

The assumptions that will be used are: a torque upper limit of 400 Nm, a maximum rotational speed of 15000 RPM (equivalent to 1571 rad/s); both assumptions are reasonable given the existing technologies [41, 10]. Figure 4.1 indicates that, given a power requirement of 150 kW, a good choice for the minimum speed is 524 rad/s corresponding to 5000 RPM. This figure allows for a maximum power transfer of 209 kW, reasonably above the desired

150 kW. A further assumption is about the inertia of the rotor of the motor powering the flywheel, which has been set to 0.5 kg m^2 , reasonably below the typical inertia of a high speed motor. Given the figures above, it is possible to calculate the minimum inertia that a flywheel needs to possess in order to be suitable. From (4.5) it is possible to calculate the inertia required for the assembly of the motor rotor and the flywheel:

$$I = 2 \frac{E_{max}}{\omega_{max}^2 - \omega_{min}^2} = 2 \frac{3.6 \text{ MJ}}{(1571^2 - 524^2) \text{ rad/s}} = 3.2828 \text{ kg m}^2 \quad (4.9)$$

therefore the inertia of the flywheel must be no less than 2.7828 kg m^2 .

4.2.2 Example of a physical flywheel

This section tries to answer the question regarding the feasibility of a flywheel possessing the characteristics specified in the previous section by providing a plausible example. It shows how to achieve an inertia of 2.7828 kg m^2 using a glass fibre hollow cylinder which is both easy to manufacture and relatively cheap.

By selecting $L = 0.6 \text{ m}$ as the length of the cylinder and $r_{max} = 0.25 \text{ m}$ for the external diameter, and knowing that glass fibre has a density of approximately 2500 kg/m^3 [105], the resulting r_{min} is equal to 0.229 m . This ensures a minimum thickness of 21.52 mm , which is reasonable for the type of material. The total mass M of the flywheel will be the following:

$$M = \rho L \pi (r_{max}^2 - r_{min}^2) = 15.45 \text{ kg} \quad (4.10)$$

which is relatively low and feasible. The calculations for the moment of inertia of a hollow cylinder can be found in Appendix B.

4.3 Powering a flywheel

A flywheel can be powered using any electrical motor that can efficiently produce enough torque in the range of speeds specified when designing the energy storage, either directly or through a gearbox. Ideally, a motor should offer high efficiency and minimal losses and should be able to maintain high speed for relatively long periods of times (hours, in the case of applications in RTG cranes). It is often convenient to run the motor in vacuum as it reduces windage losses, therefore low rotor losses are preferred as it becomes difficult to

dissipate the heat accumulated in the rotor[32, 106]. There is a wide range of technologies available in terms of electric motors, and the most suited for the application in a flywheel energy storage are described below.

4.3.1 Induction motor

The most common electric motor has been used successfully for powering flywheels [107–109]. This kind of motor is very cheap and its widespread adoption reduces the design effort. The high rotor losses are the limiting factor, as in vacuum the only two paths for thermal dissipation are through the bearings and through radiation. This poses great limitations on the power rating of the machine, also indirectly increasing size and weight. Furthermore, at high speed this type of motor generates high iron losses and switching losses in the converter compared to other motors. For these reasons their application is very limited and it is only indicated in situations where there are no constraints in size and weight whilst budget is very limited.

4.3.2 Permanent magnet motor

Permanent Magnet (PM) motors are the most commonly used motors for flywheel energy storage systems [79, 88, 110, 111, 106] thus many applications using this technology can be found in literature [19, 112–115]. The advantages are:

- High efficiency;
- Low rotor losses;
- No excitation circuit required.

While they do not share the disadvantages of induction motors, the presence of permanent magnets limit the temperature at which the machine can operate and losses must be heavily monitored to ensure that the magnets do not get damaged by the heat. Also, other disadvantages are that PM are brittle, can be demagnetised if incorrectly operated and have a very high cost. For applications that have very strict constraints of size and weight, PM motors can be a reasonable choice, but they will inevitably cause increased budget requirements.

4.3.3 Homopolar induction motors

Homopolar motors are not widely used but they found an application in flywheel energy storage [106] due to their simplicity and low rotor losses. The robust rotor structure could also be used as the inertia element, reducing the need for an external flywheel.

4.3.4 Switched reluctance motor

Switched Reluctance (SR) motors are DC stepper motors that run by reluctance torque. Current is delivered to stator windings creating a magnetic field that forces the rotor, a solid salient-pole made of soft magnetic material, to align its pole to the nearest stator pole [116–118]. To move the rotor it is then necessary to generate a sequence of current pulses in the phases of the stator, and this is done by using modern electronic devices that also allow to shape the waveform of the current. Figure 4.2 shows a cut-out of an SR motor perpendicularly to the rotational axis. The need for high speed and high current power electronics is the reason why SR motors have only started being widely adopted recently, thanks to advances in semiconductors research[116].

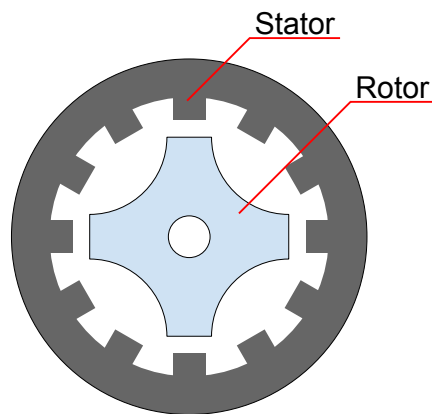


Fig. 4.2 Basic visualisation of a 6/4 switched reluctance motor.

SR motors are used in flywheel applications [108, 111, 50, 32, 48] because of the high efficiency, high robustness, low rotor losses and high temperature tolerances. In [119] SR motors have been compared with induction motors of similar size and weight showing that SR motors have superior performances. The absence of rotor windings reduce rotor losses, while the absence of permanent magnets reduce costs and temperature constraints. Given all these reasons, the SR motor is a good candidate for flywheel energy storage systems; in particular, it is a good choice for the installation in RTG cranes, as the weight and size

constraints are more relaxed compared to other applications (like electric vehicles), ruling out more expensive PM motors.

One important limitation of SR motors is the inevitable torque ripple caused by the characteristics of the motor. Carefully studied control techniques can reduce this issue [116, 120] but in a flywheel energy storage system its impact is reduced due to the high inertia that smooths speed fluctuations.

Overall, an SR motor offers more benefits with respect to the other technologies described above, therefore in this research this technology has been chosen for powering the flywheel in order to create a Flywheel Energy Storage System (FESS).

Table 4.1 summarises the comparison between the various electric motor technologies associated with flywheels.

Table 4.1 Comparison of electric motor technologies associated with flywheel energy storage.

Technology	Cost	Rotor losses	High speed capability	Converter complexity	Robustness
Induction machine	Low	High	Low	Low	High
Permanent magnets	Very high	Low	High	Low	Low
Homopolar induction	Average	Low	Average	Low	High
Switched reluctance	Average	Low	High	High	High

4.4 Control of a switched reluctance motor

For this research it will be used a 6/4 switched reluctance motor, so called as it has 6 pairs of stator poles and 4 rotor salient poles (as is shown in Figure 4.2). By running current through a stator, flux is generated and this, in turns, creates a magnetic field that attracts the rotor poles. By carefully controlling the current flow it is possible then to generate torque in the rotor in the required direction.

Voltage pulses on the stator are responsible for the magnetic flux linkage ϕ_s which is obtained integrating the difference between the stator voltage and the voltage drop across the stator resistance R_s [69]:

$$\phi_s(t) = \int_0^t (V_s(t) - R_s(t)I_s(t)) dt \quad (4.11)$$

where I_s is the stator current and V_s the voltage across the stator windings. The currents are given by a non-linear function $I_s(\phi_s, \theta)$ which is characteristic of the properties of the

stator and that are often pre-calculated in a lookup table which can be extracted from the magnetization characteristic of the particular motor. The inductance is higher when a rotor pole is aligned to a stator pole, whilst its minimum is reached in the unaligned position. In the latter, the flux increases linearly with the current amplitude, while in the aligned position the higher inductance results in a higher flux (the slope is equal to the inductance) and in this condition it also saturates at low current (growing with the lower slope given by the “saturated” inductance). Torque is produced in the direction of the movement by flux present with increasing inductance: Figure 4.3 shows the inductance with varying rotor angle and the current in the stator coil needed to produce motoring torque. When generating it is necessary first to induce current in the stator to produce flux in the aligned position, then current will be generated by the magnetised stator with a decreasing inductance (the rotor pole moves towards the unaligned position). Thus, in order to generate torque in the direction of movement, the turn-on angle (when the current starts to flow in the stator) is around 45° while the turn-off angle (when current stops flowing in the stator phase) is lower than 90° . Vice-versa, when opposing torque is required, the turn-on angle is around 0° and the turn-off angle at 45° .

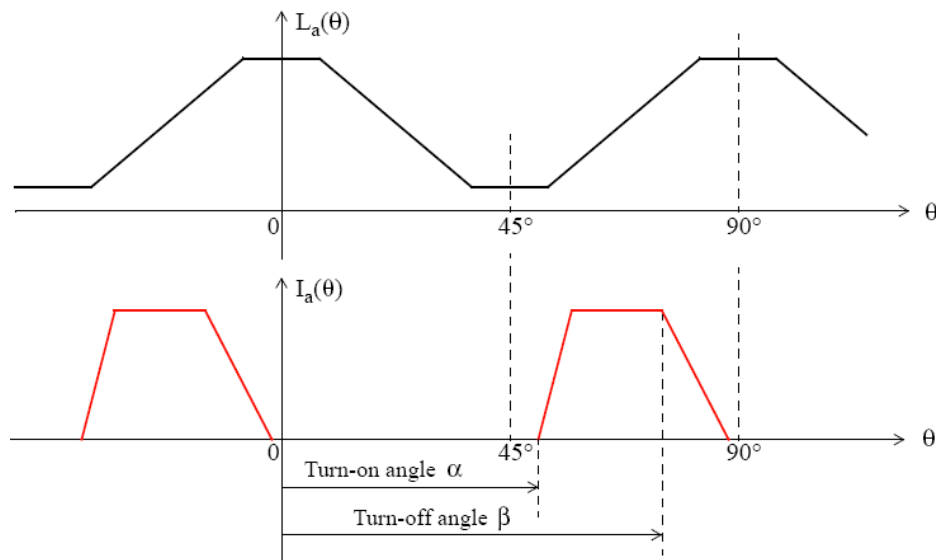


Fig. 4.3 Inductance and current of a single phase of an SR motor with respect to the rotor angle. Source: Mathworks.

In order to control the current flow in the stator, an asymmetric bridge is usually used; it is composed of one “half-leg” per phase, as shown in Figure 4.4. This configuration requires two switches, usually IGBTs, that are activated at the turn-on angle and deactivated at the turn-off angle. At low speeds it is also possible to limit the current by deactivating either

switch when it reaches a predetermined threshold, allowing the current to flow freely; at high speeds this is not necessary as usually the current does not have enough time to reach critical levels. By varying the distance between the turn-on and turn-off angle it is possible to control how much flux is generated and how much current flows into the coils (as it increases depending on the inductance), thus limiting the torque applied. While it is not necessarily a linear correlation, a fast PI control is usually enough to obtain a specific torque [116].

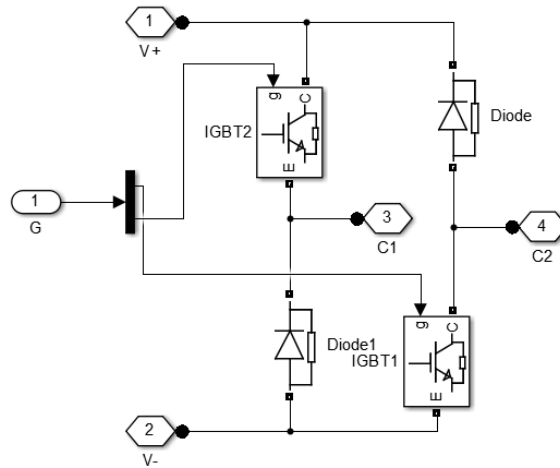


Fig. 4.4 Single phase of a SR motor converter: half leg configuration. C1 and C2 are connected to a single phase of the SR machine, V+ and V- are the positive and negative connections to a DC voltage source.

The control algorithm can be a simple pulsed control that energises the stator coils when the rotor reaches predetermined angles. This simple control is not optimised for the high speeds (5000 to 15000 RPM) required by the FESS, so a new control algorithm has been developed that changes the firing angles depending on the speed of the motor and it is shown in Figure 4.5. The control system described below is based on typical SR motor control algorithms that use lookup tables in order to determine the best on and off angles depending on the speed and torque demand[116].

The rotor angle at which the converter activates a phase is defined as α while at the angle β the semiconductors are deactivated. When generating, the default ON and OFF angles are $\alpha_0 = 82 \text{ deg}$ and $\beta_0 = 107 \text{ deg}$, respectively. The control algorithm changes them accordingly to the following formula:

$$\alpha = \alpha_0 - \frac{\omega_{RPM}}{2000}$$

$$\beta = \beta_0 + \frac{\omega_{RPM}}{1600}$$

where ω_{RPM} is the rotational speed of the rotor expressed in RPM. The ON angle moves backwards and the off angle move forwards as the speed increases, anticipating the rotation and increasing the duty cycle of the voltage pulses to compensate for the activation delay of the IGBTs and the stator high inductance. When motoring, the formula is divided in four parts, depending on the speed of the rotor.

- Zero speed (0 to 5000 RPM):
 $\alpha = 45 \text{ deg}$
 $\beta = 85 \text{ deg}$
- Low speed (5000 to 10000 RPM):
 $\alpha = 43 \text{ deg} - 0.0016(\omega_{RPM} - 5000) \text{ deg}$
 $\beta = 85 \text{ deg} - 0.001(\omega_{RPM} - 5000) \text{ deg}$
- High speed (10000 to 15000 RPM)
 $\alpha = 35 \text{ deg}$
 $\beta = 80 \text{ deg} - 0.0014(\omega_{RPM} - 10000) \text{ deg}$
- Top speed (15000 to 16000):
 $\alpha = 35 \text{ deg}$
 $\beta = 73 \text{ deg}$

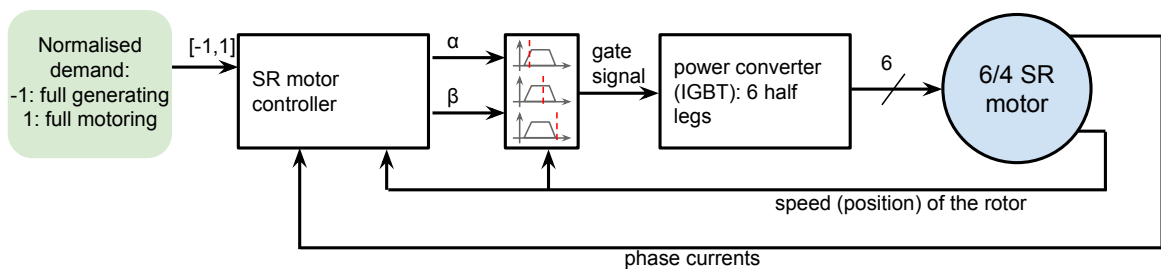


Fig. 4.5 Diagram of the low-level controller for the SR motor.

The complexity of the formula is due to the necessity to obtain a high maximum power curve along all the range of speeds. The control algorithm that manages the power flow in the ESS is expected to output a normalised control value between -1 (when fully generating) and 1 (fully motoring) and the switching angles change accordingly to this value, shrinking symmetrically. This crude controller scheme may not be good when implemented in a real system, but it gives a good approximation of a switched reluctance controller that performs adequately when linked to a high-inertia flywheel.

The controller presented in this section has been implemented in Matlab/Simulink to be included in the hybrid RTG crane model, and its implementation is presented in detail in Section 5.2.2.

4.5 Summary

In this chapter the design of a flywheel energy storage system has been introduced, presenting the definition of the requirements, the detailing of the physical constraints and the general definition of a mechanical flywheel that is suitable for the application in RTG cranes. Electric motor technologies usually associated with flywheels have been presented, in particular the switched reluctance motor which appears to be the best technological solution given the requirements. Finally, a low-level controller for a SR motor is presented, allowing the control of the power flow through the storage and finalising the foundations of a flywheel energy storage system.

This chapter demonstrated how the electrical characteristics required by the objectives can be successfully obtained by a flywheel storage device whose weight and dimensions are suitable for the applications. This ensures that the subsequent work presented later in this thesis is, in fact, based on realistic assumptions of the energy and power rating of the storage.

Chapter 5

Modelling

This thesis presents novel control strategies that have been developed in order to increase the efficiency of an RTG crane using energy storage. In order to analyse the qualities and benefits of the control strategies it is necessary to implement them in realistic scenarios consisting of RTG cranes performing normal operations.

The literature shows many works that use Matlab and Simulink to create basic RTG crane models (see Section 2.3). The objective of this chapter is to produce a more complete model that is also validated against actual measured data. This model will be used to simulate the behaviour of the crane so that it could be possible to calculate energy, power and fuel consumption in configurations that differ from the original, for example when including energy storage.

This chapter will present the process that led to the development of a validated model of a single RTG crane as well as three different models of an energy storage system which could be implemented in the RTG.

5.1 Model of an RTG crane

This section presents an RTG crane model which has been developed in Matlab/Simulink using the Simscape Power Systems toolbox [70]; this library provides basic power components which can be used to build complex power systems that accurately simulate real systems [121]. The particular crane in question has been described in detail in Chapter 3, and the key parameters are specified in Appendix A; it is the most common type of RTG crane used at

the Port of Felixstowe and has been equipped with high-accuracy measurement systems that are able to record high quality data.

In order to limit the complexity of the model of the RTG crane it was necessary to narrow down the number of components being simulated, limiting the scope to the only ones that are relevant to energy consumption and savings. From the analysis shown in Section 3.5 it is clear that the large majority of consumed and regenerated energy of a working crane is due to the hoist motor, thus it is the key element of the simulation and the subject of a very strict validation process. The hoist motor is powered by either a diesel generator (in D-RTG cranes) or a three-phase source (in E-RTG cranes) therefore the model contains elements that simulate the primary power sources of a typical crane. Other elements that are necessary for the operation of the crane have been modelled as well, and they include brake resistors, power converters and other minor capacitive/resistive elements.

The crucial feature of the model is the ability to read activity data measured on a real RTG crane (speed of the motors, weight of the container, etc.) and produce power profiles that should match those measured on a crane; this characteristic has been essential for validating the model, as it will be shown later.

5.1.1 Hoist motor

The hoist operation is performed by a three-phase induction motor with a rated power of 185 kW at the nominal speed of 700 RPM. As shown in Figure 3.4, it is connected to a common DC bus through a variable voltage and variable frequency power converter that enables four-quadrant operation. Figure 5.1 below shows the configuration that has been chosen for simulating its operation. A field oriented control system (part of the Simscape Power Systems toolbox) takes care of generating the control signal for an IGBT converter that powers the motor; this type of low-level controller has been thoroughly demonstrated to be effective and efficient [42, 43] and for this reason it has been chosen for this model.

The controller takes as input the reference speed, which is either an artificial signal or the actual speed measured on a real RTG crane, and aims to maintain the motor speed as close as possible to a reference. An external torque is applied to the motor itself, reproducing the load applied to the real motor; this external torque cannot be directly determined from the measured weight of the container due to the peculiar geometry of the hoisting mechanism, as it will be shown in the following section.

The objective that the model needs to achieve is to replicate the power output of the real motor with equal motor speed and container weight: an example of measured power and speed when the hoist motor is lifting a 19 tonne container is presented in Figure 5.2.

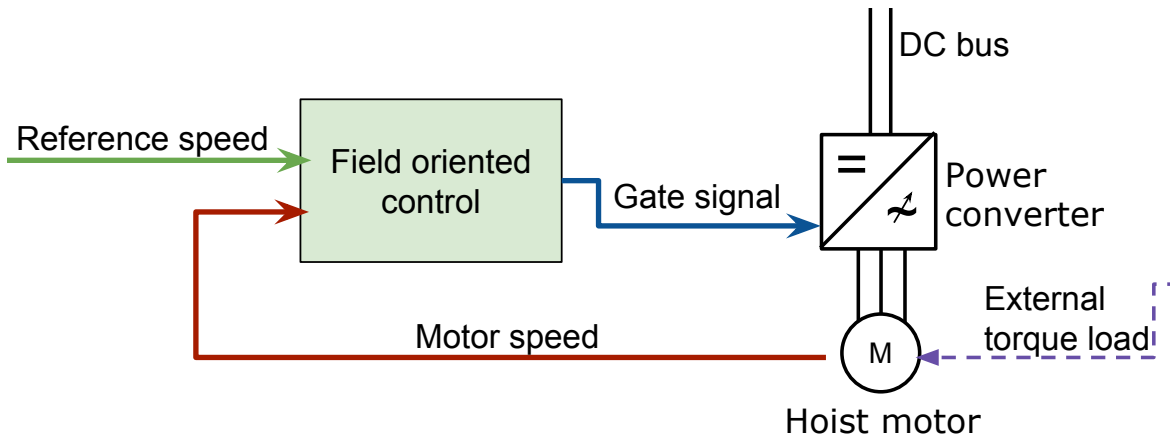


Fig. 5.1 Diagram of the electrical and control connections for the model of the hoist motor.

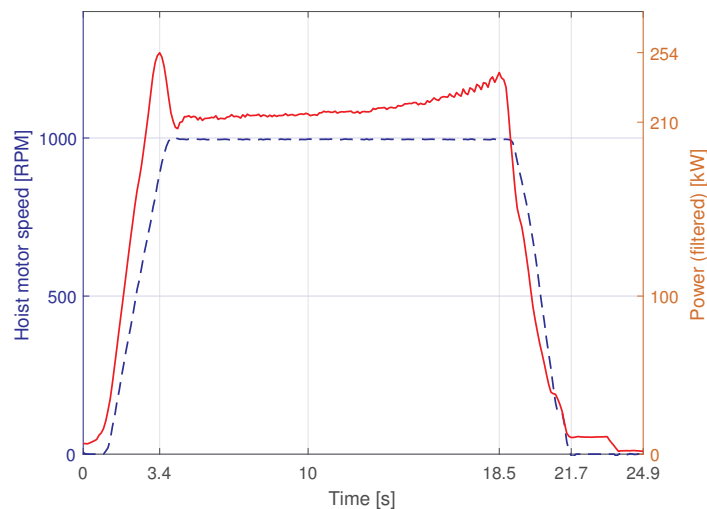


Fig. 5.2 Measured power and speed of the hoist motor when lifting a 19 tonne container.

5.1.2 Load applied to the hoist motor

The hoist geometry of a gantry crane has been historically modelled as a single rope lifting a mass whose dynamic equation were used to control the swinging [122]. Later, the research problem moved towards multi-cable spreaders with parallel cables [123, 124] which result in a constant power consumption in the steady state phase with constant rotor speed. Parallel

ropes create a configuration equivalent to the one shown in Figure 5.3 where the mechanical power $P_m(t)$ of the hoist motor only depends on the vertical speed of the container:

$$P_m(t) = (m_s + m_c)g v(t) \quad (5.1)$$

where m_s and m_c are, respectively, the spreader and container weights, g is the acceleration of gravity (constant) and $v(t)$ is the instantaneous vertical velocity of the load. With constant mass and velocity, the mechanical power is constant, as well as the torque T at the motor:

$$T = \frac{d_{drum}}{2n_{red}}g(m_s + m_c) \quad (5.2)$$

where d_{drum} is the diameter of the hoist drum and n_{red} is the reduction ratio of the transmission.

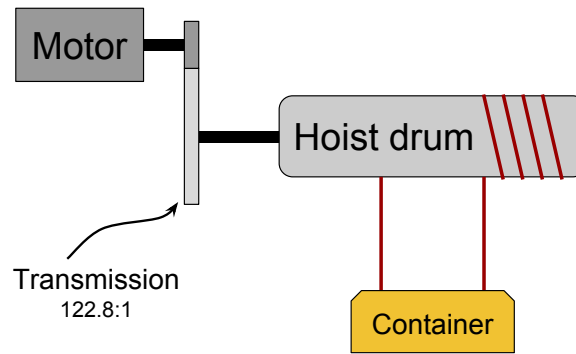


Fig. 5.3 Mechanical system of the hoist motor with parallel ropes.

By analysing data acquired on RTG cranes at the Port of Felixstowe it was observed that the power demand cannot be modelled only by calculating (5.1), as the demand is not constant during a constant speed phase. Figure 5.2 and, in more detail, Figure 5.4 show how power demand increases during the lifting phase, even with constant speed. The same behaviour, reversed, also occurs when lowering the container. This is due to the peculiar geometry of the crane hoisting mechanism that uses non-parallel cables, causing an increase in power demand with container height because of the changing vertical angle of the ropes: when the container is at the top, the power consumption (per unit of time) is higher due to the different rope angle [74].

The hoist motor is connected to the hoist drum through a reducer with a ratio of 122.8:1, which is then attached to the eight wire ropes that pass across sheaves; the ropes are then connected to the headblock, each rope forming the same angle with respect to the vertical axis.

For the purposes of calculating container position and speed, only one rope is considered in the simplified geometry (Figure 5.6), assuming that the ropes contribute evenly to transfer the forces (due to gravity and inertia) from the container to the hoist drum and that the mass is restricted to only move vertically.

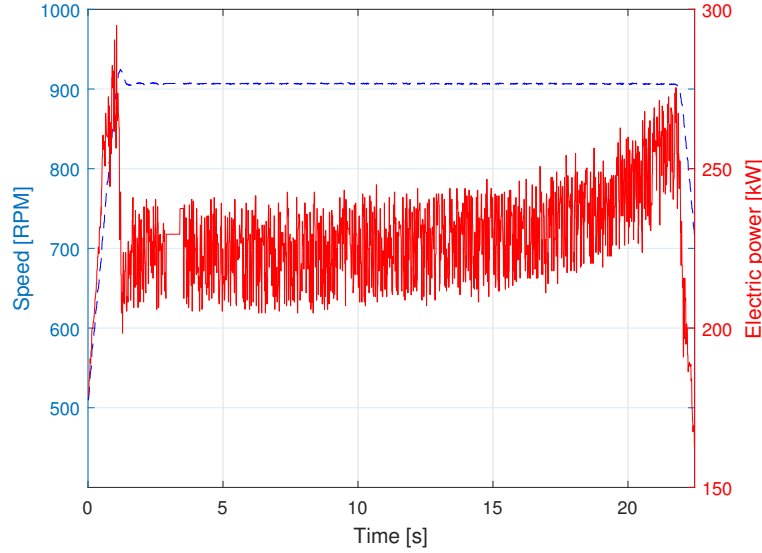


Fig. 5.4 Hoist motor speed (dashed blue line) and hoist motor power consumption (red) when lifting a 25 t container.

Kinematics

Defining $c(t)$ as the length of a hoist rope at time t in meters, we assume that only the value of the speed $\dot{c}(t)$ is known, and it is calculated as:

$$\dot{c}(t) = -\frac{\omega_{hoist}(t) d_{drum}}{n_{red} 2\pi} \quad (5.3)$$

where ω_{hoist} is the angular speed of the hoist motor in rad/s (known), $n_{red} = 122.8$ is the gear ratio of the reducer and $d_{drum} = 1.285$ metres is the diameter of the drum; $\dot{c}(t)$ is integrated to obtain the value of the rope length at time t . From the crane's schematics the range of values of $c(t)$, $b(t)$ and $\theta(t)$ have been extracted and are presented in Table 5.1. The initial condition $c(0)$ is unknown so it is initially chosen from the range of admissible values and then during the integration of $\dot{c}(t)$ the value of $\theta(t)$ is calculated at each interval verifying that it does not step out of the boundaries, in which case the initial condition $c(0)$ is changed

accordingly. In case it happens, the integration is restarted and the cycle is repeated until a suitable initial condition is found.

From the geometry in Figure 5.6 it can be seen that the value of $c(t)$ is linked to the values of lengths a and $b(t)$:

$$c(t)^2 = a^2 + b(t)^2.$$

The value of a measured from the crane schematics provided by the manufacturer is approximately 2.640 m. Assuming that $c(t) > a \forall t$, the vertical position $b(t)$ is the following:

$$b(t) = \sqrt{c(t)^2 - a^2} \quad (5.4)$$

and speed of the container $\dot{b}(t)$ is then:

$$\dot{b}(t) = \frac{d}{dt} \sqrt{c(t)^2 - a^2} \quad (5.5)$$

$$= \frac{c(t)}{\sqrt{c(t)^2 - a^2}} \dot{c}(t). \quad (5.6)$$

Equation (5.5) implies that when the hoist motor speed is constant (and $\dot{c}(t)$ is constant) the vertical speed of the container changes with the length of the rope $c(t)$. The vertical speed of the container and the rope speed have a ratio which then depends on $c(t)$:

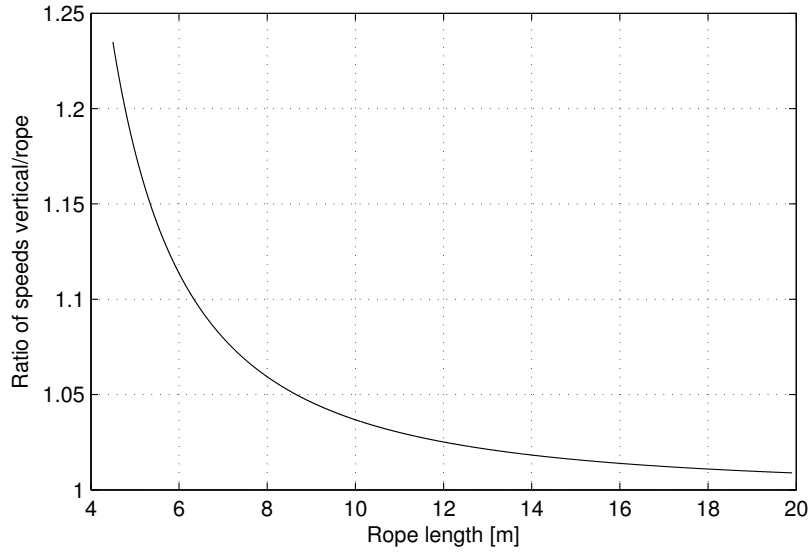
$$\frac{\dot{b}(t)}{\dot{c}(t)} = \frac{c(t)}{\sqrt{c(t)^2 - a^2}}. \quad (5.7)$$

The ratio in (5.7) is plotted in Figure 5.5 and it is noticed that, with constant hoist motor speed, the vertical container speed $\dot{b}(t)$ increases as the rope length $c(t)$ decreases. The angle $\theta(t)$ varies as the container moves vertically:

$$\theta(t) = \arcsin \left(\frac{a}{c(t)} \right).$$

Table 5.1 Measured ranges of rope length c , container vertical position b and rope angle θ .

$\forall t$	Maximum height	Minimum height
$c(t)$	4.200 m	19.908 m
$b(t)$	3.643 m	19.732 m
$\theta(t)$	$\approx 39^\circ$	$\approx 7.4^\circ$

**Fig. 5.5** Ratio between vertical speed and rope speed in function of rope length.

The vertical acceleration can be calculated by further differentiating the speed:

$$\ddot{b}(t) = \frac{d}{dt} \left(\frac{c(t)\dot{c}(t)}{\sqrt{c(t)^2 - a^2}} \right) \quad (5.8)$$

$$= \frac{c(t)\ddot{c}(t) + \dot{c}(t)^2}{\sqrt{c(t)^2 - a^2}} - \frac{c(t)^2\dot{c}(t)^2}{(c(t)^2 - a^2)^{3/2}} \quad (5.9)$$

$$= -\frac{c(t)(a^2 - c(t)^2)\ddot{c}(t) + a^2\dot{c}(t)^2}{(c(t)^2 - a^2)^{3/2}}. \quad (5.10)$$

Limiting the calculations in the constant hoist motor speed phase, i.e. $\ddot{c}(t) = 0$, Equation (5.10) can be simplified:

$$\ddot{b}(t) = -\frac{a^2\dot{c}(t)^2}{(c(t)^2 - a^2)^{3/2}}. \quad (5.11)$$

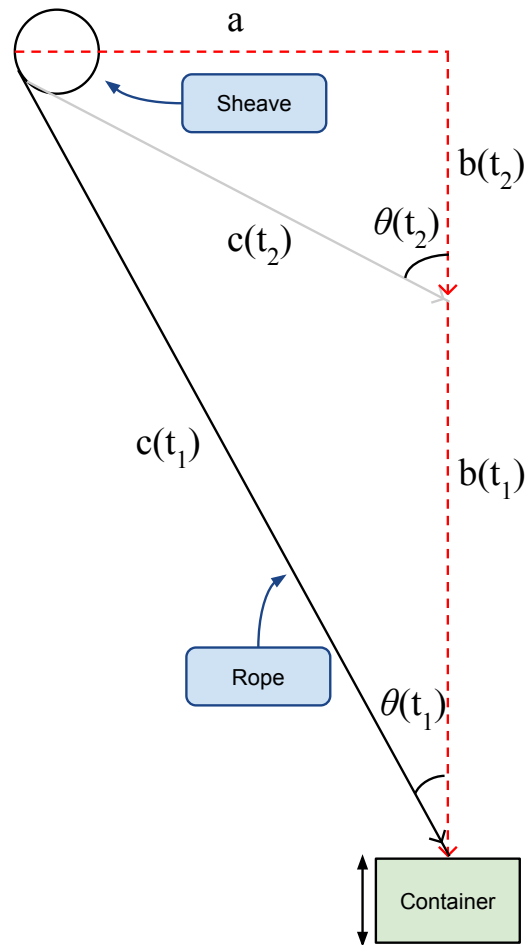


Fig. 5.6 Simplified 1-rope geometry of the hoisting mechanism. At time t_1 the container vertical position is lower so $b(t_1)$ and $c(t_1)$ are higher, therefore angle $\theta(t_1)$ is smaller. At time t_2 the vertical position is higher.

The vertical acceleration, which varies depending on the height of the container, will be used to calculate the load torque on the motor.

Dynamics

To calculate the hoist motor power flow $p_L(t)$, an instantaneous load torque input $T(t)$ is needed as well. As already stated, the power consumption increases with the container height when the speed is constant. The motor mechanical power $P_m(t)$ is proportional to the torque $T(t)$ times the rotational speed $\omega(t)$; it is then evident that the variable that changes with height is the torque. In Figure 5.7 it can be seen that a torque $T(t)$ is applied to the hoist drum causing it to lift the container by applying equal forces \vec{F}_1 and \vec{F}_2 whose sum results in the

vector \vec{F}_b . By calculating the magnitude of \vec{F}_b and the value of the angle $\theta(t)$ it is possible to calculate the torque which the motor needs to apply to the drum (of known diameter). The vector \vec{F}_b is the sum of two symmetrical components:

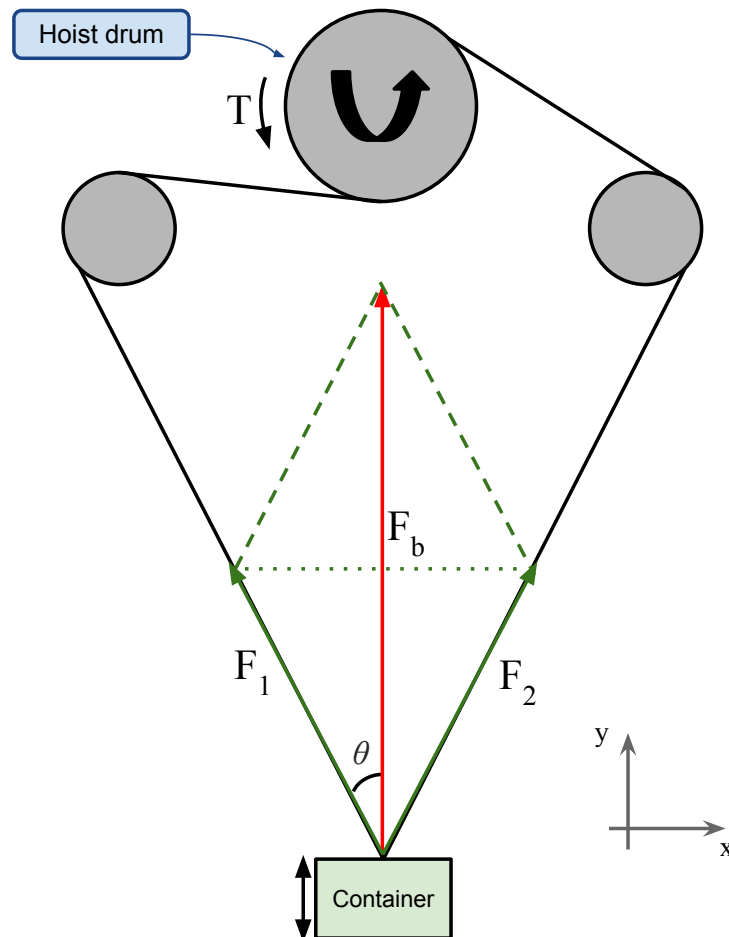


Fig. 5.7 Forces imposed by the hoist motor on the container when lifting.

$$\vec{F}_b = \vec{F}_1 + \vec{F}_2$$

and the modulus depends on the vertical components as the horizontal components cancel out:

$$|\vec{F}_b| = F_{1,y} + F_{2,y} = 2F_{1,y}$$

with $F_{n,y}$ being the component on the y-axis of \vec{F}_n . The component $F_{1,y}$ can be calculated from the values of $\theta(t)$, a and $c(t)$ (from Figure 5.6):

$$\sin(\theta(t)) = \frac{a}{c(t)}$$

$$\cos(\theta(t)) = \sqrt{1 - \frac{a^2}{c(t)^2}}$$

$$F_{1,y}(t) = |\vec{F}_1(t)| \cos(\theta(t)) = |\vec{F}_1(t)| \sqrt{1 - \frac{a^2}{c(t)^2}}.$$

The magnitude of the force vector \vec{F}_1 that needs to be applied to generate a vertical force \vec{F}_b on the container is then:

$$|\vec{F}_1(t)| = \frac{|\vec{F}_b(t)|}{2\sqrt{1 - \frac{a^2}{c(t)^2}}}. \quad (5.12)$$

At rest, the only force that the hoist motor needs to compensate is gravity. However, when the container is moved the sum of forces acting on the mass is:

$$\vec{F} = (m_s + m_c)(\vec{g} + \ddot{b}(t)\vec{u}_y) + \vec{F}_b = \vec{0}$$

$$|\vec{F}_b| = (m_s + m_c)(|\vec{g}| + \ddot{b}(t))$$

where $m_s = 13000$ kg is the mass of headblock and spreader, m_c is the mass of the container, \vec{g} is the acceleration given by gravity, \vec{u}_y is the unit vector in the positive y direction and $\ddot{b}(t)$ is the instantaneous vertical acceleration imposed by the hoist motor as calculated in (5.11). Given the diameter d_{drum} of the drum, the torque $|\vec{T}_d|$ that needs to be applied to the drum is then:

$$|\vec{T}_d| = |\vec{F}_b| \frac{d_{drum}}{2} \quad (5.13)$$

and, taking into account the presence of a reducer with ratio n_{red} , the hoist motor must provide the following instantaneous load torque T :

$$T(t) = \frac{1}{n_{red}} \frac{(m_s + m_c)(g + a_c(t)) d_{drum}}{\sqrt{1 - \frac{a^2}{c(t)^2}}}. \quad (5.14)$$

When the container is at rest, $\ddot{b}(t) = 0$ and the only acceleration acting on the container is gravity:

$$T(t) = \frac{d_{drum} g(m_s + m_c)}{2n_{red} \sqrt{1 - \frac{a^2}{c(t)^2}}}. \quad (5.15)$$

If it is possible to measure the vertical position of the spreader, the value of $c(t)$ can be calculated directly from $b(t)$ using (5.4) resulting in a more accurate calculation as the integration step can be skipped, increasing the accuracy.

Validation of hoist load calculations

A proper validation of the power demand with the torque load calculations shown above will be presented later in this chapter as the whole model of the crane is run and compared to the measurements. Nonetheless, it is possible to show that (5.15) provides an output that lies between upper and lower limits calculated from known values.

The torque T_{rest} that a hoist motor needs to provide to keep a 10 tonne container at rest can be calculated as:

$$T_{rest} = \frac{d_{drum} g(10 + m_s)}{2n_{red}} \quad (5.16)$$

$$= \frac{9.81 \text{ m/s}^2 \cdot (10 \text{ e}3 \text{ kg} + 13 \text{ e}3 \text{ kg}) \cdot 1.285 \text{ m}}{2 \cdot 122.8} \quad (5.17)$$

$$= 1180 \text{ Nm}. \quad (5.18)$$

Measurements were taken during a controlled test consisting in lowering and lifting a 10 tonnes container. The values of $\dot{c}(t)$ (and, by integration, $c(t)$) have been extracted and used in (5.14) in order to calculate the load torque on the motor. The result is shown in Figure 5.8. The gray signal of the calculated torque is highly sensible to noise in the hoist rotor speed measurement; for this reason the moving average of the torque value is also shown. Assuming no vertical acceleration beside gravity and rope length spanning the whole admissible range, equation (5.15) indicates an expected torque range of approximately 1191 to 1518 Nm during the whole movement, confirming the validity of the results shown in Figure 5.8.

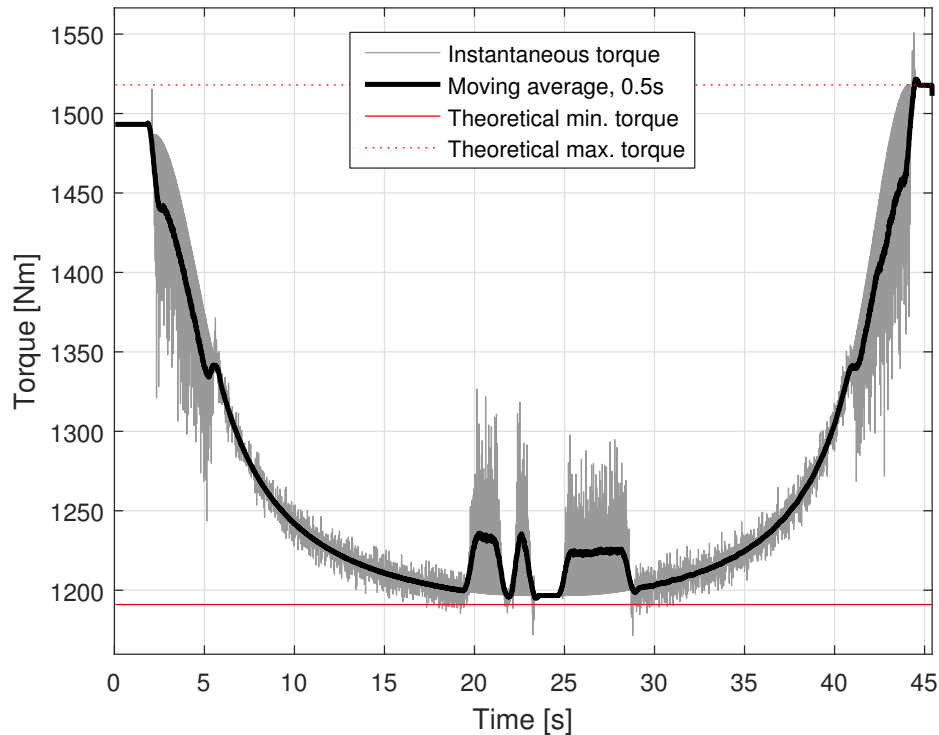


Fig. 5.8 Load torque on the hoist motor calculated from mass and acceleration of the container and the geometry of the system. A 10 t container is lowered (first 23 seconds) and later it is raised again to approximately the same height. The boundaries (in red) are the theoretical maximum and minimum values for the calculated torque.

5.1.3 Primary source

In order to assess the impacts that a control strategy has on the energy and power consumption of a crane, it is necessary to accurately model the primary power source of a crane, which can be either the terminal power network or a diesel generator.

Diesel generator

Diesel powered RTGs are widespread but are being phased out due to environmental regulations and energy costs [75, 78, 76]. They still account for high fuel consumption and it may be interesting to calculate how much fuel is consumed by a crane and how much is saved by using energy storage associated with various control techniques.

Validated and accurate models of diesel generators exist in the literature and are used to calculate the estimated fuel consumption of an engine [125, 126]. Information on the engine used by the crane is limited, therefore it has not been possible to accurately model the diesel

generator and, instead, it has been preferred to model the fuel consumption using information provided by manufacturer (Table 5.2); this has the added benefit of reducing the complexity of the model as it avoids modelling the mechanical dynamics that are not of interest in this research.

Table 5.2 Volvo Penta TAD1641GE diesel generator fuel consumption [82].

Power [kW]	Specific fuel consump. [g/kWh]	Instantaneous fuel consump. [g/s]
137	217	8.83
273	197	15.6
410	196	23.1
546	200	31.9

The instantaneous fuel consumption appears to be proportional to the power output, therefore it has been decided to interpolate those values in order to estimate the fuel consumption throughout all possible power outputs. For the interpolation, a Piecewise Cubic Hermite Interpolating Polynomial (PCHIP) has been chosen to use [127, 128]. It is a variant of cubic Hermite interpolation that, unlike methods like *Spline* and *Bessel*, preserves monotonicity avoiding “bumps” and overshoots in the resulting signal. Figure 5.9a shows the data points along with the interpolated and extrapolated values for the instantaneous fuel consumption; those interpolating values will be used in the model in order to calculate the fuel consumption of the diesel generator. Figure 5.9b shows instead the specific fuel consumption at various power levels.

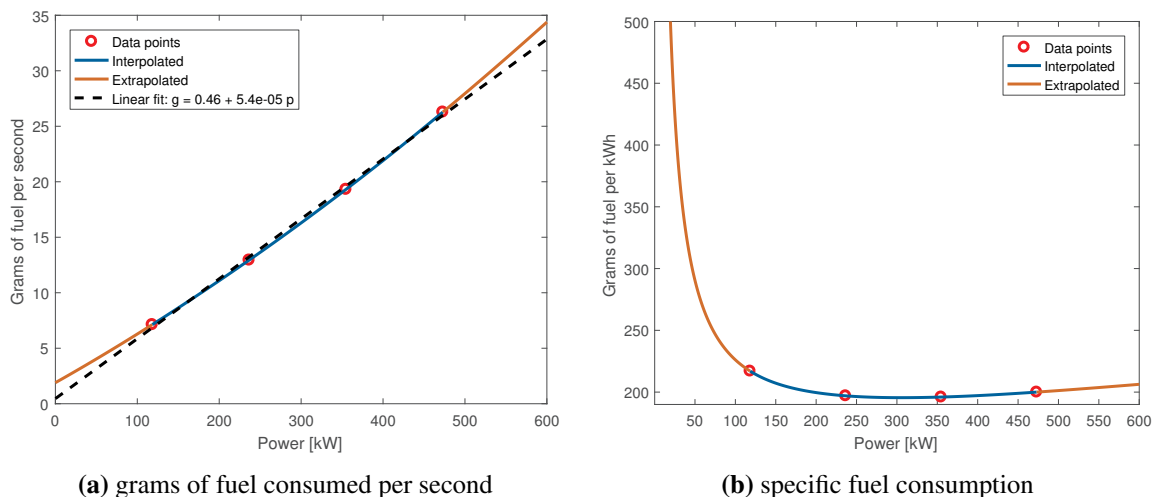


Fig. 5.9 Fuel consumption of a Volvo Penta TAD1641GE diesel generator with interpolated and extrapolated values.

It was not possible to obtain high-quality measurements for the fuel consumption of an RTG crane yet, therefore the diesel generator model could not be included in the validated model. Nonetheless, estimations on the fuel consumption will be used to assess and compare control strategies when reducing CO₂ emissions caused by the combustion of diesel fuel.

E-RTGs and Active Front-End

Container terminals are starting to introduce E-RTGs or to convert D-RTGs into E-RTG cranes, reducing the global amount of D-RTG cranes in circulations. In E-RTGs the primary source can be simply modelled as an ideal three-phase power source as the scope of the research does not include the study on power quality. On the real crane used for the analysis the three-phase source is connected to the container terminal power network and powers the motors through a diode rectifier (see Figure 3.4) which cannot offer regeneration into the grid. It is interesting, though, to assess the potential benefits of adding regenerative capabilities to a crane by substituting the diode rectifier with an Active Front-End (AFE).

The main use for AFEs in the generic application is to improve the power quality, both reducing harmonics and stabilising the power factor to the desired value, and their use is widespread and well documented [97, 98, 100, 101, 1]. Crane manufacturers are equipping new models of E-RTGs with AFEs in order to obtain high power quality, reducing the total harmonic distortion to around 3%, which is an order of magnitude less than what achieved with passive filters [102, 103]. The regenerative feature of an AFE could potentially reduce the energy consumption of a container terminal if the energy recovered from one crane is simultaneously used by other cranes. The reduction of energy consumption directly translates into a reduction in costs and greenhouse gas emissions; it could also lower the stress on the terminal's electric network as the regenerated power can feed neighbouring cranes causing a reduction in the peak power demand. Its regenerative capability make them similar to energy storage in terms of recovering otherwise wasted energy; therefore, it is crucial to determine their qualities and compare them with energy storage: an energy storage controlled by a good control strategy should perform better than an AFE.

Modelling of Active Front-End

An AFE is incorporated into the model using a Voltage Source Converter (VSC). The VSC has been modelled using an averaged model that preserves the dynamics from the interaction between the control system and the power system. The averaged model allows for faster

simulations but it cannot represent harmonics; nevertheless, the research is focused on the regenerative capabilities and not on the improvement of power quality.

The VSC is controlled using a control system (Figure 5.10) developed in [129–131] which has been adapted for the use in an RTG crane. The controller aims to regulate the DC bus voltage by setting the reference current of the VSC in the dq0 coordinate system. This controller is also designed to eliminate the reactive currents on the AC side maintaining a constant power factor of 1. In order to regulate the DC voltage, a PI controller reads the voltage error and sets the I_d reference current accordingly; the I_q and I_0 reference values are set to 0 in order to maintain a balanced system and eliminate reactive power. The current reference in the dq0 space is sent to a second PI controller that controls the current flow through the VSC [101, 132].

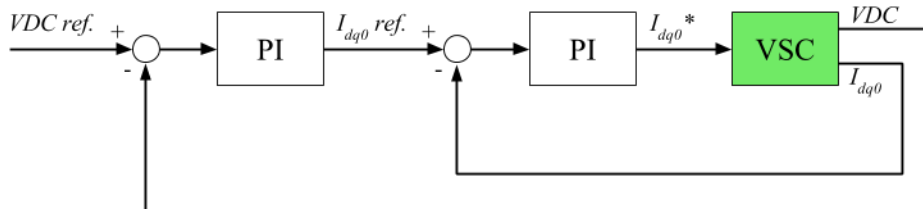


Fig. 5.10 VSC control system used in the model. VDC and $VDCref$ indicate the DC voltage and the reference value; I_{dq0} , I_{dq0ref} and I_{dq0}^* indicate, respectively, the current in the dq0 coordinate system, the reference value generated by the first PI controller and the current imposed by the second PI to the VSC.

In a standard crane fitted with a diode rectifier the DC voltage decreases as the hoist motor draws power when lifting; the voltage then increases when the motor regenerates into the DC bus during the lowering phase, ultimately reaching the voltage threshold at which the brake resistors activate (750 V). The power will then move from the grid to the crane (positive I_d and positive power) when the hoist motor is lifting a container, and it will move in the opposite direction (negative I_d and power) during a lowering. A crane equipped with the modelled AFE will not see the DC bus voltage deviating significantly from the constant value due to the controller action. The AFE effectively prevents the activation of the brake resistors by not allowing the DC bus voltage to reach the 750 V threshold of the brake resistor, therefore no energy is dissipated.

5.1.4 Additional secondary elements of the model

Brake resistors

When a motor on the crane is regenerating power and no energy storage system (or AFE) is present, the excessive energy is dissipated into resistor banks that convert it into heat. Brake resistors are often designed to activate when the DC bus voltage reaches a predetermined threshold which is usually much higher than the standard voltage level, in order not to interfere in any other crane activity.

In the model the brake resistors have been implemented by using a resistor connected to the dc bus through an ideal switch (Figure 5.11). The switch is controlled by a PWM generator with a switching frequency of 1 kHz whose duty cycle is given by a signal which is the difference between the activation threshold and the instantaneous voltage multiplied by 0.2; with an activation threshold of 745 V, the duty cycle will be 100% when the voltage reaches 750 V, emulating what is happening on the crane.

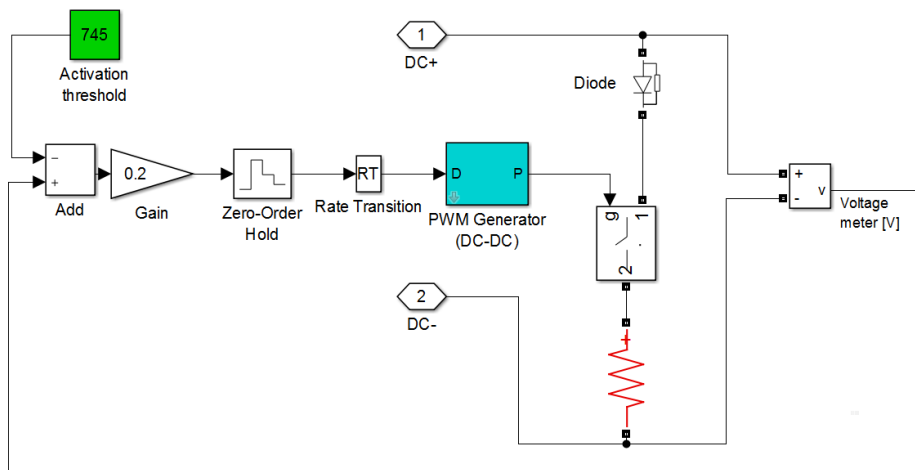


Fig. 5.11 Simulink model of the brake resistor and resistor chopper.

DC capacitors and persistent power draw

The crane is equipped with large capacitors installed on the DC bus in order to smooth voltage fluctuations. On the crane under analysis there is a total of 38 capacitors rated at 6 mF on the DC bus, for a total capacitance of 228 mF. An ideal 228 mF capacitor has been installed on the DC bus of the model in order to emulate the real ones and their smoothing effect on voltage fluctuations.

From the measurements it has been found that the crane motors consume 5 kW when in standby and not operating. The cause of this power draw has not been identified, however it is possible that the electric motors, power converters and other elements attached to the DC bus cause this small power draw. For example, capacitors, diodes and other elements may be affected by leaking currents; snubber elements may cause power loss due to voltage fluctuations. Although improbable, the current transducers used for measurements may also be affected by a small bias. Nonetheless, the standby power draw has been modelled by connecting a current source between the DC lines.

5.1.5 Validation of the RTG model

The final version of the model, shown in Figure 5.12, has been subjected to an extensive validation using high resolution data collected on an RTG crane by the UoR during 25 days, starting on the 15th of April 2016 till the 10th of May 2016. The validation process focused on assessing the accuracy of the model when replicating the power and energy consumption of the real crane.

Regarding power consumption, the statistical measure chosen for determining the quality of the simulation is the coefficient of determination R^2 [133] which is defined as follows:

$$R^2 = 1 - \frac{\sum_{i=0}^N (y(i) - x(i))^2}{\sum_{i=0}^N (y(i) - \bar{y})^2} \quad (5.19)$$

where $x(i)$ and $y(i)$ are, respectively, the simulated and measured power from sample 0 to N , and \bar{y} is the mean value for $y(i)$. A value of R^2 higher than 0.5 indicates that the model is a better representation of the system compared to the average value, while $R^2 = 1$ indicates a perfect representation and it is the highest value that R^2 can reach for this particular formulation and model. Unlike the power consumption, evaluating the accuracy of the energy consumption is straightforward as the energy consumed, regenerated and net can be compared directly with the measured one.

The model has been validated firstly when performing a single sequence of lift cycles. Figure 5.13 shows the power consumption of the crane performing a series of lifts lasting 5 minutes, and the simulation power output has an R^2 value of 0.90. Single lifts are simulated with higher accuracy, as in the example shown in Figure 5.14 where the R^2 metric reaches 0.93.

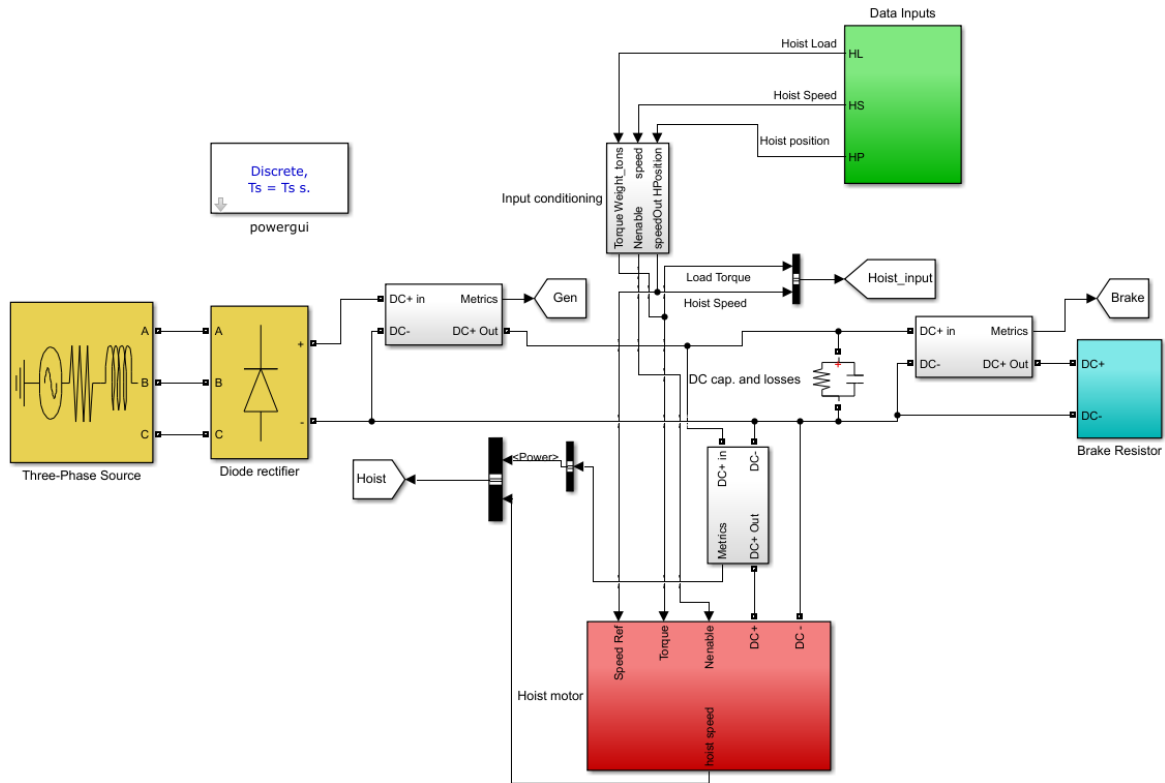


Fig. 5.12 Simulink model of the RTG crane. On the left, the primary power supply and the diode rectifier. At the top, the data inputs that are processed in order to be fed to the model. At the bottom, the hoist motor. On the right, the passive components of the DC bus and the brake resistors.

In order to validate the model for long term simulations, measurements have been taken during a typical day (24 hours) during normal operation, then the same activity has been simulated for the same duration using the data collected. The results for both the measurements and the simulation are shown in Figure 5.15, Table 5.3 and Table 5.4, where it can be noted that the simulation accurately reproduces the power ($R^2 = 0.88$) and energy flows (error $< 5\%$) of the real crane. From these results it is clear that it is now possible to use the model presented in this section for testing various control strategies for energy storage and also assess their benefits in an RTG crane. However, before being able to test the control strategy, it is necessary to use a model of the energy storage system. The next section is dedicated on modelling the energy storage system to be implemented in the model of the RTG crane.

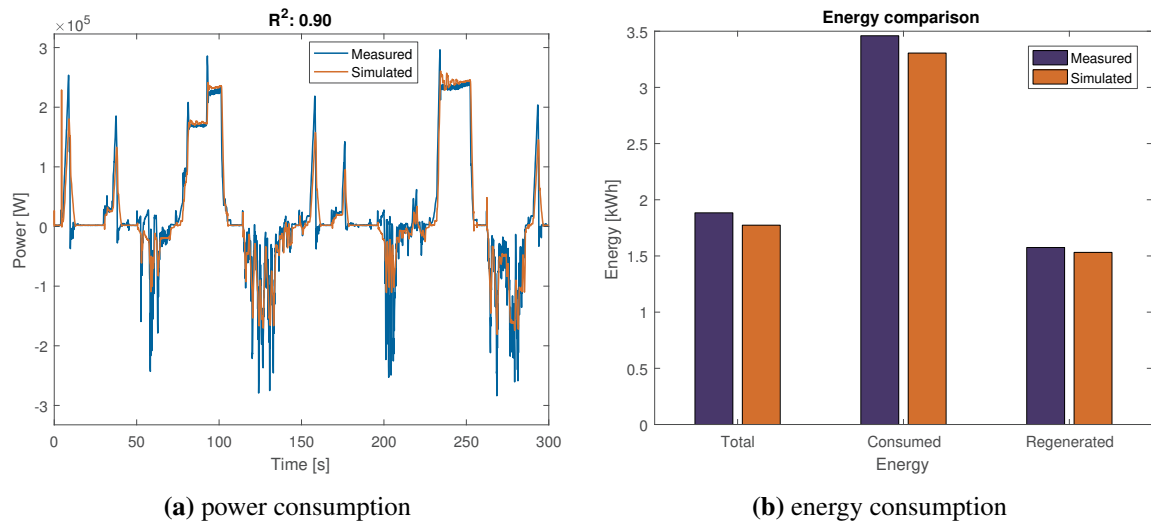


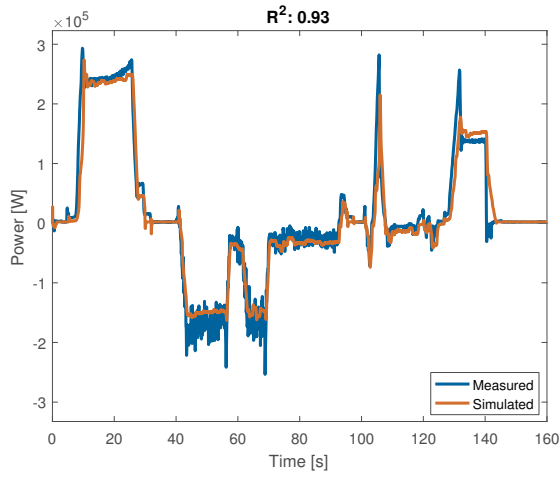
Fig. 5.13 Comparison of measured and simulated data showing a series of lift cycles accurately simulated by the RTG model.

Table 5.3 Energy consumption, as measured and simulated, of a single RTG crane for a duration of 24 hours.

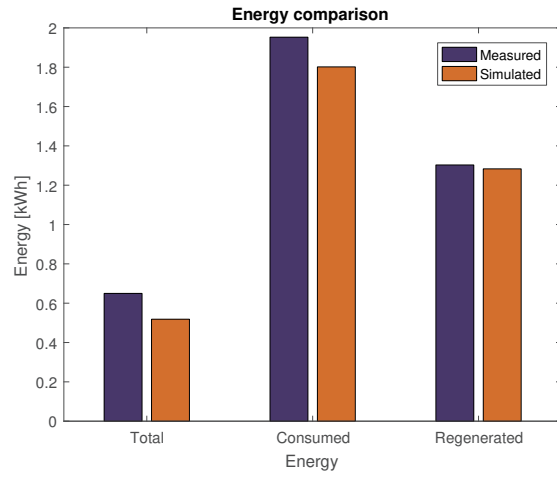
	Net energy	Consumed	Regenerated
Measured [kWh]	112.18	239.30	127.12
Simulated [kWh]	106.63	228.34	121.71
Error [%]	4.95	4.58	4.26

Table 5.4 RTG model validation results for power flows.

Test time duration	R^2 coefficient ($R^2 \in (0,1)$)
Single lift cycle (160 s)	0.93
5 minutes	0.90
24 hours	0.88

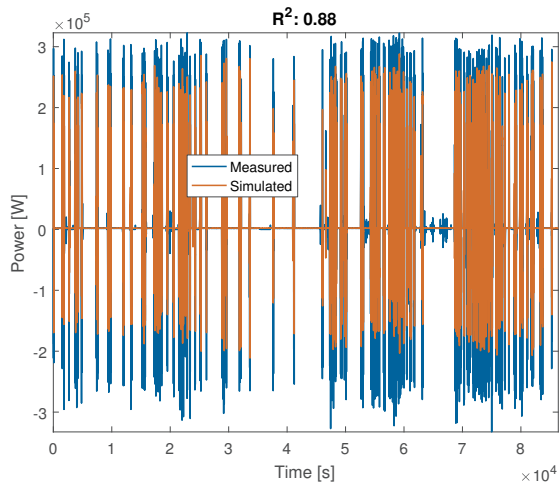


(a) power consumption

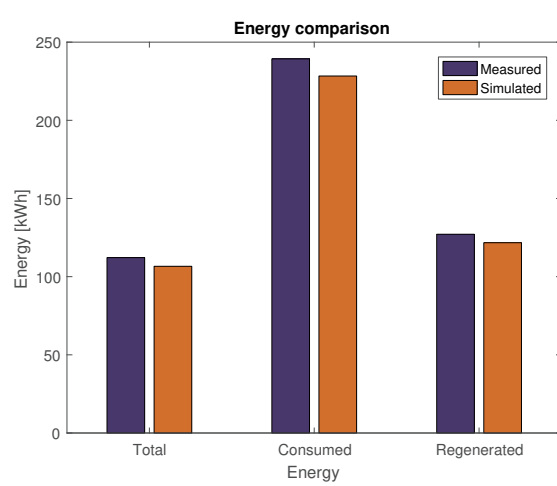


(b) energy consumption

Fig. 5.14 Comparison of measured and simulated data showing a single lift cycle accurately simulated by the model.



(a) power consumption



(b) energy consumption

Fig. 5.15 Comparison of measured and simulated data for long-term simulation (24 hours) of the RTG crane.

5.2 Model of energy storage

With the availability of a validated model of an RTG crane it is possible to start experimenting with solutions that could increase the efficiency of RTGs, all without impacting on the operation of real cranes or using expensive electrical equipment.

A key element needed for analysing the impacts and benefits of the work presented in this thesis is an accurate model of energy storage. During the course of the research, three models were developed, refined and implemented. Each model has its advantages and disadvantages with respect to the others and the following sections describe the development and the characteristics of each.

5.2.1 Generic energy storage model

An energy storage is a device that can absorb substantial amounts of energy from a system and deliver it back when requested. A control system usually is designed to output a desired instantaneous power flow when requested up to a certain power limit, storing energy up to the maximum capacity and it is inherently characterised by losses and other dynamics. The idea behind a generic storage model is that to produce a system that behaves like a typical storage system without modelling the electrical, mechanical or electrochemical dynamics behind it.

In order for a model to be generic, it needs to be able to reproduce the most common storage technologies only by changing its parameters. Therefore, a generic model has been developed that is characterised by a limited number of parameters that are associated with the main features of a storage system and can be chosen depending on the application.

Three-phase generic energy storage

Initially it has been decided to develop a storage system designed to be connected to a three-phase network. It is formed of three controlled current sources that are governed by a control unit that impose a current waveform whose amplitude depends on the power demanded; frequency and phase of the current are synchronised to the three-phase network the storage is connected to. The control unit also calculates the amount of energy stored, ensures that energy stored does not become negative or goes above maximum capacity and also takes into account of the losses. The parameters that can be chosen are shown below.

- Reference voltage [V]
- Maximum power [kW]
- Energy capacity [MJ]
- Starting energy [MJ]
- Recharge factor

The model implemented in Simulink is shown in Figure 5.16 and Figure 5.17 shows an example of the simulation of this system.

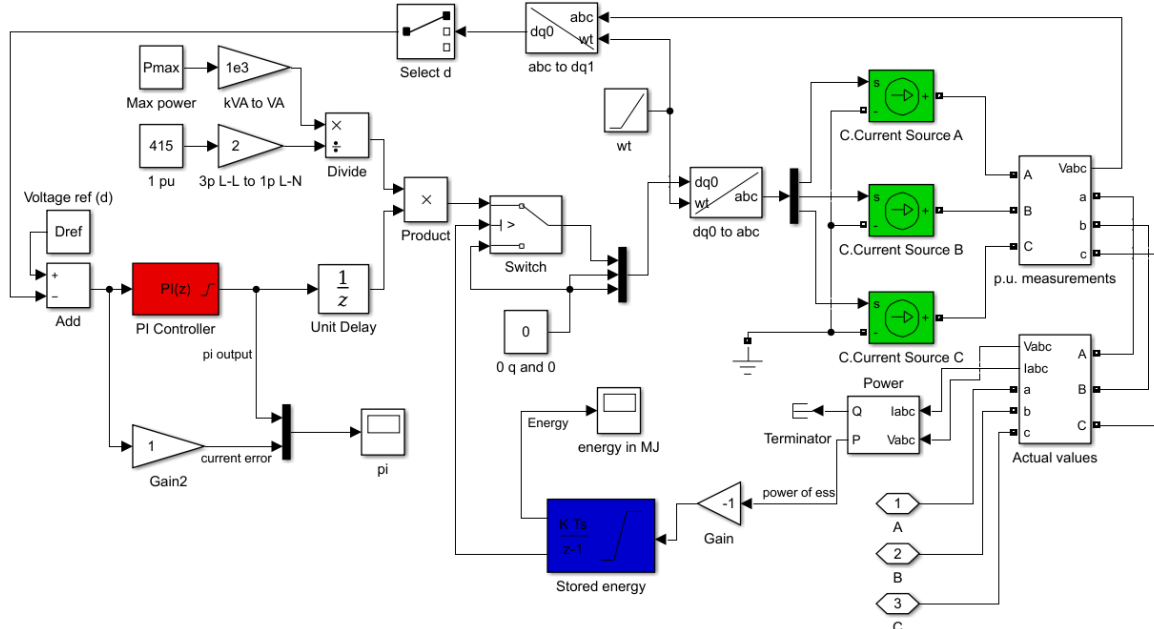


Fig. 5.16 Simulink model of the three-phase energy storage system. Note, on the left, the PI controller and, on the right, the three controlled current sources. The blue block at the bottom is responsible for calculating the amount of energy stored.

This model has been used in [134] as it is now exclusively implemented in simulations that involve a network of container cranes. For storage located inside RTG cranes it is more appropriate to model DC storage systems that connect directly to the internal DC bus.

DC generic energy storage system

Batteries and supercapacitors are often connected to DC networks as they work naturally in DC. Flywheel energy storage, on the other hand, are powered by electrical machines which

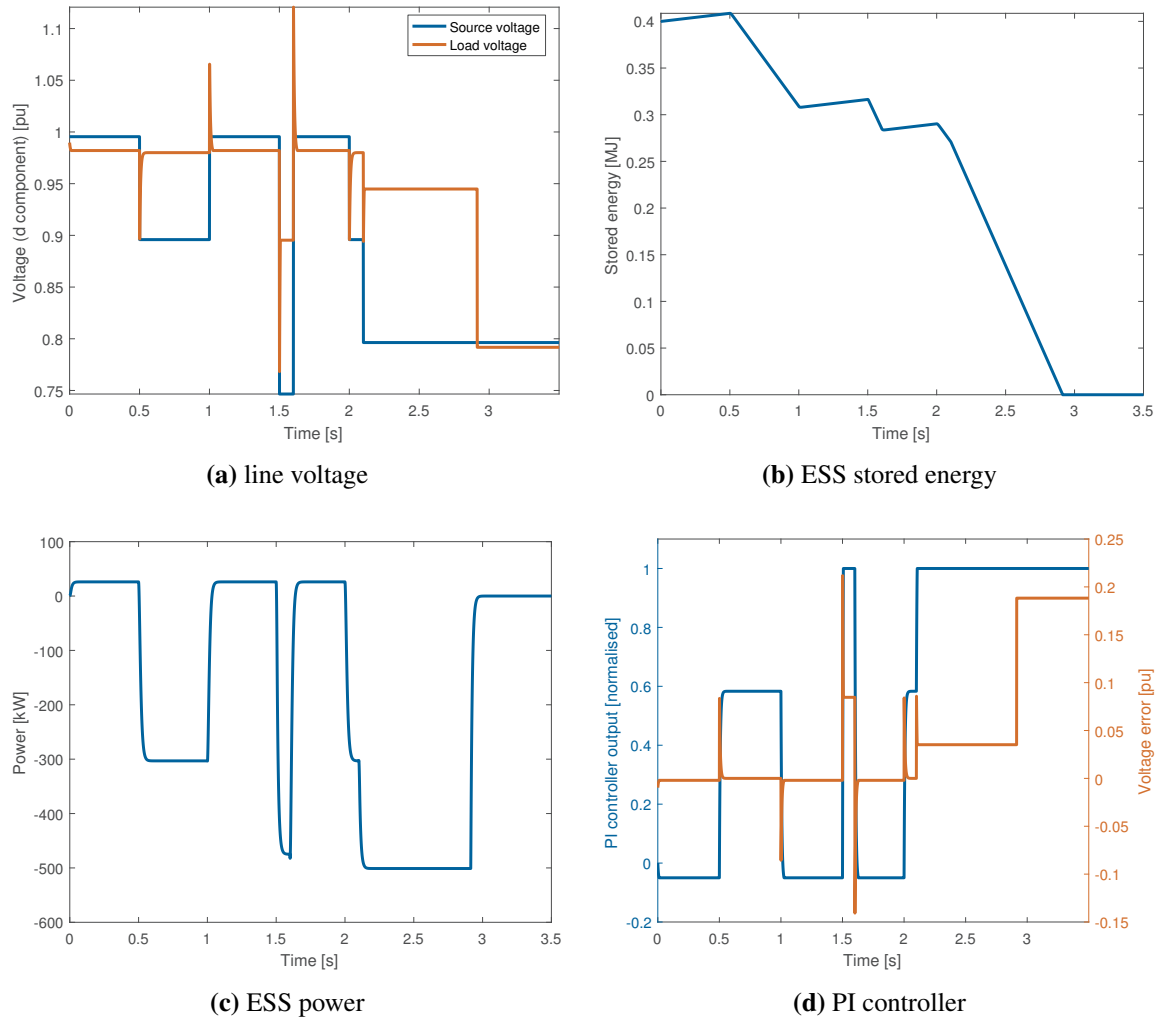


Fig. 5.17 Simulation of a three-phase ESS supplying power during voltage sags (a) on the input line. The storage provides up to 500 KVA maintaining the voltage on the load at 0.98 pu until it is depleted (at second 2.9).

usually are AC, nonetheless they are equipped with power converters that can possess a DC stage [43, 135, 111, 136]. Therefore, a generic energy storage model should preferably be modelled as a DC component that connects to a DC bus.

A generic storage device will accumulate energy depending on the power flowing in and out of it, and the stored energy will usually decay over time due to losses, with a rate that depends on the technology, e.g. flywheels will deplete the stored energy in the span of hours whilst batteries can hold charge for weeks or more. Equation (3.6) describe the behaviour of the storage, but it needs to be discretised in order to be simulated properly with the Simscape Power Systems toolbox in MATLAB/Simulink [70]. The equations of the storage model implemented in simulink are shown below:

$$E(t) = \sum_{k=0}^t \hat{p}_s(k) - fE(k) \quad (5.20)$$

where f is the term linked to the charge decay and \hat{p}_s is the actual power (in Watts) flowing to the storage. An internal resistance of value R is used to model the losses linked to the current:

$$p_s(k) = \hat{p}_s(k) - Ri^2 \text{sgn}(i) \quad (5.21)$$

where i is the current flowing from the ESS, which is controlled in order to impose a power flow to the storage.

The generic energy storage as been implemented in Simulink and it is shown in Figure 5.18. The list below presents the tunable parameters, which can be modified in order to adapt the model to any technology (flywheels, batteries, supercapacitors) which can be fully characterised by its energy and power specifications.

- Energy capacity [MJ]
- Power rating [kW]
- Starting energy [MJ]
- Standing losses [s^{-1}]
- Internal resistance [Ω]
- Power rate limit [kW/s]

A controlled current source is used to impose a current i which determines the power flow, while a discrete-time integrator calculates the stored energy. A MATLAB script defines the other dynamics of the system, including the lower and upper saturation of the energy stored.

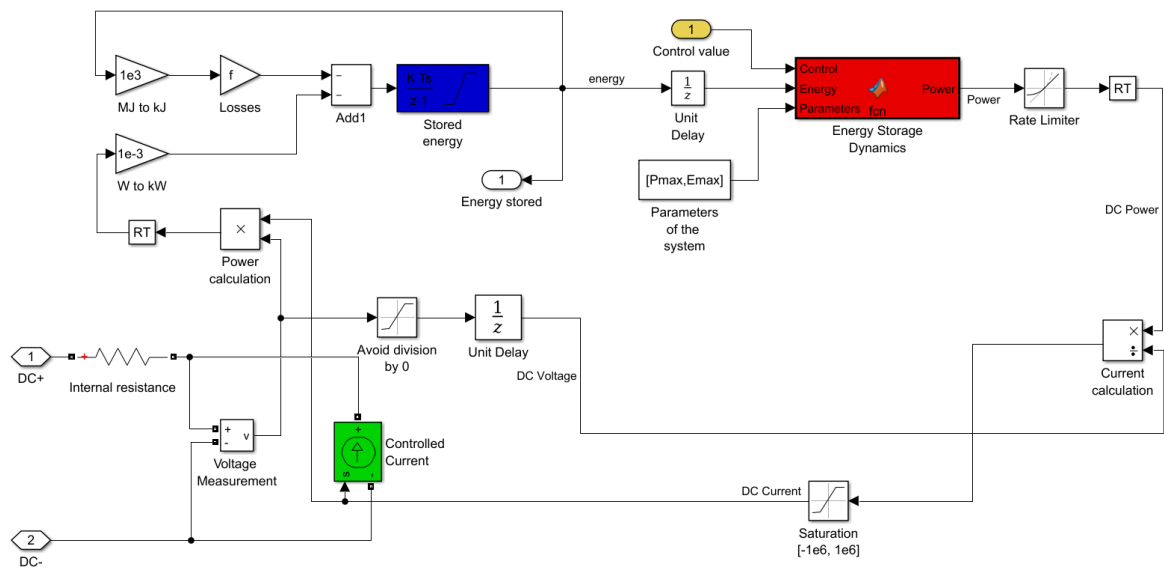


Fig. 5.18 Generic DC energy storage system model implemented in Simulink. Note, on the bottom left, the controlled current source which is governed by the block named “Energy Storage Dynamics”, on the top right, which in turns receives an external control input named “Control value”. The block at the top named “Stored energy” is responsible for representing the accumulated energy.

5.2.2 Generic flywheel energy storage model

As discussed in Section 4.3, a good solution for powering flywheels is using an SR motor, therefore for this work it has been decided to develop the model of a flywheel storage powered by an SR motor. A downside of an SR motor is the need of a very fast converter with switching frequency of the order of tens of kHz. For example, a 6/4 motor (composed of 4 rotor poles and 6 stator poles) that runs at a speed of 15000 RPM, equivalent to 250 Hz, will have a rotor pole sweep near a stator pole at a frequency of 1000 Hz; a converter needs to be able to quickly switch on a phase with good timing and switch it off very fast when the rotor has moved past the stator. The fast dynamics of this type of motor, then, are not easy to simulate with good accuracy, especially for long periods of time. A solution is to model the motor as an equivalent circuit which is powered from a DC bus and outputs the desired mechanical torque, mimicking a real motor. Nonetheless, high time resolution is still needed, slowing down simulations [68, 69].

The generic Flywheel Energy Storage System (FESS) model has been developed by modelling a switched reluctance motor in Simscape Power Systems [70] and connecting it to a mechanical flywheel which has been modelled mathematically and it is described in the next section. The SR motor model, shown in Figure 5.19, implements the SR motor model developed in [68] and it uses the bespoke control strategy described in Section 4.4 in order to provide power depending on the normalised control input (in the interval $[-1, 1]$, where -1 is full generating and 1 is full motoring).

The mechanical flywheel

The electrical energy is converted by the motor into mechanical energy that is stored in a rotating mass, as it had been shown in (4.6):

$$E(t) = \frac{1}{2}I(\omega(t)^2 - \omega_{min}^2). \quad (5.22)$$

and it is evident how the stored energy is directly proportional to the square of the rotational speed $\omega(t)$ minus a term that is dependent on the minimum rotational speed ω_{min} of the flywheel. Eq. (4.1), on the other hand, correlates the mechanical power $p_f(t)$ imposed to the flywheel with the torque.

$$p_f(t) = \tau(t)\omega(t) \quad (5.23)$$

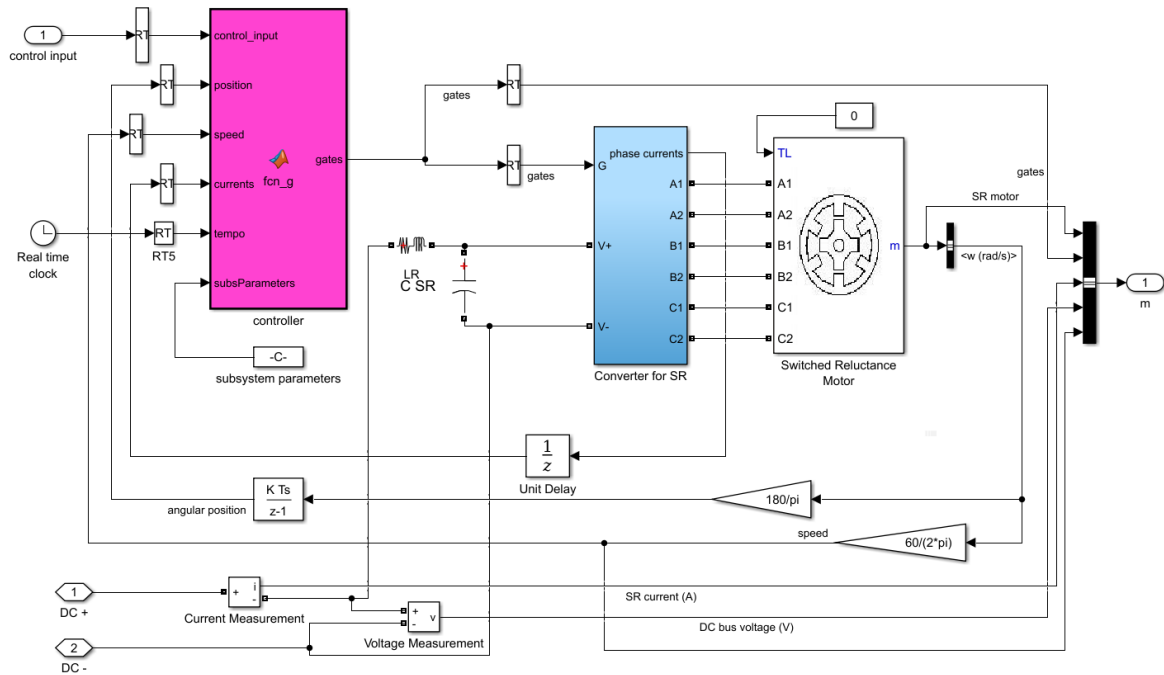


Fig. 5.19 Switched reluctance motor model, motor drive and controller implemented in Simulink. On the left, the block named “controller” reads the external control input and outputs the gate signal to be fed to the power converter (middle) which, in turns, powers the 6 phases of the SR motor (right).

The SR motor converts electric power to mechanical torque, usually with an efficiency lower than 1:

$$T_m(t) = \eta_1 \frac{p_s(t)}{\omega(t)} \quad (5.24)$$

where $T_m(t)$ is the motoring torque, $p_s(t)$ is the electric power, $\omega(t)$ is the rotational speed of the rotor and $\eta_1 \in [0, 1]$ is the efficiency when motoring. Note that, in reality, the value of η_1 may not be a constant and could depend on the status of the system, as the efficiency of the motor may vary due to multiple factors, including speed. When generating, the torque associated with an unit of electric power is higher than the ideal as the losses will have an impact the amount of energy that is extracted when the flywheel is slowed down. The power loss is dependent on the term $\eta_2 \in [0, 1]$, and in the following equation it is shown how the generating torque $T_g(t)$ needs to be higher than the mechanical torque due to the presence of η_2 :

$$T_g(t) = \frac{1}{\eta_2} \frac{p_s(t)}{\omega(t)}. \quad (5.25)$$

The losses caused by the energy transformation are included in the model of the SR motor, as they have been considered in the equivalent circuit which is characterised by the presence of resistances, especially in the stator. Therefore it is not necessary to calculate the values for η_1

and η_2 as the motor will automatically produce the correct torque output. Nonetheless, it is important to account for their effect on the torque applied to the flywheel, and the controller cannot regulate the power flow to the energy storage by merely acting on the mechanical torque or the speed of the flywheel. As an example, if the objective is to impose an electrical power flow $\hat{p}_s(t)$ on the ESS, the resulting torque we demand from the motor depends on $\omega(t)$ and also the values of η_1 and η_2 , therefore the mechanical power will differ from the electrical, being the former larger (in absolute value) when motoring, and lower when generating. A power management controller will usually monitor the power flow and react accordingly, therefore it will automatically compensate for any losses. For these reasons, the generic term $T(t)$ will be used to identify the instantaneous torque produced by the motor, which is positive during motoring and negative when generating.

The rotor dynamics in the SR motor are then modelled by the following equation:

$$\frac{d\omega(t)}{dt} = \frac{1}{I} (T(t) - B\omega(t)) \quad (5.26)$$

where B is a parameter that is related to the windage losses and converts the rotational speed to torque, slowing down the rotor in proportion to the speed. This model has been adapted to be used in conjunction with a flywheel by selecting a value for B that approximates the friction induced on the flywheel, estimating the effect of windage and friction. This initial model has also been initially used with the specific SR motor model (described in Section 5.2.3) until it was superseded by a more advanced model based on measurements (presented later in this chapter). The flywheel model described by (5.26) has been used in [85], where the value for B has been set to 0.002 N m s / rad.

5.2.3 Specific flywheel energy storage model

Generic models offer a high flexibility and allow to simulate a wide range of technologies or an entire subset of a single technology, but they may fail at accurately reproduce a single device as they may lack complexity or, on the contrary, model dynamics which are not present in the particular system. High quality measurements obtained after the development of the previous models allowed for the creation of a specific model of a flywheel energy storage powered by a switched reluctance motor. The specific model requires less assumptions as it is purely based on data provided by manufacturers, thus it intrinsically includes all the dynamics which are difficult to estimate, like losses and efficiency.

The specific model is composed of two major components: a mechanical flywheel modelled by a differential equation, and a SR motor based on electrical data. Figure 5.20 shows a diagram with the various components of the model and their interconnections; the apparent complex topology will appear clearer after finishing reading this section.

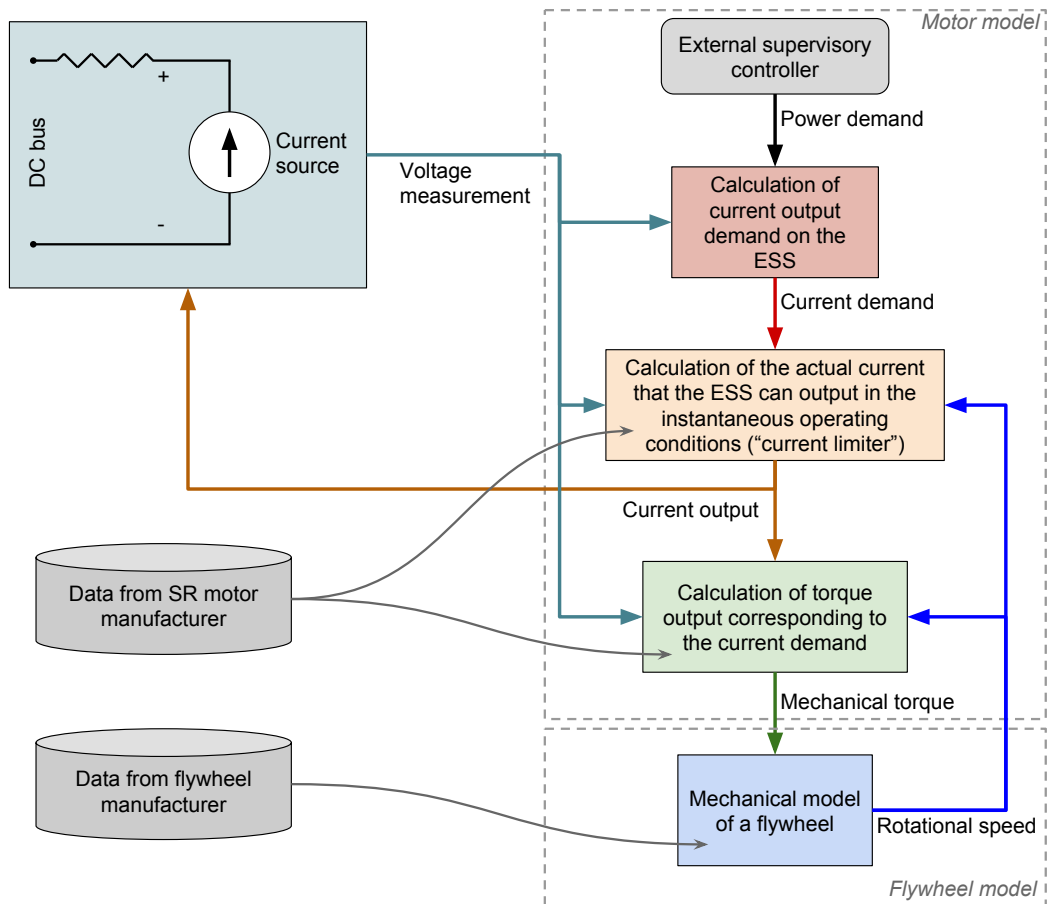


Fig. 5.20 Diagram of the components of the specific FESS model.

Updated model for the mechanical flywheel

In September 2016 a high quality set of measurements were collected on a flywheel energy storage developed by CRESS Systems, allowing for a more accurate model of the flywheel to be developed. The system has been metered during spin-down phases consisting in the motor and flywheel slowing down from 12000 RPM to 0 under friction and windage effects only, with the motor powered down. The motor rotor and flywheel operated under a constant pressure differential of 0.88 bar in order to reduce drag.

A first order differential equation of second degree has been used for modelling the spin-down:

$$\frac{d\omega(t)}{dt} = \frac{1}{I} (T(t) - b_1\omega^2(t) - b_2\omega(t) - b_3) \quad (5.27)$$

where b_1 , b_2 and b_3 represent, respectively: the aerodynamic drag, the bearing friction, and a constant torque load caused mostly by the viscous friction due to the bearing lubricant and vibrations [137]. The latter should only dominate at low speeds. This equation is only valid when speed is positive, which is true in the operating range of the flywheel. To generalise this equation for any speed it is possible to express it as following:

$$\frac{d\omega(t)}{dt} = \frac{1}{I} (T(t) - b_1\omega^2(t)\text{sgn}(\omega) - b_2\omega(t) - b_3\text{sgn}(\omega)) \quad (5.28)$$

The constants b_1 , b_2 and b_3 were found by minimising the RMS error between the data measured during the spin-down and the modelled data; the motor torque $T(t)$ is 0 $\forall t$ during spin-down. As the motor is powered down, the constants b_1 , b_2 and b_3 determine the mechanical losses of the flywheel and motor rotor and can be used to model the mechanical flywheel of the energy storage. In Table 5.5 presents the parameters of the flywheel, the calculated constants and the modelling error NRMSD¹, whilst Figure 5.21 shows the measured spin down against the model; the model was used also to calculate the speed profile from 15000 RPM.

It is interesting to calculate how much mechanical power is lost with respect to the rotational speed: this value determines the electrical energy demanded by the motor in order to maintain a certain constant speed. The power loss is calculated from (3.7) as follows:

$$P_{loss} = \frac{dE(t)}{dt} = J\omega(t)\frac{d\omega(t)}{dt}. \quad (5.29)$$

From (5.27), and assuming $T(t) = 0 \forall t$, Eq. (5.29) becomes:

$$P_{loss} = -b_1\omega^3(t) - b_2\omega^2(t) - b_3\omega(t) \quad (5.30)$$

which corresponds to 8.33 kW at 15000 RPM. Figure 5.22 shows the mechanical power loss calculated from the model.

¹Normalised Root-Mean-Square Deviation

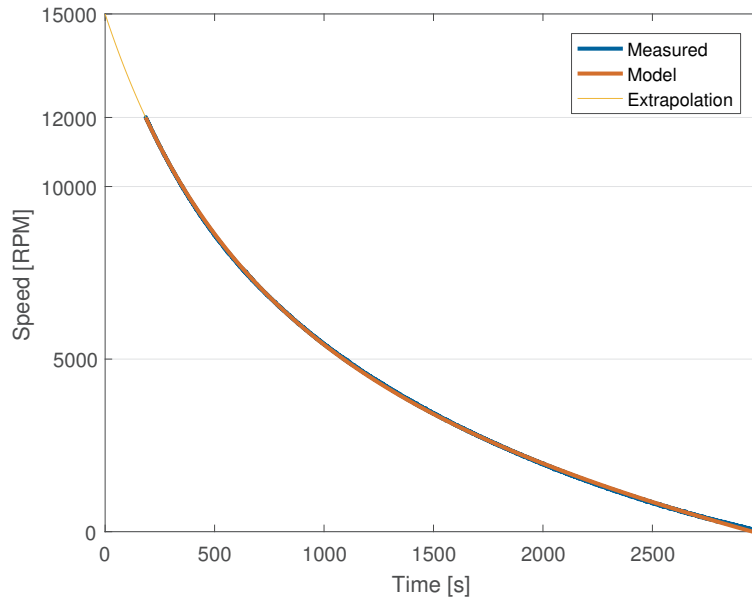


Fig. 5.21 Measurements from a flywheel during a spin-down compared to the model calculated from the measurements.

Table 5.5 Parameters of the flywheel and best-fit values.

Parameter	Value
I	2.62 Kg m ²
b_1	1.543e-6
b_2	6.436e-4
b_3	0.4835
NRMSD	4.7e-5

Equation (5.27) is implemented in Simulink as shown in Figure 5.23. The only input to the system is the external torque imposed by the motor, while the only output is the instantaneous flywheel speed in rad/s.

SR motor

The SR motor is manufactured by Nidec SR Drives, which provided data collected during dynamic testing of the motor. The data contains information measured on the motor under the following operating conditions:

- 3 voltage levels: 550 V, 650 V, 750 V;
- 15 speeds level, from 0 to 15700 RPM;

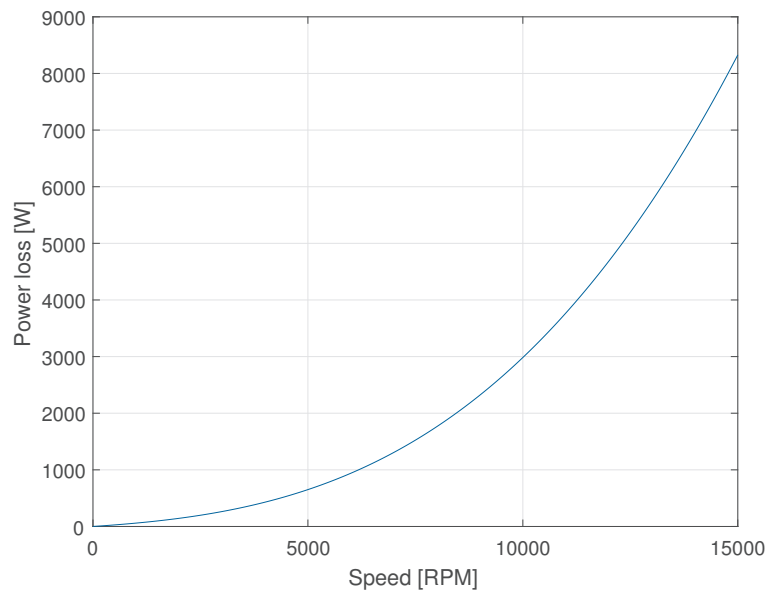


Fig. 5.22 Mechanical power lost from friction at various rotational speeds.

- 31 torque levels in Nm, from -100% to 100% of the rated value at that speed and voltage.

The data measured in the above conditions includes DC current, losses and efficiency. The data is imported in the Simulink model and it is processed at each instant in order to calculate what is the torque output associated with a particular power output that is demanded to the FESS by the control system. The steps, which are visualised in Figure 5.20, are the following:

1. The external supervisory controller asks the motor to produce a particular power output, either positive or negative depending whether the storage is importing or exporting energy.
2. The instantaneous voltage on the DC bus is measured and used to calculate what is the current necessary to output a particular power, therefore the power demand is converted into a current demand.
3. Limitations in the power rating in the motor do not allow it to produce any current that is demanded, therefore the value is limited to the actual admissible value. Furthermore, the current limiter reads the speed and reduces the current if the speed is approaching the upper or lower limit; for example, the current absorbed by the storage is reduced as the speed climbs towards the maximum speed until it is set to 0 when it is reached.

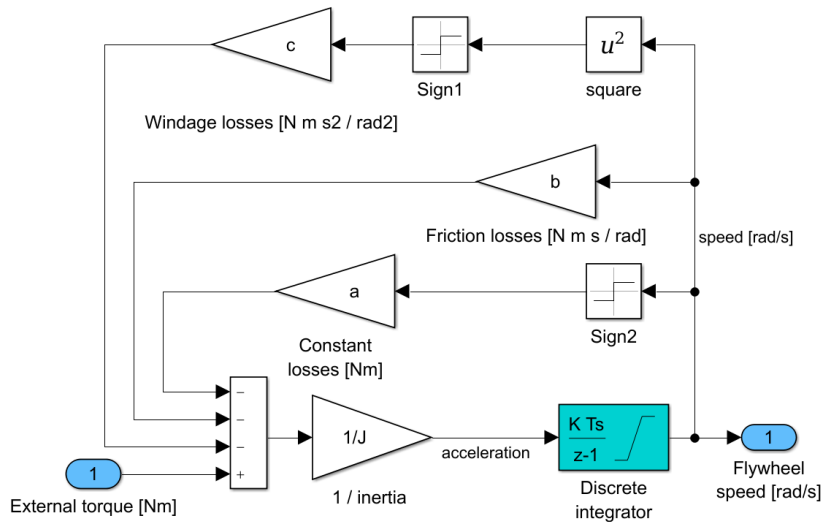


Fig. 5.23 Mechanical flywheel implemented in Simulink and representing (5.27). An external torque, coming from the left, is added to the losses, imposing an acceleration to the flywheel whose speed is represented by the discrete integrator. The constants a , b and c correspond to b_3 , b_2 and b_1 respectively.

4. The instantaneous electrical status is defined by the triplet *current*, *voltage* and *speed*, with the behaviour of the motor, in that status, defined by the data provided by the manufacturer. The model performs linear interpolation between the measured points using fast prelookup and interpolation blocks that quickly calculate the torque produced in that particular condition. Figure 5.24 shows the Simulink diagram with the blocks that read the electrical status of the system and produce a torque value as the linear interpolation of the values belonging to neighbouring statuses.
5. The torque output is then passed to the mechanical flywheel model, while the actual current consumption is passed to the electrical subsystem connected to the DC bus.

The complete model implemented in Simulink, which includes both the flywheel and the SR motor, is shown in Figure 5.25.

5.2.4 Comparison of energy storage models

This section is dedicated to the comparison of the energy storage model variants. In this chapter, 3 models have been presented:

1. Generic ESS: a generic energy storage model than can be used to represent batteries, supercapacitors, flywheels or any other common storage technology;

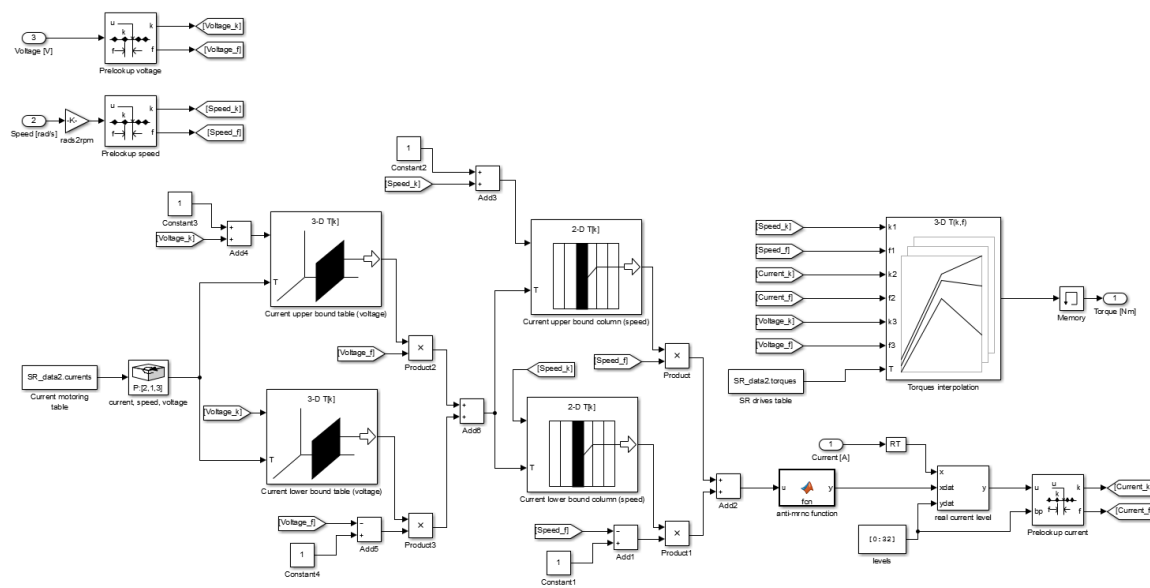


Fig. 5.24 Simulink blocks that read the instantaneous motor values from data provided by the manufacturer. These blocks perform the instantaneous data lookup by selecting and interpolating the values corresponding to the actual state (speed, voltage, etc.) of the motor. The output is the mechanical torque imposed to the flywheel.

2. Generic SR FESS: a generic flywheel energy storage model that uses equivalent circuits to reproduce a SR motor, and it uses a bespoke low-level control strategy;
3. Specific FESS: a model reproducing an actual system composed by a SR motor and a flywheel.

Usually, the more generic the model, the more versatile it is, as it can model a wider range of devices. The downside of a more generic model is potential loss of accuracy due to the reduced complexity, whilst more specific models could require more computational power for the simulation. Another critical factor is validation: a generic model requires a more strict validation process, whilst a specific model based on measurements is usually inherently accurate.

In order to test and compare the storage models it has been decided to impose the same power demand to each of them and measure their power and energy flow. The models share the following parameters:

- Energy capacity of 2.873 MJ;
- Maximum bidirectional power output of 150 kW;

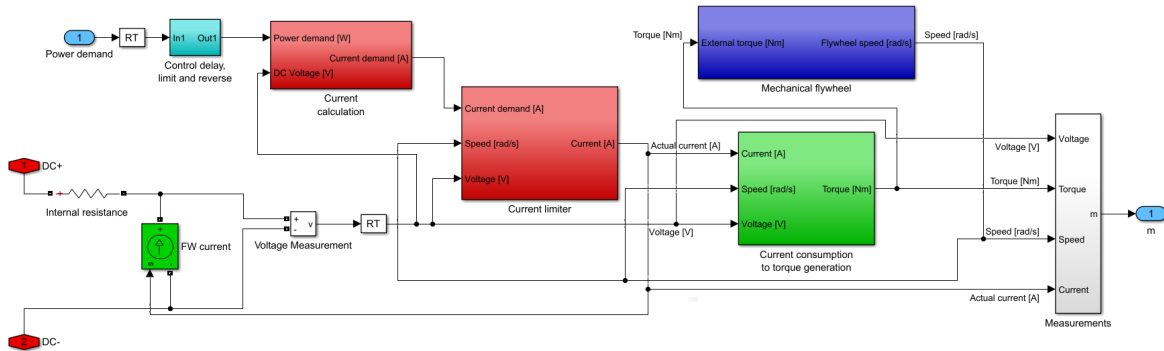


Fig. 5.25 Simulink model of the specific energy storage system. The blocks are the implementations of the logic presented in Figure 5.20.

- Starting energy of 0 MJ (empty);

The Generic ESS has been tuned to mimic the Specific FESS, whilst the Generic SR FESS has very similar parameters to the one used for [85]. Figure 5.26 shows the power flow reference as well as the output power provided by each storage model. Every variant tends to match the reference power when it is within the power limits of the storage; when empty (or full) the storage stops exporting (or importing) power. Notice how the Generic ESS power output is very similar to the Specific FESS, while it is not the case for the Generic SR FESS as it depletes its charge faster (at around 30 seconds) and reaches maximum capacity faster (at around 65 seconds), indicating a comparably higher efficiency when motoring and a lower efficiency when regenerating. The energy stored is presented in Figure 5.27, and it can be seen how the Generic SR FESS differs from the other two variants.

Knowing that the Specific FESS model is based on actual measurements, one could think that the Generic SR FESS model does not represent accurately an SR FESS, unlike the Generic ESS model. It needs to be noted, though, that the Generic SR FESS has been developed before the experimental data was available, therefore its role was to approximate the potential behaviour of an SR motor knowing its basic electrical characteristics. The Generic ESS matches almost perfectly the Specific FESS during the test shown, but the reduced complexity is evident in the simulation shown in Figure 5.28, where the three storage systems are simulated in a spin-down test. In this test, the Generic ESS loses energy differently than the Specific FESS, mostly because of the different mechanical flywheel model, which in the case of the Generic model has a lower complexity. The advantages and disadvantages of each model are summarised in Table 5.6.

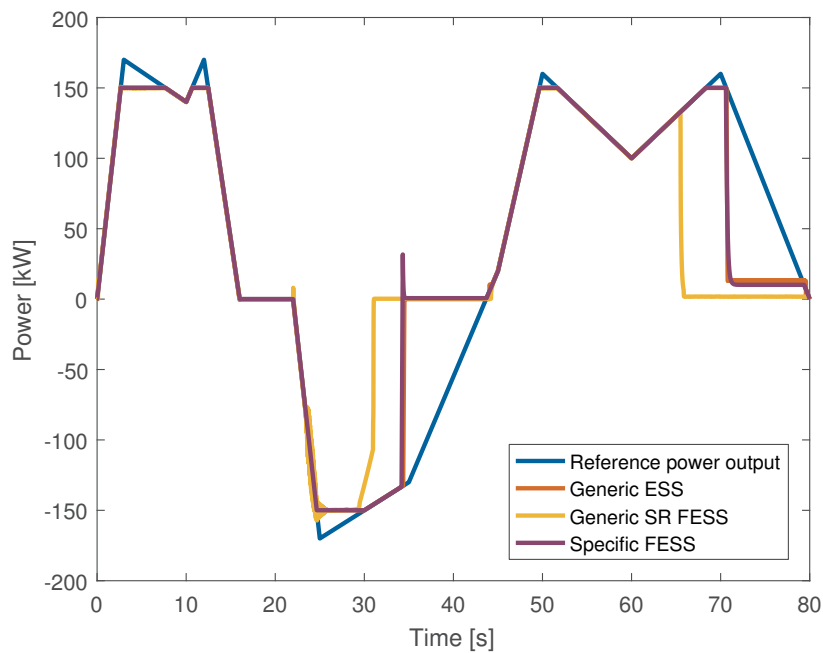


Fig. 5.26 Comparison of the three ESS models: power reference and storage outputs.

Most of the work presented in this thesis was based on the Generic SR FESS model, but the data-driven Specific model is most suited for representing an existing system, therefore the overall quality of the control strategies will be tested using the latter in Chapter 7.

Table 5.6 Comparison of energy storage models.

Variant	Advantages	Disadvantages
Generic ESS	<ul style="list-style-type: none"> • Low complexity • High versatility 	<ul style="list-style-type: none"> • Lower accuracy • Needs strict validation
Generic SR FESS	<ul style="list-style-type: none"> • High potential accuracy • SR model based on equivalent circuit 	<ul style="list-style-type: none"> • Low actual accuracy • High complexity • Needs strict validation
Specific FESS	<ul style="list-style-type: none"> • Based on measurements • High accuracy • Fast to compute 	<ul style="list-style-type: none"> • Needs no validation • Very low versatility

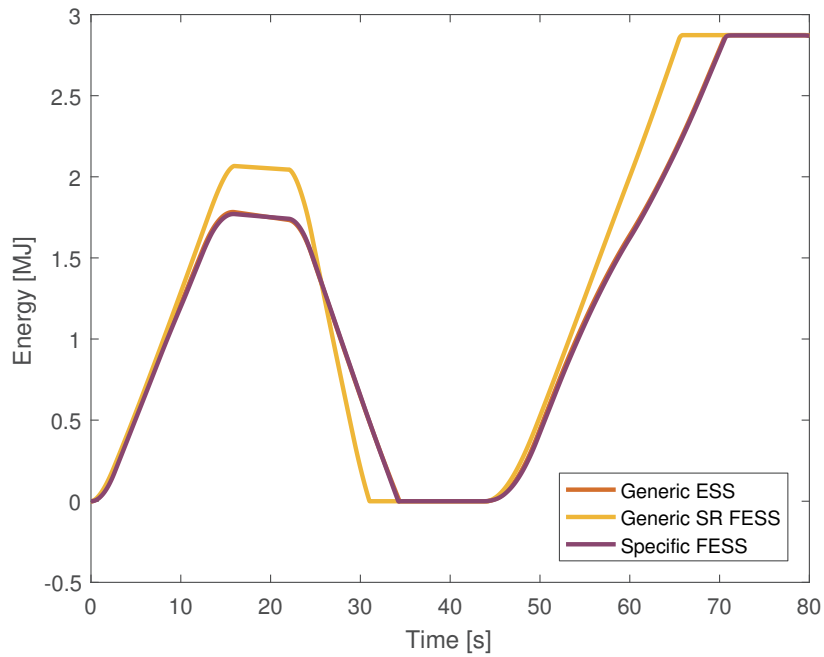


Fig. 5.27 Comparison of the three ESS models: energy stored.

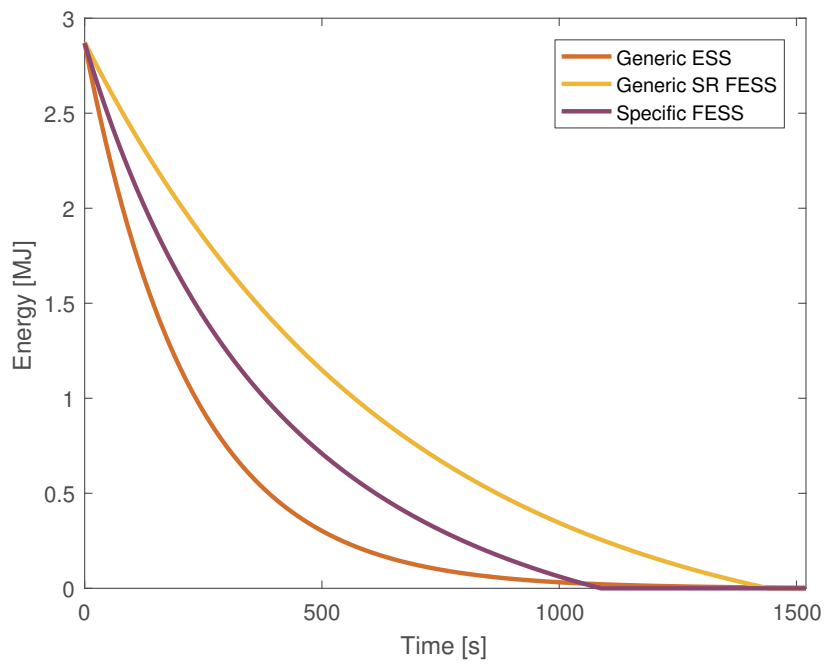


Fig. 5.28 Comparison of the three ESS models: spin-down test.

5.3 Hybrid RTG crane model

The models presented in this chapter have been developed with the objective of generating a model of a hybrid RTG crane. This model is therefore composed of the following three sub-models:

- The validated RTG crane model which includes a hoist motor, primary power source, DC bus and brake resistors;
- The specific Flywheel ESS with the above mentioned low-level control system;
- A supervisory control system which could be one of those developed for this thesis.

The diagram in Figure 5.29 shows how those components are linked together. The FESS model is linked to the DC bus bar of the RTG crane model. Voltage and power transducers transmit information to the supervisory controller which, in turns, sends a power output reference to the low-level controller of the ESS.

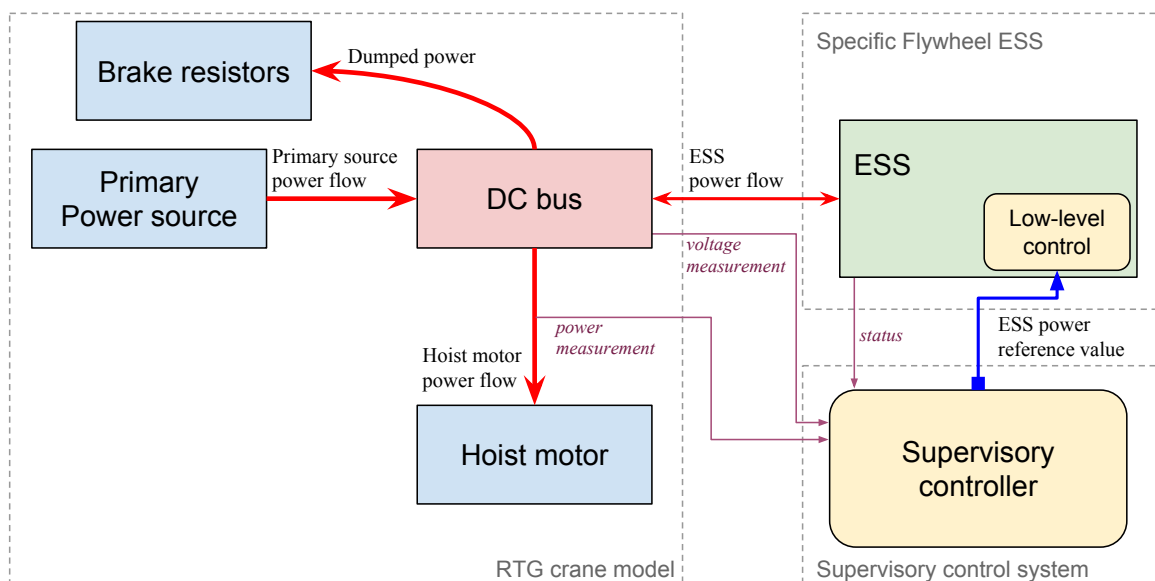


Fig. 5.29 Simplified diagram of the hybrid RTG crane model.

5.4 Summary

This chapter presented the modelling process that led to the development models that enabled the study of supervisory control strategy for energy storage in RTG cranes. The first model

presented simulates a single RTG crane and its major electrical components. The activity of an RTG crane can be replicated allowing for the inclusion of additional modules, in particular an energy storage system.

Three very different models of energy storage systems were also presented and compared, each of them with its own features and advantages. A generic storage model has been developed in order to simulate a whole range of storage technologies; a second model represents a generic flywheel storage system that can be used to test a wide range of flywheel storage technologies; the last model has been tailored to a specific flywheel storage system which is under development and whose operational data is accessible.

The RTG crane model presented in this chapter is the first known example of a Matlab/Simulink model that is validated against actual measurements. Both single cycles and long term simulations showed high accuracy when compared with high resolution data acquired from an RTG crane in use at the Port of Felixstowe. The work that led to the characterisation of the hoist motor demand has been the subject of a conference paper (presented at the *2015 IEEE Industry Applications Society Annual Meeting*) [138] and a journal paper published in *IEEE Transactions on Industry Applications* [74].

The RTG and ESS models presented will be also used to test, assess and compare the supervisory control strategies described in the following chapters.

Chapter 6

Supervisory control strategies

The previous chapter presented the potential benefits of adding energy storage units to RTG cranes, including the potential energy savings that could be obtained. It was also shown how low-level controllers can be designed to induce a desired ESS power output whilst maintaining the operating limits. The storage device, however, can provide limited power and energy, therefore it is necessary to choose accurately the time profile of the storage power output that maximises the benefits. In an RTG crane, there are two major objectives: to reduce energy consumption and to decrease the stress on the primary source. These objectives can be met by using a supervisory control system that reads the status of the crane and outputs a power reference value which is fed to the storage device.

This chapter presents three very different approaches to a supervisory control, all implemented in the same hybrid RTG crane and aiming at the same objectives. The three supervisory control systems presented are either extensions of existing control techniques or based on state-of-the-art controllers that have been used in similar applications, adapted for the particular use in hybrid RTG cranes. Each controller presented is described and simulated, with the results analysed to highlight the behaviour of the storage in association with the specific control system. Relevant scenarios are analysed in this chapter, whilst a thorough analysis and comparison is presented in Chapter 7. The first supervisory controller, based on PI controllers, is described in Section 6.1. The second is an optimal controller, presented in Section 6.2. The third supervisory control is a fuzzy logic controller, described in Section 6.3. The diagram in Figure 6.1 shows the three control strategies with the sub-strategies employed.

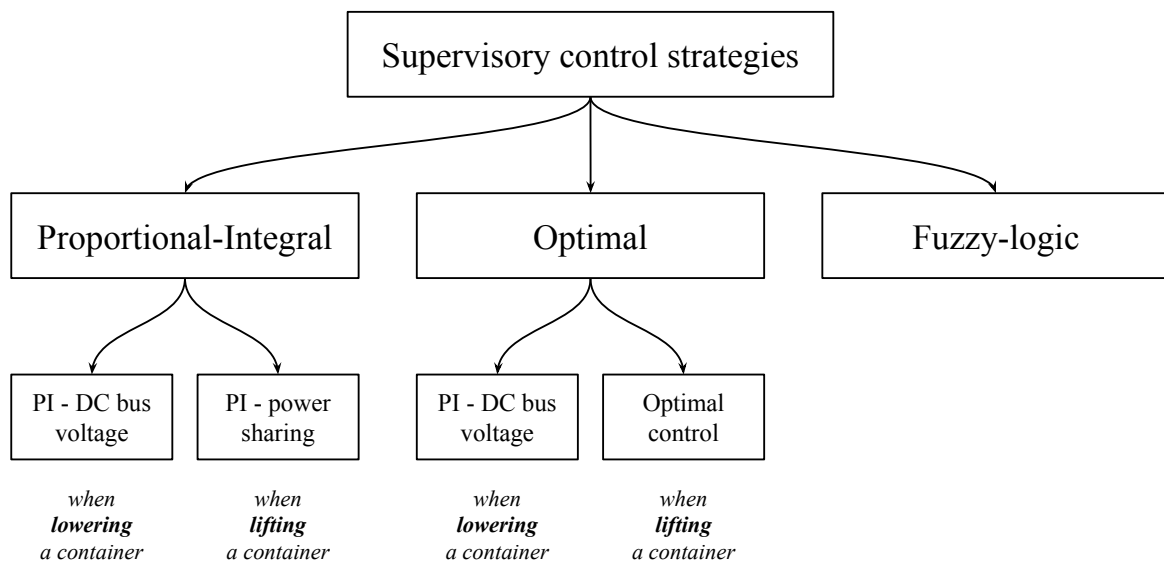


Fig. 6.1 Supervisory control strategies presented in this chapter.

This chapter will present, for each supervisory control, a short simulation demonstrating the properties of each control systems. A more thorough comparison and analysis, including a comparison with an existing supervisory controller, will be presented in Chapter 7.

6.1 Proportional-integral supervisory control

The first set of supervisory control systems presented in this chapter is based on a combination of Proportional-Integral (PI) controllers, designed to minimise the error between actual values and reference values. The controller output is linked to the energy storage control input, where the internal low-level control system is in charge of inducing a power output proportional to the control input value.

PI controllers are widely used for low level control of linear and non-linear dynamic systems, but it will be shown that they can also be used as supervisors. The following sections will show how PI controllers can effectively provide the reference power output for energy storage systems in RTG cranes in order to achieve multiple objectives.

6.1.1 DC bus voltage control

The DC bus in the RTG crane presented in Section 3.4 is powered by a 415 V three-phase source through a diode rectifier. The common DC bus is shared between the major electrical components, including the hoist motor and brake resistors. The DC bus voltage, when the crane is idling in a steady state, should hover around 560 V, but it varies dramatically when there is power flowing in and out of the motors connected to the bus. Figure 6.2 shows the measurements of the DC bus voltage on the crane when lifting and lowering a container: when the hoist motor is lifting (positive speed) the DC bus voltage is low, whilst it climbs up to 750V (brake resistors activation threshold) when the hoist motor is lowering (negative speed).

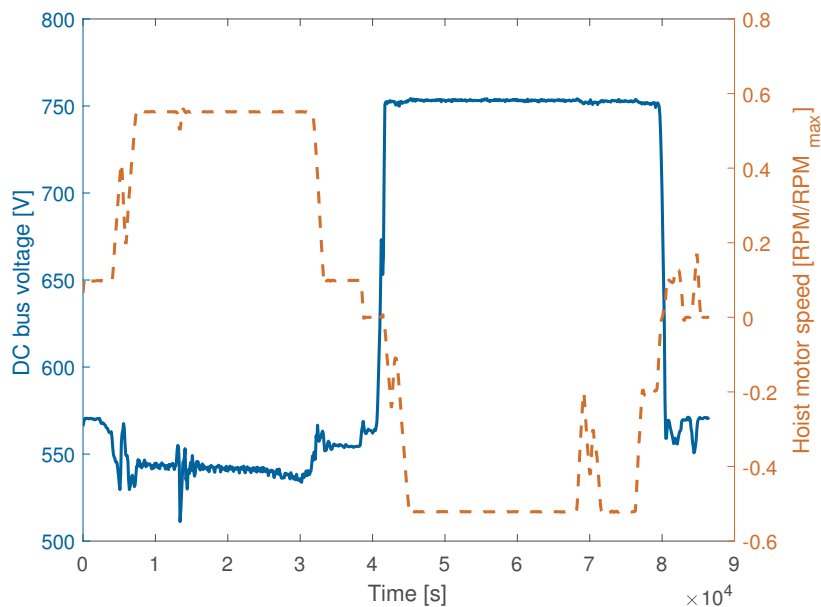


Fig. 6.2 DC bus voltage fluctuations due to the activity of the hoist motor. The voltage (solid line) changes depending on whether the hoist motor is lifting (positive speed) or lowering (negative speed) a container.

The simplified crane's electrical diagram shown in Figure 6.3 represents how the energy storage can exploit the presence of the voltage fluctuations. The load is a bidirectional power source that represent the motors, in particular the hoist motor. When the hoist motor draws power, the DC bus voltage decreases and the energy storage can detect the change and start outputting power. During a container lowering, instead, the hoist motor regenerates power into the DC bus raising its voltage; the energy storage can absorb the power as the voltage is increased. However, the storage device does not know the precise power that it needs to output or absorb. It could measure the voltage and provide power proportionally to the

deviation from the norm, using a proportional control. The issues linked with this approach are evident from Figure 6.2: the voltage oscillates too wildly, and the deviation from the normal value may be minimal and hard to detect. The solution is to use a PI controller to control the ESS power flow, selecting an adequate voltage reference that sits in between the rectifier activation level and the brake chopper threshold. The PI controller receives as input the error $e_V(t)$ between the reference voltage and the measured value, outputting a power reference that charges the storage when the voltage is high and discharging it in the opposite case. The integral action of the PI controller filters input oscillations and ensures steady-state error rejection for constant inputs, thus guaranteeing that the asymptotic output of the storage maintains the desired DC bus voltage. A more formal study of the stability and error rejection of the system is included in Appendix C. It was chosen not to use a derivative term because the system is inherently an integrator (the power target affects the derivative of the DC bus voltage) with very little inertia (power output of the storage can vary almost instantaneously). Oscillations are therefore easily avoided with proper tuning, and the derivative term provide few benefits in this case.

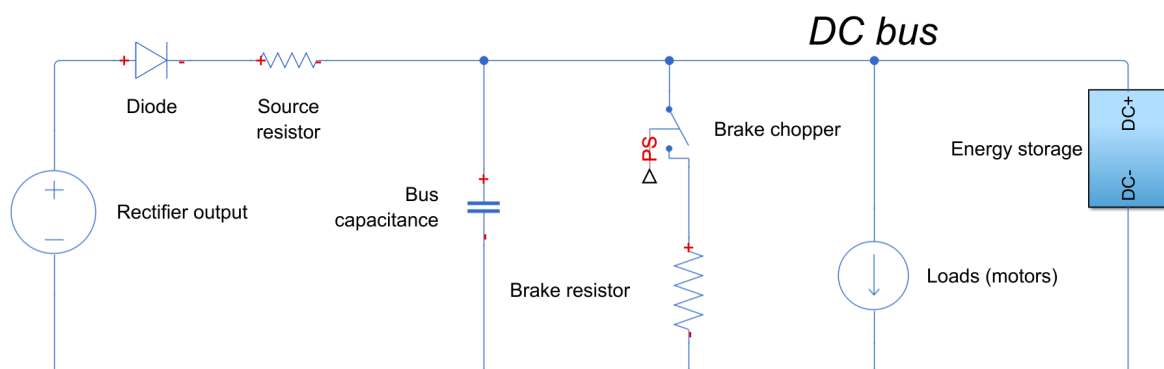


Fig. 6.3 Diagram of the RTG crane represented as basic electrical elements.

The simplicity of this control system allows its use in multiple energy storage applications, including the use in RTG cranes where it has led to significant energy savings [34, 50, 19, 45, 139]. Nonetheless, one disadvantage is that the power flows are difficult to control, because they are not controlled directly and only through their effect on the DC bus voltage. This is particularly evident during a lift: the hoist motor demands power causing a very small drop in voltage which is difficult to handle. It may not be useful to control the voltage during a lift, as it is only an indirect measure of the power output of the primary source. A more direct management of the power flows can be achieved by controlling directly the power flowing from the primary energy source.

6.1.2 Power sharing control

Reduction in crane energy consumption is not the only benefit of energy storage. An equally important objective is the reduction in peak power demand, as has been discussed in Section 3.8.2. A power management system can limit the power flowing from the primary source by supplying the extra power using energy storage. Figure 3.25 and Eq. 3.5 on page 52 indicate the potential use of the power output of the energy storage $p_s(t)$ for limiting the effort of the primary source $p_g(t)$. The objective is to shave the peak power demand on the primary source during a lift, limiting it to a chosen value P_M . The power output of the storage $p_s(t)$ is then:

$$p_s(t) = \begin{cases} 0 & \text{if } p_L(t) < P_M \\ P_M - p_L(t) & \text{if } p_L(t) \geq P_M \end{cases} \quad (6.1)$$

with $p_L(t)$ the load power and $0 < P_M \leq \max\{p_L(t)\}$. This ensures that $p_g(t) \leq P_M$, therefore achieving effective peak shaving through power sharing. In an actual system, the power output of the storage is limited by the power rating:

$$-P_s \leq p_g(t) \leq P_s \quad (6.2)$$

whilst $p_g(t)$ is not bounded. Furthermore, the storage charge may not be high enough to supply all the necessary energy. For these reasons, an important metric that can be used to compare storages and control strategies is the percentage of time that the primary power supply outputs more than a defined power level. This metric is a good indicator of the quality of the power management strategy when it is forced to deal with the limited power and energy capacity of a storage system [85].

In order to implement the power sharing control strategy above, a PI controller is used to reduce the error $e_P(t)$ between the threshold value P_M and the power flowing from the primary source through the rectifier $p_g(t)$:

$$e_P(t) = P_M - p_g(t) \quad (6.3)$$

The output of the controller, $u_P(t)$, is then inverted in sign so it is positive when the storage needs to supply power to the system. When the load demand is over the power threshold, $p_L(t) - P_M > 0$, the generated power will be greater than the desired threshold: $p_g(t) > P_M$. In this condition, the value of $u_P(t)$ is positive and the storage will output positive power $p_s(t)$. The power sharing controller needs to operate only when $p_g(t) > P_M$,

therefore the controller output is saturated and bounded to $[0, 1]$ and it can reach a saturated state in certain conditions:

$$\lim_{t \rightarrow \infty} u_P(t) = \begin{cases} 0 & \text{if } p_L(t) \leq P_M \\ 1 & \text{if } p_L(t) > P_M + P_S \\ * & \text{otherwise.} \end{cases} \quad (6.4)$$

In summary, the controller will have an output of 0 if the load is below the threshold avoiding the activation of the storage. If the load goes above the threshold, the PI will force the storage to provide enough power to limit $p_g(t)$ to P_M . Once the power required is above the capabilities of the storage, the PI will saturate to the maximum value. The behaviour of the power sharing PI described above is pictured in Figure 6.4. In order to avoid wind-up of the saturated PI, the integrator is stopped if the output is saturated and the integrator output has the same sign as the controller input.

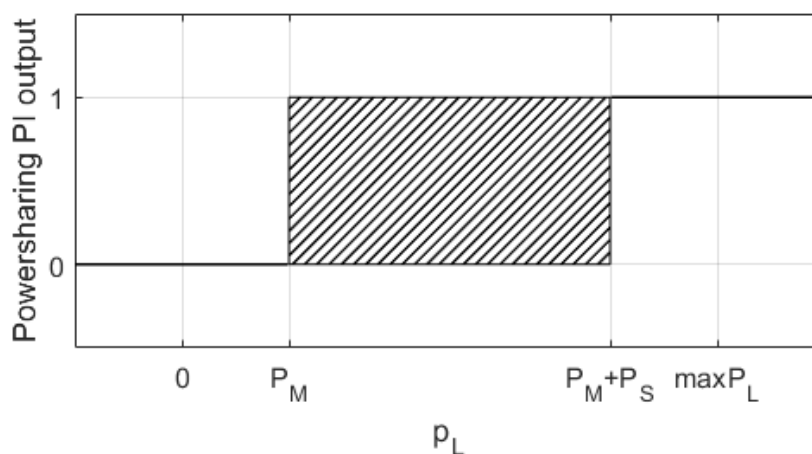


Fig. 6.4 Output of the power sharing PI depending on load power P_L . P_M is the power threshold chosen below which the ESS does not intervene. P_S is the maximum power output of the ESS.

As described above, the power sharing controller needs only to operate during a container lifting, when the demand from the hoist motor is positive. During lowering, the energy storage needs to be charged using recovered energy, and to do so a modified version of the DC voltage controller is implemented. The DC voltage PI controller is activated when the voltage $V(t)$ rises above a voltage threshold V_M smaller than the brake resistor activation threshold. The voltage PI controller reads the voltage error $e_V(t)$ and outputs a positive power command $u_V(t)$ if this error is positive. Similarly to the power sharing PI, the voltage PI controller output is saturated to $[0, 1]$ and it can reach the saturated state in certain conditions:

$$\lim_{t \rightarrow \infty} u_V(t) = \begin{cases} 0 & \text{if } V(t) \leq V_M \\ 1 & \text{if } V(t) \gg V_M \\ * & \text{otherwise.} \end{cases} \quad (6.5)$$

The voltage controller does not operate if the voltage stays below the threshold V_M , because this status never corresponds to a crane lowering a container. On the other hand, very high voltage levels may saturate the controller to the maximum value, which is associated with the maximum power level of the storage. This condition signifies that the storage cannot absorb power at a sufficient level to avoid an uncontrollable increase in voltage, resulting in the activation of brake resistors. The value of V_M needs to be chosen above the rectifier activation level but well below the brake resistors level to ensure effective energy savings.

The DC bus voltage and the power sharing PI controllers work concurrently. The control value $u(t)$ that is effectively fed to the storage is calculated as follows:

$$u(t) = P_S(u_V(t) - u_P(t)) \quad (6.6)$$

therefore $u(t) \in [-P_S, P_S]$. Figure 6.5 illustrates the process and shows how the two controllers are joined, as well as their input errors and the hybrid crane subsystem.

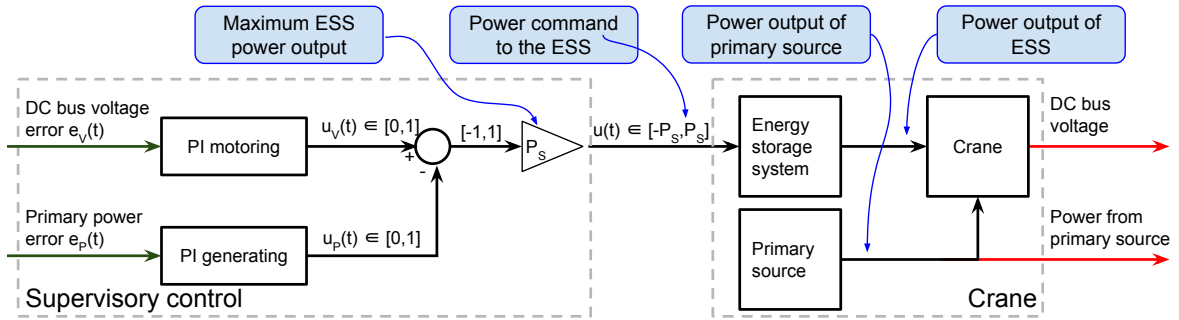


Fig. 6.5 Diagram showing the PI controllers in charge of DC voltage control operating jointly to control an energy storage system.

There is no risk of both PI controllers outputting a non-zero output at the same time (and interfering with each other) for the following three reasons:

- The voltage threshold V_M is, by design, above the diode rectifier activation threshold, so no current can flow from the three-phase source when the DC voltage error is positive. This is evident from Figure 6.6 which shows measurements of the hoist motor power versus DC bus voltage during normal operation. Therefore, if the output of the DC

voltage control PI is positive, the power sharing PI output can only be zero or negative as $V(t) > V_M$ and $p_g(t) \leq 0$. The power sharing PI output, though, cannot be negative as it has a lower bound at 0. Therefore, its output is 0 if the DC bus voltage PI has non-zero output.

- When current is flowing from the three-phase source to the DC bus, the power $p_g(t)$ is positive and the steady-state output of the PI is positive if also $p_L(t) > P_M$. Positive $p_g(t)$ can only occur if the DC voltage is below the activation threshold of the rectifier (in the case of the RTG in question it is around 560 V) which, in turns, is below V_M by design. Therefore, if the power sharing PI has positive output, the DC control PI has necessarily output 0.
- The only situation where both controllers have positive output at the same moment is if the integral portion of the PIs is slower than the dynamics of the system. By design this is not the case, as the controller needs to have larger bandwidth than the system in order to react adequately to changes in the DC bus voltage or power demand. The time it takes for the DC voltage to move between the diode activation threshold and the DC control threshold is inevitably higher than the time taken by the PIs outputs to vanish after an error sign change.

6.1.3 Simulation and results

The dual-PI control strategy has been implemented in Simulink and it has been connected to the FESS model presented in Section 5.2.3. The parameters of the PI controllers are presented in Table 6.1; they were tuned to guarantee fast compensation of voltage and power fluctuations, avoiding overshoots and oscillations. The slow dynamics, inherent stability and simplicity of the crane electrical subsystem resulted in a fast tuning process that can be replicated with little effort on a different crane. The gains of the supervisory controller have little effect on the overall result, given that the dynamics are dictated primarily by the crane and the low-level ESS control (for which this supervisory controller only provide a reference value).

An RTG crane in use at the Port of Felixstowe (described in Section 3.1) was recorded for 38 minutes during normal daily activity. The FESS model with PI supervisory control was added to the RTG crane model presented in Section 5.1 in order to replicate the operation of the crane when equipped with a storage system.

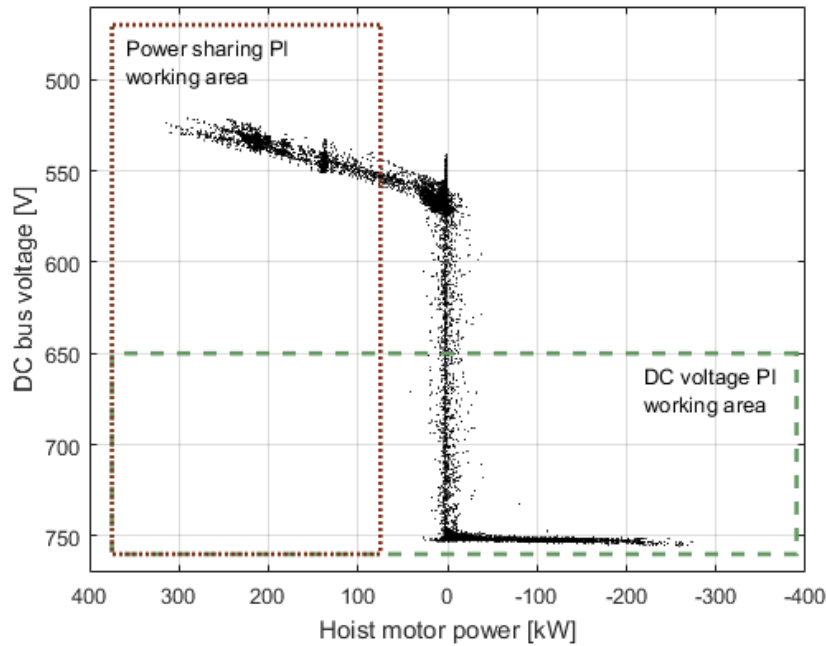


Fig. 6.6 Hoist power against DC bus voltage; every dot represents a data point collected at 10 Hz. The power sharing and voltage PI working areas are highlighted, showing that no activity happens in the overlapping zone.

During the 38 minutes, the crane performed 42 container lifts with weights ranging from 0 (spreader only) to 31 tonnes. Figure 6.7 shows the power flows and the energy stored by the ESS during the simulation. The PI controllers successfully charge and discharge the ESS as described in Sections 6.1.1 and 6.1.2, resulting in a total energy consumption of 20.44 kWh, saving 31% of energy with respect to the crane not equipped with an ESS (29.85 kWh).

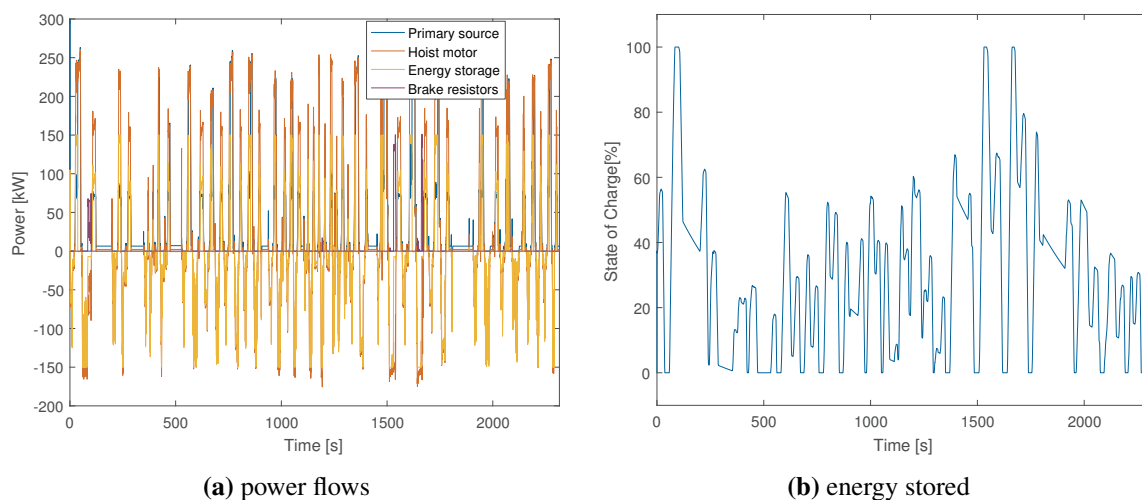
In order to present the operation of the PI control system in more detail, a single lift cycle is presented in Figure 6.8, where it is possible to discern how the PI controllers operate depending on the status of the crane. The chosen single lift is a snapshot of the simulation above (occurring at approximately $t = 1450$ seconds), and the initial conditions depend on the state of the system and the storage at this particular time.

Figure 6.8a shows the power flows, with the energy storage providing power when the hoist motor demands power. This particular lift cycle is composed of the following phases:

1. The empty spreader is lowered from a resting position to the top of a container. This occurs in the first 20 seconds of the lift cycle.
2. In the second phase the container is lifted, causing a massive power demand. This phase starts at around 20 seconds and lasts for 37 seconds.

Table 6.1 PI controllers parameters used in the simulation.

Controller	Parameter	Value
DC voltage PI	K_P	0.01
	K_I	0.1
	V_M	650 V
Power sharing PI	K_P	2×10^{-7}
	K_I	1×10^{-4}
	P_M	75 kW

**Fig. 6.7** Results from the full 38 minutes simulation using the PI supervisory control.

3. The third phase is characterised by power flowing from the hoist motor to the DC bus (showing as negative power) as the container is lowered into place. This phase occurs between 57 and 95 seconds in the simulation shown in Figure 6.8.
4. The fourth and last phase corresponds to the empty spreader being lifted back into the resting position. Energy is consumed by the hoist motor, although at a lower intensity compared to the second phase. This phase occurs in the last 25 seconds, starting at 95 seconds in the simulation.

6.1.4 Analysis of the results

The lift cycle presented in Figure 6.8 offers an interesting insight into the workings of the dual-PI supervisory control. It is an extract of the 38 minutes simulation, and it is presented as it shows the modus operandi of this supervisory control system. In this single lift cycle

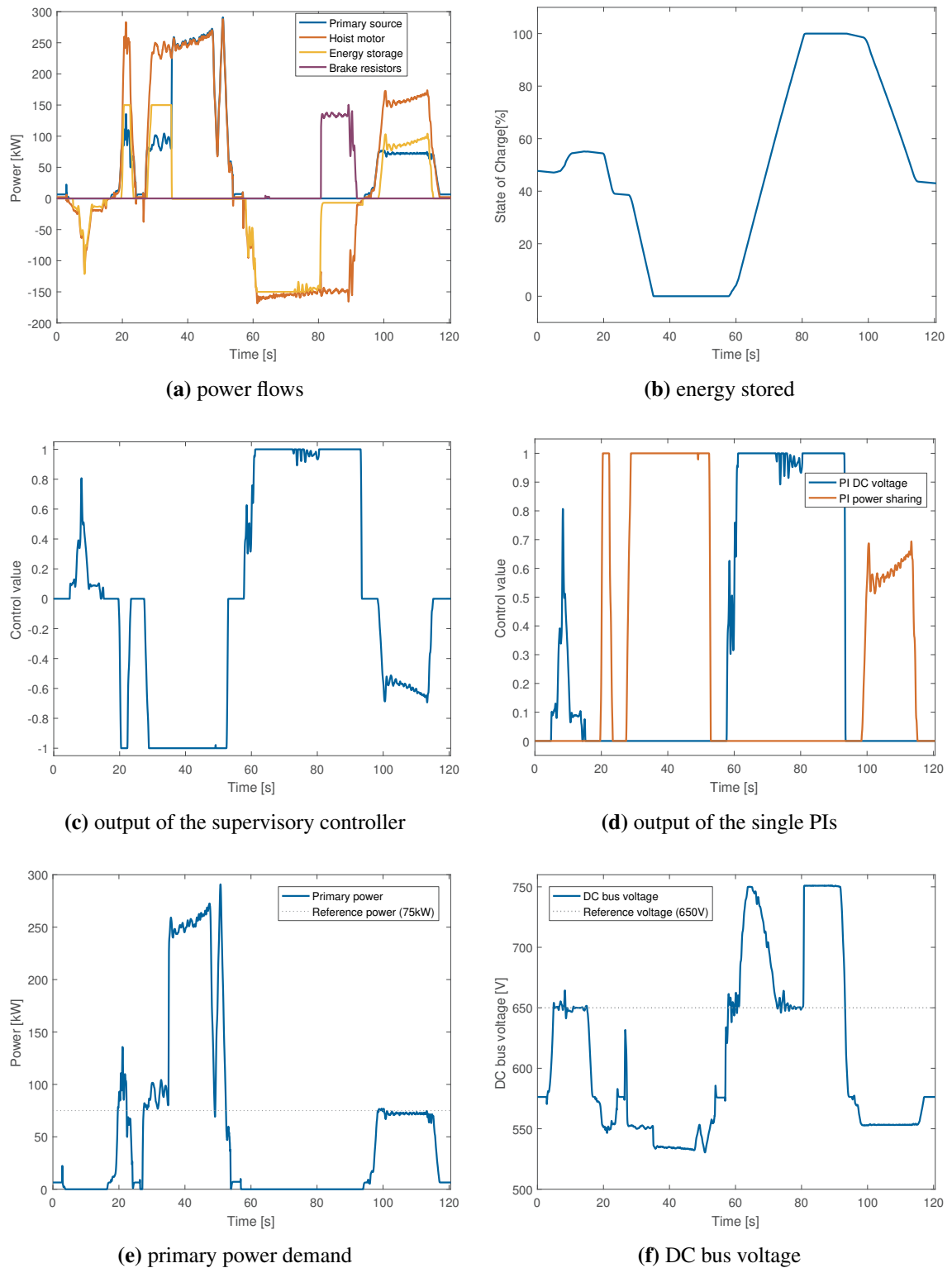


Fig. 6.8 Results from the full simulation using the PI supervisory control, single lift cycle.

the storage alternates charge and discharge, from empty to full. The supervisor successfully manages to recover and reuse stored energy, however the overall efficiency is constrained by limitations of the device and the supervisory control system. The storage device power output is limited to $P_s = 150$ kW, therefore it cannot provide all the power demanded by the hoist motor in phase 2. The primary source, therefore, needs to provide the additional power. As the storage reaches maximum power output, the PI controller responsible for the power sharing saturates to the maximum value of 1, shown in Figure 6.8d. After 38 seconds from the start of the lift cycle, the ESS is depleted (see Figure 6.8b) and its power output becomes 0, regardless of the PI output. The supervisory control has caused the fast depletion of the stored energy, whilst it would be preferable to spread it over a longer period in order to reduce overall peak demand and stress on the primary source.

In the third phase the hoist motor provides power at a high intensity, increasing the DC bus voltage over the activation threshold of the DC voltage PI ($V_M = 650V$). Figure 6.8f shows how the voltage increases in this phase, causing the activation of the DC voltage PI. The voltage PI controller successfully commands the storage to absorb the excess energy, preventing the activation of the brake resistors until the regenerated power exceeds the rating of the storage. At around 80 seconds from the start, the storage is full and cannot absorb any more power, therefore the brake resistors dissipate the extra energy.

In the fourth phase the crane lifts the empty spreader, demanding relatively low power. The power sharing PI can successfully limit the output of the generator to 75 kW by instructing the storage to provide the extra power. This activity is particularly evident from Figure 6.8d as the power sharing PI output reflects the varying demand of the hoist motor. In Figure 6.8e is shown how the primary power gets limited to the reference value of 75 kW in this particular phase.

The power and voltage reference chosen for the simulation are adequate for the generic operation of the crane. However, in this particular lift it is possible to see how the choice of P_M may not be suitable for every condition. This value is too low when lifting a heavy container, as the ESS cannot provide enough power for a long period of time in order to limit the primary power to 75 kW. During a demanding and long lift, the reference should be set to a higher value, allowing the primary source to take most of the effort. On the other hand, 75 kW is too high for the fourth phase when the crane is lifting an empty spreader: at the end of the lift, the ESS has still 43% of charge, so the primary source has been over utilised. In this case it would have been better to have a lower reference value, saving more energy. If the objective is to fully exploit the capabilities of the storage, the reference value needs to

change depending on the status of the ESS and the crane. Unfortunately, it is impossible to know beforehand what the power and energy consumption of a lift will be, but a solution exists: to treat the activity of the crane as a stochastic process and try to find the optimal reference value corresponding to the instantaneous state of the system.

6.2 Optimal supervisory control based on stochastic modelling

In the previous section it was highlighted how the choice of reference power in power-sharing mode can be a major design limitation that can reduce the effectiveness of the PI supervisory control strategy. This problem is caused by the inability to predict the future energy demand, which forced the choice of a constant power reference value for the power-sharing controller of 75 kW. This value is supposed to be lower for lifts of long duration that benefit from a sustained power output from an energy storage with limited energy capacity; on the other hand, it is supposed to be lower for short lifts that could be powered exclusively using the primary source.

An a-priori knowledge of the total energy consumption of a lift could lead to the generation of a power reference trajectory that maximises the combined benefits of the storage in terms of energy savings and peak power reduction. This thesis is based on the realistic assumption that information on future energy demand is unknown. To overcome this limitation, it is possible to develop an optimal controller that exploits known statistical information on the duration of container lifts. This controller can generate the best trajectory given the statistical and physical parameters of the system and the global objective (defined as a cost function). It can provide the optimal power trajectory for a system subjected to uncertainties that can be modelled by a random distribution, and this is the approach that has been chosen for the supervisory control presented in this section, which aims to maximise the advantages that can be obtained with the limited energy and power resources available.

As discussed in Chapter 1, optimal control has been applied in the past in conjunction with energy storage [66, 67, 62–65], including RTG cranes [22]. The innovations behind the controller presented in this section are the following:

- No knowledge is required of the future power consumption of the crane. Only statistical information of lift durations is needed.
- The cost function is not linked exclusively to fuel consumption but it can penalise a wide range of power flows, including reducing peak power demand.
- The formulation is generic and can be applied to any hybrid system subjected to a pulsed load of random duration.

6.2.1 Lift duration

As mentioned above, the total duration of the lift cycle has been assumed to be unknown. This uncertainty is due to the fact that a human operator controls the RTG crane and the choice of the container trajectory is not defined a-priori. Furthermore, in the current state the RTG taken as a reference has no knowledge of the height the container is going to reach. The maximum height is correlated with the total energy consumed in the lift cycle (with other variables being the weight and the speed), therefore the supervisory controller will not be able to produce an efficient power profile that satisfies the required objectives of energy saving and reduction in peak power demand for a single lift cycle. However, it is possible to obtain a control strategy that is mathematically optimal with a stochastic process defined by known random distributions [58]. This optimal control strategy would not be optimal for the single lift cycle, as the optimality requires the advanced knowledge of the length of the lift cycle before its start. However, the stochastic optimality would be reached over time as the lift duration distribution approaches the predicted distribution.

This chapter will present one possible optimal strategy based on measured characteristics of the lift duration distribution. The crane and the controller are assumed to have no knowledge of the future final time of the lift cycle (which defines its duration). The controller will also have access to instantaneous (not future) values of power demand and energy storage charge. The controller will then produce a reference power output for the storage from those instantaneous values and its knowledge of the optimal strategy.

It is clear that this optimal problem has significance only if the lift duration is unknown. As it will be discussed in the last chapter of this thesis, if future advances remove this uncertainty then this controller will be necessarily outperformed by one that relies on the advanced knowledge of the single lift cycle duration. In the meantime, this optimal problem will guarantee optimal performance for stochastic processes characterised by known load pulses of random duration.

6.2.2 Problem definition

Before detailing the optimal controller it is necessary to lay the foundation on which it is based, using the following assumptions:

- The primary power supply provides all the energy and power demanded by the crane and is represented as an infinite source, with the diesel generator or the power network

rated above the maximum possible load of the single crane. This is the case with cranes operating normally in container terminals: the main power source can provide enough energy and power to operate the crane without any energy storage device.

- The primary supply is unidirectional as power cannot be converted back to fuel or regenerated into the grid. This is due to the absence of an active front-end on the large majority of electric powered cranes and all diesel powered cranes.
- Crane power consumption is constant during the steady state of a container lift. This assumption reduces massively the complexity of the problem and increases the speed at which it is possible to calculate the optimal strategy. The actual power changes over time, however at runtime it can be approximated by a piecewise-constant approximation whose sampling time is equal to the sample time of the controller, reducing the impact of this assumption.

The cost associated with every unit of energy delivered can be represented by a positive definite function $D(p_g(t))$. In order to successfully achieve the objectives posed (in terms of energy and power consumption), $D(p_g(t))$ needs to include energy consumption as well as peak power demand. The objective of the proposed power management strategy is to use the stored energy to minimise the total cost of the energy production for the duration of a single lift, which is:

$$D_{tot} = \int_0^T D(p_g(t)) dt \quad (6.7)$$

with T indicating the maximum possible duration of the lift.

The Load

During a lift, the power required by the hoist motor is assumed known and constant with value P_L . The load profile can then be defined as following:

$$p_L(t) = \begin{cases} P_L, & \text{if } 0 \leq t \leq t_f \\ 0, & \text{otherwise} \end{cases} \quad (6.8)$$

where the instantaneous power demand $p_L(t)$ is not known because the lift duration t_f is unknown. The final time t_f is a random variable modelled by a distribution which is assumed known. It would be possible to calculate the optimal $p_s(t)$ assuming a deterministic and well-known load profile [66, 67]. However, the research presented in this thesis is based on

the realistic condition of ignorance of the future power demand, particularly regarding the lift duration which is only modelled by a probability distribution.

The Energy Storage

An energy storage system can supply the crane with power $p_s(t)$ in order to reduce the energy consumption of the crane:

$$p_g(t) = p_L(t) - p_s(t), t \in \mathbb{R}^+. \quad (6.9)$$

The storage model used in this problem is defined by the following differential equation:

$$\dot{E}(t) = -\eta_1 E(t) - \eta_2 - p_s(t) \quad (6.10)$$

where η_1 is a constant value that links losses to the stored energy (friction and windage losses) and η_2 is a constant power loss which is independent from the quantity of stored energy (e.g. power supply, cooling). The minimum and maximum stored energy levels are set as, respectively, 0 and E_{max} :

$$0 \leq E(t) \leq E_{max}. \quad (6.11)$$

After defining the generic physical systems that compose the basis of the optimal problem, it is possible to start defining the optimal management strategy.

6.2.3 Optimal power management strategy

The global objective is to minimise the total cost D_{tot} expressed in (6.7). The optimal controller is designed to find the storage output that minimises (6.7) which, given (6.9), is a functional corresponding to:

$$D_{tot} = \int_0^T D(p_g(t)) dt = \int_0^T D(p_L(t) - p_s(t)) dt \quad (6.12)$$

where T is the maximum possible value for t_f . As $D(p_g(t))$ is positive definite, there exists a trivial storage output $p_s(t) = 0$ corresponding to $p_L(t) = 0$, therefore:

$$D(p_g(t)) = 0 \quad \forall t : p_L(t) = 0 \quad (6.13)$$

Knowing from (6.8) that $p_L(t) = 0$ when $t > t_f$, we can reduce the limits of the integral in (6.12):

$$D_{tot} = \int_0^{t_f} D(p_L(t) - p_s(t)) dt + \int_{t_f}^T D(p_L(t) - p_s(t)) dt = \int_0^{t_f} D(p_L(t) - p_s(t)) dt. \quad (6.14)$$

The total cost value in (6.14) is calculated for a specific t_f which, in reality, is a random value whose distribution L is known. To account for the stochastic behaviour it is then necessary to calculate the expected value of the total cost, by considering a single value of t_f weighted by the probability of its occurrence. By defining $f_L(t_f)$ as the probability that a certain t_f occurs, the expected value of the cost D_E is the following:

$$D_E = \int_0^T f_L(t_f) \left(\int_0^{t_f} D(p_L(t) - p_s(t)) dt \right) dt_f \quad (6.15)$$

We assumed that $f_L(t_f) = 0 \forall t < 0$ as container lifts have positive duration, and also $f_L(t_f) = 0 \forall t > T$ and $T < \infty$ because duration is finite. Equation (6.15) spans the whole range of possible values of t_f and calculates the cost of applying a certain control strategy $p_s(t)$ in all possible scenarios, weighting the cost with the probability of that scenario to occur. An optimal control strategy $p_s^*(t)$ is then completed:

$$p_s^*(t) = \arg \min_{p_s(t)} \int_0^T f_L(t_f) \left(\int_0^{t_f} D(p_L(t) - p_s(t)) dt \right) dt_f. \quad (6.16)$$

By defining $F_L(t)$ as the Cumulative Distribution Function (CDF)[140] of the probability density function $f_L(t_f)$, we have:

$$F_L(t) = \int_{-\infty}^t f_L(t_f) dt_f = \int_{-\infty}^0 f_L(t_f) dt_f + \int_0^t f_L(t_f) dt_f = \int_0^t f_L(t_f) dt_f \quad (6.17)$$

and $F_L(t)$ has the following property:

$$\lim_{t \rightarrow \infty} F_L(t) = F_L(T) = \int_0^T f_L(t_f) dt_f = 1. \quad (6.18)$$

The integrand $D(p_L(t) - p_s(t))$ represents finite quantities:

$$\int_0^{\infty} |D(p_L(t) - p_s(t))| dt < \infty \quad (6.19)$$

since the load energy is limited (from (6.8)) as well as the stored energy. When taking into account (6.17) and (6.19), the expression in (6.16) is equivalent to:

$$p_s^*(t) = \arg \min_{p_s(t)} \int_0^T (1 - F_L(t)) D(p_L(t) - p_s(t)) dt \quad (6.20)$$

which is a more manageable form of minimisation as it involves a single integrand when the CDF is known. The proof of (6.20) is located in Appendix D.

Constraints

The problem in (6.20) has the trivial solution of setting $p_s(t) = p_L(t)$ if the available stored energy is infinite. In the actual world the energy capacity will be limited and this is reflected by adding the constraint (6.11) which will have the practical effect of limiting the amount of energy that can be provided by the storage, creating a *limited fuel* problem:

$$\int_0^T p_s(t) dt \leq E(0). \quad (6.21)$$

Furthermore, the dynamics of the storage system with its losses need to be taken into account; the expression in (6.10) dictates how the system loses energy over time, hence (6.21) misrepresents the available energy, and it needs to be replaced by (6.22).

$$\int_0^T (\eta_1 E(t) + \eta_2 + p_s(t)) dt \leq E(0). \quad (6.22)$$

The last constraint is the power rating of the storage which cannot exceed the maximum rated value and it is assumed to be the same, in absolute value, when motoring and generating:

$$-P_s \leq p_s(t) \leq P_s. \quad (6.23)$$

This type of optimal control problem has not yet been solved analytically [58, 141, 142] but it can be solved numerically by dynamic programming, accurately reducing the number of combinations to iterate through.

Numerical calculation

The non-convex problem defined in (6.20), with the domain defined by the constraints in (6.22-6.23), has been discretised in order to perform the numerical minimisation. This is because the numerical calculation requires the quantisation of the instantaneous control value $p_s(t)$, subject to constraints that are difficult to include in the minimisation process.

$$p_s^*(k) = \arg \min_{p_s(k)} \sum_{k=0}^N [(1 - F_L(k)) D(p_L(k) - p_s(k))] T_s \quad (6.24)$$

where T_s is the chosen sampling time. To represent the cost, $D(p_g(k))$ has been chosen as $p_g^2(k)$ as it penalises the higher costs associated with higher power demands to the generator and the network. In particular, it penalises high power demands as the cost increases with the square of the power. The constraint expressed in (6.22) is discretised as well:

$$\sum_{k=0}^N [\eta_1 E(k) + \eta_2 + p_s(k)] T_s \leq E(0). \quad (6.25)$$

The search space for the minimisation is reduced by parametrising the control function $p_s(k)$ using a PCHIP interpolant which has the characteristics of being continuously differentiable and its extrema are located at the extremal points. An interpolant function $P(k)$ is generated from a finite number N of data points (t_j, y_j) , $j = 1 \dots N$ which are then the values of the control signal. The number of values N define the complexity of the interpolant and also the computing time; N must be chosen as a trade-off between the time required by the calculation and resolution of the signal. In order to further reduce the search space, it is assumed that the optimal $p_s(k)$ is monotonically decreasing for $k \in [0, T]$ due to the monotonically decreasing characteristics of the scaling factor $(1 - F_L(k))$.

The output

The outcome of the minimisation is a control strategy which needs to be calculated for a specific range of parameters: distribution of the durations, initial conditions of the storage, load intensity and storage dynamics. In case of distinct possible initial conditions, it is necessary to calculate the optimal strategy for each scenario. For example, if the energy stored at the beginning is not a constant, the controller must account for the possible range

of initial storage level and produce an output which is appropriate for that particular initial condition.

The optimal strategy P^* that it is necessary to calculate is represented as follows:

$$P^*(k, L, E_0, P_s, \eta_1, \eta_2)$$

where k is the sample time since the start of the lift, L defines the distribution of the durations, E_0 is the starting energy of the storage, P_s is the load intensity and η_1, η_2 define the energy storage dynamics. The controller will then output an optimal reference power $p_s^*(k)$ which depend on the time and state of the system.

6.2.4 Simulation and results

The optimal problem defined in the previous Section can now be used to calculate the optimal control strategy. The optimal control is tailored for a specific system whose parameters are presented in Table 6.2. The choice of η_1 and η_2 are representative of a system with 1% energy loss over time and a constant loss of 1 kW. These values must be chosen as close as possible to the actual system in order to guarantee the optimality of the controller. Any deviation may result in a decreased efficiency of the controller. For example, a higher η_1 is characteristic of a system which loses high amounts of power at high energy levels, for example in the case of a flywheel with high friction losses. Higher values of η_2 increase standing losses that are independent of the stored energy as well as auxiliary system support (e.g. cooling, powering control systems). Whilst it may be possible to calculate the values of η_1 and η_2 , it may be necessary to estimate them a-priori, as it was done in this research because an actual flywheel was not available when the optimal calculation algorithm was run.

Table 6.2 Parameters of the system used for the calculation of the optimal control strategy.

Parameter	Value
P_s	150 [kW]
E_{max}	3.6 [MJ]
η_1	1 [%]
η_2	1 [kW]

Distribution of lift durations

Measurements of the activity of an RTG crane were recorded at the Port of Felixstowe, including the duration of container lifts measured as the interval between the start of a lift (i.e. the hoist motor speed becomes positive) and its end when reaching zero speed. The data was collected for a period of 6 days, after which it was analysed and fit to a Gamma distribution. This distribution, defined by parameters α and β , was chosen as it results in the best fit to the data. The probability density $f_L(t)$ of a Gamma distribution L is described by the following equation:

$$f_L(t) = \frac{t^{\alpha-1} e^{-\frac{t}{\beta}}}{\beta^\alpha \Gamma(\alpha)} \quad \text{for } t \geq 0 \text{ and } \alpha, \beta > 0 \quad (6.26)$$

where $\Gamma(\alpha)$ is the Gamma function evaluated at α and it is a constant:

$$\Gamma(\alpha) = \int_0^\infty x^{\alpha-1} e^{-x} dx. \quad (6.27)$$

The actual random variable t has a realistic upper limit T as the duration of the load is limited in time, so the distribution used in the calculation has been truncated at $t = T$. The parameters α and β have been found by minimising the squared error and are presented in Table 6.3. Figure 6.9 shows the histogram of lift durations superimposed on the Gamma distribution.

Table 6.3 Parameters of the Gamma distribution which fits the lift duration data.

Parameter	Value
α	5.0292
β	4.3923

The CDF $F_L(t)$ can be easily pre-calculated off-line for each instant by integration or by using the following equation:

$$F_L(t) = \int_0^t f(u) du = \frac{\gamma\left(\alpha, \frac{t}{\beta}\right)}{\Gamma(\alpha)} \quad (6.28)$$

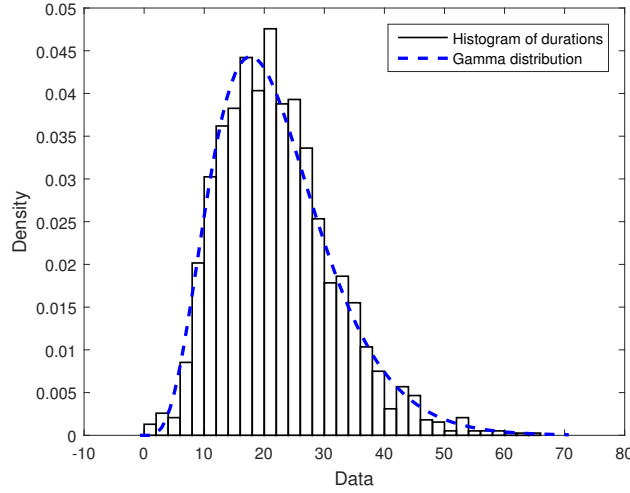


Fig. 6.9 Histogram of the lift durations superimposed on the Gamma distribution that fits the data.

where $\gamma\left(\alpha, \frac{t}{\beta}\right)$ is the *lower incomplete gamma function* and equal to:

$$\gamma(s, x) = \int_0^x t^{s-1} e^{-t} dt. \quad (6.29)$$

Numerical calculation of optimal values

The number of calculations to be performed is too large for a single system, for this reason a *HTCondor* cluster [143] composed of over 300 nodes has been used to calculate the optimal strategy when varying the values of $E(0)$ and $p_L(t) = P_L$. The nodes work concurrently on different initial conditions to find the minimum cost by searching in the \mathbb{R}^2 parameter space defined by the points (t_j, y_j) which can vary from $[0, -P_s]$ (corresponding to the initial time and minimum power output) to $[T, P_s]$. The time distribution of these points has been selected with the objective of maximising the variability of the interpolant when the changes in power output are more expected; that is, when the probability $f_L(t)$ is higher. The points need to be adequately distributed as well, so the choice for the values t_j is the following: given τ_j a series of N points linearly distributed in the interval $[0, 1]$ and given a CDF $F_L(t)$, the values t_j are:

$$t_j = F_L^{-1}(\tau_j) \forall j = 1 \dots N. \quad (6.30)$$

resulting in a distribution of t_j which tends to concentrate the values where the CDF changes more rapidly, which in turns corresponds to the instants when the probability $f_L(t)$ is higher as is shown in Figure 6.10.

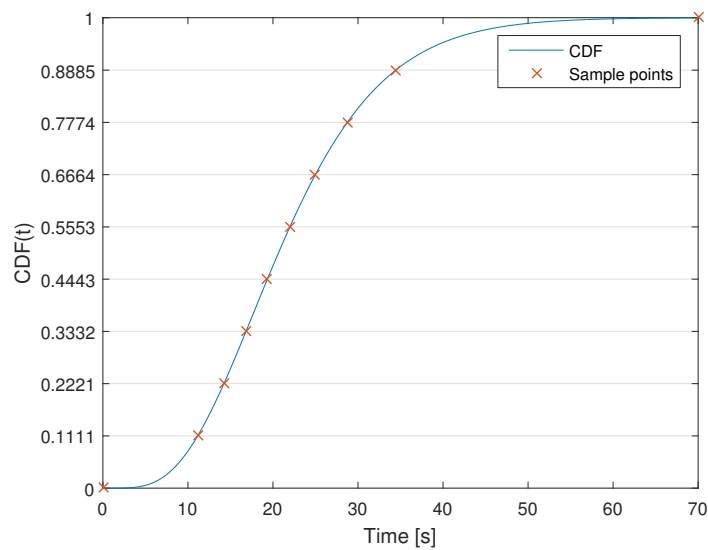


Fig. 6.10 Temporal distribution of 10 sample points of a PCHIP interpolant superimposed on the CDF. The vertical position of the PCHIP points indicates the distribution in the $[0, 1]$ region.

The output of the calculation is a matrix of parameters linked to an individual initial condition of the storage and value of the load. Given a particular scenario, the control system reads the optimal values calculated off-line and generates the optimal power output $p_s^*(k)$ in real-time via PCHIP interpolation. Figure 6.11a shows an example of the output of the calculation as well as the PCHIP interpolation used as reference for the control system. The parameters used in the minimisation (including discretisation and load ranges) are presented in Table 6.4. Parameters ΔP_L and $\Delta E(0)$ indicate, respectively, the resolution used for the load power and the initial stored energy. A sample of the results of the calculations is shown in Figure 6.11b.

Table 6.4 Parameters of the numerical minimisation.

Parameter	Value
P_s	150 kW
T	70 s
ΔP_L	10kW
$E(0)$ (range)	[720,3470] kJ
$\Delta E(0)$	101.8 kJ

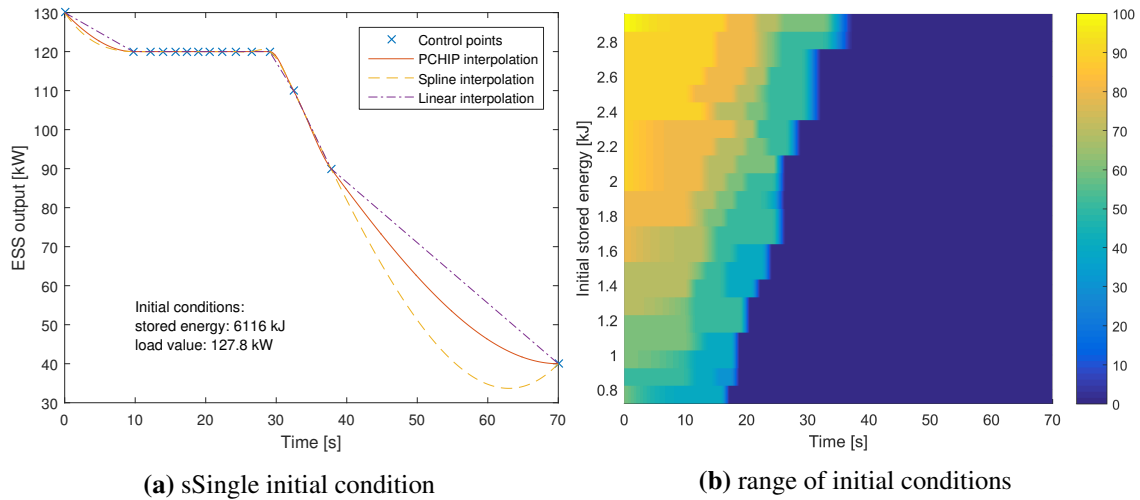


Fig. 6.11 Examples of control points calculated in the minimisation. (a) shows the control points calculated for a single pair of initial conditions. Three different interpolations are also shown (PCHIP, spline and linear). Notice how the spline interpolation does not maintain monotonicity between points. (b) shows a range of optimal control strategies calculated for $0.72\text{MJ} < E(0) < 3.00\text{MJ}$ and $Pl = 100\text{kW}$. The colour bar on the right shows the power output of the storage expressed in kW.

Simulations

Similarly to the PI control system, the optimal control system was implemented in Simulink and used in conjunction with the ESS described in Section 5.2.3, connected to an RTG crane operating for 38 minutes in normal conditions and performing 42 lifts. The results, presented in Figure 6.12, show an energy consumption of 20.52 kWh, a 31% reduction with respect to the crane not equipped with ESS.

Figure 6.13 shows a single lift cycle extracted from the simulation above, where is visualised more clearly the activity of the energy storage. Note that the behaviour of the storage during a lowering (seconds 57 to 95 seconds from the start of the cycle) is very similar to the one presented in the section regarding PI control: this phase is taken care of by a DC voltage PI controller which is equivalent to the one used previously. The optimal controller calculates the optimal trajectory only during a lift, as the regenerated power is given “for free” and there is no reason for limiting the charging of the storage

6.2.5 Analysis of the results

The lift cycle shown in Figure 6.13 offers an insight into the operation of the optimal controller. When the hoist motor is lifting a container the power output of the storage is

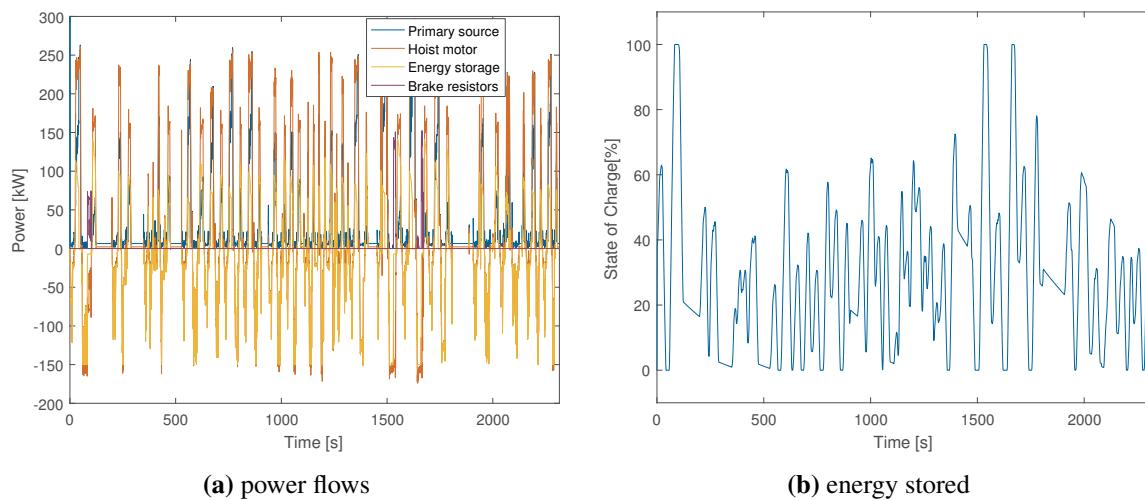


Fig. 6.12 Results from the full simulation using the optimal supervisory control.

controlled by the optimal control: the power profile depends on the conditions of the storage at the beginning of the lift, therefore with low starting energy (Figure 6.13b) the power output will be lower than one with a high starting energy. This is clearly visible in Figure 6.13e where the control output is significantly higher in the second lift (at around 100 seconds) because the storage starts delivering power when it is fully charged, unlike the first lift where it starts at around 50% charge. When calculating the optimal strategy, a low power lift like the one of the empty spreader (at 100 seconds after the start of the cycle) was linked to a high power output of the ESS: note how the controller makes use of almost all of the stored energy, finishing with less than 15% of charge at the end of the lift. If the lift had lasted 5 seconds more, the storage would have been fully depleted, indicating an efficient utilisation of the stored energy. In fact, the length of the spreader lift (around 20 seconds) is slightly below the mode of the distribution shown in Figure 6.9.

One potential limitation of this control system is the following: if the distribution of lift durations change, the control will no longer be optimal. Furthermore, this control system is tailored for a very specific storage system implemented in a particular RTG crane, whilst it may be beneficial to design a control system that renounces optimality in order to be universal and not tied to a particular system. One potential control system that has those characteristics is Fuzzy Logic Control which is presented in the following section.

A more thorough analysis of the optimal control system will be found in Chapter 7, where it will be also compared with other control systems, including the power sharing PI presented previously in this Chapter and the Fuzzy Logic Control discussed below.

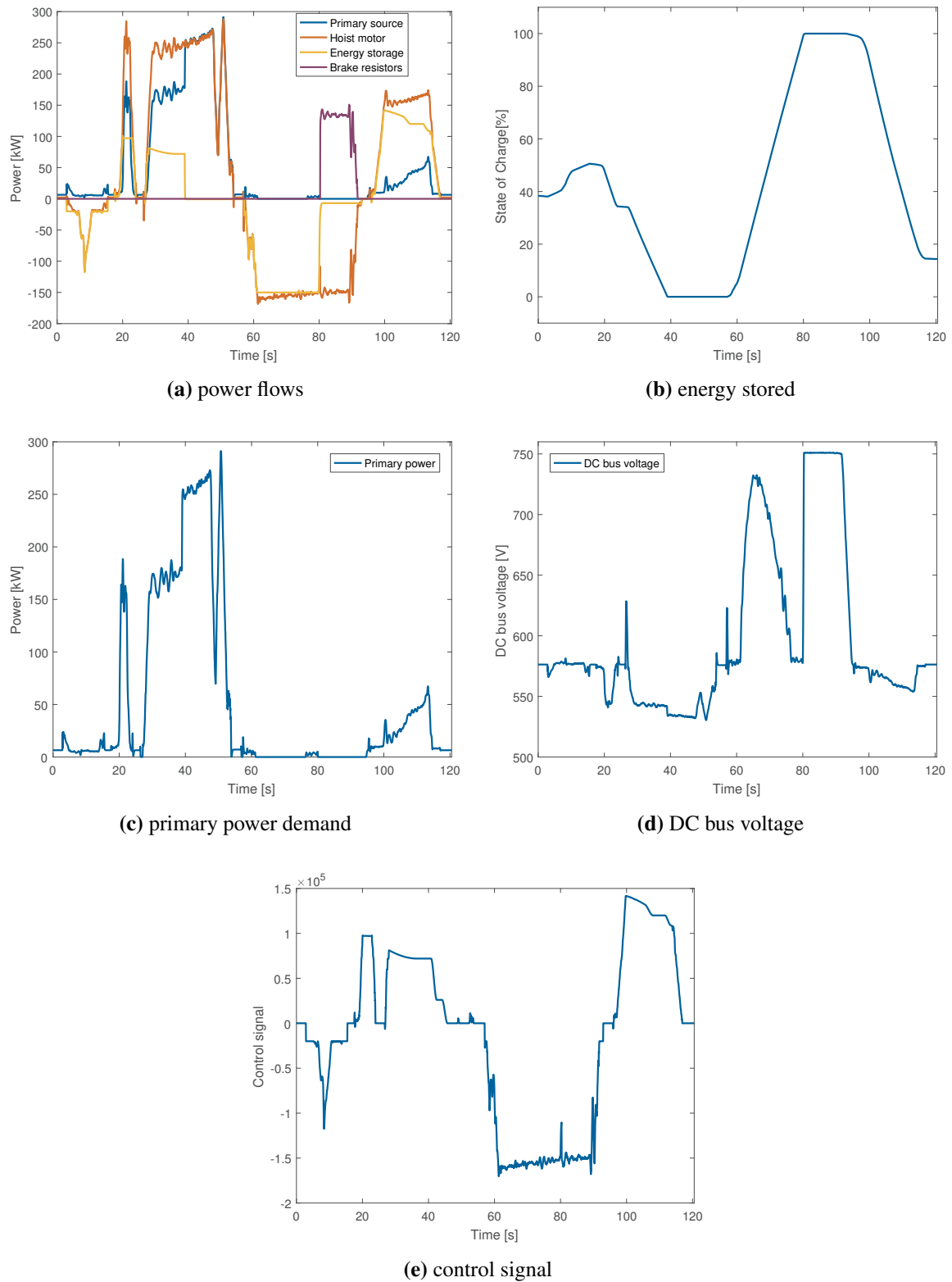


Fig. 6.13 Results from the full simulation using the optimal supervisory control, single lift cycle.

6.3 Fuzzy logic supervisory control

A Fuzzy Logic Controller (FLC) is based on fuzzy logic rules which determine the value of the control output depending on the approximate state of the inputs. For example: if the hoist motor is regenerating power, then the storage should be charged; if the hoist motor is regenerating a **large** amount of power, then the storage should be charged **faster**. Fuzzy rules allow for degrees of uncertainties on the measurements or the parameters, as the output is calculated depending on the degrees of membership of the inputs to fuzzy sets and not crisp values.

The objective of using fuzzy logic control is to increase the robustness of basic rule-based controllers, which are currently the most common controllers used in hybrid RTGs. As discussed in Section 2.2.2, FLCs are widespread in other areas (e.g. hybrid electric vehicles), however for RTGs they have only been the subject of one work [57] even though Xu *et al.* [50] recommended their use with RTGs. Their use is then proven in similar applications and comparisons have shown that they are a viable and efficient alternative [30]. FLCs possess qualities that are favourable to the use in hybrid RTGs: their structure is based on simple logic which helps the initial development. Once implemented in a control system they act as simple inputs-to-output mapping that has no dynamic and therefore they are very easy to test when associated with complex models as the RTG one presented in Chapter 5.

This work is based on the Mamdani FLC [52]: a fuzzification process transforms the input into fuzzy sets that are then processed using linguistic rules (*if X then Y*) in order to produce an output, which then undergoes a defuzzification process to produce the crisp output value [51]. This process is shown in Figure 6.14.

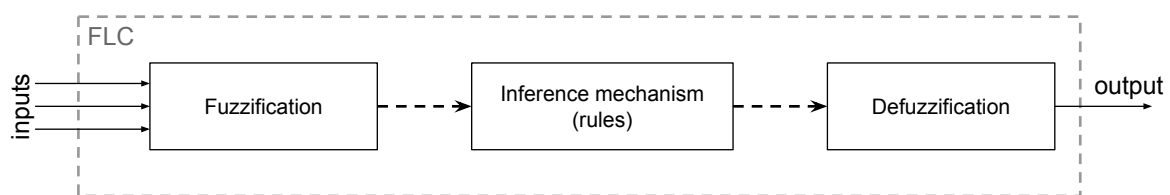


Fig. 6.14 Structure of a fuzzy system.

Designing a FLC may require a less formal approach with respect to other controllers as it is based on intentionally vague evaluations of the inputs in order to determine the output. Nonetheless, it does not mean that it is simpler or easier to do so, as it requires a deeper understanding of the complex system that needs to be controlled. In this particular case, the thorough knowledge of the operation of the RTG crane — and its power flows — is necessary

for the development of this controller. This requirement will be evident in the following sections, where the fuzzy rules are presented and explained. A FLC is usually quite robust to changes in the parameters of the system because, as the name implies, it uses fuzzy logic and it is not necessarily bound to exact values: the power flow can be defined as “low”, “medium” or “high”, with very gradual and smooth boundaries between the three levels [51].

The assumption used for the development of this controller is that the control system has access to similar inputs as the previous two controllers defined in this chapter. These inputs are: FESS rotational speed, power flowing to the hoist motor and DC bus voltage. The (single) output is normalised and bounded in $[-1,1]$, corresponding respectively to maximum power input and maximum power output.

6.3.1 Membership functions

Every signal or value that is fed as an input to the controller is associated with its own set of pre-defined fuzzification functions. The actual “crisp” value of the input is not important, what matters is its degree of membership to a particular linguistic description (e.g. “high”). A DC voltage of 750 V, in the case of a crane, can be defined as “very high” with the maximum degree, 1. On the other hand, 650 V is just in between a “normal” and “high” voltage level, therefore this value is 0.5 “normal” and 0.5 “very high”.

The inputs undergo a process of fuzzification through the application of membership functions $\mu_M(x)$ that map the input x into $[0,1]$ depending on their degree of membership to a particular set \mathbf{M} ; the membership functions belong, usually, to three categories: triangular, trapezoidal or sigmoid. Trapezoidal functions are shown in Figure 6.15, where the intensity of power flowing through the hoist motor is classified into three different fuzzy sets: low power, medium power and high power. When the power is very low, only the “low power” condition will be active and the associated membership function μ_{lp} will have positive value. As the power increases and approaches $pt1$, μ_{lp} will decrease and μ_{mp} will start to grow from 0 to 1, because the power can now be defined as “medium power”.

The three inputs that need fuzzification are: flywheel speed, hoist power and DC bus voltage. The parameters chosen for the membership functions are based on the power flows and the activity of the crane. The values presented in this thesis are the result of a trial-and-error process guided by the knowledge acquired analysing RTG data and results obtained from other control strategies. All the membership function are visualised in Figure 6.17a-c and are also described in the sections below.

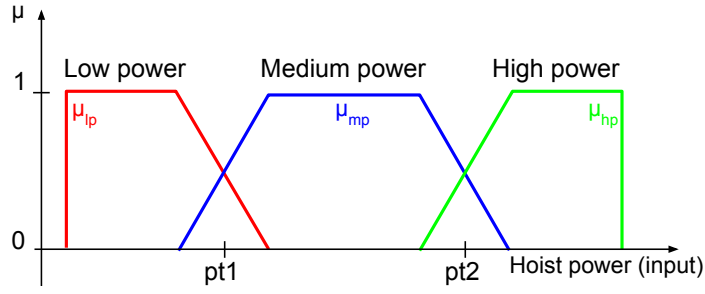


Fig. 6.15 Example of membership functions for a FLC.

Flywheel speed

The speed of the flywheel storage is bounded, therefore its power flow needs to be restricted near the limit values. The membership function $\mu_{lowSpeed}$ linked to the first input $FESSspeed$ (in RPM) is used to maintain the storage in the charge limits as in [93]:

$$\mu_{lowSpeed} = \begin{cases} 1, & FESSspeed < 5000 \\ -\frac{FESSspeed}{200} + \frac{5200}{200}, & 5000 \leq FESSspeed < 5200 \\ 0, & \text{otherwise} \end{cases} \quad (6.31)$$

where the lower limit is 5000 RPM and 5200 RPM is the highest value of the **lowSpeed** fuzzy set. The values in $\mu_{lowSpeed}$ have been chosen to achieve a soft transition to this fuzzy state, avoiding a sudden change in control output.

The set **normalSpeed** is associated to the normal operating speeds of the storage. It is characterised by a degree of membership 1 for a very large proportion of the admissible FESSspeeds:

$$\mu_{normalSpeed} = \begin{cases} 0, & FESSspeed < 5000 \\ \frac{FESSspeed}{200} - \frac{5000}{200}, & 5000 \leq FESSspeed < 5200 \\ 1, & 5200 \leq FESSspeed < 14800 \\ -\frac{FESSspeed}{200} + \frac{15000}{200}, & 14800 \leq FESSspeed < 15000 \\ 0, & FESSspeed \geq 15000. \end{cases} \quad (6.32)$$

Unlike similar Fuzzy Logic Controllers developed for batteries, as in [53, 54], there is no differentiation between a low state of charge and a high one, as flywheel storage does not

degrade when deep discharged and the SR FESS used in this research can provide maximum power at any allowed speed.

A similar membership function as the *lowSpeed* is applied to the “high” speed set **highSpeed**, where the upper boundary is set to 15000 RPM, which is the maximum rotating speed of the flywheel. The membership functions described above are shown in Figure 6.17a and are defined in detail in Appendix E, Section E.1.1.

Hoist Power

The second input, *HoistPower* in W, is the power flowing to the hoist motor, and it is positive if the motor is demanding power. The fuzzy sets depend on the sign of the power (Negative, Positive or Zero) and are categorised as High, Medium and Low depending on the intensity. For example, if the hoist power is “positive high” then it will belong to the set **PH**, from the initials of Positive and High. If the power is “negative medium”, the set will be **NM**. The last set, **POS**, is only used to identify whether the power is positive or negative, therefore it will be active if the power is positive. As an example, the membership function μ_{NH} is presented below:

$$\mu_{NH} = \begin{cases} 1, & HoistPower < -350000 \\ -\frac{HoistPower}{150000} - \frac{200000}{150000}, & -350000 \leq HoistPower < -200000 \\ 0, & otherwise. \end{cases} \quad (6.33)$$

The values that compose this function are chosen to provide a smooth transition between fuzzy sets.

The fuzzy sets that define the power level are the following: **NH**, **NM**, **NL**, **Z**, **PL**, **PM**, **PH**, **POS**. The 8 membership functions are presented in Section E.1.2 and are shown in Figure 6.17b. The rules related to these power levels will specify the amount of power that the ESS needs to provide depending on the power level of the hoist motor: intuitively, the higher the intensity, the higher the ESS power output.

DC bus voltage

The third and last input to the FLC is the DC bus voltage $DCbusV$. When the crane is idle the voltage will fluctuate around 600 V, therefore the energy storage should be kept inactive at that voltage level. During a lift, motors demand power lowering the DC bus voltage: the voltage will then be defined as “low” (**L**). However, a dramatic increase in voltage should determine an activation of the energy storage in order to absorb the regenerated energy: this happens in the “high” (**H**) and “very high” (**VH**) states of the voltage. An additional voltage state, “zero” (**Z**), is used to indicate an extreme condition determined by very low bus voltage. Below is the membership function linked to the “normal” voltage state, μ_N :

$$\mu_N = \begin{cases} 0, & DCbusV < 550 \\ \frac{DCbusV}{25} - \frac{550}{25}, & 550 \leq DCbusV < 575 \\ 1, & 575 \leq DCbusV < 600 \\ -\frac{DCbusV}{100} + \frac{700}{100}, & 600 \leq DCbusV < 700 \\ 0, & DCbusV > 700. \end{cases} \quad (6.34)$$

This function has output 1 when the voltage is between 575 and 600 V, which are voltages associated with an idle crane. Then the fuzzy set transitions to 0 as the voltage deviates from the norm.

The fuzzy sets for the input $DCbusV$ are the following: **Z**, **N**, **L**, **H**, **VH**, similar to what has been done previously in [53]. The membership functions are defined in Section E.1.3 and are shown in Figure 6.17c.

Figure 6.16 summarises the fuzzification process showing the three inputs and the associated fuzzy sets.

Output

The fuzzy sets defined for the inputs are then linked via a linguistic rule to an output state, which will be used later to calculate the (crisp) output value of the controller. In this work, 7 output states have been defined following a similar strategy to the one presented in [53]: the storage is either importing (charging) or exporting (discharging) power at a low, high or very high intensity. There is also a “zero” state (**Z**) that is related to a zero output power. The fuzzy states are, in order from maximum import to maximum export, are: import very

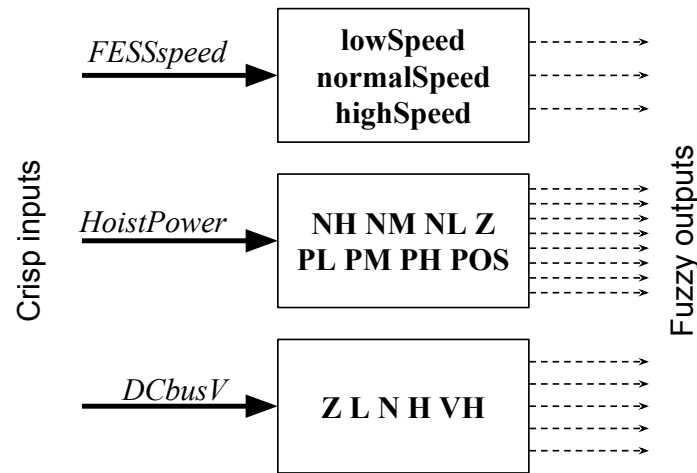


Fig. 6.16 Fuzzification process of the three inputs and their associated fuzzy sets.

high (**IVH**), import high (**IH**), import low (**IL**), zero (**Z**), export low (**EL**), export high (**EH**), and export very high (**EVH**). The membership functions are defined in Section E.2.1 and are shown in Figure 6.17d. An example of an output membership function is the following:

$$\mu_{EH} = \begin{cases} \frac{i - 0.5}{0.5 - 0.5}, & 0.5 \leq i < 1 \\ -\frac{i}{0.5} + \frac{1.5}{0.5}, & 1 \leq i < 1.5 \\ 0, & \text{otherwise} \end{cases} \quad (6.35)$$

where i is the control output.

The inputs and output of the FLC are summarised in Table 6.5, with each signal associated to a particular symbol that identifies it in the rules definition. The following section will discuss how logic rules can link input fuzzy states to each of the output states.

Table 6.5 Input and output signals of the FLC with their associated symbols.

Signal	Type	Symbol
Flywheel storage rotational speed	Input	<i>FESSspeed</i>
Hoist motor power	Input	<i>HoistPower</i>
DC bus voltage	Input	<i>DCbusV</i>
Control output to the ESS	Output	<i>ESScontrol</i>

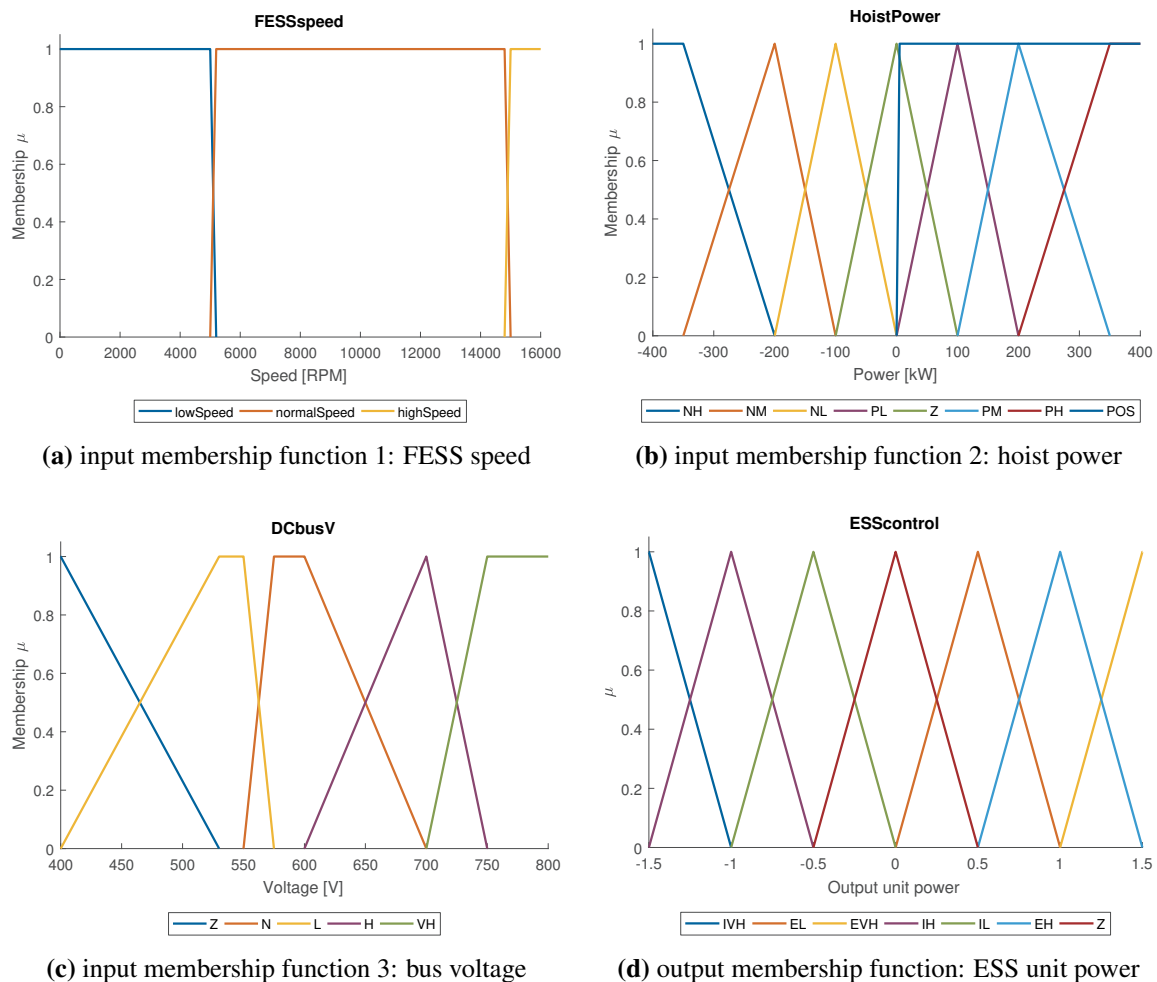


Fig. 6.17 Membership functions of the Fuzzy Logic Controller.

6.3.2 Rules

The Mamdani type FLC is characterised by linguistic rules that link fuzzy states to output fuzzy states using logic and if/then operators [52]. An input state, or a combination of input states, can then activate an output state with a degree that depends on the degree of membership of the input states. This process, called inference, determines the degree of firing of each rule [51]. Later, it will be explained how a crisp output is extracted from the resulting aggregation of rules.

Using a single membership function $\mu_M(x)$ and a single rule R as an example, it is possible to define the simplest rule as:

R : if x is \mathbf{M} , then y is \mathbf{O}

where \mathbf{M} is an input fuzzy state, \mathbf{O} is an output state and y is a fuzzy output. The rule R will be fired to the extent $\mu_M(x)$ (which maps x to $[0,1]$) and it corresponds to a certain implicit fuzzy set \mathbf{O} with associated membership function μ_O . Multiple inputs can cooperate to fire a rule by using logic operators (e.g. AND, OR, XOR). In this work, all the rules have been designed with the AND (or, when negated, AND NOT) operator, and the method chosen to intersect the sets is the “minimum”: only the lowest output of the membership functions belonging to this rules is carried over:

$$\mu^{M_1 \cap M_2 \cap \dots \cap M_n}(x) = \min\{\mu_{M_1}(x), \mu_{M_2}(x), \dots, \mu_{M_n}(x)\} \quad (6.36)$$

where $\mathbf{M}_1, \mathbf{M}_2, \dots, \mathbf{M}_n$ are the n input fuzzy sets that are part of that rule. If the rule includes an AND NOT, the associated function will be negated: AND NOT $\mu(x) = \text{AND } \bar{\mu}(x)$, where $\bar{\mu}(x) = 1 - \mu(x)$. Every rule is also associated with a weight which determines the strength of the effect of that rule on the output during the defuzzification phase; a low weight (which is independent of the degree of membership) indicates that the rule has a minor impact on the output with respect to rules with higher weight.

It is useful to provide an example which visualises the effect of a rule firing with varying extents. In Figure 6.18a a rule is fired and it is translated to an output fuzzy set, but with two distinct degrees, the first with degree 1 and the second with degree 0.7. The effect is that the first will have a larger impact on the output in the presence of multiple firing rules with respect to the second. In fact, Figure 6.18b shows what happens when two rules fire with different degree: the first dominates visually on the second, prevailing also for the choice of the output value. The defuzzification process will be presented later in this Chapter, where the method chosen for determining the crisp value of the output will be described.

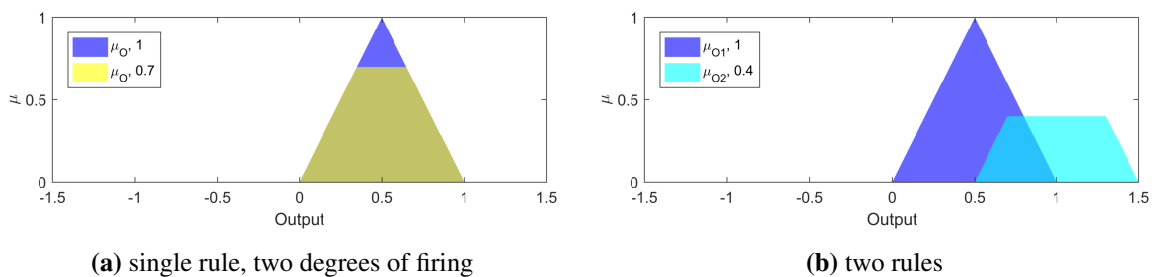


Fig. 6.18 Examples of an FLC inference stage.

The rules chosen for the FLC are divided into four categories and are shown below:

1. Import rules

- (a) If (*FESSspeed* is **not highSpeed**) and (*DCbusV* is **VH**) then (*ESScontrol* is **IH**) , weight: 1.00
- (b) If (*FESSspeed* is **not highSpeed**) and (*DCbusV* is **H**) then (*ESScontrol* is **IL**) , weight: 1.00
- (c) If (*FESSspeed* is **not highSpeed**) and (*HoistPower* is **NH**) and (*DCbusV* is **not Z**) then (*ESScontrol* is **IVH**) , weight: 1.00
- (d) If (*FESSspeed* is **not highSpeed**) and (*HoistPower* is **NM**) and (*DCbusV* is **not Z**) then (*ESScontrol* is **IH**) , weight: 1.00

2. Export rules

- (a) If (*FESSspeed* is **not lowSpeed**) and (*HoistPower* is **PH**) and (*DCbusV* is **not VH**) then (*ESScontrol* is **EVH**) , weight: 1.00
- (b) If (*FESSspeed* is **not lowSpeed**) and (*HoistPower* is **PM**) and (*DCbusV* is **not VH**) then (*ESScontrol* is **EH**) , weight: 1.00
- (c) If (*FESSspeed* is **not lowSpeed**) and (*HoistPower* is **PL**) and (*DCbusV* is **not VH**) then (*ESScontrol* is **EL**) , weight: 1.00

3. Idle rules

- (a) If (*HoistPower* is **not POS**) and (*DCbusV* is **N**) then (*ESScontrol* is **Z**) , weight: 1.00
- (b) If (*FESSspeed* is **not lowSpeed**) and (*HoistPower* is **not POS**) and (*DCbusV* is **L**) then (*ESScontrol* is **Z**) , weight: 1.00
- (c) If (*HoistPower* is **Z**) and (*DCbusV* is **N**) then (*ESScontrol* is **Z**) , weight: 1.00

4. Input-space filling rule

- (a) If (*FESSspeed* is **not normalSpeed**) then (*ESScontrol* is **not Z**) , weight: 0.01

The first category relates to the import phase: the storage absorbs power that is generated by the hoist motor when lowering a container. All the 4 rules in this category begin with negating the **highSpeed** set for the input *FESSspeed*, indicating that the flywheel speed must not be too high in order to activate this rule. The first two rules link a DC voltage input state (**VH** or **H**) into a corresponding output state (**IH** and **IL**), so the ESS will absorb power with an intensity that depends on the voltage level of the DC bus. Rules 1c and 1d are activated

by the hoist motor power being negative (with varying intensity), and also by the DC bus voltage not being very low; the effect is that the control output will increase the imported power as the hoist regenerates more power.

The second category relates to the export phase: the hoist motor starts demanding power (and *HoistPower* is positive). All the three rules in this category include a check for *FESSspeed*: the rule decreases the degree of firing as the speed enters the **lowSpeed** fuzzy state. They also include a check on the DC bus voltage level: if it is very high, the rules are not fired, because that would indicate an excessive storage power output which causes an undesired increase in DC bus voltage. The three rules differ only by the *HoistPower* fuzzy set: as the hoist power decreases (from **PH** to **PL**) the control output goes from **EVH** to **EL**, thus decreasing the ESS power output; this will cause the storage to output power depending on the intensity of the demand.

The third category defines the logic that limits the control output magnitude. Rule 3a checks that the hoist motor power is not positive (which would indicate a power demand) while also checking if the voltage level is in normal state. If that is the case, then the output state selected is zero (**Z**). Similarly, the second rule of this category inhibits the storage when the voltage is low with a simultaneously negative hoist motor power. The reason behind those two rules is to limit the activity of the storage when the hoist motor has not yet increased the DC bus voltage to a level above the rectifier activation threshold. The last rule of this category is trivial: if the host motor power is zero and the DC bus voltage is normal, then do nothing.

The last category has only one rule and its purpose is to fill the input space so every combination of inputs is mapped into an output, ensuring there are no ambiguous situations where no rule is firing. Note that this is the only rule that has weight different than 1: the low weight ensures minimal impact of this rule on the FLC global output.

In summary, the import rules determine the storage output based on the DC bus voltage measurement, whilst the export rules are mostly based on the hoist motor power. The idle rules determine the conditions where the storage needs to stop outputting power whilst the input-space filling rule is only used to avoid ambiguous output conditions. Table 6.6 presents the rules in a tabular form which helps visualise the logic.

Table 6.6 Rules defined for the FLC.

Rule	<i>FESSspeed</i>	<i>HoistPower</i>	<i>DCbusV</i>	<i>ESScontrol</i>	weight
1a	not highSpeed		VH	IH	1
1b	not highSpeed		H	IL	1
1c	not highSpeed	NH	not Z	IVH	1
1d	not highSpeed	NM	not Z	IH	1
2a	not lowSpeed	PH	not VH	EVH	1
2b	not lowSpeed	PM	not VH	EH	1
2c	not lowSpeed	PL	not VH	EL	1
3a		not POS	N	Z	1
3b	not lowSpeed	not POS	L	Z	1
3c		Z	N	Z	1
4a	not normalSpeed			not Z	0.01

6.3.3 Defuzzification

The fired rules will produce a collection of recommendations, each produced by the implied fuzzy set associated with each rule. When multiple rules associated with the same output fuzzy set are fired, only the one with the highest weighted degree of firing is considered. Figure 6.18 shows an example of one or two implied fuzzy sets fired with different degrees. The crisp output is generated from the aggregate of these recommendations by using some form of weighted averaging on the area formed by the superimposition of the output membership functions (in Figure 6.18b, this is the area occupied by the trapezoids). For example, the crisp output could be one of the points where the resulting output set has the maximum (corresponding to 0.5 in Figure 6.18b), or the value corresponding to vertical line that divides the figure in two regions of equal area (bisector). The method chosen in this work is the centroid, which is the centre of gravity of the area, and the crisp output is the output value associated with that particular point. Note that the centroid and bisection methods result in the same output if the shape of the area is vertically symmetrical. Figure 6.19 shows the result of calculating the centroid, bisector and Middle of Maximum (MOM: the point which is in the middle of all the points with maximum value) of an area; if the centroid method is chosen, the resulting crisp output will be 0.64.

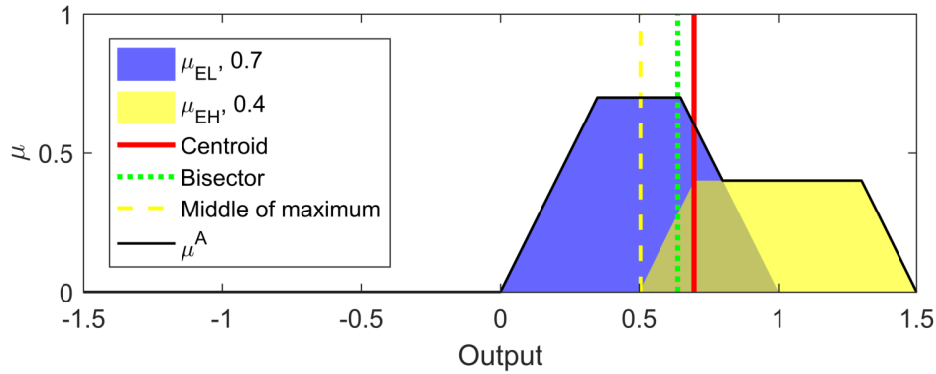


Fig. 6.19 Example of the defuzzification process: crisp output calculation using 3 methods.

The centroid and bisector of an aggregated membership function $\mu^A(y)$ (formed by the maximum of all the output fuzzy states) are calculated as follows [51]:

$$y_{\text{centroid}} = \frac{\int \mu^A(y)y dy}{\int \mu^A(y) dy} \quad (6.37)$$

$$y_{\text{bisector}} = \arg \min_{y_i} \left\{ \left| \int_{-\infty}^{y_i} \mu^A(y) dy - \int_{y_i}^{\infty} \mu^A(y) dy \right| \right\} \quad (6.38)$$

whilst the middle of maximum is the average value of \bar{y} : $\mu^A(\bar{y}) = \max \mu^A(y)$.

6.3.4 The output

Figure 6.17d shows the output membership functions whose image is defined in the interval $[-1.5, 1.5]$. The FLC controller output is truncated to the range $[-1, 1]$ which correspond to the normalised ESS power output. Figure 6.20 shows the FLC output when the flywheel speed is in the **normalSpeed** range, which is the operating state where the storage can both import and export energy. This three-dimensional figure shows what is the output of the controller (*ESScontrol*) with respect to two inputs: instantaneous hoist power in W (*HoistPower*) and instantaneous DC bus voltage in V (*DCbusV*). For example, at a normal flywheel speed with an hoist power of around 100 kW and a DC bus voltage of approximately 600 V, the controller will output 0.4, corresponding to a 40% positive ESS power output. The figure shows that, in general, the output of the FLC is positive when the hoist power is positive and the DC bus voltage is below 600 V, as this corresponds to the lifting phase when the hoist motor demands power. Conversely, the output is negative when the motor power is negative

and, most importantly, when the voltage approaches its higher value, thus indicating that the crane is lowering a container and the storage can be charged.

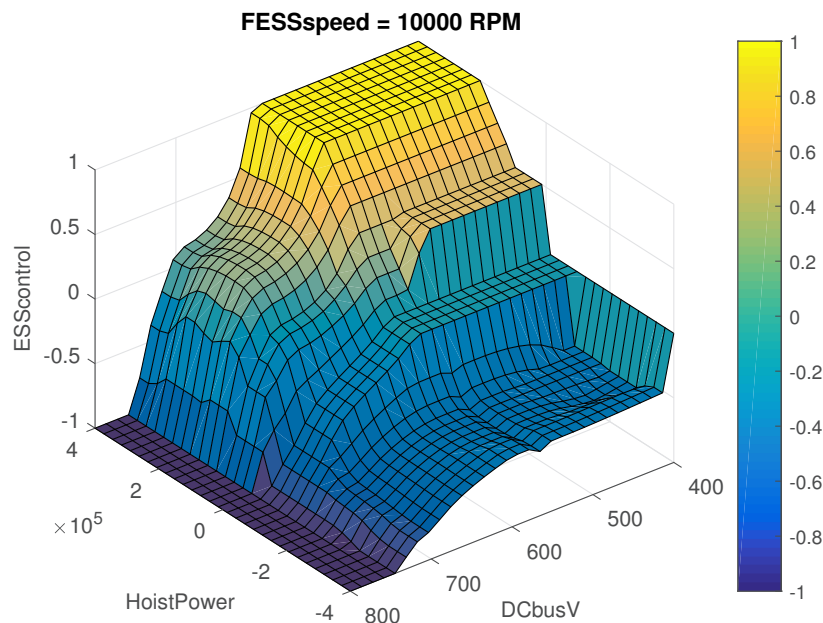


Fig. 6.20 Output of the Fuzzy Logic Controller when the flywheel is in the normal speed range. The output value is limited to the interval $[-1,1]$.

The output of the FLC changes dramatically when the speed of the flywheel is very low (<5000) or very high (>15000): positive outputs should not be allowed in the first case, whilst it is the opposite for the second case. Figure 6.21 shows how it is the case, as *ESScontrol* is non-positive in Figure 6.21a and it is non-negative in Figure 6.21b.

The aforementioned figures show the output for any combination of voltage and power, showing a clear trend: the output reaches its maximum when voltage is low and hoist motor power is positive. As voltage decreases and hoist power decreases, the output becomes negative. The output of the fuzzy controller depends on the whole input space, but it is expected to concentrate its activity in a relatively narrow area as DC bus voltage and hoist power are not independent. During normal activity, DC bus voltage is low when hoist power is positive and vice-versa. This is more evident in Figure 6.22, where the voltage and power measured on a crane during typical operation have been superimposed on the output of the FLC.

Not all rules will fire at the same time, and some rules will exclude others as they will be pertinent to separate fuzzy sets of the inputs. However, as mentioned above, some states of the system are more common due to the dynamics of the electrical components of the crane.

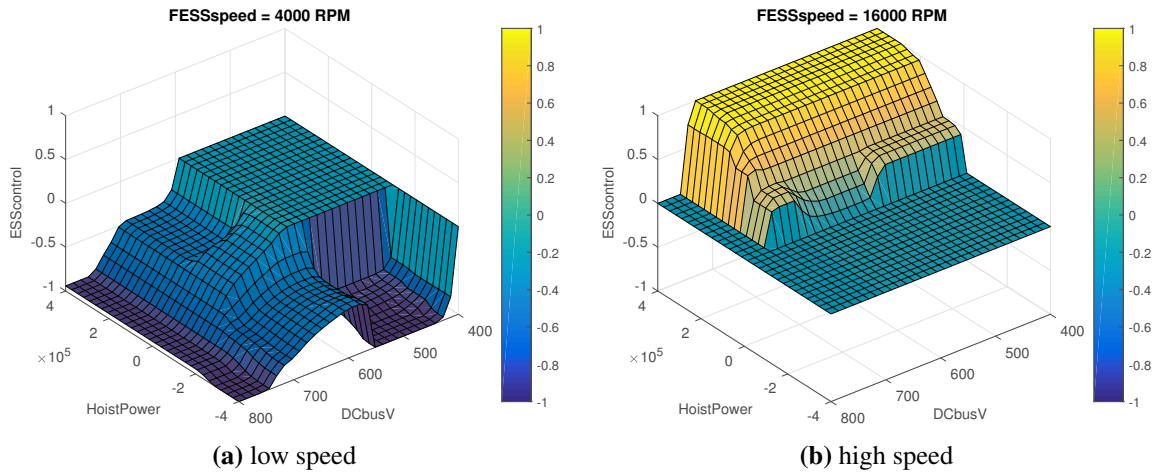


Fig. 6.21 Output of the Fuzzy Logic Controller when the flywheel speed is lower than the minimum **(a)** and higher than the maximum **(b)**. The output value is limited to the interval $[-1,1]$.

For example, the DC bus voltage will necessarily be over a certain threshold when the hoist motor is regenerating power into it. Vice-versa, when the hoist motor is drawing power from the bus it will cause the DC bus voltage to drop below the activation threshold of the rectifier diodes. Nonetheless, the fuzzy logic strategy presented in this thesis has been designed to completely fill the input space, therefore every input combination is associated with a valid output state, regardless of the probability of it happening. The surjective property of this fuzzy logic is necessary to avoid any undefined output state but also improves the transitions between more common states.

6.3.5 Simulation and results

The FLC was implemented in Simulink and tested with the ESS model presented in Section 5.2.3. The output of the controller was multiplied by the maximum power output of the storage P_s and used as the input of the storage. The same 38 minutes simulation used for the PI and optimal control were repeated with the fuzzy logic control, with the results shown in Figure 6.23. The energy consumed by the crane reached a total of 20.19 kWh, corresponding to a 32% reduction with respect to a crane not equipped with ESS.

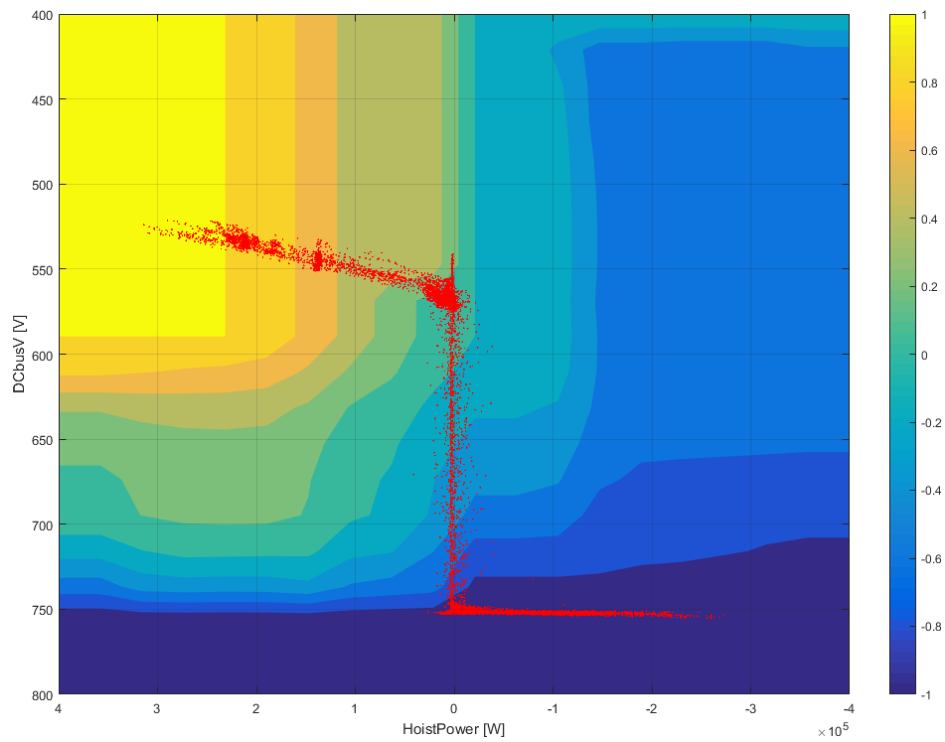
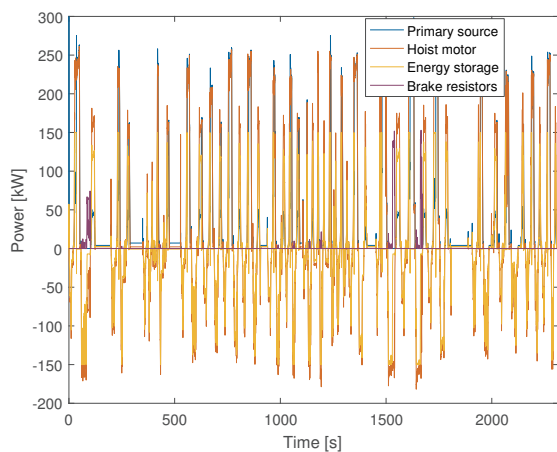
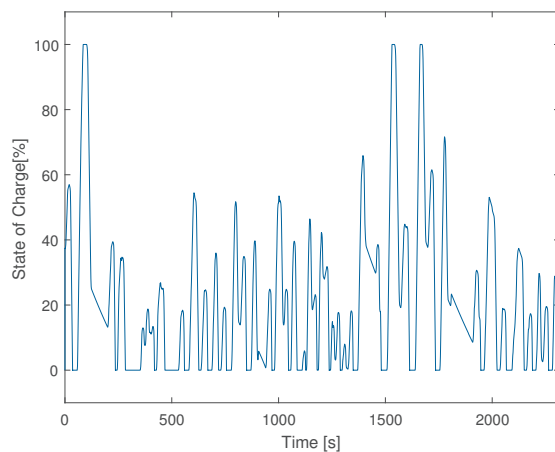


Fig. 6.22 Hoist power vs. DC bus voltage (in red, measured during the activity of the RTG crane) superimposed on the output logic of the Fuzzy Logic Controller when the flywheel is in the normal speed range.



(a) power flows



(b) energy stored

Fig. 6.23 Results from the full simulation using the Fuzzy Logic Control.

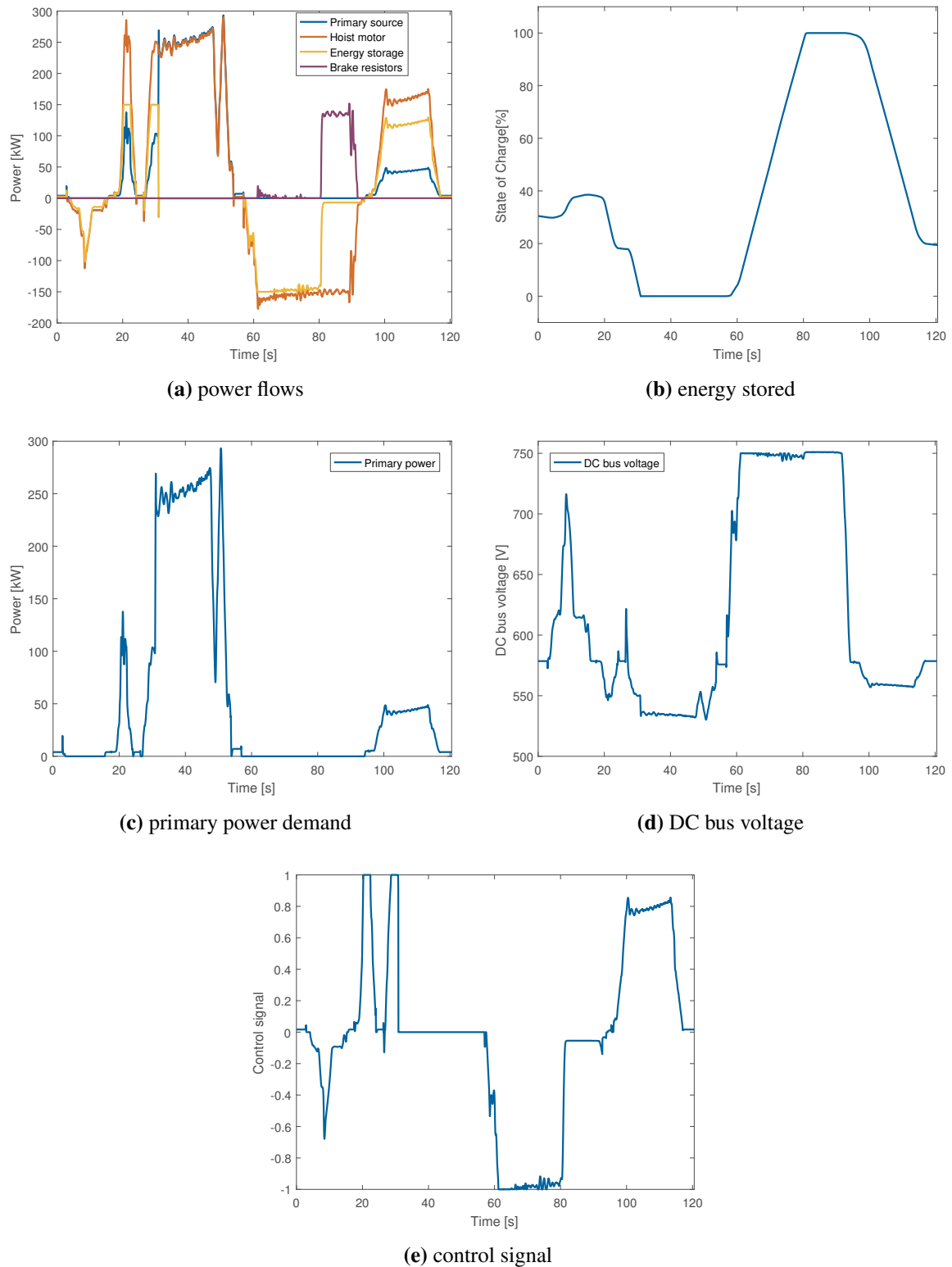


Fig. 6.24 Results from the full simulation using the Fuzzy Logic Control, single lift cycle.

6.3.6 Analysis of the results

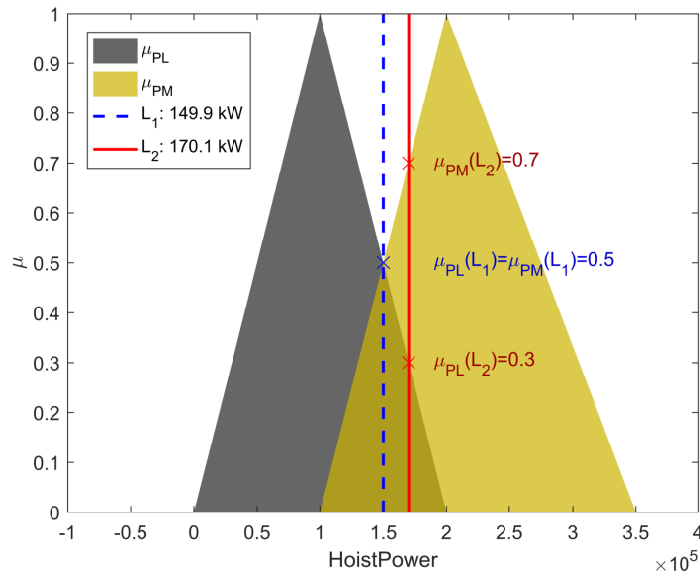
In the single lift cycle shown in Figure 6.24 the FLC shows similar behaviour to the PI and optimal controllers. In the first spreader lowering, the first 20 seconds of the cycle, the ESS successfully recovers the regenerated power without causing the activation of the brake resistors. During the container lift (from second 20 to 55) the storage outputs maximum power whenever the hoist motor demands high power, until the depletion of the stored energy (Figure 6.24b). Although being characterised by a completely different control architecture, the FLC behaves as the PI controller during the container lowering, successfully absorbing the regenerated energy until the storage is full. The spreader lift (from 95 to 120 seconds) shows the ESS outputting power proportionally to the hoist power demand: this clearly shows the effect of the export rules, which activate a different output state (**EVH**, **EH** or **EL**) depending on the *HoistPower* input state (**PH**, **PM** or **PL**). Figure 6.25 shows in detail the underlining process that causes this behaviour, focusing on two peculiar input states. The first input state, L_1 , happens at around 100 seconds in the lift cycle and is characterised by a hoist motor demand of 150 kW; the second state, L_2 , is at the end of the lift at around 115 seconds, when the demand is 170 kW. In this example, export rules 2b and 2c are active, with the output state **EH** linked to **PH** and with **EL** linked to **PM**. Given the conditions of the inputs in the states L_1 and L_2 , in this particular example the rules can be simplified as follows:

R 2b: if *HoistPower* is **PH** then *ESScontrol* is **EH**;

R 2c: if *HoistPower* is **PM** then *ESScontrol* is **EL**.

Figure 6.25a shows the fuzzification process for both states L_1 and L_2 . For the first state the degree of membership of 150 kW in **PL** and **PM** is the same: 0.5. Rules 2b and 2c are then both active with the same degree of firing of 0.5, and this results in the output states **EH** and **EL** being both active with maximum value 0.5 (Figure 6.25b). The resulting centroid is linked to a crisp output value of 0.75.

For the second state, **PM** has a higher degree (0.7) than **PL** (0.3), therefore **EH** will be predominant, and this is reflected in the output being different from L_1 , as the crisp output has value 0.833. The ESS output in L_1 should then be $0.75P_s$ which has a value of 112.5 kW, whilst in L_2 the output should be $0.833P_s$ which is equivalent to 124.95 kW. A 20 kW difference in the input then caused a 12.45 kW difference in the ESS output due to the various degree of activation of the fuzzy sets.



(a) fuzzification

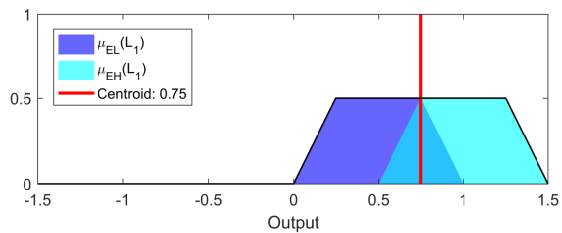
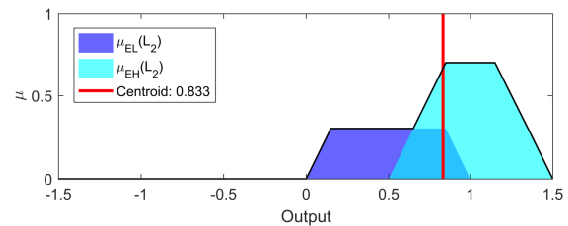
(b) defuzzification of L_1 (c) defuzzification of L_2

Fig. 6.25 Example of the fuzzy logic process for 2 peculiar states.

6.4 Summary

Three very distinctive strategies have been presented in this chapter: a PI-based controller, an optimal controller and a Fuzzy Logic Controller.

The PI control system presented is based on the combination of two PI controllers, each in charge of the DC voltage control or the power sharing mode; the operation of the two controllers is inherently isolated avoiding simultaneous activation but guaranteeing significant energy savings. The two PI controllers are used commonly on their own, but the combination of the two for both voltage control and power sharing is novel. There is the possibility, though, that existing work uses PI controllers for obtaining the same end results, especially in the work presented by Flynn et al. [19], although this is not explicitly stated.

The optimal control system presented in this chapter is based on the minimisation of a cost function that includes energy consumption and peak power demand, therefore the ESS operation is optimised for the achievement of those two main objectives. This optimal controller based on stochastic processes is completely novel as it is not found in any application. This controller has been the subject of a journal paper published in *Energies (MDPI)* [85] and of a seminar at the City University of London held by Victor M. Becerra and titled *Optimal Power Management Strategy for Energy Storage with Stochastic Loads*.

The Fuzzy Logic Controller presented in this chapter is based on linguistic rules that describe the desired behaviour of the ESS under certain conditions, ensuring an effective operation of the storage. Each controller is designed for the same objective and the behaviour may appear similar, nonetheless their differences are prominent, as will be shown in the next chapter where they will be analysed in more detail and compared. This is only the second Fuzzy Logic Controller for RTG cranes present in the literature, and it is the first one which is tested in simulation with a validated model of an RTG crane.

The three control strategies have been tested, showing the desired behaviour of the storage and resulting in a reduced energy consumption. They are now ready to be included in the RTG model equipped with ESS for extensive testing of the benefits of energy storage in the normal operation of the crane.

Chapter 7

Analysis and comparison of supervisory control strategies

This chapter presents an analysis of the three supervisory control systems proposed in this thesis. The first section shows the results of simulations of the hybrid crane when controlled by each of the supervisory control systems. The subsequent section will then focus on the analysis of the results, comparing the properties and characteristics of each controller. Finally, in the third section, the controllers are assessed on their implementability, complexity, sensitivity and other factors that may impact their use in the real world.

7.1 Hybrid RTG simulation

The activity of an RTG crane at the Port of Felixstowe — described in Chapter 3 — has been recorded continuously for approximately 6 days. The data obtained represents typical crane activity, including approximately 3000 container movements, real idle time and gantry movements. The data has been analysed and fed into the Simulink model described in Section 5.1 and the flywheel storage system presented in Section 5.2.3. The model has been simulated in the configurations listed in Table 7.1.

All the scenarios are simulated using the same data (power, energy, storage starting energy, system parameters) which lasts exactly 514950 seconds (5 days, 23 hours, 2 minutes, 30 seconds). The first scenario is the baseline and it represents the normal activity of the actual crane in operation at the Port of Felixstowe. Its results will be used in this chapter to quantify the potential energy savings obtained by installing energy storage.

Table 7.1 List of RTG configurations simulated

Configuration	Short Name
No energy storage system	No ESS
Energy storage with DC voltage control	DCV
Non realistic energy storage of infinite energy capacity	Ideal
Energy storage with PI supervisory control system	PI
Energy storage with optimal supervisory control system	Optimal
Energy storage with supervisory fuzzy logic control	Fuzzy

In the second scenario the crane is equipped with a controller that is set to maintain a constant DC bus voltage (here named “DCV”); this control system is common in the industry as well as in the literature where it has been the subject of numerous studies (see Section 2.2). In this scenario, the energy storage is set to maintain a constant DC bus voltage of 650 V, absorbing energy if the voltage tends to rise (for example during a lowering) and providing energy to the system if the voltage tends to decrease (during a lift). If the storage is empty or full, it cannot provide or absorb enough energy to maintain a constant voltage, and in that situation either the diesel generator or the brake resistors will take over.

The third scenario, the ideal case, delineates an upper-bound to the possible amount of energy that could be saved with the same storage system under analysis. This scenario is run removing limits on the maximum capacity of the storage, corresponding to an infinite upper bound on the rotating speed of the flywheel. This is equivalent of an energy storage with no upper bound on the amount of energy that can be stored, thus the storage will continue to accumulate energy indefinitely. However, the storage can still be depleted and reach no stored energy. In this case, the ESS will not provide any power until recharged. In this ideal scenario the ESS is unmanaged and its only role is to absorb power when it is regenerated by the hoist motor and to deliver it back as soon as it is demanded by the system. By removing energy capacity constraints it is possible to remove the impact of the control strategy on the amount of energy saved, providing a quantifiable upper bound to the possible energy savings. The results from this case will then be used as a reference for the best possible results when energy constraints are removed, and the closer the supervisory controllers results will be to the ideal, the better they manage the energy constraints.

Scenarios 4 to 6 are a direct application of the supervisory control strategies presented in this thesis. The data provided by these three scenarios will be used to quantify the benefits of the proposed strategies. Thus, the first, second and third scenarios provide a reference that can be used to assess how the supervisory control strategies manage the limited storage

capacity and also how they can improve upon existing technologies. Figure 7.1 shows the energy consumption of the RTG crane in the 6 days that compose the simulation. The following sections presents the results of the simulations.

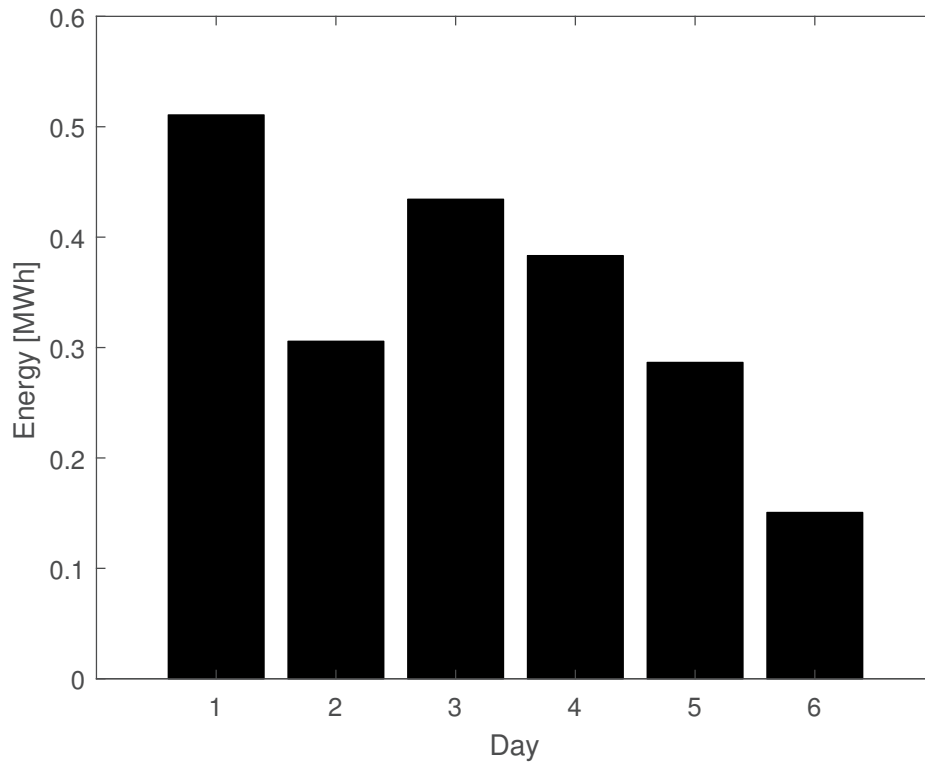


Fig. 7.1 Energy consumption of the hybrid RTG crane in the six days recorded.

7.1.1 Energy consumption

In this application, the first objective of an effective supervisory control system for energy storage is the reduction of energy consumption. The results obtained from the simulations will quantify the performance of the supervisory control strategy in the data set used, allowing a comparison with the other reference scenarios. The length of the simulation and the high number of lift cycles increase the chance of simulating every possible lift cycle. Furthermore, the crane was recorded during typical activity in normal operating conditions.

Figure 7.2 presents the energy consumed by the crane under the six different scenarios. Without an ESS, the crane consumes 2.07 MWh whilst under the ideal case it would only consume 1.23 MWh. The simple DC voltage controller achieves a 22.9% energy reduction by consuming 1.6 MWh. The fuzzy logic controller achieves the best performance, with a reduction of 31.6% compared to the 26.1% of the PI controller and 21.6% of the optimal controller. The results show a reduced energy consumption in a hybrid crane, an improvement from the baseline regardless of the control strategy implemented. However, this will not be the same with another indicator: peak power demand. The full energy results are displayed in Table 7.2.

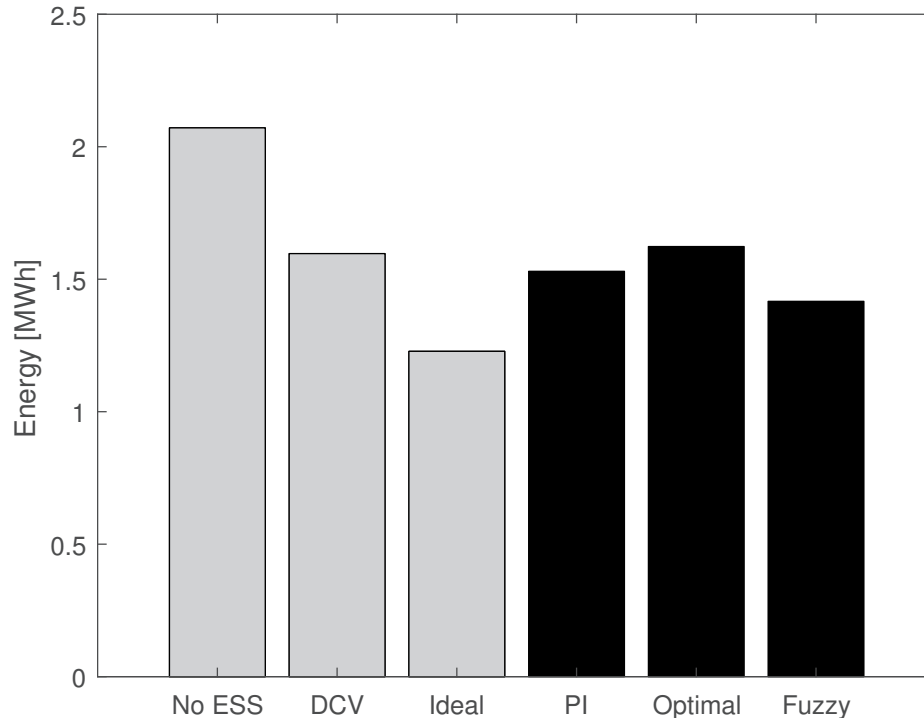


Fig. 7.2 Energy consumption of the hybrid RTG crane in the six scenarios.

Table 7.2 Results of the simulation: energy consumption

Scenario	Energy consumed [MWh]	Reduction w.r.t no ESS
No ESS	2.07	0%
DC voltage control	1.60	22.91%
Ideal case	1.23	40.72%
PI control	1.52	26.13%
Optimal control	1.62	21.62%
Fuzzy logic control	1.42	31.61%

7.1.2 Peak power demand

The storage system is required to achieve a key objective: to reduce the peak power demand from the RTG crane, diminishing the impact on the diesel generator or the local power network. The power produced by the primary source has been recorded and analysed. Figure 7.3 shows two indicators: the fraction of time that the crane demands either more than 150 kW or 200 kW. The results show that all three supervisory controllers reduce the amount of time that the crane demands peak power, especially over the 200 kW threshold which is the most demanding on the primary source.

The PI controller reduces massively the peak demand above 150 kW, although most of this time corresponds to a demand over 200 kW. This outcome is due to the power-sharing characteristics of the controller: it handles correctly power demands up to 75 kW, but then it fails to limit it when the stored energy is depleted. This is also the reason why the ideal case is not the best of the six: in this scenario the ESS is unmanaged and delivers all the power demanded by the system, and it usually depletes the storage very quickly. The crane is then forced to finish most lifts using the primary power source exclusively. The same pattern occurs under DC voltage control, which produces even worse results. Similarly to the ideal case, this strategy does not manage the power output and provides passively what is required by the crane until its energy is quickly depleted — but unlike the ideal case, its energy capacity is limited.

Adequate performance is achieved by the fuzzy logic controller, which results in a modest but noticeable reduction in peak power demand. The controller that achieves the best results is the optimal controller, which significantly reduces the demand over 200 kW; with the optimal controller, the amount of time that the crane demands over 200 kW is reduced by 1/5 with respect to the original RTG. This result is due to the cost function chosen which penalises high power demands. The PI supervisor could be tuned to further reduce peak

power demand by increasing the reference power when in power sharing mode (which in this test is set to 75 kW). However, increasing it will massively reduce the energy savings obtained with this controller. The reference value of 75 kW has been found to be a good compromise between energy savings and peak power demand reduction. The difficulties and implications of choosing the correct reference power will be discussed later in this chapter. The full peak power results are displayed in Table 7.3.

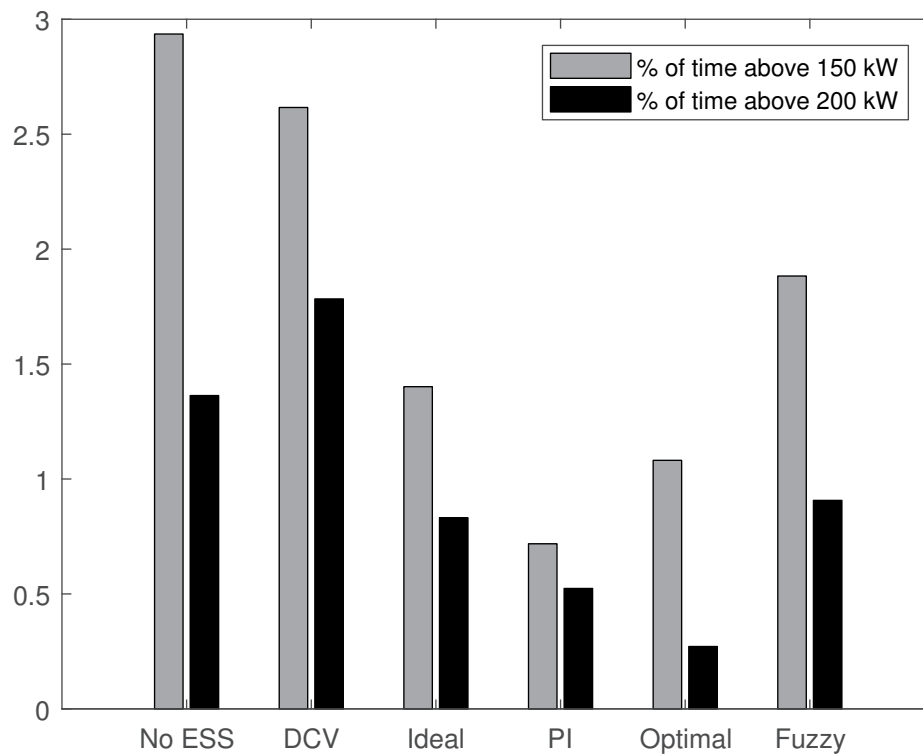


Fig. 7.3 Percentage of time that the RTG crane load is above specified thresholds.

Table 7.3 Results of the simulation: peak power demand

Scenario	Fraction of time over 150 kW	Fraction of time over 200 kW
No ESS	2.94%	1.36%
DC voltage control	2.62%	1.78%
Ideal case	1.40%	0.83%
PI control	0.72%	0.52%
Optimal control	1.08%	0.27%
Fuzzy logic control	1.88%	0.91%

7.1.3 Estimated fuel consumption

Fuel consumption was not measured directly on the RTG crane, however it can be estimated from power consumption as explained in Section 5.1.3. Fuel is consumed both when moving container and when waiting idling for a new task (see Section 3.3.4). Most RTG cranes automatically shut down the diesel generator after a certain amount of time with no activity, therefore the generator will not always be consuming fuel. This issue is not present in E-RTG cranes because they are powered by the local power network and do not need an idling diesel generator.

It was not possible to meter the diesel generator, therefore it is not known when it had been idling or shut down. For this reason, the decision was made to simulate the worst case scenario consisting of the diesel generator always on and either idling or actively powering the crane. Whilst unrealistic, this condition is associated with the highest fuel consumption and also the least benefits of the ESS: the flywheel storage chosen for this research does not provide benefits during idling. The results, presented in Figure 7.4, show relatively modest fuel savings that reach 10.40% in the ideal case, or 8.07% in the fuzzy logic control which is the best performing supervisory controller. The results indicate that the fuel savings from three supervisory controllers follow the same pattern as energy savings: most fuel is saved by the fuzzy logic controller, followed by the PI controller and the optimal controller. The DC voltage controller provide a reduction of 5.64% in fuel consumption. Table 7.4 displays the full results.

Table 7.4 Results of the simulation: fuel consumption

Scenario	Fuel consumed [kg]	Reduction w.r.t. no ESS
No ESS	1306	0%
DC voltage control	1232	5.64%
Ideal case	1170	10.40%
PI control	1214	7.03%
Optimal control	1228	5.96%
Fuzzy logic control	1201	8.07%

7.1.4 Impact on the ESS

Shifting the focus from the crane to the energy storage device, it is useful to investigate the impact the control strategies have on the ESS. A flywheel storage device maintenance

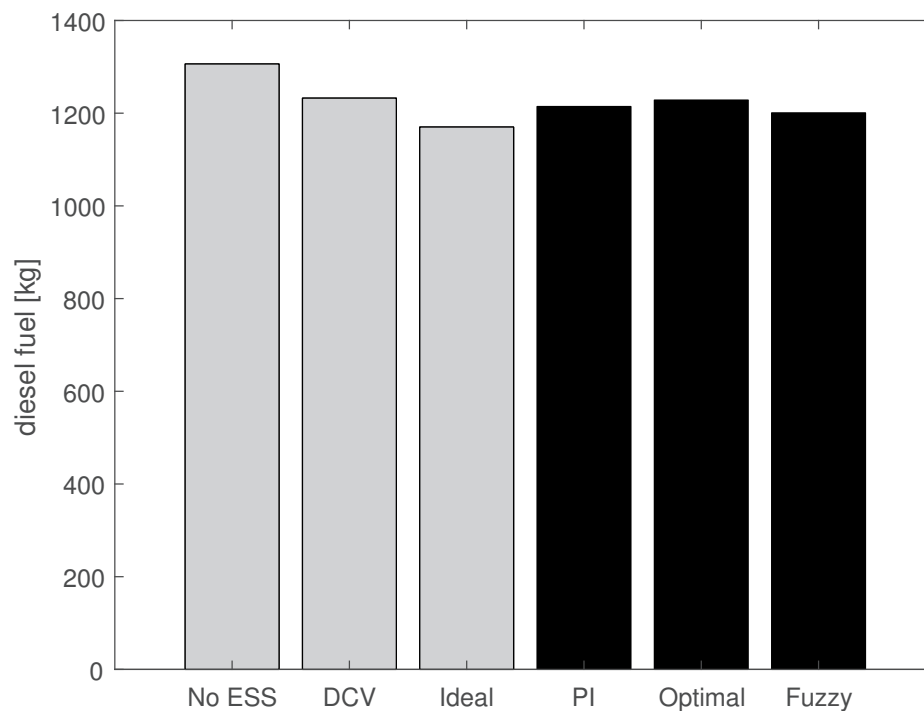


Fig. 7.4 Estimated fuel consumption in the six scenarios.

schedule and lifetime depend on the activity the controller subjects it to. One indicator of the impact on the ESS is the average power output as it correlates with reduced lifetime of the electric machine (due to wear on the mechanical components). The average power output was calculated as the sum of the absolute value of the output divided by the total time. The results, shown in Figure 7.5, indicate that the PI puts the ESS under the highest stress with an average power of 9.04 kW, whilst the optimal controller and fuzzy logic controller have, respectively, 7.96 kW and 8.37 kW. The ideal ESS, having no upper bound in the amount of stored energy and no power management, reach a substantially higher average power of 17.14 kW, whilst the DC voltage controller is the one with the best results with an average power of 6.89 kW.

A second indicator of the stress applied to the ESS is the average state of charge. A flywheel storage degrades faster when the rotational speed is kept high, because of the wear on the mechanical components (bearing, motor rotor, shaft, flywheel). Figure 7.6 presents the average charge hold by the storage depending on the control strategy. These results are similar to the ones about average power (described above). The DC voltage controller provides the best results with an average stored energy of 0.46 MJ (approximately 6100 RPM); the optimal controller maintains the storage at the average of 0.61 MJ (7100 RPM). The fuzzy logic controller, at 0.76 MJ (7650 RM), comes third, whilst the worst result in

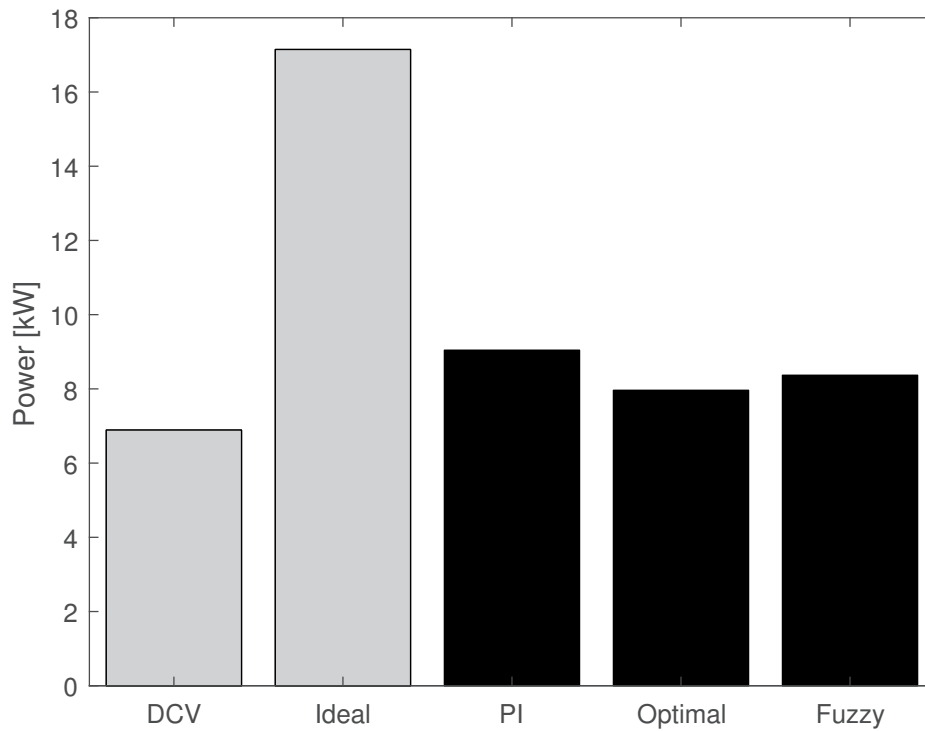


Fig. 7.5 Average absolute power output of the storage device under the supervisory controllers.

this test is associated with the PI controller at 1 MJ (8500 RPM). The ideal ESS has no boundaries for stored energy, and this is reflected in the very high average energy (8.38 MJ, 34000 RPM), therefore it is not shown in Figure 7.6 among the other results.

From these results it is possible to deduce that the optimal controller can help to increase the lifetime of the storage device when compared to the other proposed controllers, however the existing DCV controller shows better results. The results also show how increasing the capacity of the storage may not be an alternative to an advanced supervisory control: in this test, the ideal ESS is subjected to a higher stress because of higher power outputs and higher rotational speeds, affecting the lifetime and maintenance costs.

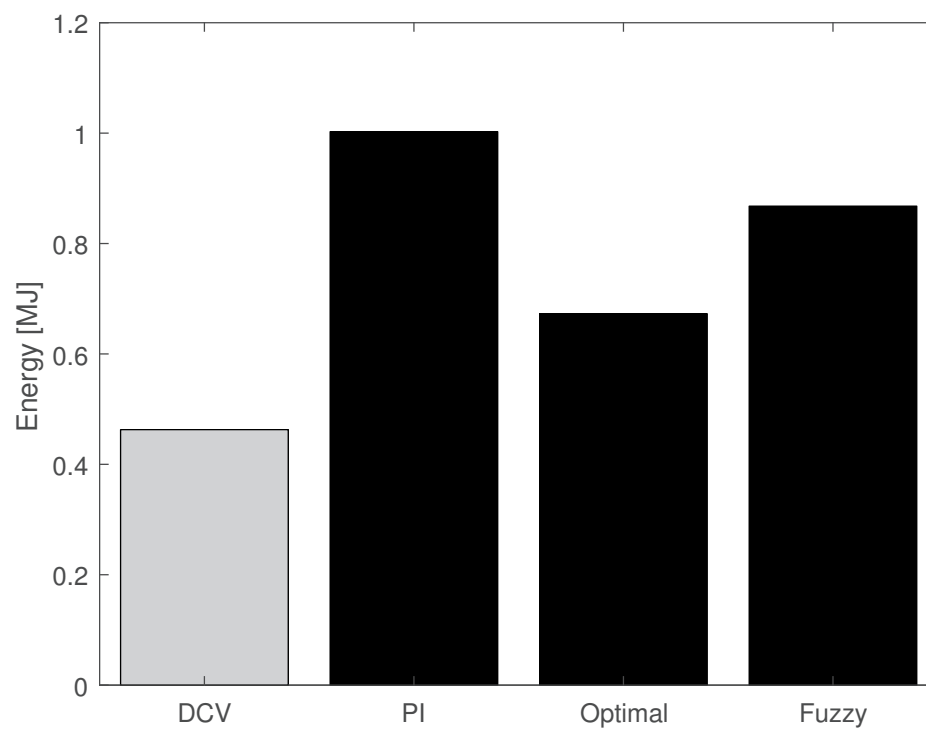


Fig. 7.6 Average energy stored in the ESS under the supervisory controllers.

7.2 Analysis of supervisory control strategies

The results of the simulations show the potential benefits of each control strategy in terms of energy consumption, peak power demand and impact on the storage device. However, other criteria need to be analysed, mainly related to the sensitivity to change in parameters or in the activity of the crane. This section will analyse the results of the simulation study focusing on these aspects, evaluating each control strategy and comparing it to the others.

7.2.1 PI control strategy

Section 6.1 described how the supervisory PI controller is divided into two systems: one activated when the crane is lifting, one when the crane is lowering a container. During lowering, the hoist motor regenerates into the DC bus increasing the voltage. A DC voltage control is active and all the available energy (minus losses) is absorbed by the storage if there is enough capacity. The voltage activation threshold is chosen by the designer to avoid charging the storage outside the regeneration phase. Furthermore, the reference voltage was chosen high enough to avoid interference between the DC voltage controller and the power sharing one. This means that there is no possibility of charging the storage when the crane is not lowering, creating the possibility that the storage cannot provide a significant amount of energy to the crane when lifting. This is an issue linked to the peculiar design and could only be avoided by further increasing the complexity of this control system.

In the simulations the PI control strategy showed a significant decrease in energy consumption: 26% with respect to the normal crane (which is an improvement on the 23% obtained by the simpler DC voltage controller). This value places the PI controller in between the other two proposed controllers. The situation is repeated with peak power demand, where the PI controller reduces the peak more than Fuzzy Logic but fails to reach the reduction in very high (above 200 kW) power demands offered by the optimal controller. This mediocre peak power demand behaviour may be the cause of the high average power: of all the controllers, the PI resulted in the higher stress on the storage device. Overall, in this test its performance resulted to be a middle ground between the other two strategies, but this may only be due to the choice of controller parameters, as will be explained later.

There are constraints to consider when choosing the PI gains due to the dual PI system (see Section 6.1.2). However, if it can be assumed that the storage behaves like a simple first order lag system (with second and higher order dynamics being stable or negligible) and

if the low-level control system is stable (which it is, by design) then there is no possibility of instability. Reference tracking is only guaranteed for constant references, and the motor load in power sharing mode can be categorised as a disturbance which is, generally, not constant. Therefore, there will always be a non-zero error but it is negligible if the integral action is sufficiently fast. This error only affects the speed at which the storage reacts to fast fluctuations in the load power, with minimal impacts on the overall energy consumption. The issues in this controller lay in its lack of versatility: the reference power (in power sharing mode) is chosen a-priori and it is constant. A lift characterised by high energy (e.g. lifting a heavy load, or a light load to the maximum height) should be associated with a low power reference to ensure that the storage can provide energy for the entire duration of the lift. On the other hand, a quick or light load should be associated with a high power reference to ensure that all the stored energy is used. This research is based on the assumption that it is impossible to know in advance the total energy and duration of a lift, and therefore it is impossible to determine the appropriate power output of the storage. A high output may deplete the storage prematurely, whilst a low output may underutilise it. The power reference chosen for the simulations shown previously has been chosen slightly below the average power demand (see Section 3.6.4 on pg. 41) in order to increase the performance of the storage for longer lifts. This choice has been made as a trade-off between energy savings and peak power demand: higher power equals higher savings, but it increases the number of times the storage is depleted during a lift. Any variation in reference power has an effect on the performance of the system, therefore this control strategy is highly susceptible to variations in control parameters as well as the activity of the crane. Thus this controller is not easy to tune, due to the non-trivial choice of reference power in power-sharing mode. The next controller under analysis, the optimal controller, hides the complexity under a simple choice of the cost function.

7.2.2 Optimal

In the current configuration of the crane under analysis, it is not possible to determine in advance the exact characteristics of the lift cycle. It would be useful to know what will be the energy consumption and duration of a lift in order to adjust the power output of the storage for the best performance. The optimal controller presented in this thesis (Section 6.2) tackles this problem by exploiting the characteristics of the stochastic process that models the lifts. By knowing the distribution of container lift durations, it is possible to pre-calculate the optimal trajectory for the given distribution. In theory, this controller will provide the best

benefits, determined by the cost function chosen. The results of this simulation reflect this aspect: energy savings are limited — only slightly worse than DC voltage control — but high power demand is greatly reduced, with a result that is significantly lower than any other scenario. This is due to the choice of the quadratic cost function which penalises high power flows. Any cost function can be chosen depending on the requirements and desired output; the only major constraint is that it needs to be semi-definitive positive. This aspect increases the versatility of this control strategy with respect to the potential applications and desired outcomes. In terms of burden on the storage device, the optimal controller offers the best results of the three control strategies with the lowest average power and stored energy.

Unfortunately, once the control strategy is calculated off-line, it is limited to a specific application and storage parameters, e.g. energy capacity, power rating and load power ranges. Changing those parameters without re-calculating the optimal strategy may reduce the performance of the controller. This aspect affected the simulations: the optimal strategy was calculated around a different set of measurements than the one used for the simulation, and the lift duration distributions may have not matched. Nonetheless, the optimal strategy tries to optimise the single lift weighted by the probability that it occurs, therefore the performance of the controller will not be massively affected by small changes in the probability distribution.

Regarding the design inputs, the quality of the optimal control is not determined by the choice of reference values (as the PI controller was). Instead it is based on the characteristics of the activity that the crane is subjected to, and how well they are represented by the modelled stochastic process. Once the characteristics of the system are defined, the only design input is the cost function. However, in a real application it is generally based on real costs (energy, fuel, peak power demand) therefore it is usually pre-defined. Generally, a cost function can be tuned to favour energy savings or limit peak power demand by varying the cost associated with the single unit of power. For example, by using $D(p_g(k)) = p_g(k)^4$ instead of $p_g(k)^2$ peak power demand is linked to an even higher cost and is greatly penalised.

7.2.3 Fuzzy Logic

The Fuzzy Logic controller has been designed by using the knowledge of the crane activity that has been gained with the data analysis and the development of the other supervisory control systems (see Section 6.3). The choice of the input and output fuzzy functions is completely dependent on human knowledge and intuition, and there is no asymptotic error rejection (like in the PI control) or mathematical optimisation that will facilitate the work

of the designer. The proposed FLC is effectively a time-invariant surjective mapping of the inputs and the outputs, i.e. for every output state there is at least one combination of inputs that will result in that particular output. There is no underlying dynamic, no internal state of the controller, and no time-varying output. It is equivalent to defining an output for every one of the infinite combinations of inputs, however fuzzy logic will facilitate the design process by using linguistic rules. These rules are arbitrarily chosen by the designer from knowledge of the system and its behaviour, and there is no established methodology that produces the best results for any application. The proposed FLC is the result of many iterations, and it is heavily based on the results obtained from the simulation. In this research, the FLC may have been the control system with the less complex theoretical background and study, but it is the one that required the highest insight on the energy storage problem and the longest tuning process.

After the controller is developed, tested and tuned for a certain activity of the crane, it is not guaranteed that it may also work for a different RTG. The FLC has small sensitivity to changes in the frequency and duration of the lifts (unlike optimal control) as it is not based on statistical properties of the activity. However, changes in the power and energy level do have an impact, because the input and output functions are based on the typical activity observed in the past by the designer. For example, if the lifts start to demand unusual amounts of power, the input function linked to hoist motor power needs to be retuned. It is quite straightforward to change the input (or output) functions, but any change needs to be tested and tuned. Of the three supervisory control systems presented, this is the one where it cannot easily be determined a-priori if changes are potentially beneficial. For example, it is possible to decrease the power reference in the power sharing PI in order to increase the share of power contributed by the storage during a lift; in the optimal control, the cost function can be changed to penalise peak power demand more. During the development phase it has been observed how small changes to the FLC may have a non-linear impact on the performance. Intervening on a single fuzzy set is not ideal as all the fuzzy sets linked to the same variable are designed to ensure a smooth transition from set to set and may interfere with the effect given by other variables. Nonetheless, the FLC has no internal dynamic: it is a simple input to output mapping and there is little risk of instability caused by unmodelled dynamics. The only potential hazard is selecting the wrong output value for a given input that may damage the system or reduce its efficiency. The complex operation of choosing effective fuzzy sets and logic rules makes this controller the hardest to tune of the three under analysis. The optimal controller requires more computational power due to the numerical optimisation, however the optimal strategy is generated automatically by software. The PI

requires more effort than the previous one, but choosing its gains is not burdensome, and the reference power can be found by testing. Any operation on the fuzzy sets of the FLC, on the other hand, can dramatically change the intrinsic input-output mapping and generate unwanted behaviour.

In the simulation, the Fuzzy Logic controller produced the highest energy savings of the three supervisory controllers — 32%. This result is obtained to the detriment of peak power demand, where it produced the worst results among the supervisory controllers considered. In fact, peak power demand was worse than the ideal scenario, where the energy storage is not subjected to any power management. This is due to the difficulty of managing the power flowing from the primary energy source: an FLC produces an instantaneous reaction to a change in power demand. Changing the activation functions linked to primary power may alleviate this problem, but it will also significantly reduce the performance of the controller because it will decrease the magnitude of the reaction to high power demands.

7.3 Feasibility, tuning and implementation

Whilst previous sections discussed the qualities of the supervisory control systems and their sensitivity to parameter change, this section focuses on the real-world difficulties linked with the design and implementation of the controllers. Each control strategy is assessed to check whether its implementation is feasible and if it is easy to tune and implement.

7.3.1 Tuning difficulty of supervisory controllers

The tuning difficulty has already been discussed in Section 7.2: it is the effort that is required to adapt a controller to the specific application. The PI controller exploits the asymptotic error rejection capability to compensate for variations in the crane electrical system and the storage. The voltage and power reference need to be readjusted to the crane and its activity, and they can be selected in advance knowing the electrical characteristics of the crane. The optimal control requires an off-line calculation of the optimal strategy each time the system or the activity change, otherwise the optimality is lost. These two control systems then require little effort for tuning, unlike the FLC which may need multiple simulations with a trial-and-error approach to verify that the chosen input to output mapping causes the desired behaviour of the storage. During the development of the FLC it has been observed that the fuzzy sets and functions are very easy to change but they may not bring the beneficial effects

expected as the inputs states interact with each other through the logic rules. The non-linear fuzzification and defuzzification process creates an inherently non-linear interaction between variables that is not easy to predict and is often only apparent after simulating the system.

7.3.2 Portability and generalisation

The supervisory control systems proposed were designed for the use on a specific model of RTG with a flywheel storage system. This section studies how each control system can be applied to a different crane, a different storage system or even a completely different application, for example in hybrid electric vehicles.

The PI control system has been specifically designed for the electrical configuration of the RTG crane used in this analysis, but all that is required in order to accomplish the DC bus voltage control, as well as the power sharing control, is a common DC bus. Any electric system characterised by a primary energy source and a regenerating electric machine connected by a DC bus can be augmented by a DC storage controlled by the PI supervisory control. The tuning challenges are similar to those for the RTG crane under analysis.

The optimal control supervisor is not only tailored around the specific crane and energy storage system, but also a single distribution of lift durations. Nonetheless, the theoretical idea behind it can be applied to any hybrid system characterised by load pulses of random duration and known distribution. Once the characteristics of the load, system and energy storage are set, it is just a matter of calculating the optimal strategy, regardless of the application behind it. As an example, let's consider an HEV whose front wheels are powered by an internal combustion engine and the back wheels by electric motors connected to a storage system. If the demand to the engine and motors can be approximated as pulses of random duration (modelled by a Gamma distribution), then the optimal control presented in the previous chapter can be used to determine what is the mechanical power output of the electric motors that will best reduce fuel consumption and peak power demand. It is counter-intuitive to imagine that a controller that requires a recalculation of the optimal strategy for every minute parameter change is the one that offers the best potential portability. However, the theoretical work behind this controller is based on a generic hybrid topology and not on a specific electrical diagram, therefore any system or application that satisfies the assumptions posed above can adopt this control system.

The FLC presented in this thesis conforms to a standard Mamdani-type fuzzy logic which has been applied in many other contexts, including HEVs [30, 51]. It is then very versatile

and could be applied to any hybrid crane under any sort of activity. The most laborious parts, though, are the tuning and testing that need to be performed for every application, therefore its high portability is not straightforward to exploit in practice.

7.3.3 Computational burden

One aspect that may be overlooked is the on-line computational burden of the controller. PI controllers are ubiquitous in industry and there is no problem running two PI controller at the same time, as is required by the first supervisory strategy. The fuzzy controller can run in real-time with minimal delay as it is based on fast mathematical calculations and logic rules. If necessary, the performance of the FLC can be improved by creating a lookup table with the pre-calculated output value for a very wide range of input combinations (an example is shown in Figure 6.20). The optimal controller can run easily in real-time because it is based on pre-calculated optimal strategies for an array of system conditions. Therefore, all the proposed supervisory control strategies can be implemented on an industrial micro-controller.

The optimal strategy at the base of the optimal controller, however, cannot be calculated on-line. The optimal controller reads the optimal strategy based on the characteristics of the crane activity and the system parameters, but any change on these variables require a new calculation which is too computationally intensive for a real-time application. However it cannot be excluded that advances in micro-controller performance may one day enable the calculation of the optimal strategy in real time, removing the need of the pre-calculation. This would increase the robustness and versatility of the controllers to changes in the parameters of the system: the optimal strategy can be re-calculated each time parameters change. Nonetheless, in the current state this control system is very computationally intensive during the design phase and the optimal strategy cannot be updated in real time.

7.4 Sensitivity analysis

This section presents results of simulations of the controllers presented in previous chapters when varying the energy capacity and power rating of the energy storage device. Although this thesis is focused on the whole process of designing supervisory strategies that are tailored to the specific application, it is necessary to study the effects of varying the ESS main parameters to see how the results change for each control system under analysis.

Neither supervisory control strategy has been re-tuned for the new ESS parameters, all the conditions of the system have been kept constant apart from one single parameter for each simulation (either energy capacity or maximum power output). All simulations are based on the same metered data (which corresponds to day 1 of the simulations presented at the beginning of this chapter).

7.4.1 Change in energy capacity

The control systems were tested when varying the energy capacity of the energy storage system. The variations tested are listed below:

1. -50%
2. -25%
3. -5%
4. +5%
5. +50%
6. +100%

The results for energy savings and peak power demand reductions are presented in Table 7.5 and Table 7.6. They are also visualised in Figures 7.7 and 7.8. The ideal control strategy has not been tested in this scenario as its peculiarity is the unbounded energy capacity, therefore it is not affected by a variation in energy capacity.

Of the four strategies tested, the DCV is showing the highest sensitivity to a reduction in storage capacity. This is due to its tendency on using the stored energy to power the crane when idling, reducing its effectiveness during high-power lift cycles. The PI controller shows an increase in effectiveness when energy storage increases, although the peak power demand is increased at lower capacities. These two aspects are probably caused by the arbitrary choice of the power sharing threshold of 75 kW which limits the energy savings effectiveness of the ESS at low capacities, and on the other hand creates a performance bottleneck at higher capacities with regards to peak power demand. This aspect is highlighted by the relatively higher robustness of the optimal control to a reduction in energy capacity: the optimal strategy has been calculated along all possible SoC values below the maximum value, thus obtaining

good results even at reduced storage capacities. However, at increased capacities the optimal controller exits the optimal strategy calculation area: the controller works sub-optimally because it has no information on the optimal strategy outside its pre-defined parameter area. This is expected and emphasises how the optimal controller must be tied to a particular application with pre-defined parameter bounds.

The fuzzy logic controller shows no unexpected variation in performance in both energy savings and peak power demand reduction when varying energy capacity. The performance of this system when capacity increases is limited by the design of its fuzzy sets, which are bounded to the original energy and power parameters, whilst the performance under capacity reduction decrease linearly as it is expected by a controller which is inherently based on piecewise linear fuzzy sets.

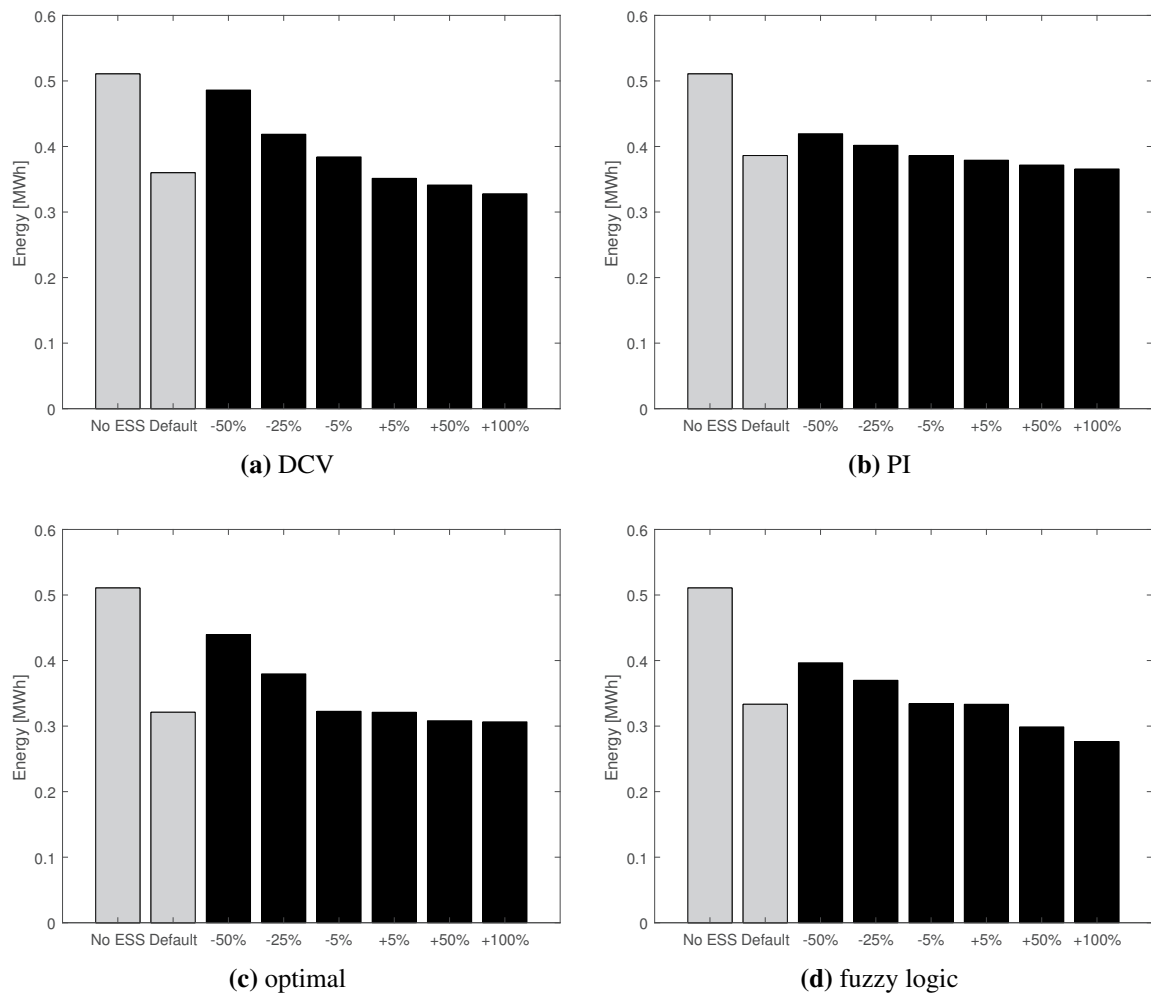


Fig. 7.7 Variation in energy capacity: consumed energy

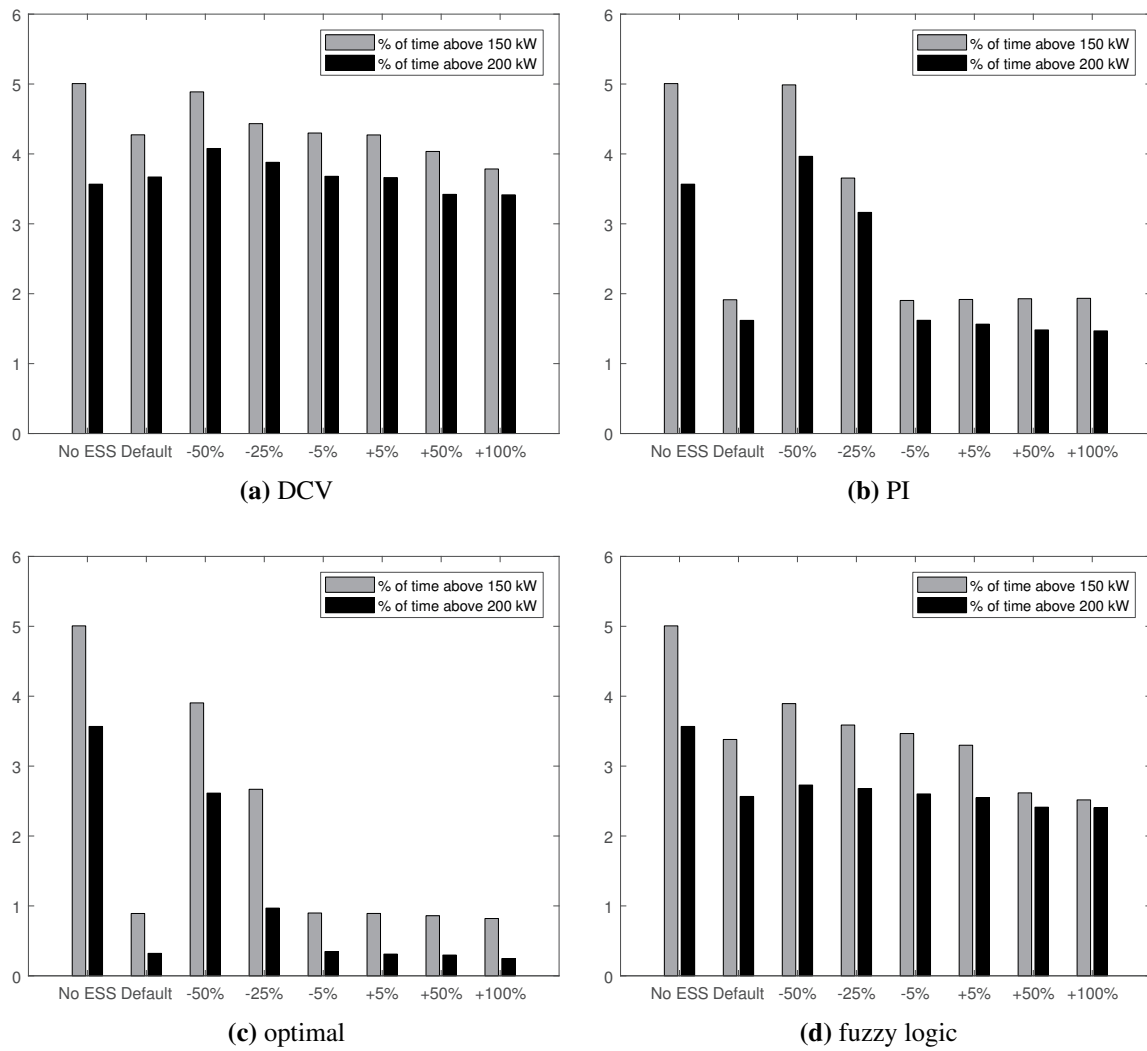


Fig. 7.8 Variation in energy capacity: peak power demand

Table 7.5 Changes in primary source energy consumption when varying the energy storage capacity

System	<i>Variants</i>						
	<i>Default</i>	<i>-50%</i>	<i>-25%</i>	<i>-5%</i>	<i>+5%</i>	<i>+50%</i>	<i>+100%</i>
DCV							
Energy [MWh]	0.36	0.49	0.42	0.38	0.35	0.34	0.33
% w.r.t default	100.00%	135.07%	116.34%	106.72%	97.64%	94.80%	91.11%
PI							
Energy [MWh]	0.39	0.42	0.40	0.39	0.38	0.37	0.37
% w.r.t default	100.00%	108.62%	104.05%	99.95%	98.17%	96.25%	94.70%
Optimal							
Energy [MWh]	0.32	0.44	0.38	0.32	0.32	0.31	0.31
% w.r.t default	100.00%	136.92%	118.24%	100.46%	100.00%	95.97%	95.45%
Fuzzy							
Energy [MWh]	0.33	0.40	0.37	0.33	0.33	0.30	0.28
% w.r.t default	100.00%	118.99%	110.98%	100.24%	100.00%	89.64%	82.92%

Table 7.6 Changes in primary source peak power demand when varying the energy storage capacity

System	<i>Variants</i>						
	<i>Default</i>	<i>-50%</i>	<i>-25%</i>	<i>-5%</i>	<i>+5%</i>	<i>+50%</i>	<i>+100%</i>
DCV							
Over 150 kW [% of time]	4.27%	4.89%	4.43%	4.30%	4.27%	4.04%	3.78%
Over 200 kW [% of time]	3.67%	4.08%	3.88%	3.68%	3.66%	3.42%	3.41%
PI							
Over 150 kW [% of time]	1.91%	4.99%	3.65%	1.90%	1.92%	1.93%	1.93%
Over 200 kW [% of time]	1.62%	3.97%	3.16%	1.62%	1.56%	1.48%	1.47%
Optimal							
Over 150 kW [% of time]	0.89%	3.90%	2.67%	0.90%	0.89%	0.86%	0.82%
Over 200 kW [% of time]	0.32%	2.61%	0.97%	0.35%	0.31%	0.30%	0.25%
Fuzzy							
Over 150 kW [% of time]	3.38%	3.89%	3.59%	3.47%	3.30%	2.62%	2.52%
Over 200 kW [% of time]	2.57%	2.73%	2.68%	2.60%	2.55%	2.41%	2.40%

7.4.2 Change in maximum power output

The control systems were tested when varying the maximum power output of the energy storage system. The variations tested are listed below:

1. -50%
2. +100%

The results for energy savings and peak power demand reductions are presented in Table 7.7 and Table 7.8. They are also visualised in Figures 7.9 and 7.10.

When decreasing the maximum power output, all controllers show a decrease in effectiveness in reducing energy consumption. The ideal controller is particularly affected due to its peculiarity: its good performance in other tests is due to its ability to store infinite amounts of energy, but this advantage could be crippled by the inability to *absorb* or *provide* this energy due to the limitations in power output. This controller also shows interesting results in peak power demand reduction when increasing power capacity: in this condition, the primary source is only subjected to high-power peaks, corresponding to the instants when the ideal ESS has run out of charge and the primary source is providing all the necessary power to the crane.

The PI, optimal and fuzzy logic supervisors do not perform significantly better when increasing the maximum power output. This is due to their design characteristics that limit the maximum power output to the original rating. This is particularly evident with the optimal controller for the same reason discussed previously: an increase (or decrease) in maximum power output cause a sub-optimal performance due to a change in the underlying optimal strategy, which is uniquely based on different performance bounds.

Table 7.7 Changes in primary source energy consumption when varying ESS maximum power output

System	<i>Variants</i>		
	<i>Default</i>	<i>-50%</i>	<i>+100%</i>
DCV			
Energy [MWh]	0.51	0.36	0.41
% w.r.t default	141.90%	100.00%	113.28%
Ideal			
Energy [MWh]	0.51	0.14	0.37
% w.r.t default	353.91%	100.00%	255.34%
PI			
Energy [MWh]	0.51	0.39	0.40
% w.r.t default	132.25%	100.00%	104.02%
Optimal			
Energy [MWh]	0.51	0.32	0.41
% w.r.t default	159.05%	100.00%	127.89%
Fuzzy			
Energy [MWh]	0.51	0.33	0.38
% w.r.t default	153.24%	100.00%	112.75%

Table 7.8 Changes in primary source peak power demand when varying ESS maximum power output

System	<i>Variants</i>		
	<i>Default</i>	<i>-50%</i>	<i>+100%</i>
DCV			
Over 150 kW [% of time]	4.27%	4.58%	4.26%
Over 200 kW [% of time]	3.67%	4.16%	3.28%
Ideal			
Over 150 kW [% of time]	3.74%	4.64%	1.97%
Over 200 kW [% of time]	2.87%	3.02%	1.96%
PI			
Over 150 kW [% of time]	1.91%	2.54%	1.91%
Over 200 kW [% of time]	1.62%	2.00%	1.62%
Optimal			
Over 150 kW [% of time]	0.89%	2.88%	0.89%
Over 200 kW [% of time]	0.32%	2.18%	0.32%
Fuzzy			
Over 150 kW [% of time]	3.38%	3.57%	3.38%
Over 200 kW [% of time]	2.57%	2.79%	1.01%

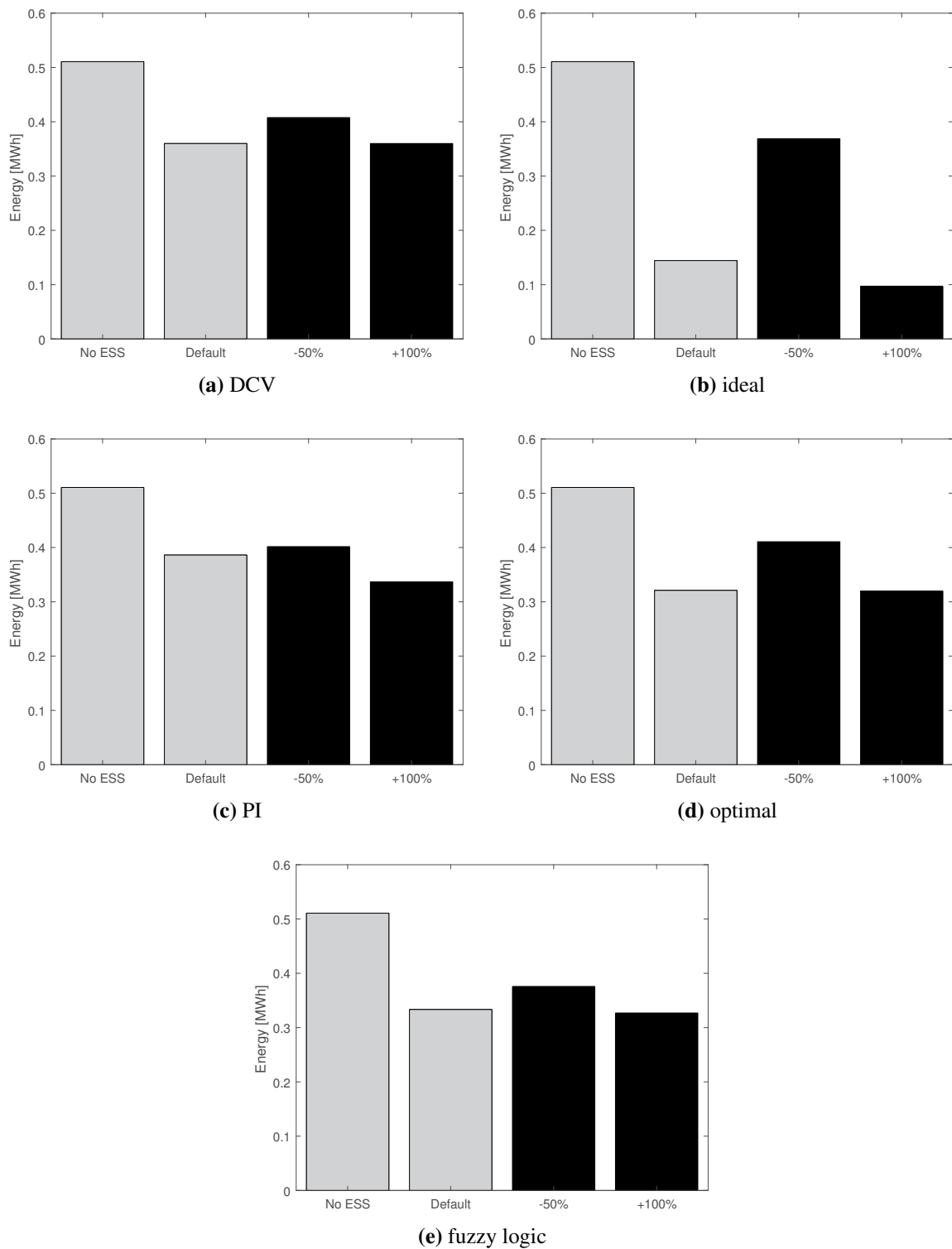


Fig. 7.9 Variation in power rating: energy demand

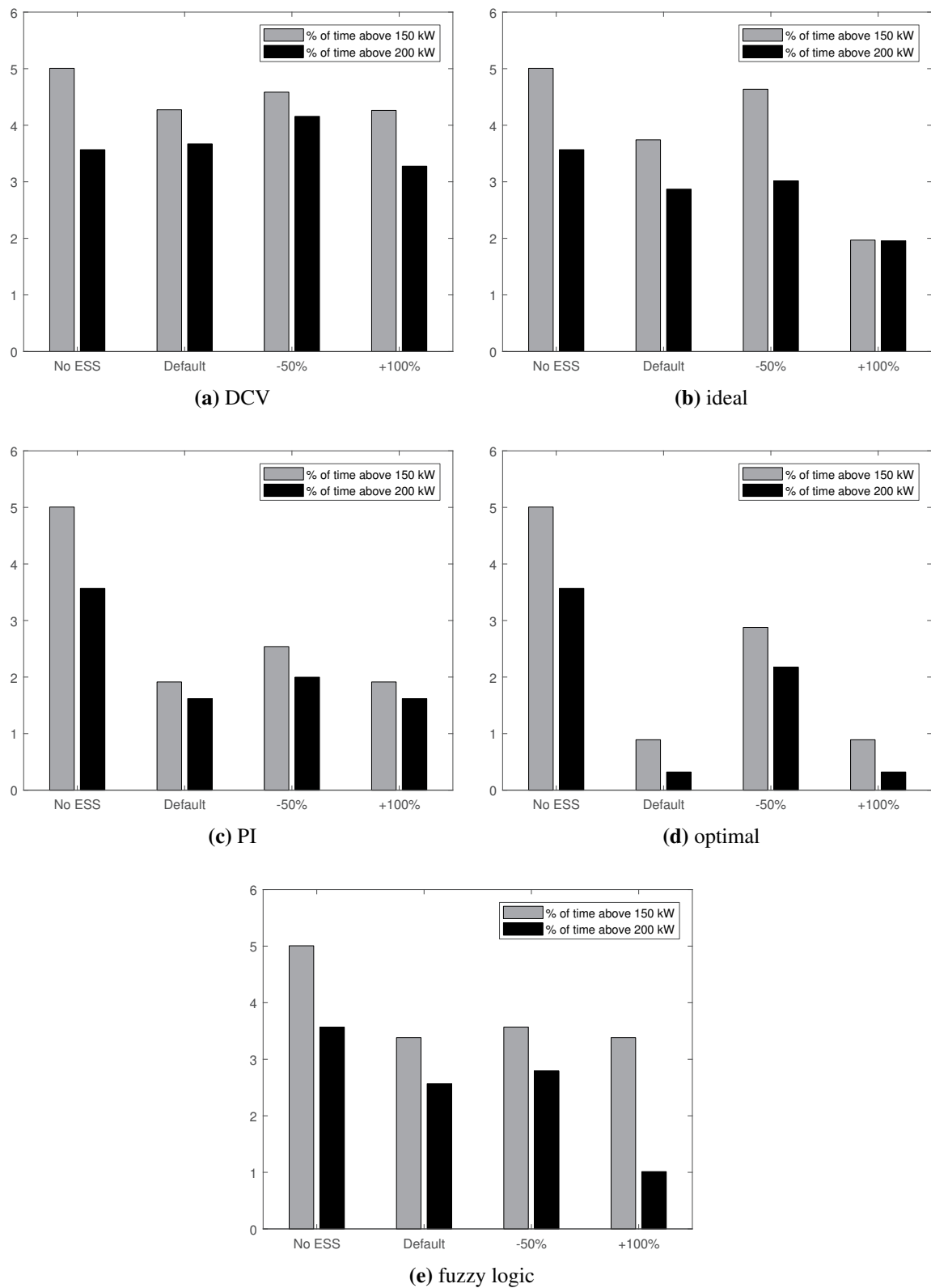


Fig. 7.10 Variation in power rating: peak power demand

In summary, changing the parameters of the energy storage system resulted in expected variations in performance. The three supervisory strategies presented in this thesis are based on the particular characteristics of the hybrid RTG crane under analysis, and therefore they show a reduction in effectiveness when those characteristics are changed. This is particularly evident with the optimal controller: its optimality is based on assumptions on the parameters of the systems, and any significant change in the parameters causes a significant reduction in the quality of the results. The PI controller continues to show limitations due to the arbitrary choice of the power sharing threshold of 75 kW, which limits its robustness. The FLC shows lower sensitivity, although it seems to perform worse in this dataset (corresponding to day 1 in the 6-days dataset) compared to the other controllers. This robustness is probably due to its simplicity and to the quasi-linearity of the equations composing the fuzzy sets.

Summary table

Table 7.9 shows a summary of the advantages and disadvantages of each supervisory control system analysed in this chapter, taking into consideration all the metrics and characteristics discussed in this chapter.

Table 7.9 Main advantages and disadvantages of each control strategy

Strategy	Advantages	Disadvantages
PI	<ul style="list-style-type: none"> • Easy to implement • Low complexity 	<ul style="list-style-type: none"> • Not versatile • Does not excel in any metric • Sensitive to change in tuning parameters
Optimal	<ul style="list-style-type: none"> • Easy to tune • Reduces peak power demand • Reduces burden on ESS • Easy to port to other applications 	<ul style="list-style-type: none"> • Low energy savings • Design is computationally intensive • Requires extensive knowledge of the system
FLC	<ul style="list-style-type: none"> • Best energy savings in the simulation • Not computationally intensive 	<ul style="list-style-type: none"> • Requires long tuning process • Difficult to tune and design • Requires extensive knowledge of the system

7.5 Summary

This chapter analysed and compared the supervisory control strategies proposed in this thesis. Activity of the crane was simulated for 6 days in 5 different scenarios with varying storage configurations. Energy savings, peak power demand reduction and other metrics were calculated from the results; the performance of each supervisory control strategy has been analysed and compared. All three strategies showed improvements over an existing technology, although none prevailed in all the metrics and each strategy has its own advantages and disadvantages that make it more suitable for a specific objective. The PI controller in the simulation showed average energy and power results, whilst it appears to be the most onerous to the storage device. The optimal controller saves the least amount of energy but excels in peak power demand and burden on the storage device. The FLC shows the best performance in terms of energy but the worst in peak power, and average strain on the ESS.

The sensitivity to change in control parameters or activity of the crane has been discussed. The PI controller is highly sensitive to changes in the activity of the crane and mildly affected by change in the tuning of control parameters. The optimal controller, instead, has no control parameter to tune but it is moderately affected by a change in the activity of the crane. The Fuzzy Logic controller is lightly sensitive to changes in the activity but a change in control parameters requires a full process of tuning and testing.

Lastly, the real-world feasibility and implementability were discussed. The PI controller and FLC are the easiest to implement and require the least computational power. The optimal controller requires little power in its final implementation but, on the other hand, it requires very large computational power in the design and calculation phases. The latter, though, is the simpler to tune and requires no guesswork.

Chapter 8

Conclusions

This chapter presents the conclusions for the research presented in this thesis and is divided into two sections. The first summarises the main contributions of the thesis and highlights the original contributions to knowledge. The second introduces areas for future work.

8.1 Summary and conclusions

8.1.1 Summary of the thesis

This thesis has presented three supervisory control systems for energy storage in Rubber Tyred Gantry (RTG) cranes. These manage the energy storage power flow with the objective of increasing the crane efficiency and reducing the impact on the primary energy source. The first control strategy is based on PI controllers that track a reference voltage or power output depending on the status of the crane, producing a reference power output for the ESS. The second strategy aims to minimise a cost function applied to the probability distribution of lift durations; an optimal problem is defined around parameters of the system and then a numerical computation outputs the optimal power output for any admissible initial condition. The third strategy uses Fuzzy Logic to determine the power output with linguistic rules applied to the value of variables of the system, creating an input-output mapping that selects the appropriate power output depending on the status of the crane and the storage.

The three proposed control strategies were implemented in a hybrid RTG model and showed significant benefits in terms of energy savings and reduction in peak power demand. The RTG model was developed specifically for this research and is composed of two main

components: a flywheel energy storage model based on data acquired by the manufacturer, and a RTG crane model representing the main electrical components of a crane which was validated using measurements taken on a real crane. The flywheel storage model used in this thesis is based on realistic mechanical and electrical assumptions, as well as a control system purposely-designed to ensure that the storage device provides the desired electrical power output.

This research is based on energy and power objectives that were quantified by analysing data collected at the Port of Felixstowe. The data provided insight on the potential benefits of energy storage and how to best improve the efficiency of the crane. Examining power flows in a typical lift cycle helped identifying the power and energy flows associated with normal operation. This knowledge was used to draft the base requirements for a storage device. The topology of electric components in the crane was studied in order to identify potential locations for placing storage devices.

The motivations and objectives of this thesis are based on the need for more efficient container cranes. Container terminals are major producers of CO₂ emissions and RTG cranes are one of their most energy demanding element. Reducing their energy consumption and reducing the peak power demand would be highly beneficial both in terms of energy costs and greenhouse gases emissions. The literature review identified energy storage as a powerful tool to achieve these objectives, however gaps were found in regards to supervisory control systems that can use storage devices to achieve a reduction in both energy consumption and peak power demand. This research has then been focused firstly on laying the foundation for analysing data and testing new supervisory control strategies, and then to develop new supervisory control strategies that improve over existing ones.

8.1.2 Summary of the chapters

This section will summarise the work presented in each chapter that compose this thesis.

Chapter 1

The first chapter introduces the background of the research, describing the context as well as the motivations. It also provides a literature review on the topics that will be discussed in subsequent chapters: energy storage systems, control of energy storage (including supervisory control) and modelling of power systems (focusing on RTG cranes). Then, it lays down

the objectives of the research that guided the rest of the research process, which consist in reducing energy consumption and decreasing the burden on the primary energy source by decreasing the peak power demand. This research led to journal papers and conference papers being published, and they are listed in this chapter along with papers still in the submission process.

Chapter 2

The RTG crane is thoroughly described in this chapter, including a description of the main electrical components and their activity during a typical lift cycle. It also introduces the actual crane (in use at the Port of Felixstowe) that is used as a reference for this research: this is the crane whose data was used to validate the RTG model presented in Chapter 5. The typical container lift cycle is described in terms of movements and associated energy flows, identifying potential opportunities for increasing the efficiency. These opportunities are defined clearly in the second half of the chapter: energy saving and peak power demand reduction are placed into a context of a crane working in a container terminal. This chapter showed that reducing energy consumption is beneficial both in economical and environmental terms, but a reduction in power demand can enable more environmentally-friendly alternatives to be implemented by port operators, as it is explained in this chapter. Finally, various storage technologies are analysed, resulting in the choice of flywheel energy storage as the best suited for the application on an RTG crane.

Chapter 3

Chapter 3 focuses on the storage device, starting with the description of a mechanical flywheel that can accumulate kinetic energy by rotating, and that is subjected to physical constraints of size and weight. The rotational mass is powered by an electric motor which can be one of the many available electric machines (e.g. induction motor or permanent magnet motor). The best suited solution was found to be a switched reluctance motor as it achieves high rotational speed with low rotor losses and high resilience. Finally, a low-level control system has been developed for tracking the desired instantaneous reference power output by acting on the power controller that drives the switched reluctance motor.

Chapter 4

The two Matlab/Simulink models that compose the hybrid RTG model are presented in this chapter. The RTG crane model represents the main electrical components of an RTG crane, i.e. main motors, power converters, primary power source and brake resistors. This model was successfully validated using high-resolution measurements acquired during controlled tests performed on an actual crane at the Port of Felixstowe; it enables the simulation of the activity of an RTG crane and the associated power flows. After the RTG crane model, the second component required to model a hybrid RTG is the energy storage device. Three different models were developed: one very generic model that represents any storage device by its electrical characteristics, a generic flywheel storage model that simulates a switched reluctance motor by its dynamic equations, and finally a switched reluctance flywheel storage which is based on data acquired by the motor manufacturer. The latter was chosen because, being based on actual data, requires the least number of assumptions. The flywheel storage model was then developed by linking the mechanical equations to the electrical motor model.

Chapter 5

This chapter presents the three proposed supervisory control strategies: PI supervisory control, Optimal supervisory control and Fuzzy Logic supervisory control. For each of the strategies, the development process has been described in detail; the final version of each controller is then tested in a short simulation and its behaviour is compared to the expectations.

The PI supervisory control is based on two PI controllers operating in two different phases on a lift cycle. A DC-voltage control limits the DC bus voltage increase (which is a characteristic of a crane lowering a load) by letting the storage absorb the excess energy. In a different phase, a power-sharing PI controller limits the output power of the primary energy source by acting on the power output of the storage during a container lift.

The Optimal supervisory controller exploits stochastic properties of container lift durations to anticipate the energy required by a lift, choosing an adequate power profile for the energy storage. During a lowering it operates similarly to the PI controller, however during a lift this controller varies the storage device power reference over time to follow an optimal trajectory that has been found with numerical calculations.

The Fuzzy Logic supervisory controller was developed using linguistic rules that act on fuzzy sets composed of various input variables. The instantaneous status of the crane and the storage are read by the controller which then produces a power reference that is fed to the device. The fuzzy sets are designed to produce a smooth transition between different fuzzy states which, combined, produce an output reference power. Each possible combination of the monitored variables is associated with one reference power value, therefore any phase of the lift cycle is governed by the input/output mapping generated by the controller.

Chapter 6

The supervisory control strategies presented in Chapter 5 are analysed in detail in this chapter. A total of 6 days worth of activity was recorded on an RTG in operation at the Port of Felixstowe and then this data was used to simulate the hybrid RTG equipped with various control strategies, including the three discussed above. The results were analysed and energy consumption and peak power demand for each controller were presented, among other metrics. The results of the simulations were used to analyse each strategy individually and also to compare the three supervisory controllers between themselves and with other reference scenarios. Other aspects of the controllers were discussed, including their sensitivity to a change in system parameters and the sensitivity to change in the activity of the crane. Finally, practical aspects were analysed, e.g. computational complexity and design difficulty.

8.1.3 Assumptions

The research that led to this thesis was based on the following major assumptions:

Simplified crane model: the RTG crane has been modelled using its major electrical components, ignoring smaller elements that produce low power demands. This is in line with similar works in the literature where simpler topologies are preferred (see Section 2.3).

Unknown future energy demand: this research is based on the supposition that the knowledge of the characteristics of future container lifts is unknown. Whilst this may change in the future with advanced container terminal logistic systems, it is assumed that at the present the typical crane has no knowledge of the energy power requirements of future lifts. Furthermore, this information would be of limited use without the associated timings (i.e. the exact moment at which the future lift is planned to start).

Data availability: data collected at the Port of Felixstowe has been the basis of this research.

Data from other container terminals was not directly available, however other works in the literature show similar patterns that suggest the data acquired is representative of a large sample of container terminals and RTG cranes. It was then assumed that the analysis of energy and power flows in an RTG crane operating in the Port of Felixstowe is valid for a generic container terminal.

8.1.4 Overview of original contributions to knowledge

- A validated MATLAB/Simulink model of the main electrical components of an RTG crane that allows for the study of novel solutions for increasing energy efficiency, including energy storage;
- Novel power sharing supervisory control system that uses existing PI controllers to produce an effective peak power demand reduction in hybrid RTG cranes;
- An optimal control strategy based on statistical properties of RTG activity in order to maximise the benefits of energy storage;
- An advanced fuzzy logic controller applied to energy storage in RTG cranes that enables both energy recovery and power sharing.

8.2 Future work

8.2.1 Models and simulations

The RTG crane model developed for this research is based on a single RTG crane in use at the Port of Felixstowe. The electrical topology of this particular crane is shared with all the modern RTG cranes that have been mentioned in the literature: a main power source connected to a series of electrical motors, which in turns are connected to one or more brake resistors. The model presented in this thesis could be expanded by including minor electrical components, e.g. trolley and gantry motors. Furthermore, it could be expanded by allowing the simulation of cranes using electric motors of different power rating, investigating the potential alternatives of slowing down or speeding up container lifts further increasing the efficiency boost given by energy storage. For example, an energy storage device could

provide extra peak power that would enable higher accelerations and reduce the duration of a typical container lift. A more generic model would allow more flexibility in the research and development process.

Generic ESS models were presented in Chapter 5 and they are perfect candidates for an investigation on the benefits of alternative energy storage devices (batteries, supercapacitors or alternative flywheel storage devices) in RTG cranes.

Multiple RTG models could be linked together to investigate the benefits of an array of cranes connected to a single power source. The use of energy storage as well as active front-end rectifiers shows promising results in preliminary studies [134]. The ESS models developed in this research could be strategically placed to provide peak power to one or multiple cranes, mitigating the fluctuations that are already diminished by aggregating the loads.

8.2.2 Crane Activity

One of the assumptions of this research is that the future energy and power consumption of RTG cranes is unknown or not accessible. Knowing in advance the characteristics of future container lifts may provide opportunities for using intelligent supervisory control systems that take into account the future demand. Knowing, instead of predicting, future demand would enable a true optimal control strategy to be developed, one that guarantees the minimisation of cost functions without uncertainties. It would be interesting to quantify the benefits of this knowledge in order to assess whether it would be cost effective to implement a precise logistic strategy that plans and coordinates container movements and that exposes this information to the crane. A supervisory control strategy that has access to this information may increase dramatically the efficiency of the crane.

As discussed above, multiple cranes could be connected together to form a network powered by a single source. Coordinating the activity of RTG cranes, for example performing a container lift whilst a second RTG is lowering a container, may reduce the impact on the primary source both in terms of peak power and energy. A storage device could mitigate short peaks and sags caused by non-perfect synchronisation. The aggregate load will then be a fraction of the sum of the loads, because regenerated energy is transferred to another crane and idle energy consumption is negligible.

8.2.3 Supervisory control strategies

The development, analysis and simulation of the three supervisory control strategies revealed potential improvements and new areas for research. Listed below are some ideas and concepts for future research.

PI supervisory control strategy

The proposed PI control strategy tracks successfully a desired power output. The research problem lays completely on deciding the appropriate power reference for the primary source. This problem has been handled by the optimal and Fuzzy Logic control strategies in two peculiar ways, but there is also the possibility of varying the primary source reference power output depending on the status of the storage device. For example, the reference could increase as the storage loses charge and vice-versa. This research has found that tackling this problem with advanced techniques does increase the performance of the controller but also increase the complexity of either the development or implementation. Effort could be spent by identifying the possibilities of increasing the performance of PI supervisory controllers without a large increase in complexity, maintaining the low characteristics of this particular strategy in terms of development and implementation costs.

Optimal supervisory control strategy

As discussed earlier, the knowledge of future demands would open new possibilities for developing an optimal controller that minimises the future cost. The unavailability of this information led to the development of the optimal control strategy based on stochastic properties of crane activity, forecasting future demand based on the status of the crane. A complete knowledge of future loads removes the uncertainty that affects this strategy, therefore future research could concentrate on modifying the optimal supervisory controller to minimise the actual (and not predicted) energy cost.

Even if complete knowledge of future demand is not possible or not cost effective, improvements are still possible for this type of controller. Simulations and analysis showed that the distribution of container lift durations may not match the predicted model, causing deviation from the optimal strategy. A solution for this would be to update the modelled distribution using new data acquired in real time: at every new container lift, the measured duration can be used to update the parameters of the distribution at the base of the optimal

strategy. This would require a recalculation of the whole optimal control strategy at each lift, therefore it may not be feasible at the moment but it could be interesting to investigate the potential benefits.

The cost function at the base of this strategy has been chosen arbitrarily as it penalises high power demands more than high energy demands. As already discussed in the analysis, this function can be changed to anything that is appropriate and reflects the actual costs (either monetary, logistics or infrastructural) associated with crane activity. Future research could investigate the use of alternative cost functions and their effects on the behaviour of the storage and the efficiency of the crane.

The main area for future research related to this particular controller, though, is the search for a closed-form solution to the optimal problem. This research uses numerical calculations to find the optimal strategy, based on the fact that the problem, as it is posed, is not convex and therefore does not allow the use of convex methods to calculate an optimal control strategy. A closed-form solution would be extremely beneficial because it would allow an instantaneous calculation of the optimal strategy given the set of constraints and initial conditions. The search for a closed-form solution is not trivial as it may require major changes in the optimal problem, for example removing or linearising constraints, adding assumptions, or add limitations to the controller.

Fuzzy Logic supervisory control

The FLC presented in this thesis is based on the Mamdani method. A future development could point to using other methods, including the Takagi-Sugeno-Kang method for fuzzy inference [144, 145]. This method allows the use of linear systems in the fuzzy system, for example for switching between optimal linear controllers as the crane operating state changes.

In the simulations, the FLC showed poor performance in reducing peak power demand. A desired outcome of a supervisory control strategy would be a reduction in peak power demand, therefore a an obvious continuation of this research would be to improve the performance of the FLC supervisory control in this key metric.

References

- [1] S. Pietrosanti, I. Harrison, A. Luque, W. Holderbaum, and V. M. Becerra. Net energy savings in Rubber Tyred Gantry cranes equipped with an active front end. In *2016 IEEE 16th Int. Conf. Environ. Electr. Eng.*, pages 1–5, Jun 2016.
- [2] V. Papaioannou, S. Pietrosanti, W. Holderbaum, V. M. Becerra, and R. Mayer. Analysis of energy usage for rtg cranes. *Energy*, 2017.
- [3] WTO. International Trade Statistics. Technical report, World Trade Organization, 2015.
- [4] IMO Maritime Knowledge Centre. International Shipping Facts and Figures – Information Resources on Trade, Safety, Security, Environment. *IMO Rep.*, (March):47, 2012.
- [5] M. Levinson. *The Box: How the Shipping Container Made the World Smaller and the World Economy Bigger*. Princeton University Press, 2016.
- [6] United Nations Conference on Trade and Development. Secretariat (Geneva). *Review of maritime transport 2015*. United Nations, 2015.
- [7] M. Acciaro and G. Wilmsmeier. Energy efficiency in maritime logistics chains. *Res. Transp. Bus. Manag.*, 17:1–7, Dec 2015.
- [8] PoF. Environment Report 2014-15. Technical report, Port of Felixstowe, 2014.
- [9] F. A. Allner. An analysis of hydro-regeneration. *Electr. Eng.*, 52(8):547–550, Aug 1933.
- [10] A. G. Ter-Gazarian. *Energy Storage for Power Systems*. IET, The Institution of Engineering and Technology, Michael Faraday House, Six Hills Way, Stevenage SG1 2AY, UK, Jan 2011.
- [11] EPRI. Bulk Energy Storage Impact and Value Analysis. Technical report, Electric Power Research Institute, 2012.
- [12] A. B. Hart and A. H. Webb. Batteries for bulk energy storage on the uk electricity supply system. In *10th International Power Sources Symposium Committee*, volume 1, 1976.
- [13] K. M. Abraham. Rechargeable lithium batteries-An overview. In *Recharg. Lithium Batter.*, volume 1, pages 1–20, 1990.

- [14] R. F. Post and S. F. Post. Flywheels. *Sci. Am.*, 229(6):17–23, Dec 1973.
- [15] J. Jensen and B. Sorensen. *Fundamentals of energy storage*. John Wiley and Sons, Inc., New York, NY, USA, 1984.
- [16] H. I. Becker. Low voltage electrolytic capacitor, 1957.
- [17] R. Kötz and M. Carlen. Principles and applications of electrochemical capacitors. *Electrochim. Acta*, 45(15-16):2483–2498, May 2000.
- [18] F. Díaz-González, A. Sumper, and O. Gomis-Bellmunt. *Energy Storage in Power Systems*. Wiley, 2016.
- [19] M. M. Flynn, P. McMullen, and O. Solis. High-speed flywheel and motor drive operation for energy recovery in a mobile gantry crane. *Conf. Proc. - IEEE Appl. Power Electron. Conf. Expo. - APEC*, pages 1151–1157, 2007.
- [20] F. Baalbergen, P. Bauer, and J. A. Ferreira. Energy Storage and Power Management for Typical 4Q-Load. *IEEE Trans. Ind. Electron.*, 56(5):1485–1498, May 2009.
- [21] K. Lin, C. Meier, J. Nelson, and Z. Papar. The Greening of Rubber-Tired Gantry Cranes in Ports. Technical report, Environmental Defense Fund, 2014.
- [22] H.; Hellendoorn, S.; Mulder, and B. D. Schutter. Hybrid Control of Container Cranes. *IFAC Proc. Vol.*, 44(1):9697–9702, jan 2011.
- [23] G. O. Cimuca and C. Saudemont. Control and performance evaluation of a flywheel energy-storage system associated to a variable-speed wind generator. *Ind. Electron.*, 53(4):1074–1085, 2006.
- [24] J. P. Barton and D. G. Infield. Energy storage and its use with intermittent renewable energy. *IEEE Trans. Energy Convers.*, 19(2):441–448, 2004.
- [25] F. Díaz-González, A. Sumper, O. Gomis-Bellmunt, and F. D. Bianchi. Energy management of flywheel-based energy storage device for wind power smoothing. *Appl. Energy*, 110:207–219, Oct 2013.
- [26] M. Rowe, T. Yunusov, S. Haben, W. Holderbaum, and B. Potter. The Real-Time Optimisation of DNO Owned Storage Devices on the LV Network for Peak Reduction. *Energies*, 7(6):3537–3560, May 2014.
- [27] M. Rowe, T. Yunusov, S. Haben, C. Singleton, W. Holderbaum, and B. Potter. A Peak Reduction Scheduling Algorithm for Storage Devices on the Low Voltage Network. *IEEE Trans. Smart Grid*, 5(4):2115–2124, Jul 2014.
- [28] T. Yunusov, D. Frame, W. Holderbaum, and B. Potter. The impact of location and type on the performance of low-voltage network connected battery energy storage systems. *Appl. Energy*, 165:202–213, 2016.
- [29] M. Ehsani, Y. Gao, and A. Emadi. *Modern Electric, Hybrid Electric, and Fuel Cell Vehicles: Fundamentals, Theory, and Design, Second Edition*. Power Electronics and Applications Series. CRC Press, 2009.

- [30] F. R. Salmasi. Control Strategies for Hybrid Electric Vehicles: Evolution, Classification, Comparison, and Future Trends. *IEEE Trans. Veh. Technol.*, 56(5):2393–2404, Sep 2007.
- [31] X. Liang and T. Virvalo. An energy recovery system for a hydraulic crane. *Proc. Inst. Mech. Eng. Part C J. Mech. Eng. Sci.*, 215(6):737–744, Jan 2001.
- [32] H. A. Toliyat, S. Talebi, P. McMullen, Co Huynh, and A. Filatov. Advanced high-speed flywheel energy storage systems for pulsed power applications. In *IEEE Electr. Sh. Technol. Symp. 2005.*, pages 379–386. IEEE, 2005.
- [33] VYCON REGEN Kinetic Energy Recycling Systems. <https://www.calnetix.com/regen-kinetic-energy-storage-system>. Last accessed 2017-12-03.
- [34] Sang-Min Kim and Seung-Ki Sul. Control of Rubber Tyred Gantry Crane with Energy Storage Based on Supercapacitor Bank. In *IEEE 36th Conf. Power Electron. Spec. 2005*, volume 21, pages 262–268. IEEE, 2006.
- [35] S. Mulder. *Energy management strategy for a hybrid container crane*. PhD thesis, TU Delft, Delft University of Technology, 2009.
- [36] M. Antonelli, M. Ceraolo, U. Desideri, G. Lutzemberger, and L. Sani. Hybridization of rubber tired gantry (RTG) cranes. *J. Energy Storage*, 12:186–195, 2017.
- [37] Konecranes. Power options for RTGs. http://www.konecranes.co.uk/sites/default/files/download/konecranes_power_options_brochure_final.pdf, 2012. Last accessed 2017-12-03.
- [38] M. Winter and R. J. Brodd. What Are Batteries, Fuel Cells, and Supercapacitors? *Chem. Rev.*, 104(10):4245–4270, Oct 2004.
- [39] Y.-S. Lee and M.-W. Cheng. Intelligent Control Battery Equalization for Series Connected Lithium-Ion Battery Strings. *IEEE Trans. Ind. Electron.*, 52(5):1297–1307, Oct 2005.
- [40] A. Ndokaj, A. Di Napoli, G. Pede, and M. Pasquali. Regulation strategy of an Ultracapacitor storage model for a gantry crane. In *IECON 2013 - 39th Annu. Conf. IEEE Ind. Electron. Soc.*, pages 1209–1216. IEEE, Nov 2013.
- [41] Mechanical Storage Sub-program. Kinetic Energy Storage Based on Flywheels : Basic Concepts , State of the Art and Analysis of Applications. Technical Report March, EERA JP Energy Storage, 2013.
- [42] B. K. Bose. *Power Electronics And Motor Drives: Advances and Trends*. Academic Press, 2010.
- [43] N. Mohan. *Electric Machines and Drives*. Wiley Global Education, 2011.
- [44] A. M. Phillips. Vehicle system controller design for a hybrid electric vehicle. *Control Appl.*, pages 0–5, 2000.

- [45] D. Iannuzzi, L. Piegari, and P. Tricoli. Use of supercapacitors for energy saving in overhead travelling crane drives. In *2009 Int. Conf. Clean Electr. Power*, pages 562–568. IEEE, Jun 2009.
- [46] W. Niu, X. Huang, F. Yuan, N. Schofield, L. Xu, J. Chu, and W. Gu. Sizing of Energy System of a Hybrid Lithium Battery RTG Crane. *IEEE Trans. Power Electron.*, 8993(c):1–1, 2016.
- [47] P. Pisu and G. Rizzoni. A comparative study of supervisory control strategies for hybrid electric vehicles. *Control Syst. Technol. IEEE ...*, 15(3):506–518, 2007.
- [48] Z. Li, H. Li, and Y. Zheng. Research of coordinated control method of hybrid power crane system. In *Model. Identif. Control (ICMIC), 2012 Proc. Int. Conf.*, pages 1093–1097, 2012.
- [49] Nan Zhao, N. Schofield, and W. Niu. Energy Storage System for a Port Crane Hybrid Power-Train. *IEEE Trans. Transp. Electrif.*, 2(4):480–492, Dec 2016.
- [50] J. Xu, J. Yang, and J. Gao. An integrated kinetic energy recovery system for peak power transfer in 3-DOF mobile crane robot. In *2011 IEEE/SICE Int. Symp. Syst. Integr.*, pages 330–335. IEEE, dec 2011.
- [51] J. H. Lilly. *Fuzzy Control and Identification*. Wiley, 2011.
- [52] E. H. Mamdani and S. Assilian. An experiment in linguistic synthesis with a fuzzy logic controller. *Int. J. Man. Mach. Stud.*, 7(1):1–13, jan 1975.
- [53] J. Lagorse, M. G. Simoes, and A. Miraoui. A Multiagent Fuzzy-Logic-Based Energy Management of Hybrid Systems. *IEEE Trans. Ind. Appl.*, 45(6):2123–2129, 2009.
- [54] N. J. Schouten, M. A. Salman, and N. A. Kheir. Fuzzy logic control for parallel hybrid vehicles. *IEEE Trans. Control Syst. Technol.*, 10(3):460–468, May 2002.
- [55] A. A. Ferreira, J. A. Pomilio, G. Spiazzi, and L. de Araujo Silva. Energy Management Fuzzy Logic Supervisory for Electric Vehicle Power Supplies System. *IEEE Trans. Power Electron.*, 23(1):107–115, Jan 2008.
- [56] C. Knight, V. Becerra, W. Holderbaum, and R. Mayer. Development and deployment of a control system for energy storage. pages 3–9, 2013.
- [57] C. Knight. *Fuzzy logic control of a flywheel energy storage system for DRTG crane application*. PhD thesis, University of Reading, 2015.
- [58] D. E. Kirk. *Optimal Control Theory: An Introduction*. Courier Corporation, 2004.
- [59] C. Lin, H. Peng, J. W. Grizzle, and Jun-Mo Kang. Power management strategy for a parallel hybrid electric truck. *IEEE Trans. Control Syst. Technol.*, 11(6):839–849, Nov 2003.
- [60] G. Paganelli, G. Ercole, A. Brahma, Y. Guezennec, and G. Rizzoni. General supervisory control policy for the energy optimization of charge-sustaining hybrid electric vehicles. *JSAE Rev.*, 22(4):511–518, 2001.

- [61] C. Lin, H. Peng, and J. W. Grizzle. A stochastic control strategy for hybrid electric vehicles. In *Proc. 2004 Am. Control Conf.*, volume 5, pages 4710–4715 vol.5, Jun 2004.
- [62] S. Teleke, M. E. Baran, S. Bhattacharya, and A. Q. Huang. Optimal Control of Battery Energy Storage for Wind Farm Dispatching. *IEEE Trans. Energy Convers.*, 25(3):787–794, Sep 2010.
- [63] K. M. Chandy, S. H. Low, U. Topcu, and H. Xu. A simple optimal power flow model with energy storage. In *49th IEEE Conf. Decis. Control*, pages 1051–1057. IEEE, dec 2010.
- [64] I. Koutsopoulos, V. Hatzi, and L. Tassiulas. Optimal energy storage control policies for the smart power grid. In *2011 IEEE Int. Conf. Smart Grid Commun.*, pages 475–480. IEEE, Oct 2011.
- [65] A. Brahma, Y. Guezennec, and G. Rizzoni. Optimal energy management in series hybrid electric vehicles. In *Proc. 2000 Am. Control Conf. ACC (IEEE Cat. No.00CH36334)*, volume 1, pages 60–64. IEEE, 2000.
- [66] Y. Levron and D. Shmilovitz. Optimal Power Management in Fueled Systems With Finite Storage Capacity. *Ieee Trans. Circuits Syst. Regul. Pap.*, 57(8):2221–2231, 2010.
- [67] Y. Levron and D. Shmilovitz. Power systems’ optimal peak-shaving applying secondary storage. *Electr. Power Syst. Res.*, 89(0):80–84, Aug 2012.
- [68] H. Le-Huy and P. Brunelle. Design and implementation of a switched reluctance motor generic model for simulink simpowersystems. In *Electrimacs2005 Conference*, 2005.
- [69] H. Le-Huy and P. Brunelle. A versatile nonlinear switched reluctance motor model in simulink using realistic and analytical magnetization characteristics. *IECON Proc. (Industrial Electron. Conf.)*, 2005(c):1556–1561, 2005.
- [70] Simscape Power Systems - MATLAB Simulink.
- [71] V. Perelmuter. *Electrotechnical Systems: Simulation with Simulink® and SimPower-Systems™*. CRC Press, 2012.
- [72] A. Di Napoli and A. Ndokaj. Ultracapacitor storage for a 50t capacity gantry crane. In *2012 XXth Int. Conf. Electr. Mach.*, pages 2014–2018. IEEE, Sep 2012.
- [73] C. E. Knight, V. Becerra, W. Holderbaum, and R. Mayer. Modelling and simulating the operation of RTG container cranes. *6th IET Int. Conf. Power Electron. Mach. Drives (PEMD 2012)*, pages F24–F24, 2012.
- [74] S. Pietrosanti, W. Holderbaum, and V. M. Becerra. Modeling Power Flow in a Hoist Motor of a Rubber-Tired Gantry Crane. *IEEE Trans. Ind. Appl.*, 52(3):2088–2094, May 2016.

- [75] EPRI. Electric Cable Reel Rubber-Tired Gantry Cranes: Costs and Benefits. Technical report, Electric Power Research Institute, 2010.
- [76] Yi Chih Yang and Wei Min Chang. Impacts of electric rubber-tired gantries on green port performance. *Research in Transportation Business and Management*, 8(2013):67–76, 2013.
- [77] C. W. Gellings. *Saving Energy and Reducing CO2 Emissions with Electricity*. Lulu.com, 2013.
- [78] WCN. RTG electrification proceeding apace. *World Cargo News*, pages 30–32, Jan 2015.
- [79] P.F. Ribeiro, B.K. Johnson, M.L. Crow, a. Arsoy, and Y. Liu. Energy storage systems for advanced power applications. *Proc. IEEE*, 89(12), 2001.
- [80] I. Harrison, S. Pietrosanti, A. Luque, R. Mayer, and W. Holderbaum. Recording and analysing measurements from an RTG crane. *Meas. J. Int. Meas. Confed.*, 125:284–293, 2018.
- [81] Amendments to the International Convention for the Safety Of Life At Sea (SOLAS), Resolution MSC.380(94), 2014.
- [82] Volvo Penta. TAD1640GE Product Bulletin, 2014.
- [83] Defra. Guidelines to Defra/DECC GHG Conversion Factors for Company Reporting. *Dep. Energy Clim. Chang.*, pages 1–54, 2012.
- [84] DECC. 2014 UK Greenhouse Gas Emissions. Technical Report March, Department of Energy & Climate Change, 2015.
- [85] S. Pietrosanti, W. Holderbaum, and V. Becerra. Optimal Power Management Strategy for Energy Storage with Stochastic Loads. *Energies*, 9(3):175, Mar 2016.
- [86] C. K. Morehouse, R. Glicksman, and G. S. Lozier. Batteries. *Proc. IRE*, 46(8):1462–1483, 1958.
- [87] X. Luo, J. Wang, M. Dooner, and J. Clarke. Overview of current development in electrical energy storage technologies and the application potential in power system operation. *Appl. Energy*, Oct 2014.
- [88] T.M.I. Mahlia, T.J. Saktisahdan, A. Jannifar, M.H. Hasan, and H.S.C. Matseelar. A review of available methods and development on energy storage; technology update. *Renew. Sustain. Energy Rev.*, 33:532–545, May 2014.
- [89] M. C. Block. RTG EcoCrane In-Use Emissions and Fuel Economy Test Program at POLA, 2013.
- [90] X. Zhou, M. Dong, and D. Zhou. Study on hybrid power system of wheeled crane. In *2010 3rd International Conference on Biomedical Engineering and Informatics*, volume 7, pages 2667–2672, Oct 2010.

- [91] J. R. Miller and A. F. Burke. Electrochemical capacitors: challenges and opportunities for real-world applications. *Electrochem. Soc. Interface*, 2008.
- [92] J. R. Miller and S. Patrice. MATERIALS SCIENCE: Electrochemical Capacitors for Energy Management. *Science (80-.)*, 321(5889):651–652, Aug 2008.
- [93] B. Ferreira and W. Van Der Merwe. *The Principles of Electronic and Electromechanic Power Conversion: A Systems Approach*. John Wiley & Sons, 2014.
- [94] T. Coombs, A. M. Campbell, R. Storey, and R. Weller. Superconducting magnetic bearings for energy storage flywheels. *IEEE Trans. Applied Supercond.*, 9(2):968–971, Jun 1999.
- [95] T. Ichihara, K. Matsunaga, M. Kita, I. Hirabayashi, M. Isono, M. Hirose, K. Yoshii, K. Kurihara, O. Saito, S. Saito, M. Murakami, H. Takabayashi, M. Natsumeda, and N. Koshizuka. Application of Superconducting Magnetic Bearings to a 10 kWh-Class Flywheel Energy Storage System. *IEEE Trans. Applied Supercond.*, 15(2):2245–2248, Jun 2005.
- [96] Haisheng Chen, Thang Ngoc Cong, Wei Yang, Chunqing Tan, Yongliang Li, and Yulong Ding. Progress in electrical energy storage system: A critical review. *Prog. Nat. Sci.*, 19(3):291–312, 2009.
- [97] H. Akagi. New trends in active filters for power conditioning. *IEEE transactions on industry applications*, 32(6):1312–1322, 1996.
- [98] B. Singh, K. Al-Haddad, and A. Chandra. A review of active filters for power quality improvement. *IEEE transactions on industrial electronics*, 46(5):960–971, 1999.
- [99] J.W. Kolar and H. Ertl. Status of the techniques of three-phase rectifier systems with low effects on the mains. *21st International Telecommunications Energy Conference. INTELEC '99 (Cat. No.99CH37007)*, page 279, 1999.
- [100] C. Klumpner, M. Liserre, and F. Blaabjerg. Improved control of an active-front-end adjustable speed drive with a small dc-link capacitor under real grid conditions. *PESC Record - IEEE Annual Power Electronics Specialists Conference*, 2:1156–1162, 2004.
- [101] A. Yazdani and R. Iravani. *Voltage-sourced converters in power systems: modeling, control, and applications*. Wiley, 2010.
- [102] WCN. Crossing the gantry divide. *World Cargo News*, pages 30–32, Feb 2016.
- [103] G. L. Fischer. Comparison of dc and ac container crane drive systems. In *Power Electronics and Drive Systems, 1999. PEDS '99. Proceedings of the IEEE 1999 International Conference on*, volume 1, pages 297–302 vol.1, 1999.
- [104] A. Gabriel-Buenaventura and B. Azzopardi. Energy recovery systems for retrofitting in internal combustion engine vehicles: A review of techniques. *Renew. Sustain. Energy Rev.*, 41:955–964, jan 2015.
- [105] F.T. Wallenberger and P.A. Bingham. *Fiberglass and Glass Technology: Energy-Friendly Compositions and Applications*. Springer US, 2009.

- [106] P. Tsao, M. Senesky, and S.R. Sanders. An integrated flywheel energy storage system with homopolar inductor motor/generator and high-frequency drive. *IEEE Trans. Ind. Appl.*, 39(6):1710–1725, Nov 2003.
- [107] H. Akagi and H. Sato. Control and performance of a doubly-fed induction machine intended for a flywheel energy storage system. *IEEE Trans. Power Electron.*, 17(1):109–116, 2002.
- [108] R. Cardenas, R. Peña, G. Asher, and J. Clare. Control strategies for enhanced power smoothing in wind energy systems using a flywheel driven by a vector-controlled induction machine. *IEEE Trans. Ind. Electron.*, 48(3):625–635, Jun 2001.
- [109] F. Hardan. Bi-directional power control for flywheel energy storage system with vector-controlled induction machine drive. In *Seventh Int. Conf. Power Electron. Var. Speed Drives*, volume 1998, pages 477–482. IEE, 1998.
- [110] R. Sebastián and R. Peña-Alzola. Control and simulation of a flywheel energy storage for a wind diesel power system. *Int. J. Electr. Power Energy Syst.*, 64:1049–1056, Jan 2015.
- [111] R. Cardenas, R. Peña, M. Perez, J. Clare, G. Asher, and P. Wheeler. Power Smoothing Using a Flywheel Driven by a Switched Reluctance Machine. *IEEE Trans. Ind. Electron.*, 53(4):1086–1093, Jun 2006.
- [112] P. Gamboa, S. Ferreira Pinto, J. Silva Fernando, and E. Margato. A flywheel energy storage system with Matrix Converter controlled Permanent Magnet Synchronous Motor. *2008 18th Int. Conf. Electr. Mach.*, pages 1–5, Sep 2008.
- [113] R. Hebner, J. Beno, and A. Walls. Flywheel batteries come around again. *IEEE Spectr.*, 39(4):46–51, Apr 2002.
- [114] R.L. Hockney and C.A. Driscoll. Powering of standby power supplies using flywheel energy storage. *Proc. Power Energy Syst. Converging Mark.*, pages 105–109, 1997.
- [115] R.H. Jansen, R.C. Wagner, K. Duffy, D.S. Hervol, R.J. Storzuk, T.P. Dever, S.M. Anzalone, J.J. Trudell, K.E. Konno, and A. Kenny. Redesign of Glenn research center D1 flywheel module. *IECEC '02. 2002 37th Intersoc. Energy Convers. Eng. Conf. 2002.*, pages 209–213, 2002.
- [116] T. J. E. Miller. *Electronic Control of Switched Reluctance Machines*. Newnes, 2001.
- [117] A. Hughes. *Electric Motors and Drives: Fundamentals, Types and Applications*. Newnes, 2005.
- [118] D. A. Torrey. Switched reluctance generators and their control. *IEEE Trans. Ind. Electron.*, 49(1):3–14, 2002.
- [119] H. C. Lovatt. Comparative performance of singly salient reluctance, switched reluctance, and induction motors. In *Eighth Int. Conf. Electr. Mach. Drives*, volume 1997, pages 361–365. IEE, 1997.

- [120] Minh C. Ta and C. Dufour. Real-time simulation and control of reluctance motor drives for high speed operation with reduced torque ripple. *IECON 2011 - 37th Annu. Conf. IEEE Ind. Electron. Soc.*, pages 4176–4181, Nov 2011.
- [121] H. Le-huy. Modeling and Simulation of Electrical Drives using MATLAB Simulink and Power System Blockset. *Annu. Conf. IEEE Ind. Electron. Soc.*, 27(C):1603–1611, 2001.
- [122] B. D’Andréa-Novel and J. Lévine. Modelling and Nonlinear Control of an Overhead Crane. In *Robust Control Linear Syst. Nonlinear Control*, pages 523–529. Birkhäuser Boston, Boston, MA, 1990.
- [123] L. Morrish, M. P. Cartmell, and A. J. Taylor. Geometry and kinematics of multicable spreader lifting gear. *Proc. Inst. Mech. Eng. Part C J. Mech. Eng. Sci.*, 211(3):185–194, 1997.
- [124] M. P. Cartmell, L. Morrish, and A. J. Taylor. Dynamics of spreader motion in a gantry crane. *Proc. Inst. Mech. Eng. Part C J. Mech. Eng. Sci.*, 212(2):85–105, jan 1998.
- [125] K. E. Yeager and J. R. Willis. Modeling of emergency diesel generators in an 800 megawatt nuclear power plant. *IEEE Trans. Energy Convers.*, 8(3):433–441, Sep 1993.
- [126] C. Knight, V. Becerra, W. Holderbaum, and R. Mayer. A Consumption And Emissions Model Of An RTG Crane Diesel Generator. In *TSBE EngD Conf.*, number July 2011, 2011.
- [127] F. N. Fritsch and R. E. Carlson. Monotone Piecewise Cubic Interpolation. *SIAM J. Numer. Anal.*, 17(2):238–246, Apr 1980.
- [128] D. Kahaner, C. Moler, and S. Nash. *Numerical methods and software*. Prentice-Hall, 1989.
- [129] P. Giroux, G. Sybille, and H. Le-Huy. Modeling and simulation of a distribution STATCOM using Simulink’s Power System Blockset. In *IECON’01. 27th Annu. Conf. IEEE Ind. Electron. Soc. (Cat. No.37243)*, volume 2, pages 990–994. IEEE, 2001.
- [130] G. Sybille and P. Giroux. Simulation of FACTS controllers using the MATLAB Power System Blockset and Hypersim real-time simulator. In *2002 IEEE Power Eng. Soc. Winter Meet. Conf. Proc. (Cat. No.02CH37309)*, volume 1, pages 488–491. IEEE, 2002.
- [131] P. Giroux, G. Sybille, C. Osorio, and S. Chandrachood. Two demonstrations of a grid-connected pv array using simpowersystems. *File Exchange–MATLAB Central, The MathWorks, Inc., Natick, MA, USA*, 2012.
- [132] F. Hernandez, L. Moran, J. Espinoza, and J. Dixon. A multilevel active front-end rectifier with current harmonic compensation capability. In *30th Annu. Conf. IEEE Ind. Electron. Soc. 2004. IECON 2004*, volume 2, pages 1446–1451. IEEE, 2004.
- [133] J. O. Rawlings, S. G. Pantula, and D. A. Dickey. *Applied Regression Analysis: A Research Tool*. Springer Texts in Statistics. Springer New York, 2006.

- [134] A. Luque, I. Harrison, S. Pietrosanti, F. M. M. Alasali, W. Holderbaum, R. M. Mayer, and V. M. Becerra. Energy reduction on eRTG. In *2016 IEEE 16th Int. Conf. Environ. Electr. Eng.*, pages 1–6, Jun 2016.
- [135] S. Talebi. Analytical model-based analysis of high-speed flywheel energy storage systems for pulsed power applications. *IEEE Electr. Sh. Technol. Symp.*, pages 65–72, 2009.
- [136] R. W. Erickson and D. Maksimović. *Fundamentals of Power Electronics*. Springer US, Boston, MA, 2001.
- [137] G. Genta. *Kinetic Energy Storage: Theory and Practice of Advanced Flywheel Systems*. Elsevier Science, 1985.
- [138] Stefano Pietrosanti, William Holderbaum, and Victor M Becerra. Modelling power flow in a hoist motor of a Rubber Tyred Gantry crane. In *2015 IEEE Ind. Appl. Soc. Annu. Meet.*, pages 1–6. IEEE, oct 2015.
- [139] M. M. Flynn, P. McMullen, and O. Solis. Saving energy using flywheels. *IEEE Ind. Appl. Mag.*, 14(6):69–76, 2008.
- [140] D. C. Montgomery and G. C. Runger. *Applied Statistics and Probability for Engineers*. John Wiley & Sons, 2010.
- [141] B. J. Driessen. On-off minimum-time control with limited fuel usage: Near global optima via linear programming. *Optimal Control Applications and Methods*, 27(3):161–168, 2006.
- [142] W. Singhose, T. Singh, and W. Seering. On-off control with specified fuel usage. *Journal of dynamic systems, measurement, and control*, 121(2):206–212, 1999.
- [143] D. Thain, T. Tannenbaum, and M. Livny. Distributed computing in practice: the condor experience. *Concurrency - Practice and Experience*, 17(2-4):323–356, 2005.
- [144] M. Sugeno. *Industrial Applications of Fuzzy Control*. Elsevier Science Inc., New York, NY, USA, 1985.
- [145] T. Takagi and M. Sugeno. Fuzzy identification of systems and its applications to modeling and control. *IEEE transactions on systems, man, and cybernetics*, (1):116–132, 1985.

Appendix A

Characteristics of the RTG crane used as a reference in this work

In Table A.1 it is presented the full list of characteristics of the RTG crane, including the parameters of its main electrical components.

Table A.1 Characteristics of the RTG crane in use at the Port of Felixstowe

Group	Parameter	Value	Unit
Crane	Crane span	26.45	m
	Wheel Base	7.5	m
	Total number of wheels / driven wheels	16/8	
	Diesel engine power	395	Kw
	Diesel engine speed	1500	rpm
	Alternator power	670	kVA

continues in the next page

Group	Parameter	Value	Unit
Hoist	Rated lifting capacity (under spreader)	40	tonne
	Rated lifting capacity (under headblock)	51	tonne
	Lifting height	18.3	m
	Hoisting speed (full load)	23	m /min
	Hoisting speed (no load)	50	m /min
	Number of hoist motors	1	
	Hoist motor nominal power	185	kW
	Hoist motor rotational speed (nominal/max)	700/1522	RPM
	Hoist motor voltage	415	V
	Hoist motor nominal frequency	50	Hz
	Hoist drum diameter	1285	mm
Hoist reducer ratio	122.8		
Gantry	Gantry travelling speed (full load)	40	m/min
	Gantry travelling speed (no load)	140	m /min
	Number of gantry motors	4	
	Gantry motor power	45	kW
	Gantry motor rotational speed	915	RPM
	Gantry motor voltage	415	V
Trolley	Gantry motor frequency	50	Hz
	Trolley traversing speed	70	m /min
	Number of trolley motors	2	
	Trolley motor power	18.5	kW
	Trolley motor rotational speed	1765	RPM
	Trolley motor voltage	415	V
Trolley motor frequency	50	Hz	

Appendix B

Calculations of the moment of inertia of a hollow cylinder

B.1 Hollow cylinder

A hollow cylinder (Figure B.1) has an inertia that is dependent on its length L , external radius r_{max} and internal radius r_{min} :

$$I = \rho L 2\pi \int_{r_{min}}^{r_{max}} r^3 dr = \rho L 2\pi \left[\frac{r_{max}^4}{4} - \frac{r_{min}^4}{4} \right] \quad (\text{B.1})$$

so a maximum value for the internal radius can be calculated as follows:

$$r_{min} = \left(\frac{K r_{max}^4 - I}{K} \right)^{\frac{1}{4}} \quad (\text{B.2})$$

with

$$K = \frac{\rho L 2\pi}{4}. \quad (\text{B.3})$$

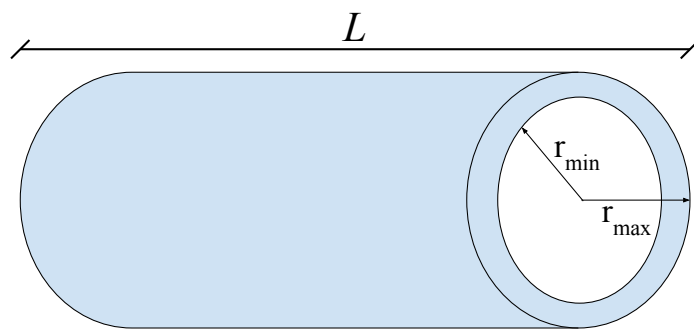


Fig. B.1 Hollow cylinder.

Appendix C

Stability and error rejection of the DC voltage PI control

A PI controller dynamic is governed by the following transfer function:

$$u(t) = K_P e(t) + K_I \int_0^t e(\tau) d\tau \quad (\text{C.1})$$

where $u(t)$ is the control output, $e(t)$ is the error between the reference and the measured value and K_P , K_I are, respectively, the proportional and integral gains. In the frequency domain, the controlled can be expressed as following:

$$U(s) = \frac{K_P s + K_I}{s} E(s) = G(s) E(s) \quad (\text{C.2})$$

where $U(s)$ is the control output and $E(s)$ the error in the Laplace domain. The plant system $P(s)$ (Figure C.1) is formed by the energy storage, the hoist motor and the DC bus. The following assumptions are made:

- The energy storage system low-level control is well-designed, with the storage output following the control input with a simple scaling factor as the difference;
- The energy storage transients are significantly faster than the crane dynamics;
- The system is of first order and type 0;
- The system is stable for bounded inputs.

From the assumptions, the plant system can be represented by a transfer function $P(s)$ which is stable and characterised by fast dynamics; therefore it can be modelled by a simple lag system:

$$P(s) = \frac{K}{\tau s + 1} \quad (\text{C.3})$$

with $\tau > 0$ the time constant and K a positive constant gain. From basic knowledge of control theory, it can be shown that the closed loop system formed by $G(s)$ and $P(s)$ is stable and that the error $E(s) = R(s) - Y(s)$, where $R(s)$ is the reference signal and $Y(s)$ the output signal, vanishes asymptotically for bounded constant reference signals:

$$E(s) = \frac{1}{1 + \frac{K_P s + K_I}{s} \cdot \frac{K}{\tau s + 1}} R(s) \quad (\text{C.4})$$

which, with a step reference signal $R(s) = A/s$ and $A > 0$, becomes:

$$E(s) = \frac{A}{s \left(1 + \frac{K_P s + K_I}{s} \cdot \frac{K}{\tau s + 1} \right)} \quad (\text{C.5})$$

$$= \frac{A s (\tau s + 1)}{s^2 \tau + s K K_P + K K_I} \quad (\text{C.6})$$

The system is stable when choosing positive K_P , K_I and the steady state error e_{SS} can be computed using the final value theorem:

$$e_{SS} = \lim_{s \rightarrow 0} s E(s) = 0. \quad (\text{C.7})$$

A properly designed supervisor can successfully control the output power of the storage in order to respond to changes in the voltage caused by a constant power demand of the hoist motor. Unfortunately, the hoist motor power flow is subject to transients, therefore it is useful to investigate what is the steady state error for ramp reference signals $R(s) = A/s^2$, as it is equivalent to:

$$E(s) = \frac{A}{s^2 \left(1 + \frac{K_P s + K_I}{s} \cdot \frac{K}{\tau s + 1} \right)} \quad (\text{C.8})$$

$$= \frac{A (\tau s + 1)}{s^3 \tau + s^2 K K_P + s K K_I} \quad (\text{C.9})$$

and the steady state error is the following:

$$e_{SS} = \frac{A}{K_I} \neq 0. \quad (\text{C.10})$$

The steady state error for non-constant reference signals is non-zero, thus reflecting the limitations of this control system. Nonetheless, by choosing a high integral gain it is possible to limit it, and the crane dynamics are slow enough that the error is minimal, therefore it is not necessary to use more complicated control systems like second order PID controllers.

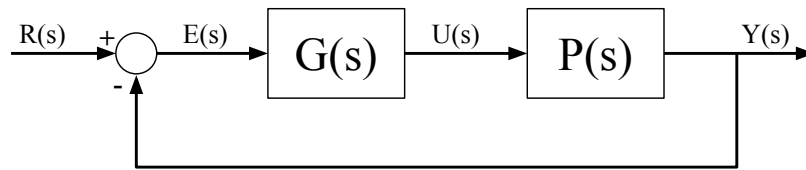


Fig. C.1 Control system topology for the PI supervisory control system.

Appendix D

Proof to the CDF Theorem

Theorem

Given a distribution L whose known probability density function is $f(x)$, with $x \in [0, T]$, and whose CDF is $F(t)$, and given continuous functions $g : \mathbb{R} \rightarrow \mathbb{R}$ and $u : \mathbb{R} \rightarrow \mathbb{R}$ that satisfy the following:

$$\int_0^{\infty} |g(u(t))| dt < \infty. \quad (\text{D.1})$$

then the following is true:

$$\arg \min_{u(t)} \int_0^T f(t_f) \left(\int_0^{t_f} g(u(t)) dt \right) dt_f = \arg \min_{u(t)} \int_0^T (1 - F(t)) g(u(t)) dt \quad (\text{D.2})$$

Proof

A sufficient condition for the equality in (D.2) is that (D.3) is true given the assumptions stated in the Theorem.

$$\int_0^T f(x) \int_0^x g(u(t)) dt dx = \int_0^T (1 - F(t)) g(u(t)) dt. \quad (\text{D.3})$$

The CDF $F(t)$ is the integral of $f(x)$ over x :

$$F(t) = \int_0^t f(x) dx \quad (\text{D.4})$$

and, given that the maximum value for x is T , it satisfies the following:

$$F(T) = \int_0^T f(x) dx = 1 \quad (\text{D.5})$$

Given that $f(x)$ does not depend on t , we can rewrite the left integral of (D.3) as follows:

$$\int_0^T f(x) \int_0^x g(u(t)) dt dx = \int_0^T \int_0^x f(x) g(u(t)) dt dx. \quad (\text{D.6})$$

The domain of t is $[0, x]$ while the domain of x is $[0, T]$. By using Fubini's theorem, we can invert the order of integration (given the assumption in (D.1)), resulting in the following domains: $t \in [0, T]$, $x \in [t, T]$. Equation (D.6) is then equal to:

$$\int_0^T \int_t^T f(x) g(u(t)) dx dt. \quad (\text{D.7})$$

The function $g(u(t))$ does not depend on x and can be moved outside the inner integral:

$$\int_0^T g(u(t)) \left(\int_t^T f(x) dx \right) dt. \quad (\text{D.8})$$

From (D.4) and (D.5) we know that:

$$\int_t^T f(x) dx = \int_0^T f(x) dx - \int_0^t f(x) dx = 1 - \int_0^t f(x) dx = 1 - F(t) \quad (\text{D.9})$$

which, when inserted into (D.8), results in:

$$\int_0^T g(u(t))(1 - F(t)) dt \quad (\text{D.10})$$

proving (D.3).

Appendix E

Input and output membership functions for the fuzzy logic controller

E.1 Inputs

E.1.1 Input 1: flywheel speed (in RPM) $FESSspeed$.

$$\mu_{lowSpeed}(FESSspeed) = \begin{cases} 1, & FESSspeed < 5000 \\ -\frac{FESSspeed}{200} + \frac{5200}{200}, & 5000 \leq FESSspeed < 5200 \\ 0, & \text{otherwise} \end{cases} \quad (E.1)$$

$$\mu_{normalSpeed}(FESSspeed) = \begin{cases} 0, & FESSspeed < 5000 \\ \frac{FESSspeed}{200} - \frac{5000}{200}, & 5000 \leq FESSspeed < 5200 \\ 1, & 5200 \leq FESSspeed < 14800 \\ -\frac{FESSspeed}{200} + \frac{15000}{200}, & 14800 \leq FESSspeed < 15000 \\ 0, & FESSspeed \geq 15000 \end{cases} \quad (E.2)$$

$$\mu_{highSpeed}(FESSspeed) = \begin{cases} 0, & FESSspeed < 14800 \\ \frac{FESSspeed}{200} - \frac{14800}{200}, & 14800 \leq FESSspeed < 15000 \\ 1, & FESSspeed \geq 15000 \end{cases} \quad (E.3)$$

E.1.2 Input 2: hoist motor power (in W) *HoistPower*.

$$\mu_{NH}(HoistPower) = \begin{cases} 1, & HoistPower < -350000 \\ -\frac{HoistPower}{150000} - \frac{200000}{150000}, & -350000 \leq HoistPower < -200000 \\ 0, & otherwise \end{cases} \quad (E.4)$$

$$\mu_{NM}(HoistPower) = \begin{cases} \frac{HoistPower}{150000} + \frac{350000}{150000}, & -350000 \leq HoistPower < -200000 \\ -\frac{HoistPower}{100000} - \frac{100000}{100000}, & -200000 \leq HoistPower < -100000 \\ 0, & otherwise \end{cases} \quad (E.5)$$

$$\mu_{NL}(HoistPower) = \begin{cases} \frac{HoistPower}{100000} + \frac{200000}{100000}, & -200000 \leq HoistPower < -100000 \\ \frac{HoistPower}{100000}, & -100000 \leq HoistPower < 0 \\ 0, & otherwise \end{cases} \quad (E.6)$$

$$\mu_{PL}(HoistPower) = \begin{cases} \frac{HoistPower}{100000}, & 0 \leq HoistPower < 100000 \\ -\frac{HoistPower}{100000} + \frac{200000}{100000}, & 100000 \leq HoistPower < 200000 \\ 0, & otherwise \end{cases} \quad (E.7)$$

$$\mu_Z(\text{HoistPower}) = \begin{cases} \frac{\text{HoistPower}}{100000} + \frac{100000}{100000}, & -100000 \leq \text{HoistPower} < 0 \\ -\frac{\text{HoistPower}}{100000} + \frac{100000}{100000}, & 0 \leq \text{HoistPower} < 100000 \\ 0, & \text{otherwise} \end{cases} \quad (\text{E.8})$$

$$\mu_{PM}(\text{HoistPower}) = \begin{cases} \frac{\text{HoistPower}}{100000} - \frac{100000}{100000}, & 100000 \leq \text{HoistPower} < 200000 \\ -\frac{\text{HoistPower}}{150000} + \frac{350000}{150000}, & 200000 \leq \text{HoistPower} < 350000 \\ 0, & \text{otherwise} \end{cases} \quad (\text{E.9})$$

$$\mu_{PH}(\text{HoistPower}) = \begin{cases} 0, & \text{HoistPower} < 200000 \\ \frac{\text{HoistPower}}{150000} - \frac{200000}{150000}, & 200000 \leq \text{HoistPower} < 350000 \\ 1, & \text{HoistPower} \geq 350000 \end{cases} \quad (\text{E.10})$$

$$\mu_{POS}(\text{HoistPower}) = \begin{cases} 0, & \text{HoistPower} < 0 \\ \frac{\text{HoistPower}}{5000}, & 0 \leq \text{HoistPower} < 5000 \\ 1, & \text{HoistPower} \geq 5000 \end{cases} \quad (\text{E.11})$$

E.1.3 Input 3: DC bus voltage (in V) $DCbusV$.

$$\mu_Z(DCbusV) = \begin{cases} 0, & DCbusV < 0 \\ 1, & 0 \leq DCbusV < 400 \\ -\frac{DCbusV}{130} + \frac{530}{130}, & 400 \leq DCbusV < 530 \\ 0, & DCbusV \geq 530 \end{cases} \quad (\text{E.12})$$

$$\mu_N(DCbusV) = \begin{cases} 0, & DCbusV < 550 \\ \frac{DCbusV}{25} - \frac{550}{25}, & 550 \leq DCbusV < 575 \\ 1, & 575 \leq DCbusV < 600 \\ -\frac{DCbusV}{100} + \frac{700}{100}, & 600 \leq DCbusV < 700 \\ 0, & DCbusV \geq 700 \end{cases} \quad (E.13)$$

$$\mu_L(DCbusV) = \begin{cases} 0, & DCbusV < 400 \\ \frac{DCbusV}{130} - \frac{400}{130}, & 400 \leq DCbusV < 530 \\ 1, & 530 \leq DCbusV < 550 \\ -\frac{DCbusV}{25} + \frac{575}{25}, & 550 \leq DCbusV < 575 \\ 0, & DCbusV \geq 575 \end{cases} \quad (E.14)$$

$$\mu_H(DCbusV) = \begin{cases} \frac{DCbusV}{100} - \frac{600}{100}, & 600 \leq DCbusV < 700 \\ -\frac{DCbusV}{50} + \frac{750}{50}, & 700 \leq DCbusV < 750 \\ 0, & otherwise \end{cases} \quad (E.15)$$

$$\mu_{VH}(DCbusV) = \begin{cases} 0, & DCbusV < 700 \\ \frac{DCbusV}{50} - \frac{700}{50}, & 700 \leq DCbusV < 750 \\ 1, & DCbusV \geq 750 \end{cases} \quad (E.16)$$

E.2 Outputs

E.2.1 Output 1: FLC output

$$\mu_{IVH}(i) = \begin{cases} 0, & i < -2 \\ 1, & -2 \leq i < -1.5 \\ -\frac{i}{0.5} - \frac{1}{0.5}, & -1.5 \leq i < -1 \\ 0, & i \geq -1 \end{cases} \quad (E.17)$$

$$\mu_{EL}(i) = \begin{cases} \frac{i}{0.5}, & 0 \leq i < 0.5 \\ -\frac{i}{0.5} + \frac{1}{0.5}, & 0.5 \leq i < 1 \\ 0, & \textit{otherwise} \end{cases} \quad (\text{E.18})$$

$$\mu_{EVH}(i) = \begin{cases} 0, & i < 1 \\ \frac{i}{0.5} - \frac{1}{0.5}, & 1 \leq i < 1.5 \\ 1, & 1.5 \leq i < 2 \\ 0, & i \geq 2 \end{cases} \quad (\text{E.19})$$

$$\mu_{IH}(i) = \begin{cases} \frac{i}{0.5} + \frac{1.5}{0.5}, & -1.5 \leq i < -1 \\ -\frac{i}{0.5} - \frac{0.5}{0.5}, & -1 \leq i < -0.5 \\ 0, & \textit{otherwise} \end{cases} \quad (\text{E.20})$$

$$\mu_{IL}(i) = \begin{cases} \frac{i}{0.5} + \frac{1}{0.5}, & -1 \leq i < -0.5 \\ \frac{i}{0.5}, & -0.5 \leq i < 0 \\ 0, & \textit{otherwise} \end{cases} \quad (\text{E.21})$$

$$\mu_{EH}(i) = \begin{cases} \frac{i}{0.5} - \frac{0.5}{0.5}, & 0.5 \leq i < 1 \\ -\frac{i}{0.5} + \frac{1.5}{0.5}, & 1 \leq i < 1.5 \\ 0, & \textit{otherwise} \end{cases} \quad (\text{E.22})$$

$$\mu_Z(i) = \begin{cases} \frac{i}{0.5} + \frac{0.5}{0.5}, & -0.5 \leq i < 0 \\ -\frac{i}{0.5} + \frac{0.5}{0.5}, & 0 \leq i < 0.5 \\ 0, & \textit{otherwise} \end{cases} \quad (\text{E.23})$$

Appendix F

How to run the Matlab/Simulink scripts and simulations

This Appendix provides information on how to run the Optimal control calculations and the hybrid RTG simulations. A compressed folder has been prepared with all the files necessary to run a simulation. At the moment, the files are located in a zip file in the following location:

<http://tp829284.webs.sse.reading.ac.uk/wordpress/wp-content/uploads/2017/12/PietrosantiThesisFiles.zip>

Alternatively, it is available at the address below, also accessible through the QR code displayed in Figure F.1.

<http://goo.gl/t7D4nY>

To open the file it is necessary to use 7-zip (available at www.7-zip.org/) and, when prompted, insert the following password: *regeneration*.

F.1 Optimal control calculations

The folder named *Optimal control strategy* contains the files necessary to calculate the optimal control strategy given a set of parameters and the data from measurements of lift durations. To start the calculation, read the instruction contained in the file named *main.m*. The code is commented and it is possible to interpret using the information provided in Section 6.2. Matlab version 2017a is required to run the calculations.



Fig. F.1 QR code linking to the zip file containing the Matlab scripts.

F.2 Hybrid RTG crane model

The folder named *RTG model* contains all the files necessary to run the 6 configuration presented in Chapter 7. As well as the models, a data file containing 1 hour of measured data is provided. The simulation can be run by modifying and executing the script named *run_to_simulate.m*. In order to run the simulation, the following Matlab toolboxes are required:

- fuzzy_toolbox
- power_system_blocks
- simscape
- simulink.